UNIVERSITY OF UDINE

PHD COURSE
ENVIRONMENTAL AND ENERGY ENGINEERING SCIENCE

XXIX CYCLE

PhD thesis

Innovative galvanic coatings for high temperature applications

SUPERVISOR:
Prof. Lorenzo Fedrizzi
CO-SUPERVISOR:
Dr. Maria Lekka

PHD STUDENT:
Ruben Offoiach

-2017-

Index

Preface

1 Theoretical remarks 1-1

1.1 Theory of the electrodeposition – Fundamental concepts 1-1

***1.1.1 The overpotential* 1-1**

***1.1.2 The Relationship between current and overpotential and the diffusion layer* 1-2**

***1.1.3 Electrocrystallization and grains growth* 1-4**

***1.1.4 Crystal growth mechanism and the parameters that influence the deposit microstructure development* 1-6**

1.2 Electrodeposition of alloys 1-11

1.3 Theory of the co-deposition - galvanic composite coatings 1-14

***1.3.1 Mechanism of co-deposition and mathematical models* 1-17**

***1.3.2 Influence of the process parameters* 1-18**

2 Galvanic coatings for high temperature applications 2-1

2.1 Ni/Al composite galvanic coatings – State of the art 2-1

2.2 Ni-B galvanic coatings – State of the art 2-3

3 Research project layout and experimental techniques 3-1

3.1 The research project 3-1

3.2 Experimental techniques and instruments 3-4

4 Ni/Al galvanic composite coatings 4-1

4.1 Production of Ni/Al composite coatings 4-1

***4.1.1 Preliminary tests and Al Powder characterization* 4-1**

***4.1.2 Study of the Ni/Al composite coating plating process* 4-3**

4.1.2.1 Substrate preparation **4-3**

4.1.2.2 Ni based plating baths **4-4**

4.1.2.3 Characterization of the Ni/Al composite coatings **4-5**

4.1.2.4 Study of the Electrodeposition process with Al nano powders **4-5**

4.1.2.5 Study of the Electrodeposition process with Al micro powders **4-16**

***4.1.3 Bath/Particles stability* 4-19**

4.1.3.1 pH measurements **4-19**

4.1.3.2 Zeta potential/Particles size measurements **4-20**

4.2 Microstructural characterization of Ni/Al composite coatings 4-25

4.2.1 Microstructural characterization of the As Plated **4-25**
4.2.2 Microstructural characterization after heat treatments **4-26**
4.3 Microhardness **4-36**
4.4 Corrosion resistance **4-38**
4.4.1 Micro-electrochemical behavior: Topographic and Volta potential maps **4-38**
4.4.1.1 Pure Ni deposits **4-38**
4.4.1.2 Ni/μAl composite deposits **4-40**
4.4.1.3 Ni/nAl composite deposits **4-42**
4.4.2 Potentiodynamic polarization measurements **4-43**
4.4.2.1 As plated deposits **4-43**
4.4.2.2 Pure Ni and composite deposits after heat treatments **4-45**
4.5 Partial conclusions **4-48**
5 Ni-B galvanic coatings **5-1**
5.1 Study of the Ni-B alloy plating process **5-1**
5.1.1 Study of the Ni-B alloy plating process at laboratory scale and microstructural characterization **5-2**
5.1.1.1 Substrate preparation and characterization of the Ni-B alloy coatings **5-2**
5.1.1.2 Preliminary study with Ni Watts plating bath **5-2**
5.1.1.3 Preliminary study with Ni Sulfammate "High speed" bath **5-24**
5.1.2 DMAB titration and plating baths stability **5-32**
5.1.3 Production of Ni-B deposits in the galvanic pilot plant and microstructural characterization **5-37**
5.1.3.1 Substrate **5-37**
5.1.3.2 Monolayer Ni-B coatings **5-37**
5.1.3.3 Multilayer Ni-B coating **5-42**
5.2 Evaluation of the performances of Ni-B alloy coatings **5-45**
5.2.1 Microstructural and microhardness modification after heat treatments **5-45**
5.2.1.1 Microstructure after heat treatments **5-45**
5.2.1.2 Microhardness after heat treatments **5-47**
5.2.2 Wear and Tribocorrosion resistance **5-48**
5.2.3 Corrosion resistance **5-53**
5.3 Partial conclusions **5-54**
6 Conclusions **6-1**

Preface

Degradation of metals and alloys at high temperature is a serious problem for many applications in aggressive environments, such as boilers, internal combustion engines, gas turbines, fluidized bed combustion, industrial waste incinerators etc. Different technologies can be used for the production of different types of coatings for the above mentioned applications. Among them, thermal spray coatings, PVD, diffusion coatings and galvanic coatings. Electrodeposition is widely used when the produced coatings should exhibit not only a high oxidation resistance but also a thermal expansion similar to that of the metallic substrate and high thermal conductivity. Moreover, the electrodeposition could form compact, porous free and thick coatings when the corrosion resistance and wear resistance in aggressive environments are also required.

The aim of this work is the production and characterization of two different types of Ni based galvanic coatings, which should guarantee higher performances at high temperature applications in comparison to the Pure Ni coatings. Thus, the work is divided in two parts, the first one regarding the production and characterization of Ni matrix composite coatings containing either micro- or nano- particles of Al and the second one regarding the production and characterization of Ni-B alloy coatings with low B content. In both cases, after an initial optimization of the process parameters different types of coatings have been produced and tested. The coatings microstructure, microhardness and chemical composition both prior and after heat-treatments at different temperatures have been studied and compared to pure Ni deposits. The coatings performances such as protective properties, wear and tribocorrosion resistance have been also evaluated and the results have been correlated to the microstructural and chemical modifications.

1 Theoretical remarks

1.1 Theory of the electrodeposition – Fundamental concepts

1.1.1 The overpotential [1,2]

Electrochemical deposition of metals and alloys involves the reduction of metal ions from aqueous solutions. The reduction of metals ions is represented by:

$$M^{z+}_{solution} + ze^{-} \rightarrow M_{lattice}$$

where z electrons could be provided by an external power supply (electrodeposition) or by a reducing agent in the solution (electroless deposition). In both cases, the deposition reaction occurs at the interface between a solid metal electrode and a liquid solution.
In the case of the electrodeposition process, the solid metal electrode is a part of an electrochemical cell through which current is flowing and its potential differs from the equilibrium potential. If the equilibrium potential of the electrode (in absence of external current) is E_{rev} and the potential of the same electrode as a result of external current flowing is $\Delta V(I)$ the different η between these two potentials,

$$\eta = \Delta V(I) - E_{rev}$$

is called *overpotential*.
The *overpotential* η is the macroscopic manifestation of the irreversibility that accompanies the electrode process or else the "energy" required to run the process at a finite rate.
In general the electrochemical process is composed of a sequence of partial processes: diffusion, charge transfer, chemical reaction and crystallization. Hence, the total overpotential can be divided in four components one for each kind of partial process:

$$\eta = \eta_d + \eta_{ct} + \eta_r + \eta_c$$

The slowest partial process is rate-determining for the total overall process.
The *diffusion processes* (η_d) regards the mass transport of the substances consumed or formed during the electrode reaction that are transported from the bulk solution to the electrode surface or vice versa. Pure diffusion overpotential η_d occurs if the mass transport

[1] M. Paunovic, M. Schlesinger, Fundamentals of Electrochemical Deposition, 2006, John Wiley & Sons Inc., Second Edition, pp. 77-112
[2] M. Paunovic, M. Schlesinger, D. Snyder, Modern electroplating, 2010, John Wiley & Sons Inc., Fifth Edition, pp. 1-32

is the lowest process and in this case, the diffusion is the rate-determining step (*Diffusion control*).
The *charge transfer reaction* (η_{ct}) involves transfer of charge carriers, ions or electrons, across the double layer and occurs between the electrode and ion or molecule. The charge transfer reaction is the only partial reaction directly affected by the electrode potential and it is the rate-determining step only if it is hindered and none of the other partial reaction is hindered (*Charge transfer control*).
Chemical reactions can be involved in the overall electrode process. The rate constant of the chemical reaction, that could occur in the solution and/or on the electrode surface, is independent of potential. However, the chemical reactions can be hindered and thus hinder the current flow.
Processes at metal/metal-ion electrodes include *crystallization reactions.* These are processes by which atoms are either incorporated into or removed from the crystal lattice. Hindrance of these processes results in crystallization overpotential η_c.

1.1.2 The Relationship between current and overpotential and the diffusion layer[1,2]

The general relationship between the current i and the overpotential η is shown in Figure 1-1

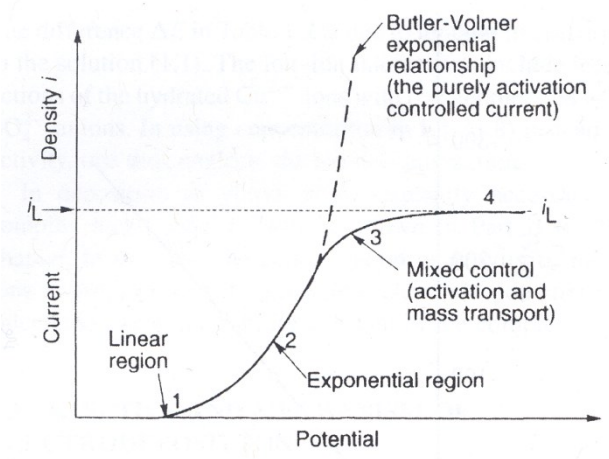

Figure 1-1: General relationship between the current density i and the potential η

Assuming that the process is in *Charge transfer control* (the charge transfer is the slowest process and the other processes are fast), the relationship between the current i and the overpotential η can be expressed in two different ways depending on the value of the overpotential.
If the overpotential is low (Linear region 1 in Figure 1-1), less than about 0.01 V (the electrode potential is near the reversible potential), the current i can be expressed as linear dependence of the η_{ct}:

$$i = i_0 \frac{zF}{RT}\eta \qquad if \qquad \eta < 0.01V$$

Where: i_0 is the exchange current density, characteristic of the particular electrochemical reaction and the electrode material; F is the Faraday constant; R is the gas constant; T is the absolute temperature.
If the overpotential is high (Exponential region 2 in Figure 1-1), above 0.1V, the relationship is exponential and the current i can be expressed as:

$$i = -i_0 \, exp\left(-\frac{\alpha z F \eta}{RT}\right) \qquad if \qquad \eta > 0.1V$$

Where: i_0 is the exchange current density; α = 0,5 for symmetric energy barrier; F is the Faraday constant; R is the gas constant; T is the absolute temperature.
Assuming that the process is in d*iffusion control* (Region 4 in Figure 1-1)*,* the rate of the reaction is limited by the transport of species ($M^{z+}_{solution}$) to the electrode surface. In this case, the current is independent to the overpotential values and is regulated by a diffusion law.

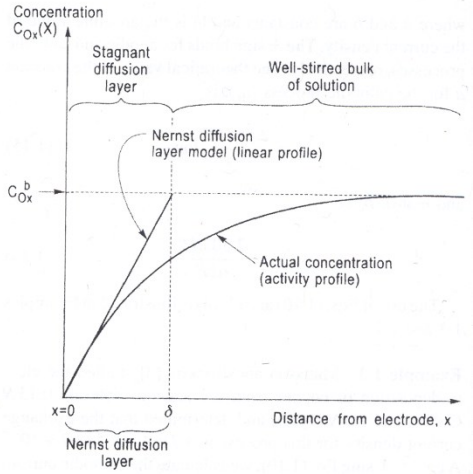

Figure 1-2: Variation of the concentration of the reactant during non-steady-state electrolysis

According to the Nernst diffusion-layer model, that assumes that the concentration of M^{z+} has a bulk concentration of C_b up to a distance of δ from the electrode surface and then falls off linearly to zero at the electrode surface, the limiting, or maximum, current density is approximated by:

$$i_L = \frac{nFD}{\delta} C_b$$

Where: D is the diffusion coefficient of the depositing species M^{z+}, δ is the diffusion layer thickness; c_b is the bulk concentration of M^{z+}.
At the values of the limiting (maximum) current density, the species M^{z+} are reduced as soon they reach the electrode surface. At this condition, the concentration of the reactant at the electrode is zero, and the rate of deposition reaction is controlled by the rate of transport of the reactant to the electrode. If an external current higher than the limiting current is forced through the electrode, the double layer is further charged, and the potential of the electrode will change until some other process, other than reduction of M^{z+}, occurs.

Electrodeposition processes in diffusion control are strictly correlated to the viscosity, the density and the temperature of the solution, the bulk concentration, and in particular to the stirring type and speed that influences the diffusion layer thickness.
The diffusion layer is also particularly influenced by the use of pulse current for the deposition. In this case the Nernst diffusion layer can be split in two diffusion layers (Figure 1-3) the pulsating diffusion layer (δ_p), close to the electrode surface where metal ion concentration pulsates with the frequency of the pulsating current, and the stationary diffusion layer (δ_s).

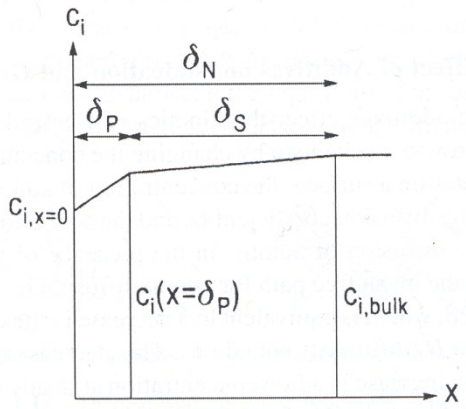

Figure 1-3: Schematic concentration profile at the cathode for pulse plating conditions

The rate determining step, in this case, is the diffusion in the δ_P diffusion layer as the drop of the concentration in the stationary diffusion layer is quite small. The use of pulse current, thus, usually leads to a thinning of the diffusion layer and to an increase of the amount of ions reaching the cathode.

1.1.3 Electrocrystallization and grains growth[1,2]

In the electrodeposition of metals, a metal ion is transferred from the solution to the ionic metal lattice. A simplified atomistic representation of this process is:

$$M^{z+}_{solution} + ze^- \rightarrow M^{z+}_{adatom} \rightarrow M_{lattice}$$

This reaction is accompanied by the transfer of z electrons from the external electron source, from the power supply, to the electron gas of the metal M.
A graphic representation of the process is shown in Figure 1-4

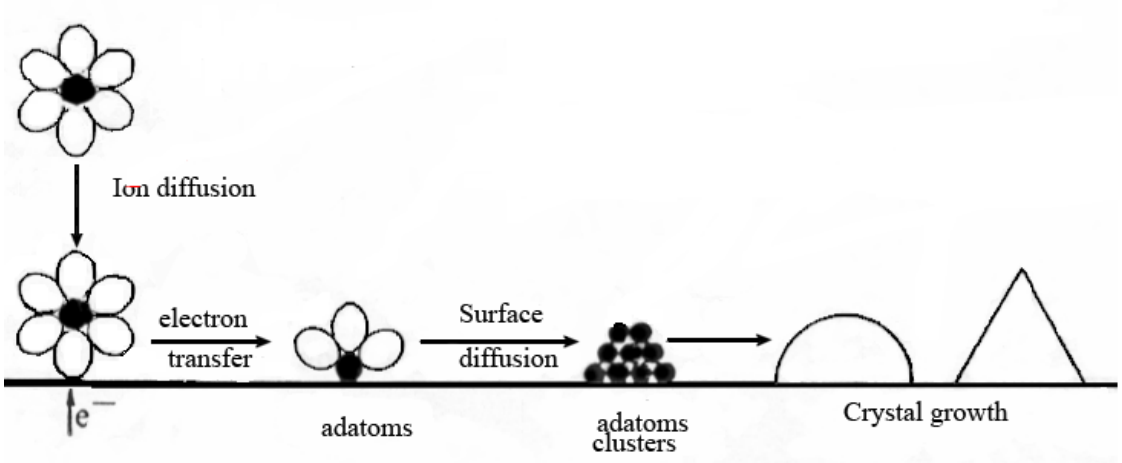

Figure 1-4: Electrocrystallization steps

The solvated ions move toward the cathode by diffusion, migration and convection. On the cathode, the ions receive electrons from the external power supply and lose partially or completely the solvation shell. The acquisition of electrons changes the atomic state of the ions in an intermediate state named adatom. The adatoms are adsorbed on the surface and spread on it until they reach a kink site. The kink site is a preferential position of lower energy where the adatom remains permanently attached contributing to the crystal growth. The adatom is reached by other adatoms forming clusters and as soon as a critical size is reached, the atomic state changes in metallic atoms of the lattice. Nucleation of a crystal starts.

The paths that the adatoms can follow to reach the kink site can be describe by two mechanisms the *step-edge ion-transfer* and the *terrace ion-transfer*. A schematic representation of the two mechanisms is presented in Figure 1-5.

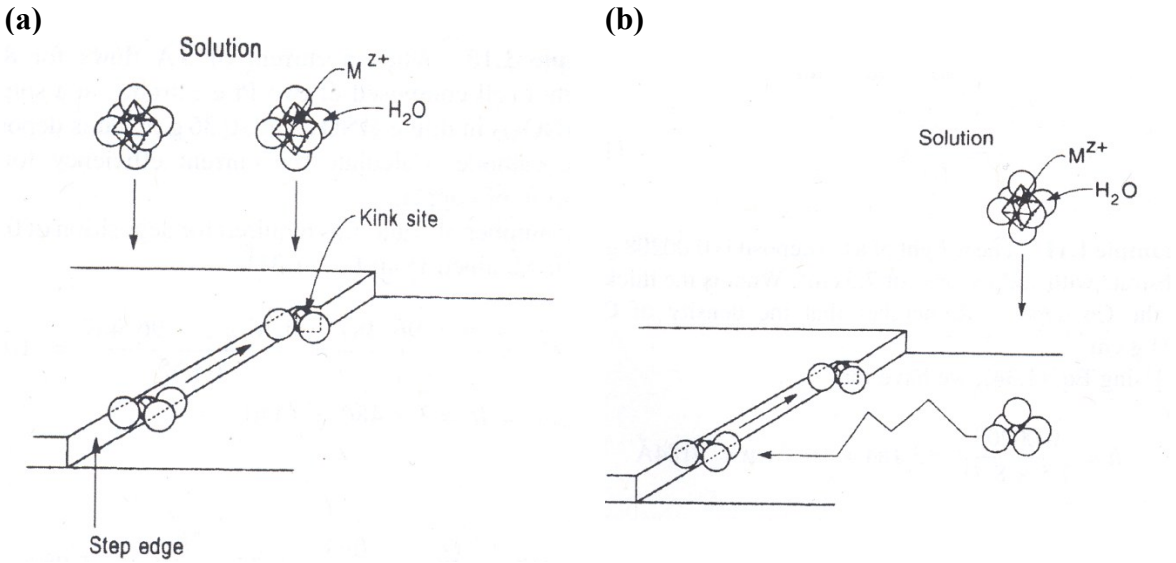

Figure 1-5: Ion-transfer mechanism: (a) step-edge transfer and (b) terrace transfer

The number of the kink sites and the path which the adatoms follow to reach it influence the rate and the mechanism of the electrocrystalization.

1.1.4 Crystal growth mechanism and the parameters that influence the deposit microstructure development [3,4]

An important contribution to understand the main aspects of the electrocrystallization and to describe the effects of the electrodeposition parameters on the crystal growth mechanism was suggested by Winand.
The Winand diagram, reported in Figure 1-6, describes in general the development of the deposit texture as function of two main parameters:

- The current density normalized with respect to the diffusion current limit
- and the *inhibition intensity* (intended as hindrance to the cathodic process, and consequently affect the various contributions to the total overpotential).

The *current density*, normalized with respect to the current limit density, is correlated to the amount of ions that reach the electrode surface and hence varies analogously to the total overpotential. While the *inhibition intensity* is correlated to the presence of other substances different to the metallic ions on the electrode surface, in the double layer and in the diffusion layer which inhibit locally the grain growth.

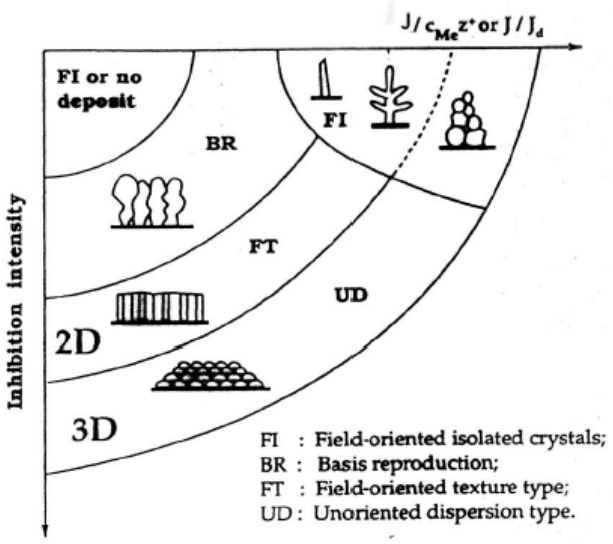

Figure 1-6:Winand diagram

The Winand model can be used as a tool for predicting the microstructural development of electrodeposits. The different zones of the diagram show the different microstructures that is possible to obtain:

- Field oriented crystals isolated (FI): obtained with low inhibitions, consisting of thin vertical columns oriented along the electric field. They can be transformed to dendrites or powders by increasing the current density

[3] R. Winand, Hydrometallurgy 29 (1992), 567-598
[4] M. Paunovic, M. Schlesinger, Fundamentals of Electrochemical Deposition, 2006, John Wiley & Sons Inc., Second Edition, pp. 113-138, 273-288

- Basis-oriented reproduction (BR): obtained with average inhibition and average current density, consisting of large grains formed by marked lateral growth, where the electrolyte could remain trapped, characterized by high roughness
- Field oriented texture (FT): obtained with strong inhibition or current density, consisting of compact elongated crystals oriented along the direction of the electric field that form a compact and coherent deposit
- Unoriented dispersion (UD): obtained with high current density and high inhibition consisting of many small crystals with no particular growth direction that form a coherent and very compact deposit

Considering the electroplating process as a whole, the two main parameters taken into account to the Winand model are strictly correlated to the "operating parameters".
The main "operating parameters" that most influence the deposit microstructure are:

- the composition of the plating bath (metal salt, support electrolyte, additives and buffers)
- the temperature of the electrolyte
- the agitation of the electrolyte
- the current density

An increase of the *current density* leads to an increase of the deposition and the nucleation rate and hence to the formation of small grains. The current density is limited by the conductivity of the electrolyte. In general, a high current density causes a dendritic growth of the deposit. The commons plating baths usually contain *metal ion concentrations* sufficient to allow high deposition rates. However high concentrations of salt favor the lateral growth at the expense of the nucleation with the formation of coarse grains. The ion concentration is dependent of the solubility and hence is influenced by the temperature and the plating bath pH.
The *pH* must be kept in an optimal operating range. Low pH facilitate the H_2 evolution instead high pH leads to the formation of hydroxides near the cathode which could form a screening film or remain entrapped into the deposit.
The *temperature* influences strongly the deposit microstructure as it increases the solubility of the salts, and hence the conductivity of the electrolyte, but in particular increases the crystallization kinetics leading to the formation of coarse grains.
The *agitation* of the plating bath assures an enrichment of metal ions near the cathodic surface reducing the thickness of the diffusion layer and in general allows to use higher current densities. However, the agitation can not be too high in order to avoid the formation of turbulent flow near the surface and thus the formation of rough deposits.
The *additives* affect the deposition and crystal building processes, in particular the ion transfer mechanism, as adsorbed substances on the surface of the electrode. There are two basic types of adsorption: chemical adsorption, where electrons are shared or transferred between the substrate and the adsorbed substances and usually the chemical bond is covalent, and physical adsorption, where there is no electron sharing or transfer and the combination is due to Van der Walls and electrostatic forces. In general the main effects of the additives are: change the number of growth sites on the cathodic surface, change the concentration of adatoms on the surface and change the diffusion coefficient D. Some additives can change also the chemical composition of the deposits due to chemical decomposition and partial co-deposition with the metal in the lattice.
A schematic representation of the influence of the different "operating parameters" on the microstructural refinement of the deposit is shown Figure 1-7.

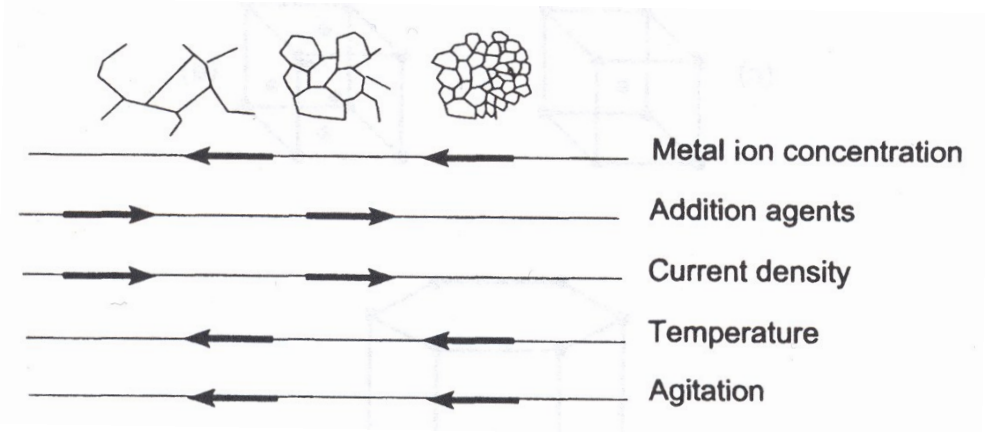

Figure 1-7: Relation of structure of electrodeposits to operating conditions of solutions.

Since the deposits properties are strongly dependent on the deposit microstructure, the formation of a coherent and compact deposit is required for many engineering applications. The formation of a coherent deposit can be described by two basic growth mechanisms:

- layer growth
- three-dimensional crystallite growth or nucleation-coalescence growth

A schematic representation of two mechanisms is shown in Figure 1-8.

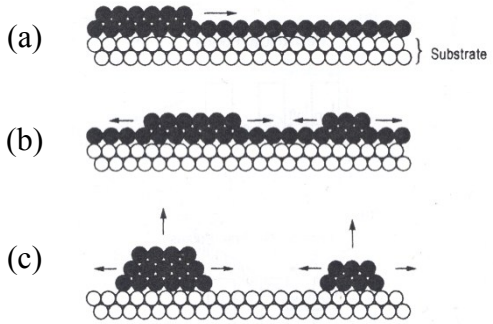

Figure 1-8: Schematic representation of (a and b) layer growth and (c) nucleation-coalescence growth

In the case of layer growth mechanism a crystal enlarges by a spreading of discrete layers (steps) one after another across the surface. In this case, a growth layer, a step, is a structure component of a coherent deposit. It is possible to distinguish among monoatomic steps polyatomic micro steps and polyatomic macrosteps. In general, there is the tendency of a large number of thin steps to bunch into a system of few thick steps. Many monoatomic steps can unite to form a polyatomic step.

In the case of three-dimensional crystallite growth mechanism the structural components are three-dimensional crystallites (TDC) and a coherent deposit is built up as a result of coalescence of these crystallite. The growth sequence of electrodeposition via nucleation–coalescence consist of four stage: formation of isolated nuclei and their growth to TDC, coalescence of TDC, formation of linked networks and formation of a continuous deposit.

Two of the most important microstructures of coherent deposits that is possible to obtain varying the "operating electrodeposition parameters" are the *columnar microstructure* and the *lamellar microstructure*.
The crystal-growth mechanism involved in the formation of the *columnar microstructure* is the nucleation-coalescence mechanism. The columnar microstructure is composed of relatively fine grains near the substrate and change to a columnar microstructure with oriented coarse grains at higher distances from the substrate. The development of the columnar microstructure can be described as the result of growth competition among adjacent grains. The low-surface-energy grains grow faster than the high-energy ones. This rapid growth of the low-surface-energy grains at the expense of the high-energy grains results in an increase in the mean grain size with increased thickness of the deposit and the transition from a fine grain size near the substrate to a coarse columnar grain size by increasing the distance from the substrate.
In general the columns are oriented along the electrical field direction but their thickness and the sub-structures of which are composed are affected by various factors.
Pure Ni deposits produced with two of the most commons Ni plating baths, the Ni Watts plating bath and the sulfammate "High Speed" bath, further described later in this study, present the typical columnar microstructure. The different counter ions of the Ni salt used in these two plating baths play a fundamental role in the deposit growth influencing the deposition mechanism.
In the case of the *Ni Watts plating bath*, mainly composed by Ni sulfate, the lower molecular weight of the anion SO_4^{2-} influences both the bath viscosity and the diffusivity of the Ni^{2+} cations toward the cathode. The high mass transfer of cations toward the electrode is not hindered thanks to an high diffusivity and low viscosity. The rate determining-step, in optimal operating conditions of overpotential, is the charge transfer.
In the case of the Ni sulfammate "High Speed" plating bath, composed by Ni sulfammate, the higher molecular weight of the anion $(SO_3NH_2)_2^{2-}$ increases the bath viscosity and reduce the diffusivity of Ni^{2+} cations toward the cathode influencing the thickness of the diffusion layer. In this case the mass transfer of cations toward the cathode is the rate determining step and the process is in diffusion control.
This two different mechanism of electrodeposition are reflected in the columnar microstructure of the Ni deposits. In fact, as observable in Figure 1-9, the microstructure of Ni deposits produced with Watts bath present thin columns composed of small single grain, while Ni deposits produced with sulfammate "High Speed" bath present a *pseudo-columnar structure* with larger and longer columns, each ones consisting of different small grains with similar orientations.

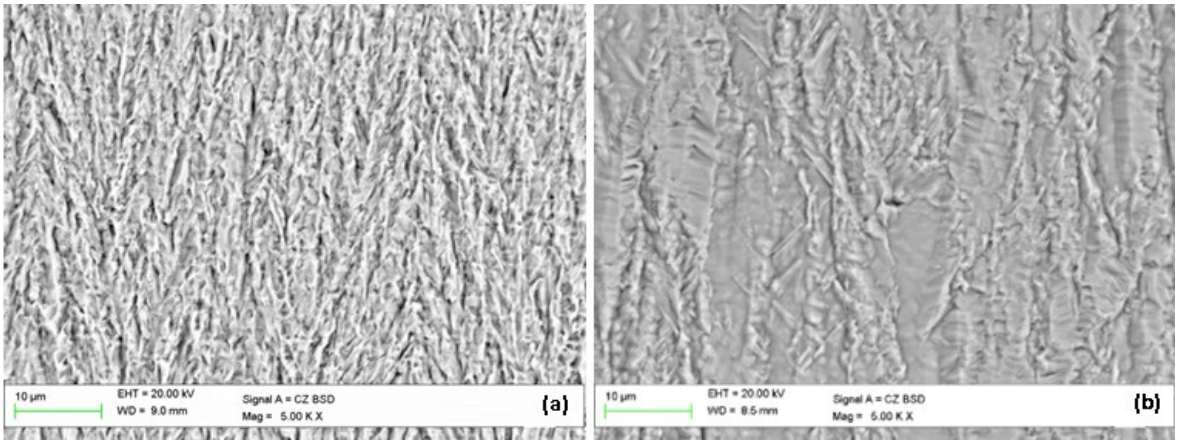

Figure 1-9: SEM micrographs in cross section after metallographic etching of: (a) Ni Watts deposit and (b) Ni sulfammate "High Speed"

The columnar microstructure is particularly affected by the deposit thickness and hence the deposition time due to the coalescence of the columns during the deposit growth.
The principal crystal-growth mechanism involved in the formation of the *lamellar microstructure* is the layer growth mechanism. The *lamellar microstructure* is typical of electrodeposits produced with strong inhibitions. Among the different factors that can hinder the cathodic process and/or modify the crystal growth mechanism, three are the most important:

- the presence of additives in the plating bath
- the co-deposition of other metals, or more in general of other elements, with the formation of an alloy deposit
- the use of the pulsed current

Cross section micrographs after metallographic etching of three Ni based deposit that present lamellar structure are observable in Figure 1-10.

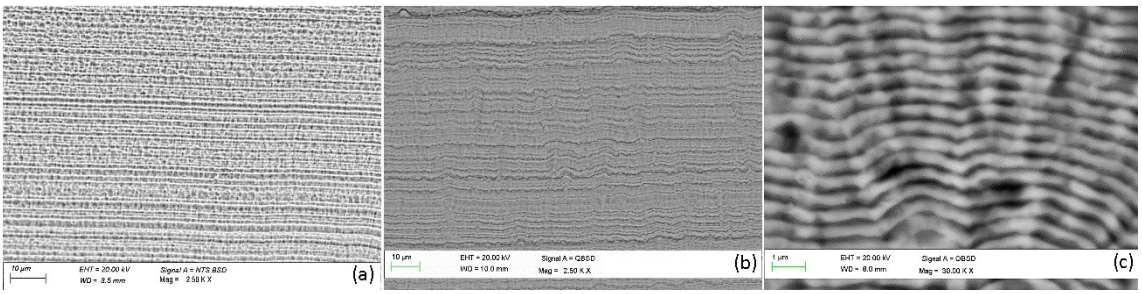

Figure 1-10: Lamellar structures of Ni based deposit produced with: (a) high concentration of saccharin, (b) co-deposition of Co, (c) pulsed current.

The lamellar microstructure is composed of very fine grains that form different sub-micrometric layers (lamella). The structure in general is non-oriented since the crystals do not have particular growth direction. Lamellar structure are usually more compact and less ductile than columnar microstructure.
Know the influence of the "operating parameters" on a specific electrodeposition process is fundamental in order to control the microstructure of the deposit and hence the overall properties of the coatings.

1.2 Electrodeposition of alloys[5,6]

The electrodeposition of an alloy regards, by definition, the co-deposition of two or more metals or, more in general, of a metal and other elements that become part of the metal lattice. The simultaneously electrodeposition of two metals is an old science as the electrodeposition of single metals. However, until today the electrodeposition of alloys is being investigated due to the vastness of the number of possible combinations and the concomitant possible practical applications. The co-deposition of two metal, in general, is possible when the ions of two metals are present in the same electrolyte and when the standard electrode potentials (E^0) of the two metals are close, or are changed to be close by modifying the chemical composition of the electrolyte.
Assuming that the standard electrode potentials of the two metals are close, the typical polarization curves for the deposition of an alloy are observable in Figure 1-11.

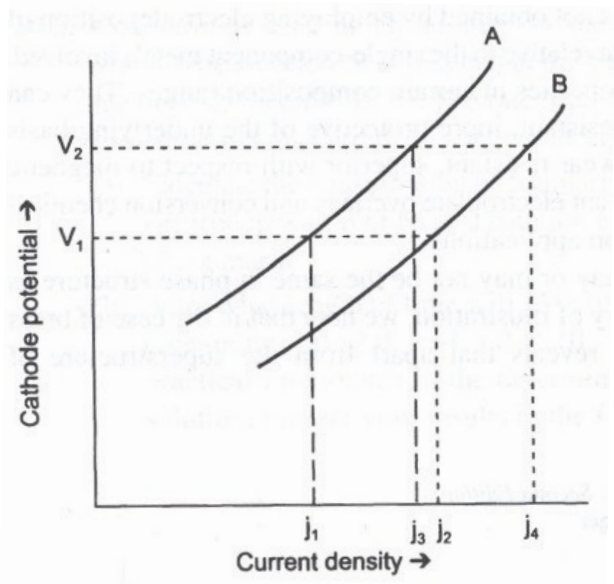

Figure 1-11: Polarization curve for the deposition of an alloy

At potential V_1, the deposition rates of metal A and B are given by the current density j_1 and j_2 respectively. Similarly, at potential V_2, the deposition rates for metals A and B are given by current densities j_3 and j_4 respectively. The amount of the metals deposited during a given interval of time may be determined from the current densities, using the relationship

$$Q = FE_q$$

Where: Q is the overall charge (C), F is the Faraday constant and E_q is the number of gram-equivalent weights of metal deposited. The values of Q can be determined from the expression

[5] M. Paunovic, M. Schlesinger, Fundamentals of Electrochemical Deposition, 2006, John Wiley & Sons Inc., Second Edition, pp. 199-208
[6] A. Brenner, Electrodeposition of Alloys – Principles and Practice, Academic Press Inc, 1963, pp. 3-11

$$Q = \int_0^t i\, dt$$

Where i is the current in amperes and t is the time in seconds.
The deposition of each metal occurs following the three main steps of *ionic migration, electron transfer* and *incorporation.* The electrodeposition occurs as an irreversible process.
The potential deposition of each metal ion however is regulated by the overpotential in accordance with:

$$E^d = E_{rev} + \eta = E^0 + \frac{RT}{zF} ln\, a^{z+} + \eta$$

Where F is the Faraday's constant, R is the gas constant, T is the absolute temperature and z number of electrons involved in the reaction.
The factor a^{z+} represents the activity value of the cation being deposited and is defined by:

$$a(M^{z+}) = \gamma c(M^{z+})$$

Where $c(M^{z+})$ is the concentration of M^{z+}in moles per liter and $\gamma(M^{z+})$ is the activity coefficient of M^{z+}. When the concentration of a solution is low the activity can be replaced by the concentration of all ions present in the solution. The activity coefficient γ is a dimensionless quantity, which depends on the concentration of all ions present in the solution (ionic strength). The individual activity coefficient of the specific ion species can not be measured experimentally, but it can be calculated. The activity a^{z+} is the parameter which is possible to modify in order to co-deposit two metals that present very different standard potentials. Varying the chemical composition of the electrolyte it is possible to form complex metal ions in order to adjust the ionic concentration and hence approach or modify completely the deposition potentials. A typical example is the co-deposition of Cu and Zn using KCN as complexing agent.
However, different binary systems present anomalies (for example Zn-Co, Ni-Co and Ni-W) due to chemical reactions that occur in the diffusion layer or electrochemical reactions that occur on the cathode surface. The triggering of these reactions may be due to local pH variations or the presence of different ionic species. Anomalous co-deposition usually leads to unexpected differences in the ratio of the amounts of co-deposited metals.
The co-electrodeposition of a metal with other elements, for example Ni-P and Ni-B, can be achieved by adding specific chemical compounds in the plating bath as element source. However, many mechanisms of the co-deposition are not yet completely understood.
The properties of electrodeposited alloys are of particular interest because, in a certain composition range, could be considerably better than those of single metal electroplates.
For example alloys usually are finer grained, harder, stronger, and may be more corrosion or wear resistant than the single metals.
Furthermore, some electrodeposited alloys can exhibit special properties, not shown by the parent metals, such as high magnetic permeability, be more suitable for subsequent electroplate overlays and conversion chemical treatments or present superior behavior in antifriction applications.
The enhanced properties compensate the increased difficulty involved in the operation of the alloy plating process. The more complex composition of alloy plating baths requires more frequent controls in order to maintain the bath composition in the operative range.

Furthermore, the alloy plating processes are more sensitive, in comparison to single metal deposition processes, to variations of the plating bath composition and plating process parameters such as current density, temperature and stirring. Small variation in the plating bath composition could lead to marked variations in the alloy chemical composition and thus in the deposit microstructure, especially in the case of anomalous co-deposition processes.

An interesting aspect of the electrodeposition of alloys is also that the phase structure of the deposits may or may not be the same as those formed metallurgically.

The grains of many electrodeposited alloys are usually smaller than that of parent metals and some alloys, for example Ni-P alloys, seem to possess no crystal structure at all and be apparently amorphous. The cross section microstructure of most electrodeposited alloys shows a laminar structure or a laminar structure superimposed on a columnar structure. The hardness of electrodeposited alloys could be considerably greater than that of parent metals, and also greater than that of thermal alloys obtained by conventional metallurgical procedures. For example, Co-P and Fe-W alloys have hardness equal to that of electrodeposited Hard-Cr, noted for its elevated hardness. Some of the electrodeposited alloys show, after heating at certain temperatures, a phenomenon similar to precipitation hardening. Coating alloys that exhibit this behavior are Ni-W, Fe-W, Co-Mo, Ni-P, Co-P and Cu-Pb. Furthermore, some of these deposits alloys, for example Co-W, are of particular interest for the preservation of their hardness at high temperatures.

Regarding the resistance to chemical attack and the corrosion resistance of electrodeposited alloys, it may be superior to that of the parent metals in certain environments. For example in outdoor and salt spray exposure, Sn-Zn alloys are superior to either Sn and Zn. Ni-Sn alloys are more resistant to attack by acids in comparison to pure Ni. Ni-High P alloys resist cold concentrated hydrochloric acid much better than pure Ni.

By virtue of their great range and diversity of properties, the electrodeposited alloys extend the field of potential applications of the deposits produced by electrodeposition. Nevertheless, the more complex process of electrodeposition of some alloys, in comparison to that of pure metals, requires more experimental efforts for both the production and the characterization.

1.3 Theory of the co-deposition - galvanic composite coatings

Electrolytic co-deposition is defined as the technique used to produce *metal matrix composite coatings* (MMCCs) or *Electrolytic composite coatings* (ECCs) by embedding particles, intentionally added to the plating bath, into a metal matrix in the course of an electrolytic deposition process. Unique, functional properties of ECCs are derived from the presence of the particles dispersed in the bulk and the microstructural modifications caused to the metal matrix and/or from the exposed particles, which are only partially embedded at the coating surface[7,8].

The particles can be co-deposited in the metal matrix by two main methods:

- by maintaining them in suspension in the plating bath for the entire deposition time by mechanical stirring. The particles are transferred to the cathode carried by the metallic ions and embedded into the metallic matrix as the metallic ions surrounding them are reduced.
- by sediment co-deposition. The particles are initially maintained in suspension in the plating bath and successively are left to sediment by gravity on the cathodic surface placed on the bottom of the cell and thus embedded in the metal matrix during the electrodeposition.

In the second case the particles content in the composite coating is usually higher but on the other hand, the geometry of pieces to be coated is bound by the peculiarities of the technique.

Many works in literature shows that ECCs could exhibit increased wear resistance, high toughness, low friction coefficient but also improved resistance to high temperatures, corrosion resistance, electromagnetic and optical properties completely different from the metal matrix. Furthermore, the electrodeposition of ECC is a relatively cheap solution to enhance the resistance of the metallic components to aggressive working conditions and to increase the component service life by increasing its mechanical, tribological, thermomechanical, and corrosion properties.

ECCs usually consist of a metal or alloy reinforced by:

- Carbides (SiC, WC, B_4C, TiC, Cr_3C_2,…)
- Oxides (SiO_2, Al_2O_3, TiO_2, ZrO_2, Cr_2O_3…)
- Nitrides (TiN, Si_3N_4, CrN, BN…)
- Sulphides (MoS, WS_2…)
- diamonds
- Graphite, PTFE, PS,…
- Metal particles (Al,Cr,Ti,…)

The type of both metal matrix and reinforcing material, the amount, the size, the shape, and the distribution of the reinforcing material in the metal matrix can be chosen based on the desired properties of the ECC.

[7] U.S. Congress, Office of Technology Assessment, Metal Matrix Composites, Advanced Materials by Design, OTA-E-351. Ed, Washington, DC: U.S. Government Printing Office, 1988, pp 99-117.

[8] W.D. Callister, Materials Science and Engineering – An Introduction..; John Wiley & Sons, Inc., 7th ed, 2007, pp 578-620

The incorporated particles do not modify the coatings properties only by their physical presence due to their intrinsic properties but also by modifying the structure of the matrix during the coating growth influencing the overall performances.
Considering the different combinations of matrixes and reinforcements and as a sequence the different properties, the composite coatings could be divided in four wide groups:

- dispersion hardened and wear resistant coatings,
- self lubricant coatings
- corrosion resistant coatings
- metal matrix / metal particles coatings

The *dispersion hardened and wear resistant coatings* are produced by co-depositing inert, hard, micrometric or submicrometric particles such as carbides, oxides, nitrides or diamonds in a metal matrix. In this kind of ECCs the matrix acts as a ductile binder able to maintain the hard particles firmly embedded during the wear process. The presence of hard particles hinders the dislocations movement through the metal lattice increasing the resistance to plastic deformation and hence the hardness[9,10,11,12,13]. The wear resistance of composite coatings does not depend only on the type and amount of incorporated particles, but it is also strongly influenced by the microstructural modifications of the metal matrix caused by the co-deposition of particles. ECCs containing hard ceramic particles present an improved hardness and wear resistance at high temperatures due to the excellent thermomechanical stability of these type of reinforcements. Contrarily to the precipitation hardened alloys, the particles in the dispersion hardened composites are not soluble to the metal matrix and do not react, maintaining the mechanical properties of the coatings also at high temperatures[14,15,16]. Since the distribution of particles in the metal matrix plays an important role to produce an isotropic coating, often ultrasounds and deposition under pulse current are used to increase the amount of co-deposited particles and to obtain a more uniform distribution within the matrix.
An another group of ECCs designed for applications that required high wear resistance are the *self-lubricating metal matrix composite coatings*. In this case, the increase of the wear resistance is obtained to co-depositing solid lubricant particles which lower the friction coefficient during the wear mechanism. The metal matrix acts as a reservoir for the particles which are released under wear condition and are smeared over the surface creating a solid lubricant layer. When the solid lubricant layer is consumed, the wear of the underneath metal matrix reveals other particles and the dry lubricant film is reformed. By lowering the friction coefficient, the material loss due to wear is decreased and the service life of the component increased. The most used particles for this application are graphite,

[9] A. Abdel Aal, K.M. Ibrahim, Z. Abdel Hamid, Wear 260 (2006), 1070-1075
[10] E. García-Lecina, I. García-Urrutia, J.A. Díez, M. Salvo, F. Smeacetto, G. Gautier, R. Seddon, R. Martin, Electrochimica Acta 54 (2009), 2556-2562
[11] P. Gyftou, M. Stroumbouli, E. A. Pavlatou, P. Asimidis, N. Spyrellis, Electrochimica Acta 50 (2005), 4544-4550
[12] M. Lekka, N. Kouloumbi, M. Gajo, P. L. Bonora, Electrochimica Acta 50 (2005), 4551- 4556
[13] Y. Zhou, H. Zhang, B. Qian, Applied Surface Science 253 (2007), 8335-8339
[14] L. Wang, Y. Gao, Q. Xue, H. Liu, T. Xu, Surface & Coatings Technology 200 (2006), 3719-3726
[15] O. A. León, M. H. Staia, H. E. Hintermann, Surface & Coatings Technology 120-121 (1999), 641-645
[16] M. Lekka, A. Lanzutti, A. Casagrande, C. de Leitenburg, P.L. Bonora, L. Fedrizzi, Surface & Coatings Technology 206 (2012), 3658-3665

molybdenum disulphide[17] and polymers such as polytetrafluoroethylene (PTFE)[18,19] or polycarbon mono fluoride (PCMF).

Corrosion resistant composite coatings present a higher corrosion resistance compared to the pure metallic coatings. The improved properties are not directly related to the intrinsic properties of the incorporated particles, but to the microstructural modifications of the metal matrix due to the co-deposition of ultrafine, mainly nano-metric, particles. Indeed, the ultrafine particles act as nucleation points or barriers to the grain growth leading to the formation of a finer and non-oriented microstructure. In this case the coatings present lower porosity, result more compact and as a consequence the corrosion resistance raises up[20,21,22]. As the corrosion properties are strictly related to the microstructure of the composite coatings the use of pulse current[23,24,25,26] or ultrasounds during the deposition[27,28] can further increase the resistance in aggressive environments.

The study of *Metal matrix/metal particles composite coatings* is relatively recent. The co-deposition of metal particles is interesting as it allows co-depositing metals that is not possible to electrodeposit from aqueous plating baths, for instance Al and Ti. Furthermore, adequate heat treatments allow the formation of specific phases, also intermetallic phases, and thus potentially extend the variety of alloy coatings that is possible to produce via galvanic processes. Among the different combinations of matrix and particles, Ni, Co or Ni/Co matrix and Al[29,30,31,32,33,34] Ti[35] or Cr[33,34,36] particles electrodeposited coatings have recently received a particular interest for their potential applications at high temperatures in oxidizing environments. However, the reactivity of the metallic particles limits the number of possible combination with the different galvanic baths.

[17] M. F. Cardinal, P. A. Castro, J. Baxi, H. Liang, F. J. Williams, Surface & Coatings Technology 204 (2009), 85-90
[18] E. Pena-Munoz, P. Berçot, A. Groesjean, M. Rezrazi, J. Pagetti, Surface & Coatings Technology 107 (1998), 107, 85-93
[19] L. X. Ying, J. T. Yang, Y. Liu, Z. K. Yang, Wang G. X., Key Engineering Materials 572 (2014), 277-280
[20] C. Zanella, M. Lekka, P.L Bonora, J. Appl. Electrochem. 39 (2009), 31-38
[21] A. F. Zimmerman, D. G. Clark, K. T. Aust, U. Erb, Mater. Lett. 52 (2002), 85-90
[22] M. D. Ger, Mater. Chem. Phys. 87 (2004), 67-74
[23] R. Mohan Reddy, B. M. Praveen, C. M. Praveen Kumar, T. V. Venkatesha, Journal of Materials Engineering and Performance 24 (2015), 1987-1994
[24] M. Lekka, A. Lanzutti, C. Zanella, G. Zendron, L. Fedrizzi, P. L. Bonora, Pure and Applied Chemistry 83 (2011), 295-308
[25] M. Lekka, G. Zendron, C. Zanella, A. Lanzutti, L. Fedrizzi, P. L. Bonora, Surface & Coatings Technology 205 (2011), 3438-3447
[26] S. Ghaziof, W. Gao, Journal of Alloys and Compounds 622 (2015), 918-924
[27] I. Tudela, Y. Zhang, M. Pal, I. Kerr, A. Cobley, Surface & Coatings Technology 259 (2014), 363-373
[28] C. Zanella, M. Lekka, S. Rossi, F. Deflorian, Corrosion Reviews 29 (2011), 253-260
[29] F. Cai, C. Jiang, X. Wu, Journal o Alloys and Compounds 604 (2014), 292-297
[30] H. Liu, W.Chen, Intermetallics 13 (2005) 805-817
[31] L. Zheng, X. Peng, F. Wang, J. Mater Sci 47 (2012) 7759-7763
[32] D.F.Susan, W.Z.Misiolek, A.R.Marder Metallurgical and Materials Transactions A 32A (2001), 379-390
[33] X. Peng, Y. Zhou, Y. Zhang, F. Wang, Materials Science Forum 461-464 (2004), 409-416
[34] X. Yang, X. Peng, C. Xu,F. Wang, J. Electrochem. Soc. 156 (2009), C167-C175
[35] I. Naploszek-Bilnik,A. Budniok,B. Losiewicz, L. Pajak, E. Lagiewka, Thin Solid Films 474 (2005),146-153
[36] X. Peng, Y. Zhang, J. Zhao, F. Wang, Electrochimica Acta 51 (2006) 4922-4927

1.3.1 Mechanism of co-deposition and mathematical models

Two processes are mainly involved in the co-deposition of particles into the metallic coatings: the physical dispersion of particles in the plating bath and the electrophoretic migration of the particles versus the cathode.
A lot of research groups tried, starting from the early 60's, to develop mathematical models of the co-deposition mechanism in order to predict the co-deposited particles amount but the complexity of the mechanisms and the peculiarity of the different systems has led in many cases to formulate models too simplistic or incorrect, not confirmed by experimental experience.
However, the most widely accepted model from the scientific community is the Celis and Ross one[37]. Celis and his group in 1987, after systematical study of the co-deposition mechanisms of different plating baths and particles, developed a detailed theory, proposing a co-deposition mechanism of 5 steps and a mathematical model to predict the amount of co-deposited particles in a metal matrix[38].
The basic assumptions of this model are:

1. An absorbed layer of ionic species, mainly metal ions, is created around the particles immediately after their dispersion in the plating bath or during the pretreatment of these particles in ionic solutions.
2. The particles can be embedded into the metal matrix if and only if an efficient part of these chemical species is reduced on the cathode.

The model consists of 5 steps as illustrated in Figure 1-12.

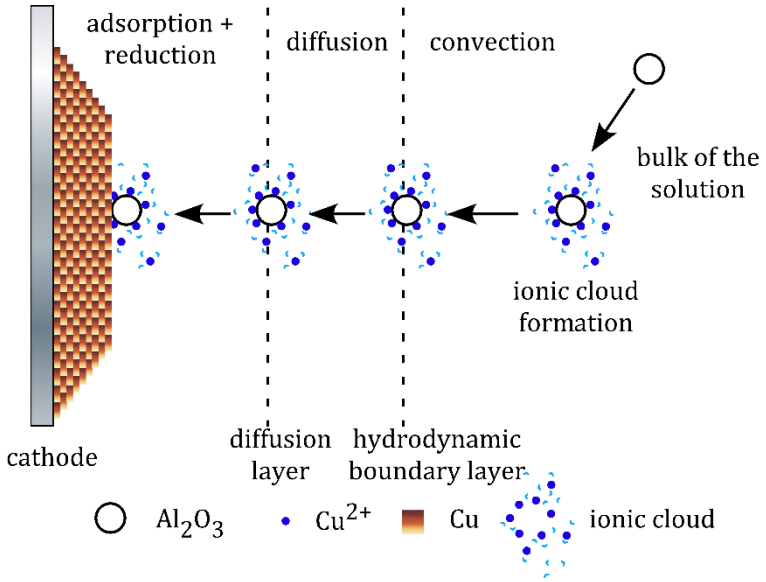

Figure 1-12: The deposition stages in the deposition of a particle according Celis et al.[39]

On its way from the bulk of the electrolyte to the site of incorporation at the cathode surface a particle has to proceed through:

1. Absorption of ionic species on its surface

[37] J. -P Celis, J. R. Roos, J. Electrochem. Soc. 124 (1977), 1508–1511
[38] J.-P. Celis, J. R. Roos, C. Buelens, J. Electrochem. Soc. 134 (1987), 1402–1408.
[39] M. Lekka, Electrochemical Deposition of Composite Coatings, Elsevier Reference Module in Chemistry, Molecular Sciences and Chemical Engineering, 2016, Reedijk, J. (Ed.)Waltham, MA: Elsevier

2. Transfer of the particle by forced convection towards the hydrodynamic boundary layer (δ_o)
3. Diffusion of the particle through the diffusion layer
4. Absorption of the particle, surrounded with the ionic cloud, at the cathode surface
5. Reduction of a sufficient amount of the ionic species by which the particle becomes irreversibly embedded into the metal matrix

For the construction of the model, it was assumed that steady-state conditions exist, so that no concentration, pressure, temperature and overpotential variations occur during the process. The cathode surface is uniformly accessible for all the particles and an homogeneous dispersion of the particles in the plating bath is achieved. Moreover, the current efficiency is considered 100% and the particles spherical. Based on this mechanism Celis et al. developed a mathematic model for the evaluation of the weight percentage of the co-deposited particles into the metal matrix, which was confirmed for the systems Cu/Al_2O_3 and Au/Al_2O_3.

Till now it is widely accepted that the particles are transported to the cathodic surface due to mechanical stirring and to electrophoretic phenomena and are codeposited into the metal matrix due to the reduction of the absorbed species. The mathematical expression which have been till now developed to predict the amount of codeposited particles can not be universally used.

1.3.2 Influence of the process parameters[39]

The properties of the composite electrodeposits are related to the presence of two distinct phases and to their interactions. During the deposition, the presence of particles on the cathodic surface and their incorporation into the growing metal matrix can cause important changes to the mechanism of nucleation and grow of the metal deposit. The final properties thus, do not depend only on the presence of the particles and their intrinsic properties, but also to the microstructural modifications of the metal matrix. The co-deposition of particles into metal electrodeposits depends on many process parameters related to the nature of the particles (particle concentration, type, shape, size, surface charge), to the electrolyte composition (electrolyte concentration, pH, temperature, surfactants type and concentration), plating parameters (current density, current type: direct current, pulse current, duty cycle, pulse time, hydrodynamics, plating cell geometry, use of ultrasounds).

Due to the high number of parameters influencing the co-deposition at the same time, it is not so easy to distinguish a clear effect of each one. However, the most important factor influencing the amount of co-deposited particles in the metal matrix from a specific plating bath and under specific plating conditions are the particles themselves.

Different researchers confirm that the amount of codeposited particles in the metal matrix generally increases by increasing their *concentration* in the plating bath till reaching a plateau. Further increase of the particles concentrations does not lead to an increase of the co-deposited amount in the metal matrix. In any case, a very high concentration of particles in the plating bath leads to a noticeable increase of the plating bath density and can cause a strong agglomeration of the particles and decrease the bath conductivity[9,40].

Regarding the effect of the *particles size* to the amount of co-deposited particles there are different and contradictory results. The particles size can not be considered as a single variable as it is difficult to obtain particles with the same composition, shape, surface

[40] S. K. Kim, H. J. Yoo, Surf. Coat. Technol. 108–109 (1998), 564–569.

charge and just different size. In many cases, a decrease of the amount of co-deposited particles was reported by decreasing the particles size[40,41,42], but it is important to specify that the co-deposition amount is usually referred to weight or volume percentage. If we transform the weight or volume percentage to number of co-deposited particles per unit of mass, volume or surface of composite deposit the number of smaller size particles is always much higher.

This is also confirmed, indirectly, by the microstructural modifications of the metal matrix caused by incorporating micro- or nano-particles. Usually the co-deposition of nano-particles in comparison to micro-particles leads to a strong refinement of the matrix microstructure due to an increase of the number of nucleation points.

The *structure of the particles* is also a very important parameter as confirmed mainly in composite systems with Al_2O_3 particles, which are much more difficult to co-deposit than other types of particles. No specific references have been found regarding the influence of the particles shape on the co-deposited amount of particles. However, the particles shape affects the absorption of ions on the particles surface, the suspension stability and the interactions with the growing metal matrix.

[41] E. A. Brandes, D. Goldthorpe, Metallurgia 76 (1967), 195–198
[42] R. Bazard, P.J. Boden, Trans. Inst. Met. Finish. 50 (1972), 63–69.

2 Galvanic coatings for high temperature applications

Degradation of metals and alloys at high temperature is a serious problem for many applications in aggressive environments, such as boilers, internal combustion engines, gas turbines, fluidized bed combustion, industrial waste incinerators etc. Solutions can be found in the use of sophisticated materials, that are resistant to oxidation and corrosion at high temperatures and exhibit high strength and wear resistance e.g. nickel based superalloy Inconel 625. However, coatings resistant at high temperatures on cheaper metals would be cheaper that bulk super alloys. The main industrial sectors interested on coatings for high temperature applications are energy plants (components of furnaces, heat exchangers, valves, etc.), the automotive industry (car engines components, pistons etc.), ceramic and glass manufacturing (molds, mixing paddles, stirrers etc.), aerospace industry (turbine engine parts), nuclear industry, cement industry, waste treatment and others.
Different technologies can be used for the production of different types of coatings for the above mentioned applications. Among them, thermal spray coatings, PVD coatings, diffusion coatings and galvanic coatings. Electrodeposition is widely used when the produced coatings should exhibit not only a high oxidation resistance but also a thermal expansion similar to that of the metallic substrate and high thermal conductivity. Moreover, the electrodeposition could form compact, porous free and thick coatings when the corrosion resistance and wear resistance in aggressive environments are also required.
Some works report that the presence of ceramic particles such as SiC or La_2O_3[1] improves also the high temperature oxidation resistance of pure Ni electrodeposits by limiting the thickness of the NiO scale. The same effect has been monitored by the use of Y_2O_3[2]. The NiO scale, however, cannot be considered fully protective for the underneath composite nickel matrix coatings. Hence, a different approach has been taken into consideration in the last years and considers the co-deposition of metallic particles.

2.1 Ni/Al composite galvanic coatings – State of the art

The scientific interest for the enhancement of the oxidation resistance of Ni coatings by the codeposition of metallic particles such as Al[3,4,5,6-17], Ti[7] or Cr[8,9] due to the tendency to form a continuous Cr_2O_3, Al_2O_3 or TiO_2 layer on the coatings surface at high temperatures is continuously increasing. The choice of adding Al or Ti in the form of particles is due to the

[1] X. Peng, D. Ping, T. Li, W. Wu, J. Electrochem. Soc. 145 (1998), 389-398
[2] Y.B. Zhou, J.F. Sun, S.C. Wang, H.J. Zhang, Corrosion Science 63 (2012) 351–357
[3] F. Cai, C. Jiang, X. Wu, Journal o Alloys and Compounds 604 (2014), 292-297
[4] H.Liu, W.Chen, Intermetallics 13 (2005) 805-817
[5] L. Zheng, X. Peng, F. Wang, J. Mater Sci 47 (2012) 7759-7763
[6] D.F.Susan, W.Z.Misiolek, A.R.Marder Metallurgical and Materials Transactions A 32A (2001), 379-390
[7] I. Naploszek-Bilnik,A. Budniok,B. Losiewicz, L. Pajak, E. Lagiewka, Thin Solid Films 474 (2005),146-153
[8] X. Peng, Y. Zhou, Y. Zhang, F. Wang, Materials Science Forum 461-464 (2004), 409-416
[9] X. Yang, X. Peng, C. Xu,F. Wang, J. Electrochem. Soc. 156 (2009), C167-C175

fact that the deposition of these elements is not possible from aqueous electrolytes. It has been reported that Ni matrix deposits containing Al micro-particles, obtained by sediment co-deposition, leads to the increase of the oxidation resistance by decreasing the thickness of the NiO scales due to the formation of a continuous and protective Al_2O_3 film on the coatings surface[10]. In order to form a continuous Al_2O_3 layer a critical amount of Al in the coating is necessary. The critical amount of codeposited Al is decreased noticeably by the codeposition of Al nano-particles instead of Al micro-particles[11,12]. Moreover, an annealing treatment in vacuum at 600^{o}C for 4h can further increase the oxidation resistance of the Ni-Al nanocomposite coatings due to the formation of $\gamma' Ni_3Al$ and γ Ni containing Al phases[13]. On the other hand, the pores which are formed due to fast diffusion of Al in the Ni matrix can negatively affect the oxidation resistance of the composites[14]. In this case, a high amount of Al (7-11%) decreases the oxidation resistance in the initial stage if compared to deposition with an Al amount less than 7% due to the formation of large pores. Anyway, more detailed studies on the oxidation kinetics on Ni-Al micro-composites produced using a parallel plates geometry and high amounts of particles both in the plating bath and in the produced deposits confirmed the beneficial effect of the Al particles on the oxidation resistance at both 800°C and 1000°C[15,16,17]. The same studies confirmed the formation of different intermetallic phases between Ni and Al after heat treatments at different temperatures based on the amount of Al and the heat treatments temperature.

The co-deposition of Al or Ti particles does not affect only the oxidation resistance of the produced deposits but also the microstructure of the Ni matrix by influencing the nucleation and growth processes. Parameters such as the plating bath chemical composition, the stirring rate, the particles concentration in the plating bath, the size and type of metallic particles, the deposition current density influence the amount of co-deposited particles, their distribution in the obtained deposit and the microstructure of the matrix, as occurs in every metal matrix composite system. As mentioned before, sediment codeposition allows the incorporation of higher amounts of particles even of large dimensions. According to Naploszek et al.[7], Ti particles can be deposited in higher amounts than Al particles using the same particles loading in the plating bath and the same current densities. The optimum conditions are different for the two systems, indicating than the type of particles strongly influence the deposition[3]. Other researchers compared the deposition of micro- and nano- particles of Al using the same particles load in the plating bath and the same current density and observed that the use of nanoparticles leads to a more uniform distribution in the metal matrix, in comparison to the use of micro-particles, and to a noticeable grain refinement of the Ni matrix microstructure[4]. The amount of co-deposited particles decreases by increasing the current density, keeping stable all other plating parameters, and the preferential orientation of the obtained deposits changes from (200) to a non-oriented one. This influences also the residual stresses of the composite deposits which thus decrease by increasing the current density.

The presence of Al particles does not only influence the oxidation resistance of the obtained deposits but could also influence the mechanical properties of the bulk deposit at

[10] Y. Zhou, X. Peng, W. Wang, Scripta Materialia 50 (2004), 1429-1433
[11] X. Yang, X. Peng, F. Wang, Scripta Materialia 56 (2007), 509-512
[12] Y. Zhou, X. Peng, F. Wang, Oxidation of Metals 64 (2005), 169-183
[13] X. Yang, X. Peng, F. Wang, Corrosion Science 50 (2008), 3227-3232
[14] H. Liu, W. Chen, Surface & Coatings Technology 202 (2008), 4019-4027
[15] D. F. Susan, K. Barmak, A. R. Marder, Thin Solid Films 307 (1997), 133-140
[16] D. F. Susan, A. R. Marder, Oxidation of Metals 57 (2002), 131-157
[17] D. F. Susan, A. R. Marder, Acta Materialia 49 (2001), 1153-1163

high temperatures due to the formation of the intermetallic Ni-Al phases. Although different research groups have studied in depth the oxidation mechanism, and the microstructural modification of the coating bulk, the literature is scarce about studies on the mechanical properties and the wear resistance at high temperatures and the wet corrosion behavior of the electrodeposited Ni-Al composite coatings.

2.2 Ni-B galvanic coatings – State of the art

Ni/B coatings are usually deposited by electroless deposition using strong reducing agents. The deposition occurs at high temperature (70-90°C) and high pH (13-14). The coatings produced by electroless deposition present a uniform thickness even on complex geometries, a high B content and high hardness. Usually the deposition is followed by a heat treatment that leads to the formation of intermetallic phases Ni-B as precipitates in order to further increase the coatings hardness. The coatings thus produced usually present a web of cracks caused by the presence of high internal stresses.
Ni/B coatings can be also produced by electrodeposition, but the literature about the electrodeposition of Ni/B coatings is relatively scarce. The galvanic processes may allow a higher deposition rate in comparison with the electroless processes; furthermore, the easier process control allows to obtain coatings with different contents of B, even very low. A low amount of B in the Ni/B deposits does not allow the formation of Ni_3B intermetallics after heat treatment, but could hinder the recrystallization of the Ni matrix at high temperatures maintaining a higher hardness than that of pure Ni coatings. The production of Ni-B coatings can be achieved by two main ways:

- by electrodeposition of an alloy using Ni plating baths containing boron chemical compounds as boron sources
- by co-deposition of B particles. In this case the production of an alloy requires a post-plating heat treatment

The most used boron sources, as reported in literature, are amine boranes, in particular dimethylamine borane (DMAB $(CH_3)_2NH{\cdot}BH_3$) and trimethylamine borane (TMAB $(CH_3)_3N{\cdot}BH_3$). K.H. Lee et al[18], carried out deposition of Ni/B alloys coatings from a Watts plating bath at temperature of 65°C and 3 pH with the addition of TMAB. It is reported that a content of TMAB from 2 to 7 g/L leads to a B content in the deposits from 2 to 12 % at. They also noticed a considerable grain size reduction by increasing the B content, Ni-B coatings with 11 % at. of B present a nanocrystalline structure consisted of equiassic grains with a diameter of 1-3 nm. All Ni-B coatings present almost the same values of Vickers hardness around 700-800HV, even if they did not investigate the variation of hardness in the B content range between 0-2% at. The internal stresses of the coating are tensile and increase linearly by increasing the B content. A thermal treatment at temperatures up to 300°C leads to a further increase in hardness due to the formation of Ni/B intermetallics. Heat treatments at higher temperatures lead to a decrease of the hardness, more pronounced in coatings with lower content of B, due to recrystallization. The wear resistance of Ni-B coatings decreases by increasing the boron content due to a high friction coefficient and brittle fracture of coatings.

[18] K.H. Lee, D. Chang, S.C. Kwon, Electrochimica Acta 50 (2005), 4538-4543

K. Krishnaveni et al[19] investigated the influence of the current density in the range of 0.4 - 4 A/dm^2 performing electrodeposition of Ni-B alloy coatings using Ni Watts bath containing 3g/L of DMAB at temperature of 45°C and 3.5 pH. They noticed that by increasing the current density the B content in the deposit decreased despite the deposition rate of Ni-B increased. All coatings were nanocrystalline and presented a dense network of cracks due to high internal stresses. Carrying out deposition at low current densities (1A/dm^2) the amount of co-deposited B was about 3%wt. and the as plated hardness was about 600HV. Post-plating thermal treatments at temperatures up to 400°C led to an increase of hardness up to 850HV due to the precipitation of intermetallic Ni_3B phase. Above this temperature, the hardness decreased because of the microstructure coarsening. Ni-B coatings heat treated at 400°C presented higher wear resistance in comparison to the as-plated coating.
Ogihara et al[20] compared the use of DMAB and TMAB in Ni Watts plating bath at various concentrations, pH and current densities. They noticed that the effect of the current density on the co-deposited B is more marked in the case of the use of TMAB. On the contrary, the effect on the coatings hardness is more marked in the case of use of DMAB.
R.A Shakoor et al[21,22] have made a comparison study between a Ni-B and Ni-B composite coatings containing either Al_2O_3 or CeO_2 particles. All depositions have been carried out using a Ni Watts plating bath containing 3g/L of DMAB and the powder concentration in the plating bath used for the production of the composite coatings was 15 g/L. They noticed a remarkable improvement of both mechanical and corrosion properties by incorporating both oxide particles.
An interesting work that reports the use of another boron compound as boron source is that of Bekish et al[23]. They have produced Ni-B coatings using a Ni Watts bath containing sodium-decahydridodecaborate ($Na_2B_{10}H_{10}$) in a concentration range from 4 to 20 g/L. They noticed a marked increase of the B content up to a concentration of 10 g/L. Above this concentration the B amount in the deposits seems to reach a plateau at about 30% at. They asserted also that the use of sodium-decahydridodecaborate allows the production of crack free Ni-B deposits with a B content varied over a wide range from 1 to 30% at. The microstructure of the coatings is nanocrystalline up to B content of 8% at. Coatings with B content around 10% at. present a mixed nanocrystalline-amorphous structure and coatings with higher B content are completely amorphous. The corrosion resistance of the nanocrystalline Ni-B coatings is higher than that of the amorphous ones. The increase of the B content in the nanocrystalline deposits leads to an increase of the wear resistance. The formation of a heterogeneous nanocrystalline-amorphous structure causes a deterioration of the mechanical properties while the amorphization of the Ni-B coatings at high B content results in an improvement of the mechanical resistance. Although Ni-B alloy coatings produced with sodium-decahydridodecaborate could be interesting for applications at high temperature, especially for the absence of cracks also with high B content, this B compound is not easily commercially available and it is more expensive than all other additives.

[19] K. Krishnaveni, T.S.N.Sankara Narayanan, S.K.Seshadri, Materials Chemistry and Physics 99 (2006), 300-308
[20] H. Ogihara, K. Udagawa, T. Saji, Surface and Coatings Technology 206 (2012), 2933-2940
[21] R. A. Shakoor, R. Kahraman, U. Waware, Y. Wang, W. Gao, Materials and Design 59 (2014), 421-429
[22] R. A. Shakoor, R. Kahraman, U. Waware, Y. Wang, W. Gao, Materials and Design 64 (2014) 127-135
[23] Yu.N. Bekish, S.K. Poznyak, L.S. Tsybulskaya, T.V. Gaevskaya, Electrochimica Acta 55 (2010), 2223-2231

Regarding the production of Ni-B composite coatings Gajewska-Midzialek et al[24] studied the influence of different surface-active additives on the co-deposition of amorphous boron particles using low-concentration Ni Watts plating bath containing 2 g/L of B powders. The different additives exhibit a marked influence on the amount of co-deposited B particles and hence on the B content in the composite coatings. They stated that the combination of different additives allows controlling the coatings composition, the nickel grains size, the roughness, the hardness and the wear resistance. Nevertheless they did not investigate the influence of heat treatments.

Orinakova et al[25,26] investigate the effect of deposition conditions and B powder concentration in the plating bath on the B content of Ni-B coatings electrodeposited using an additive-free Ni Watts bath at room temperature and pH 2. They carried out the depositions in potentiostatic and potentiodynamic conditions on a paraffin-impregnated graphite electrode (PIGE) using crystalline B powder with sizes less than 40 μm in concentration of 2,6 and 8 g/L. They noticed that the potentiodynamic deposition method is more appropriate to co-deposit high contents of B in a range from 15 to 23 % wt.

Based on the scientific works mentioned above, is it possible to notice that there is a lack of studies about the influence of very low amounts of B on the hardness, the wear resistance and corrosion resistance. Even if low amounts of B in the deposits do not allow the formation of Ni_3B intermetallics after heat treatment, the presence of boron could hinder the recrystallization of the Ni matrix at high temperatures maintaining a higher hardness. Moreover, Ni-B deposits with high B contents, due to high internal stresses, usually present a web of cracks. Low B content could allow to produce crack-free Ni-B alloys coatings preserving the protective properties of Ni both at room and high temperatures. Moreover, all works in the literature use Watts type plating baths. No references for the production of Ni-B coatings from a sulfamate bath have been found, even if this bath is known for the production of deposits with low stresses.

[24] A.Gajewska-Midzialek, B.Szeptycka, D.Derewnicka, A.Nakonieczny, Tribology International 39 (2006), 763-768

[25] R. Orinakova, K. Rosakova, A. Orinak, M. Kupkova, J.N. Audinot, H. N. Migeon, J.T. Adersson, K. Koval, J. Solid State Electrochem 15 (2011), 1159-1168

[26] R. Orinakova, K. Rosakova, A. Orinak, M. Kupkova, M. Sabalova, A.Strakova Fedorkova, M. Kabatova, F. Kalavsky, M. Sedlarikova, Int. J. Electrochem. Sci. 9 (2014), 4268-4286

3 Research project layout and experimental techniques

3.1 The research project

This research project focuses on the production and the characterization of two types of Ni based galvanic coatings, which should guarantee higher performances at high temperature applications in comparison to the Pure Ni coatings.
The first type of galvanic coatings studied are Nickel matrix composite coatings containing either micro- or nano- particles of Al. The study of the coatings production was developed taking into account the issues related to the industrialization of the process. Based on this assumption, even if it is known that other plating cell configurations can guarantee higher amount of codeposited particles, it was chosen to use a parallel plate geometry which can be easily industrialized using existing plating plants.
A scheme that summarizes the research activity for the Ni/Al composite coatings is reported in Figure 3-1.

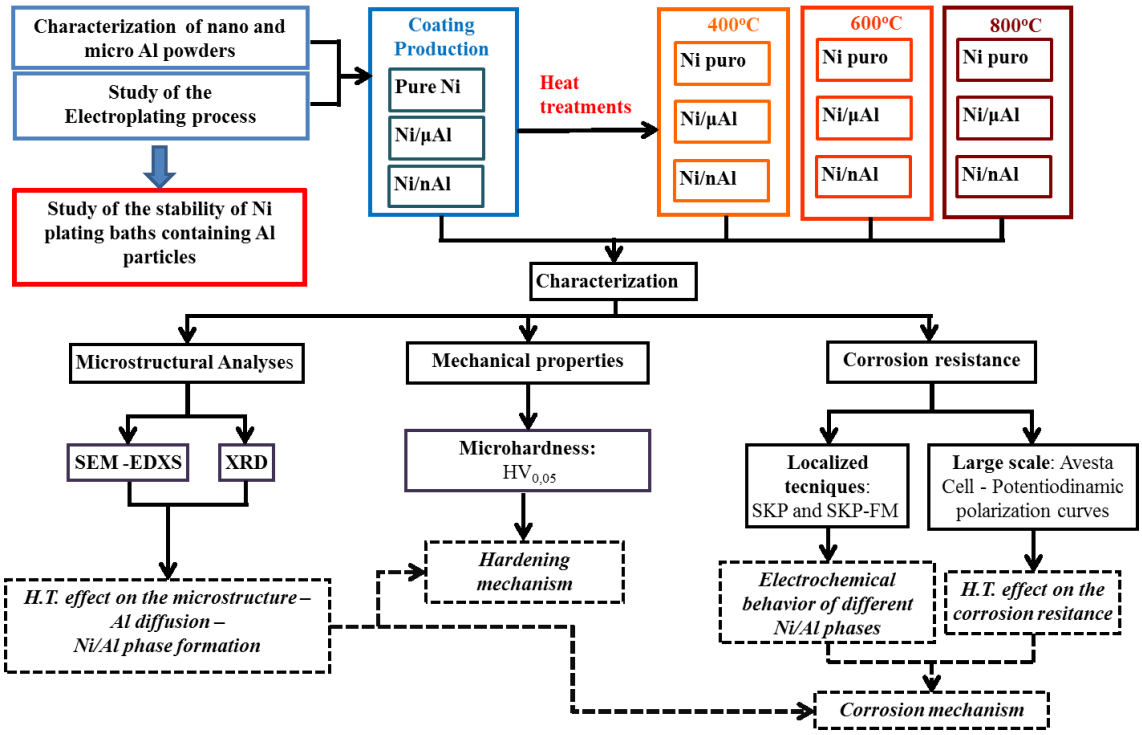

Figure 3-1: Scheme of the research activity of Ni/Al composite coatings

The study started with the characterization of different Al powders purchased from different suppliers. The powders which exhibited good wettability, dispersion, and low

precipitation rate in the Ni plating bath, have been used for the successive electrodeposition tests. The study of the influence of the electroplating parameters has been done using an electroplating cell with 1,5L of volume in order to place the study directly in between the laboratory and the industrial scale. The electrodepositions have been carried out using two different Ni plating baths: a Ni Watts bath and a Ni sulfammate "High speed" bath. The Watts plating bath has been chosen for its stability and easy-use, while the Ni sulfammate one due to the ability to produce thick and stress-free deposits.
The produced sample have been characterized by SEM and EDXS in order to evaluate the Al content, the particles distribution and the coatings microstructure. From the preliminary analyses one Ni plating bath and two Al powders, one nano and one micro, have been chosen and the plating parameters have been fixed to proceed with the production and characterization. Three groups of samples have been produced: pure Ni coatings and Ni matrix composite coatings containing either micro- or nano- Al particles. The produced coatings have been heat treated at three different temperatures: 400°C, 600°C and 800°C. Both as plated and heat treated samples have been characterized with different techniques regarding their microstructure, microhardness and corrosion resistance. The microstructure of the coatings has been analyzed by means of Scanning Electron Microscope (SEM), Energy Dispersive X-ray Spectroscopy (EDXS), and X-Ray Diffraction (XRD). The microhardness has been evaluated with Vickers-indentation in cross section. The electrochemical behavior has been evaluated by means of Scanning Kelvin Probe Force Microscopy (SKP-FM) and the protective properties with potentiodynamic polarization measurements in a 3.5% wt. NaCl solution using an Avesta cell in order to avoid crevice corrosion. The results of the microstructural analyses have been used to understand both the hardening and the corrosion mechanisms. However, stability issues of Ni plating baths containing Al powders have been encountered during the study of the electroplating process. Further investigation of the Al particles evolution in the Ni plating baths have been performed in order to better understand the causes of the degradation. Nevertheless, the instability of the plating bath did not allow to scale up the process and for this reason the research activity has been extended to the other type of galvanic coatings.

The second part of the research was focused on the production and characterization of Ni-B alloy coatings with low B content produced using Dimethylamine borane (DMAB) as B source. A scheme that summarizes the research activity for the Ni-B coatings is reported in Figure 3-2.

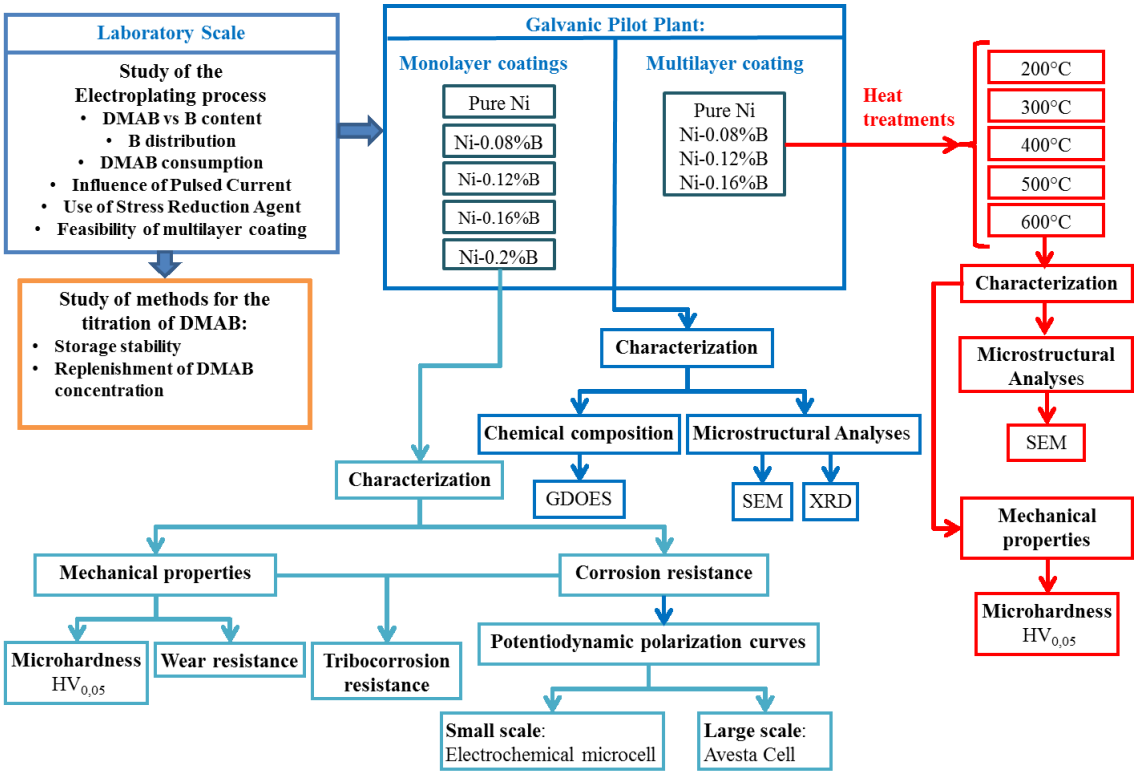

Figure 3-2: Scheme of the research activity of Ni-B alloy coatings

The research started with the production, in laboratory scale, of different series of samples in order to investigate the influence of the electroplating parameters and in particular identify a DMAB concentration range that allows to produce crack-free coatings. The preliminary tests have been performed in laboratory scale using two electroplating cells with volumes of 600mL and 1500mL. The electrodepositions have been performed using two different Ni plating baths: a Ni Watts bath and a Ni sulfammate "High speed" bath. The produced coatings have been characterized by SEM and Glow Discharge Optical Emission Spectroscopy (GDOES) in order to evaluate the microstructure, the Boron content and its distribution. The microhardness has been evaluated with Vickers-indentation in cross sections. After the optimization of the plating process parameters and the identification of DMAB concentration range allowing to produce crack-free deposits, the process was scaled up in a galvanic pilot plant with 10L deposition tanks. This was done in order to produce big samples that have been used for the evaluation of the wear, the corrosion and the tribocorrosion resistance. The wear and the tribocorrosion tests have been performed using a tribocorrosion meter equipped with a potentiostat in order to monitor the open circuit potential during the test in wet conditions. For the evaluation of the corrosion resistance potentiodynamic polarization measurements have been performed in a 3.5% wt. NaCl solution both in large scale, using an Avesta cell, and in small scale, using an electrochemical microcell. The samples have been also heat treated at different

temperatures up to 600°C in order to evaluate the microstructural and hardness modifications at high temperatures. In parallel, methods for the titration of the DMAB concentrations in the Ni plating baths have been studied.

3.2 Experimental techniques and instruments

The produced coatings were tested using different techniques.
For the microstructural analyses and the evaluation of the chemical composition, the following techniques have been used:

- Scanning Electron Microscopy (SEM)
- Energy Dispersive X-ray Spectroscopy (EDXS)
- Glow Discharge Optical Emission Spectroscopy (GDOES)
- X-Ray Diffraction (XRD)

For the evaluation of the coating hardness:

- Vickers Microhardness (HV)

The tribological and tribocorrosion test have been performed using:

- Modified Tribocorrosion meter
- Open Circuit Potential measurements
- Profilometer for the evaluation of the volume loss after the wear tests
- SEM-EDXS analyses for the evaluation of the degradation mechanism

For the evaluation of the corrosion resistance:

- Potentiodynamic polarization measurements using an Avesta cell
- Potentiodynamic polarization measurements using Electrochemical microcell

For the evaluation of the electrochemical behavior and the surface morphology:

- Atomic Force Microscope (AFM)
- Scanning Kelvin Probe Force Microscope (SKPFM)

For the evaluation of the Ni plating bath containing Al powders stability:

- analyses of the particles size distribution (PSD) and ζ-potential after different immersion times

Scanning Electron Microscopy (SEM) - Energy Dispersive X-ray Spectroscopy (EDXS)
The microstructure of the deposits and the Al powders have been examined by Scanning Electron Microscopy (Zeiss model EVO 40) both in Bask-scattered mode and in Secondary electron mode. Both surface and cross section after proper metallographic etching have been observed. Energy Dispersive X-Ray Spectroscopy has been used in combination with SEM to perform chemical analyses on different areas.

Glow Discharge Optical Emission Spectroscopy (GDOES)
Glow Discharge Optical Emission Spectroscopy (GDOES) has been used in order to evaluate the B content along the deposit thickness of the Ni-B coatings. The GDOES analyses were carried out using a JY RF-GD PROFILER HR instrument, manufactured by Horiba Jobin-Yvon, Longjumeau, France. The instrument is equipped with a standard 4 mm diameter anode, a polychromathor with 28 acquiring channels and a Quantum XP software. The source conditions were Ar pressure of 650 Pa and 35W applied power. The selected conditions are necessary to obtain a flat crater thus increasing the depth resolution. All results have been obtained with the same source conditions and with the same

calibration method. The calibration was performed with 21 samples selected among Setting-Up Samples (SUS) and Certified Reference Materials (CRM).

X-Ray Diffraction (XRD)
X-ray diffraction patterns were collected using a Philips PW3040/60 X'pert PRO diffractometer (equipped with an X'celerator detector) operated at 40 kV and 40 mA, using Ni-filtered Cu Kα radiation in the 2θ range of 10°–120° with a step size of 0.02° and a counting time of 40 s per step. The preferred orientation was evaluated by calculating the $RTC_{(h,k,l)}$ (relative texture coefficient). The exact method for the $RTC_{(h,k,l)}$ calculation is reported in the experimental part.

Vickers Microhardness (HV)
The microhardness measurements have been performed in cross section after metallographic preparation, in order to avoid the influence of the substrate, using a Struers Duramin Vickers micro-indenter. Measured microhardness were $HV_{0.05}$ and $HV_{0.025}$ with test force of 0,5 N and 0,25 N respectively.

Wear and tribocorrosion tests
Wear and tribocorrosion tests have been performed using a modified Ducom Biotribometer. The tribometer allows to perform different paths with maximum test length up to 30mm and is equipped with a loading cell from 2N to 20 N. The tribocorrosion tests have been performed using an electrochemical cell, which acts also as sample holder. The sample holder is made of PEEK and it is designed in order to avoid any electrical contact between the sample and the metallic parts of the equipment and allows to expose a specific specimen area to the electrolyte, as working electrode.
The open circuit potential (OCP) was measured continuously before, during and after the wear test vs. a Ag/AgCl (saturated with NaCl) electrode using a BIO-LOGIC SP200 potentiostat. All tribocorrosion tests were conducted in 3.5% wt. NaCl solution at room temperature. The wear and tribocorrosion tests have been performed in collaboration with the surface metallic division of IK4-CIDETEC research center.

Profilometer
The volume loss, after the wear tests, has been evaluated using a stylus profilometer DEKTAK 150 Veeco. The wear track profiles obtained have been used to calculate the wear coefficient K in order to evaluate the wear rate. The fillet radius of the stylus is 12.5 μm, with a variable load from 1 mg to 15 mg. The vertical precision is 0.002 μm, with a maximum vertical extent up to 1 mm.

Corrosion tests
For the evaluation of the corrosion resistance, potentiodynamic polarization measurements were performed in a 3.5% wt. NaCl solution at room temperature both in large and in small scale. Large scale measurements have been performed using an Avesta cell, in order to avoid crevice corrosion phenomena, in a three electrodes system. The surface of the material specimen is pressed against an opening in the bottom of the electrochemical cell. A ring of filter paper tightens the borderline of the specimen. Distilled water is passed through this filter paper ring into the cell at an extreme low rate. This prevents the corroding electrolyte to come in contact with this zone, such avoiding aggressive electrolytes in the artificial crevice. The water flow is controlled by a peristaltic pump,

which delivers 0.5 to 5 ml per hour. The volume of distilled water diluting the measuring electrolyte is too small to disturb the measurement. The working electrode area was 0.785 cm^2, and an $Ag/AgCl/KCl_{3M}$ electrode and a Pt wire have been used respectively as reference and counter electrode. The measurements in large scale have been carried out using an AUTOLAB PGSTAT 30 potentiostat. The scan rate was 0.2mV/s and the scan range was from -250mV vs. OCP till reaching $10^{-3}A/cm^2$.
Localized potentiodynamic polarization measurements were carried out by micro-cell technique in a three electrode configuration. The potentiostat used was an Elektroniklabor Peter Schrems with current resolution in the order of 10 fA. A glass capillary with internal diameter of 800 μm was selected to perform the measurements. The corresponding area of the working electrode was 0,005 cm^2. A Pt wire and an $Ag/AgCl/KCl_{3M}$ have been used respectively as counter and reference electrode. The scan rate was 1 mV/s and the scan range was from -100mV vs. OCP till reaching 10^{-2} A/cm2.

Atomic Force microscopy (AFM) and Scanning Kelvin Probe Force Microscopy (SKPFM)
Before the characterization by means of Atomic Force Microscope and Scanning Kelvin Probe Force Microscope (SKPFM), the coatings surface were grinded using abrasive SiC paper under a constant liquid ethanol jet in order to prevent a possible dissolution of different phases or corrosion phenomena caused by the contact with water. Polishing was then performed using water-free diamond suspensions in order to obtain a final surface roughness of about 20 nm Ra. After polishing, the samples were cleaned in an ethanol ultrasonic bath for about 5 minutes and then heat-dried in a heat sterilizer at constant temperature of 40°C. Samples surface were then marked in order to perform, on the same areas, analyses using different techniques. A Veeco Multimode Nanoscope IIIa AFM was used to map the samples surface. Topographic and Surface Volta Potential maps were simultaneously obtained using tapping and SKPFM-interleave mode configuration on marked 100x100 μm areas. SKPFM gives information about the anodic and/or cathodic behavior of the different particles and phases present on the sample surface.

Particles Size and ζ-potential measurements
To study the baths containing the Al particles stability and the agglomeration phenomena of the Al particles, particles size distribution (PSD) and ζ potential measurements have been performed in solutions containing the particles at different immersion times, both prior and after electrodeposition. To investigate whether the pH drop was the cause of the particles degradation or the effect of other reactions between the particles and the plating bath species, PSD and ζ potential measurements have been also performed immediately after the sonication at different pH, acidifying the bath with controlled addition of HCl. The instrument used is a Malvern Zetasizer Nano ZS with a 532nm "green" laser fitted able to perform size measurements in a range from 0.6nm to 6μm and ζ-potential measurement for a particles size range from 3nm to 10μm equipped with a narrow band filter to improve the signal that fluoresce at the wavelength of the laser fitted, a universal "Dip" cell to provide repeatable measurements with minimal quantity of samples and an MPT-2 Autotitrator to perform sample and pH titrations. The particles size and ζ-potential measurements have been performed in collaboration with Materials Science Department of University of Mons.

4 Ni/Al galvanic composite coatings

4.1 Production of Ni/Al composite coatings

The first part of the research has focused on the feasibility study of the production of Ni/Al composite coatings. The study was divided in the following steps:

- Market analysis and purchase of nano- and micro- metric powders
- Preliminary testing to evaluate the powders wettability, their dispersion in the plating bath and the suspension stability
- Characterization of the Al powders by means of SEM and EDXS in order to evaluate shape, size and presence of contaminating elements.
- Production of different series of coatings: using two different Ni plating baths, different powder concentrations and deposition parameters.

As the final goal was the industrialization of the process, the plating process by means of electroplating cell size was placed directly in between the laboratory and the industrial scale and was limited the concentration of Al powders, considering both the high cost of the powders and the plating baths management difficulties in industry.
For these reasons the study of the plating process was done:

- using a volume of electrolyte of 1.5L
- using a parallel plate geometry which can be easily industrialized using existing plating plants.
- Limiting the Al powder concentration up to a maximum of 60 g/L.

Taking in account these choices, the preliminary study of the plating process was done with the specific objectives of:

- evaluate the distribution of the Al particles along the deposit thickness,
- evaluate the maximum Al content that is possible to codeposite with both micro- and nano- powders
- study the stability of the Ni plating bath containing the Al powders with sequential deposition with the same plating bath.

4.1.1 Preliminary tests and Al Powder characterization

Nine different Aluminum powders were bought by 5 different commercial suppliers.
The list of the powder and the declared size according the technical datasheets are reported in the Table 4-1.
The powders can be divided in three classes: micrometric (powder 1 and 9), submicrometric (powder 2) and nanometric (powders 3,4,5,6,7 and 8).

Table 4-1: Reference, supplier and declared size of the Al powders

Powder reference	Supplier	Declared size
1	MK Nano	3-4.5 µm
2	US Research	800 nm
3	US Research	40 nm
4	MK Nano	50 nm
5	SkySpring	130 nm
6	SkySpring	60-80 nm
7	IoLiTec	40-60 nm
8	IoLiTec	60-80 nm
9	NanoPole	micro/nano

Preliminary tests for the evaluation of the wettability and the dispersion in the plating bath have been performed by adding 40 g/L of each Al powder in a Ni Watt plating bath and carrying out a treatment by ultrasounds for 10 minutes. The suspension stability of the powders was evaluated by leaving the bath without any stirring for 1 hour.
Powders 2 and 9 showed a very fast precipitation. After 5 min almost the whole amount of the powders were at the bottom of the becker. Powders 3 and 4 showed very scarce wettability as they were floating over the bath even after the sonication treatment.
Powders 1 and 4-8 were further characterized by means of SEM and EDXS in order to determine size, shape and presence of contaminating elements.

The micrographs of the selected powders are reported in Figure 4-1, Figure 4-2, Figure 4-3, Figure 4-4 and Figure 4-5.

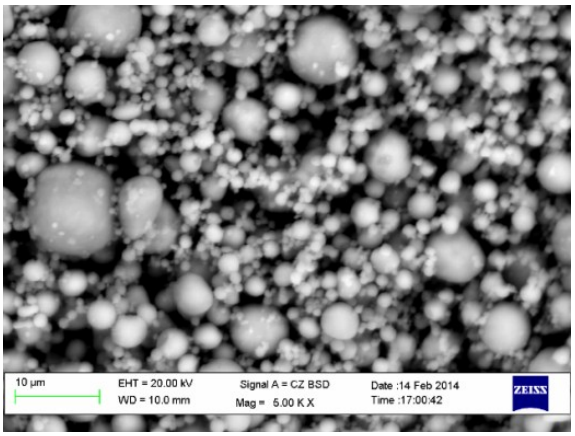

Figure 4-1: SEM micrograph of Powder 1 - MK Nano 3-4.5 µm

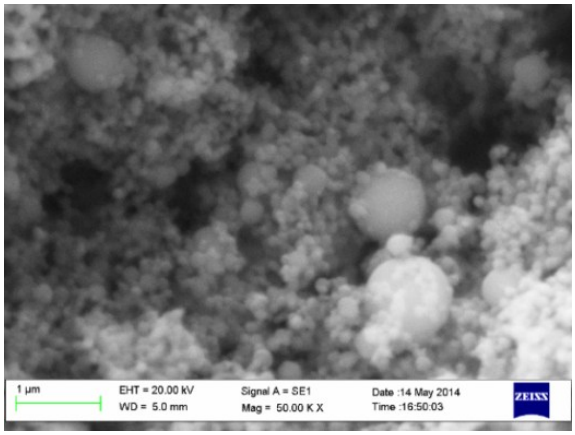

Figure 4-2: SEM micrograph of Powder 5 - Skyspring 130nm

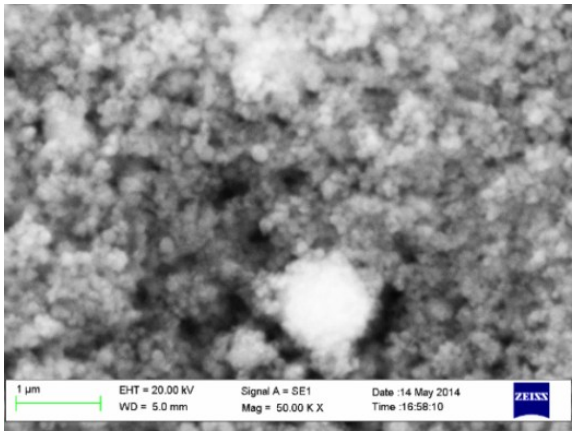

Figure 4-3: SEM micrograph of Powder 6 - Skyspring 60-80nm

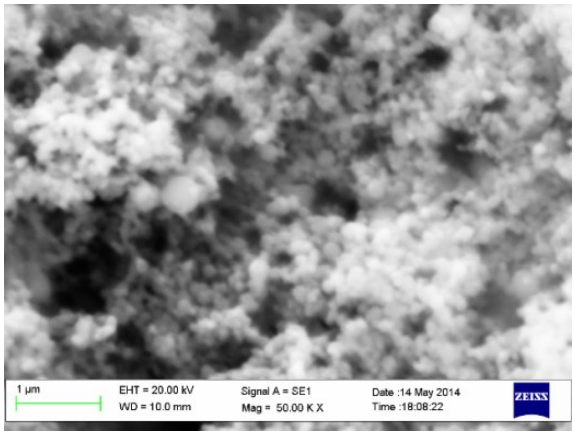

Figure 4-4: SEM micrograph of Powder 7 - IoLiTec 40-60nm

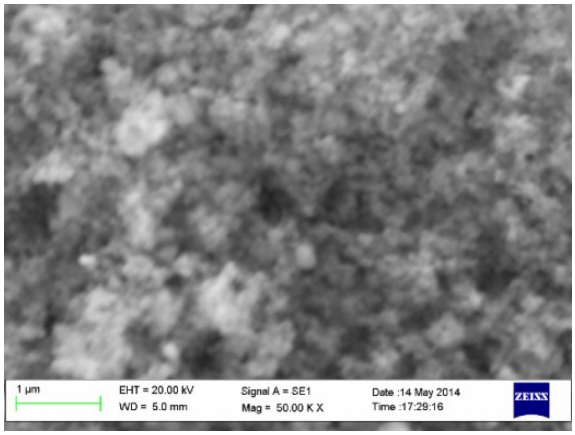

Figure 4-5: SEM micrograph of Powder 8 - IoLiTec 60-80nm

The micrographs show that all the selected powders are spherical. The powder size corresponds to declared granulometry but in the case of nano powders, some micrometric particles have been noticed. The EDXS analysis did not reveal the presence of contaminating elements.

4.1.2 Study of the Ni/Al composite coating plating process

4.1.2.1 Substrate preparation

Q panels of carbon steel (SAE 1008/1010; 0.13 max C; 0.25-0.60 Mn) with sizes of 60x60 mm were used as substrate for each electrodeposition.
Before each electrodeposition the substrates were pre-treated using the following steps:

- ultrasonic degreasing for 15 min in a aqueous solution at 70°C containing 10% in Vol. of the commercial surfactant *Galvadet* of the company *Surfatek*.
- anodic electrolytic degreasing for 10 min in an aqueous alkaline solution containing KOH using a platinized titanium net as cathode and a voltage of 6V. The alkaline

solution was prepared by adding 12% in wt. of the commercial chemical reagent *Lectrodet* of the company *Surfatek*.

- acid pickling in a solution containing 300mL/L of H_2SO_4, 100mL/L of HCl and 600mL/L of H_2O for 10 min at room temperature.

After each pre-treatment the substrates were water rinsed with deionized water.

4.1.2.2 Ni based plating baths

The electrodepositions have been carried out using two types of Ni plating bath with compositions reported in Table 4-2.

Table 4-2: Ni plating baths composition

		Ni sulfammate "High Speed"	Ni Watts
$Ni(NH_2SO_3)_2 \cdot 4H_2O$	**[g/L]**	500	-
$NiSO_4$	**[g/L]**	-	240
$NiCl_2 \cdot 6H_2O$	**[g/L]**	10	45
H_3BO_3	**[g/L]**	25	30
Surfactant	**[mL/L]**	2	2

The necessary amount of Ni ions is given by the $NiSO_4$ or $Ni(NH_2SO_3)_2*4H_2O$ and $NiCl_2$, moreover Cl^- prevents the passivation of the nickel anode. The H_3BO_3 is a buffer and maintains stable the value of the pH between 4.5 and 5.6.
The industrial surfactant used was a $C_{12}H_{25}NaO_4S$ based one and prevents the formation of "hydrogen pitting" in the deposits. By increasing the H_2 bubbles surface energy facilitates their detachment from the cathode electrode.
All the depositions of this study have been performed in a parallel plates geometry using a Pure Ni plate as anode.
Cross section SEM micrographs after metallographic etching of two coatings produced with both electroplating baths are reported in Figure 4-6.
The electrodepositions have been carried out using the optimal value of current densities for each electroplating bath: 2 A/dm^2 for the Ni Watts bath and 4 A/dm^2 for the Ni sulfammate "High Speed" bath.

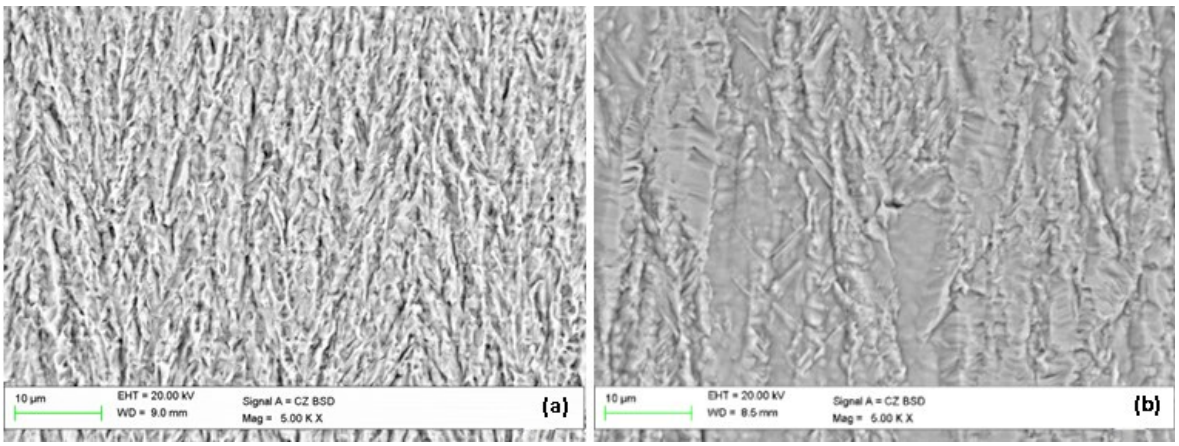

Figure 4-6: Cross section micrographs after metallographic etching of: (a) pure Ni Watts and (b) pure Ni sulfammate "High Speed"

By observing the micrographs is it possible to notice the different microstructure of the coatings. Both coatings present a columnar microstructure with the columns oriented along

the electrical field direction. The pure Ni Watts present thin, single grain, columns as the rate determination step is the charge transfer, while the "High Speed" nickel presents a pseudocolumnar structure with larger and longer columns. Each column consists of different small grains. The rate determining step during the deposition, in this case, is the diffusion. The choice of the two different plating baths was due to:

- The Watts plating bath is the most widely used among the Ni plating baths due to its stability.
- The Ni sulfammate "High Speed" bath is used in order to produce thick deposits with low internal stresses.

Usually, the coatings produced with the Ni "High Speed" bath (additives free) present lower hardness in comparison to the deposits produced with the Watts bath (additives free).

4.1.2.3 Characterization of the Ni/Al composite coatings

The produced Ni/Al coatings were observed both on top surface and in cross section by means of SEM in order to evaluate the particles distribution and the presence of defects. The Al content was determined as mean value of five measurements performed on different zones on the coatings cross section by EDXS. A demonstrative measurement is reported in Figure 4-7.

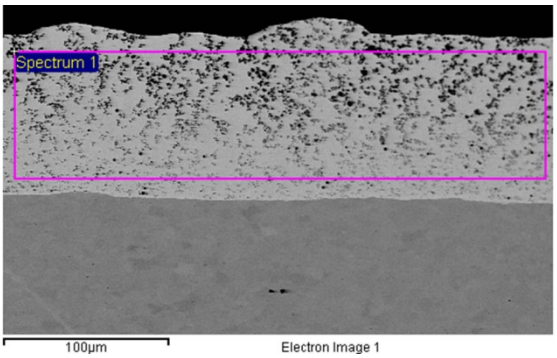

Al	Ni	Total
[Wt.%]	[Wt.%]	[Wt.%]
2.76	97.24	100.00

Figure 4-7: Example of Al content measurement by means of EDX

4.1.2.4 Study of the Electrodeposition process with Al nano powders

Comparison of Ni/nanoAl composite coatings produced with Ni Watts plating bath

The study of the co-electrodeposition process started with a comparison of a series of coatings produced using the selected Al nano powders and a Ni Watts plating bath. The Watts plating bath was chosen for its higher stability in comparison to the Ni sulfammate "High Speed" bath. Comparing the two baths, the Watts one has a slightly higher pH (4.5 instead of 4) and it is less sensitive to changes during deposition. The pH of the electrolyte was monitored prior and after each deposition.

Four Ni Watts plating baths were prepared adding 40 g/L of the selected powders 5, 6, 7, and 8. After the addition of Al powders, the plating baths were treated by ultrasound for 15 minutes in order to disaggregate the Al particles agglomerates and obtain a homogeneous dispersion. After sonication, the baths were maintained under continuous stirring using a mechanical stirrer. Sequential electrodepositions were performed changing the current density in a range around the optimal value of the deposition of the pure Ni and varying the intensity of the stirring. The pH of the electrolyte was monitored prior and after each

deposition. The lists of the produced samples and the electrodeposition parameters are reported in Table 4-3, Table 4-4, Table 4-5 and Table 4-6.

Table 4-3: Powder 5 series A produced with Ni Watts plating bath

Sample	Powder concentration	Current density	Time	Stirring	Temperature
	[g/L]	[A/dm^2]	[h]	[rpm]	[°C]
5WA.1	40	2	3	600	45
5WA.2	40	3	3	600	45
5WA.3	40	1	3	600	45
5WA.4	40	2	3	400	45
5WA.5	40	2	3	800	45
5WA.6	40	2	3	600	45

Table 4-4: Powder 6 series A produced with Ni Watts plating bath

Sample	Powder concentration	Current density	Time	Stirring	Temperature
	[g/L]	[A/dm^2]	[h]	[rpm]	[°C]
6WA.1	40	2	3	600	45
6WA.2	40	3	3	600	45
6WA.3	40	1	3	600	45

Table 4-5: Powder 7 series A produced with Ni Watts plating bath

Sample	Powder concentration	Current density	Time	Stirring	Temperature
	[g/L]	[A/dm^2]	[h]	[rpm]	[°C]
7WA.1	40	2	3	600	45
7WA.2	40	3	3	600	45
7WA.3	40	1	3	600	45
7WA.4	40	2	3	600	45

Table 4-6: Powder 8 series A produced with Ni Watts plating bath

Sample	Powder concentration	Current density	Time	Stirring	Temperature
	[g/L]	[A/dm^2]	[h]	[rpm]	[°C]
8WA.1	40	2	3	600	45
8WA.2	40	3	3	600	45

The instability of the plating baths with all Al powders was noticed straightway after the tests. As observable in the photographs reported in Table 4-7 (red frame), the surface of the coatings, after few electrodepositions, became markedly rough indicating clearly a tendency of all types of Al particles to agglomerate. Considering the entire series, the powder 5 presented the better behavior showing the lower propensity to agglomerate during the sequential depositions.

Table 4-7: Photographs of the coatings surface

	5WA Series	6WA Series	7WA Series	8WA Series
WA.1				
WA.2				
WA.3				
WA.4				

The characterization by SEM of the coatings cross-section shows more clearly the agglomeration of the Al particles during the sequential electrodepositions.
SEM micrographs of the first series of the deposits produced with powder 5 are reported in Figure 4-8 as an example. It is possible to notice a progressive agglomeration of the nano-particles that it is tolerable for the second (b in Figure 4-8) and the third specimen (c in Figure 4-8) but not for the following ones. Starting from the fourth sample (d in Figure 4-8) we can notice the formation of pronounced growths which embed the nano-particles agglomerates. When the Al particles agglomerates are big and the current density high the intensification of the electric field on the growths top leads to a formation of big protuberances (Figure 4-8 e).

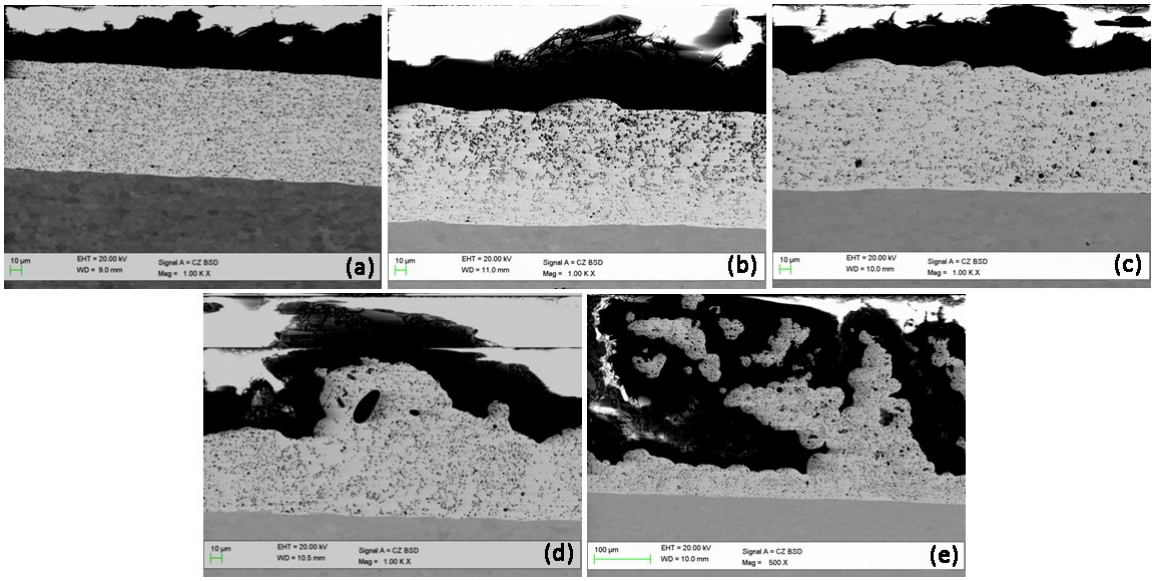

Figure 4-8: Cross section micrographs of: (a) Sample 5WA.1,(b) Sample 5WA.2,(c) Sample 5WA.3, (d) Sample 5WA.4 and (e) Sample 5WA.5

For the coatings produced with powder 6, 7 and 8 this phenomenon was even more intense and occurred earlier. Comparing the first sample of each series (a,b,c in Figure 4-9) we can notice that using the powder 6 and 8 it is possible to produce Ni/nanoAl coatings with a homogenous distribution of Al particles along the whole deposit thickness. It is not the same with powder 7.

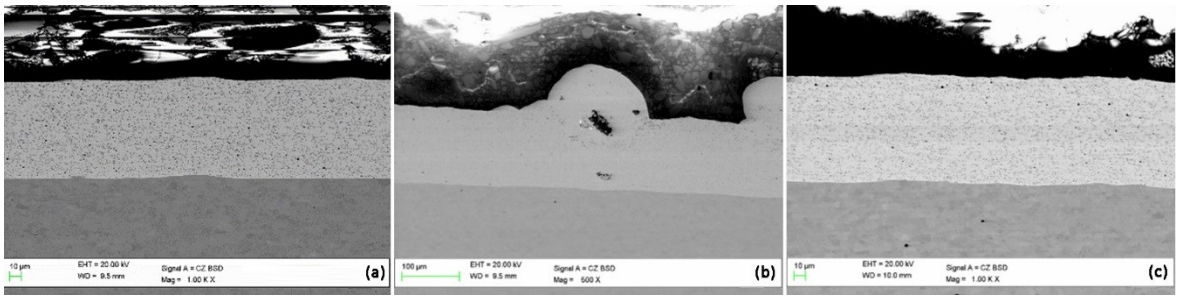

Figure 4-9: Cross section micrographs of: (a) Sample 6WA.1,(b) Sample 7WA.1,(c) Sample 8WA.1

The pH values measured both prior and after each electrodeposition with each plating bath are reported in Figure 4-10.

The progressive decrease of the electrolyte pH indicates a chemical and/or an electrochemical reaction between the Al particles and the Ni plating bath in particular during the electrodeposition. In some cases, the reaction has led to a progressive formation of foams that made unusable the galvanic baths. Corrections of the bath pH did not allow to recover the functionality of the plating baths.

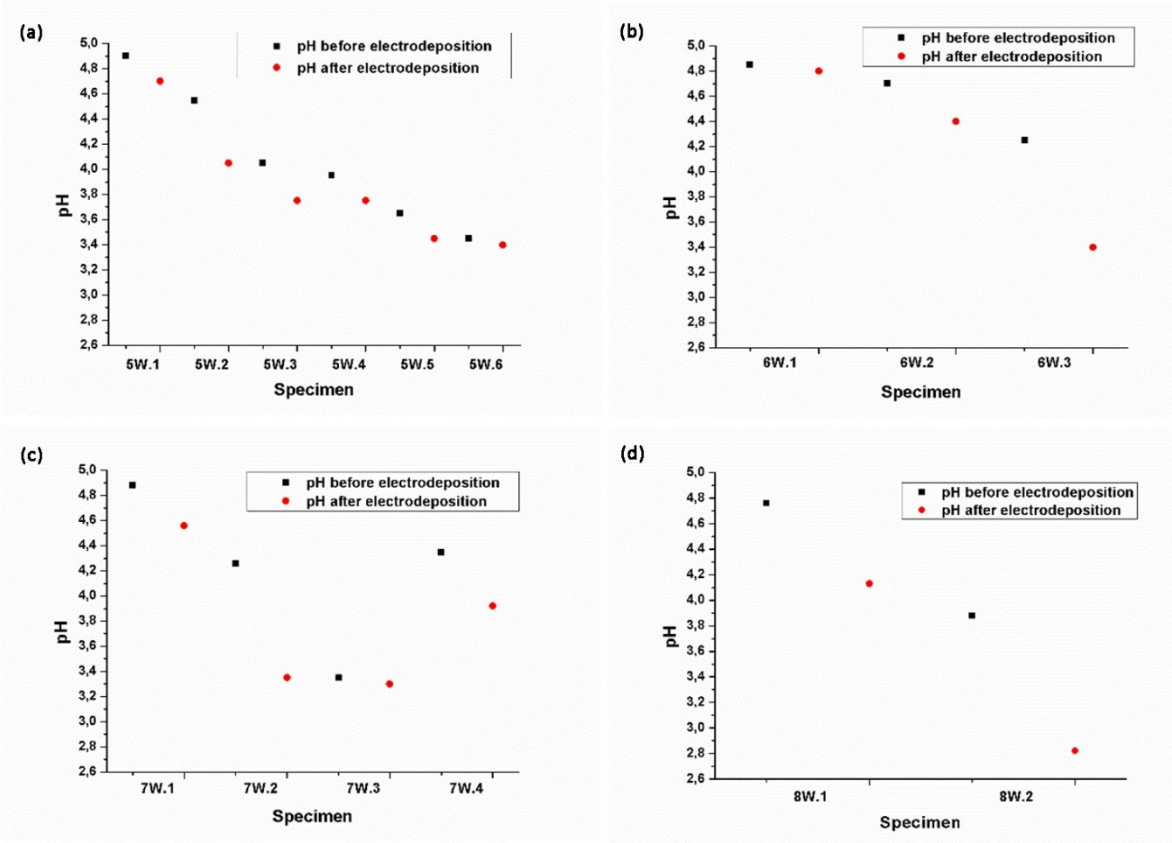

Figure 4-10: Plating baths pH prior and after the sequential depositions: (a) powder 5, (b) powder 6, (c) powder 7 and (d) powder 8.

The amount of Al incorporated (measured by EDXS in cross section) by using different powders are reported in Table 4-8. Observing the results obtained on the first coating of each series, that are the most representative considering the agglomeration phenomena which occur during the successive depositions, the maximum amount of Al incorporated were obtained with the powder 5 followed by powders 6 and 8.
From the obtained results with sequential depositions the effect of the current density, stirring or consumption of Al powders is not clear. For example the second sample produced by the 5WA bath has a higher amount of Al than the first one. On the contrary the second samples produced with baths 6WA and 7WA have a lower amount of Al in comparison to the first specimen of each series.

Table 4-8: Al content of the Ni/nanoAl coatings produced with the Ni Watts plating bath

		Sample			
		5WA.1	**5WA.2**	**5WA.3**	**5WA.4**
Al content	**[Wt.%]**	2.06 ± 0.12	2.60 ± 0.13	2.11 ± 0.19	1.72 ± 0.22
		6WA.1	**6WA.2**	**6WA.3**	
Al content	**[Wt.%]**	1.95 ± 0.15	1.65 ± 0.12	0.96 ± 0.21	
		7WA.1	**7WA.2**		
Al content	**[Wt.%]**	1.04 ± 0.28	0.89 ± 0.23		
		8WA.1			
Al content	**[Wt.%]**	1.79 ± 0.15			

Based on these results it's evident that the instability of the system Ni Watts plating bath/Al powder does not allow to investigate the influence of the electrodeposition parameters with sequential deposition as in the case of more stable systems with ceramic powders e.g. SiC, AL_2O_3, WC[1,2,3]
A correct and efficient investigation about the influence of each deposition parameter requires a big amount of Al powder in order to repeat the electrodeposition with new plating baths each time.

Comparison between Ni Watts and Ni sulfammate High Speed plating baths[4]

The powder 5, which demonstrated the lower instability in the Ni Watts plating bath was chosen to proceed with the test in order to compare deposits produced with both Ni sulfammate "High Speed" plating bath and Ni Watts plating one using different concentrations of Al powder.
Five series of specimens were deposited:

- four series using Ni sulfammate "High Speed" plating baths with 20 g/L (Series 5SA and 5SC) and with 40 g/L (series 5SB and 5SD).
- one series using a Ni Watts plating bath with a powder concentration of 60 g/L.

Also in this case different current densities and stirring speeds have been tested.
The lists of produced samples and the electrodeposition parameters are reported in Table 4-9, Table 4-10, Table 4-11, Table 4-12 and Table 4-13.

Table 4-9: Powder 5 Series 5SA produced with Ni Sulfammate "High Speed" plating baths

Sample	Powder concentration	Current density	Time	Stirring	Temperature
	[g/L]	[A/dm^2]	[h]	[rpm]	[°C]
5SA.1	20	4	2	600	45
5SA.2	20	5	2	600	45
5SA.3	20	3	2	600	45
5SA.4	20	4	2	400	45
5SA.5	20	4	2	800	45
5SA.6	20	4	2	600	45

Table 4-10: Powder 5 Series 5SB produced with Ni Sulfammate "High Speed" plating baths

Sample	Powder concentration	Current density	Time	Stirring	Temperature
	[g/L]	[A/dm^2]	[h]	[rpm]	[°C]
5SB.1	40	4	2	600	45
5SB.2	40	5	2	600	45
5SB.3	40	3	2	600	45

Table 4-11: Powder 5 Series 5SC produced with Ni Sulfammate "High Speed" plating baths

Sample	Powder concentration	Current density	Time	Stirring	Temperature
	[g/L]	[A/dm^2]	[h]	[rpm]	[°C]
5SC.1	20	4	2	600	45
5SC.2	20	4	2	800	45
5SC.3	20	4	2	400	45

[1] C.T.J. Low, R.G: A: Wills, F. C. Walsh, Surface & Coatings Technology 201 (2006) 371
[2] M. Lekka, A. Lanzutti, A. Casagrande, C. de Leitenburg, P.L. Bonora, L. Fedrizzi, Surface & Coatings Technology 206 (2012) 3658-3665
[3] L. Wang, Y. Gao, Q. Xue, H. Liu, T. Xu, Surface & Coatings Technology 200 (2006), 3719-3726

Table 4-12: Powder 5 Series 5SD produced with Ni Sulfammate "High Speed" plating baths

Sample	Powder concentration	Current density	Time	Stirring	Temperature
	[g/L]	[A/dm^2]	[h]	[rpm]	[°C]
5SD.1	40	4	2	600	45
5SD.2	40	4	2	800	45
5SD.3	40	4	2	400	45

Table 4-13: Powder 5 serie 5WB produced with Ni Watts plating bath.

Sample	Powder concentration	Current density	Time	Stirring	Temperature
	[g/L]	[A/dm^2]	[h]	[rpm]	[°C]
5WB.1	60	2	3	600	45
5WB.2	60	3	3	600	45
5WB.3	60	4	3	600	45
5WB.4	60	2	3	600	45

Also the Ni sulfammate "High Speed" plating bath has presented instability due to a reaction between the Al particles and the Ni^{2+} ions. All the series produced with Ni sulfammate showed rapid degradation of the baths, in this case the pH drop below 3.8 leads to a formation of deposits with defects and cracks (red frame in Table 4-14). Slight agglomeration of the Al particles were observed also in the samples produced with the sulfammate plating bath and powder concentration of 20 g/L (green frame in Table 4-14) but in this case, the coatings failure after few electrodeposition is mainly due to a decrease of the pH below the optimal range of 4-4.5. Higher the Al powder concentration, faster the pH drop and the plating bath degradation. The series 5SC and 5SD, produced at the same conditions of the series 5SA and 5SB, confirmed the degradation of the plating baths.
Comparing the series 5WA and 5WB produced with Ni Watts bath and 40 or 60 g/L (Table 4-7 and Table 4-14), higher the Al powder concentration faster the drop of pH and agglomeration of the Al particles (yellow frame in Table 4-14).

Table 4-14: Photographs of the coatings surface of Series 5SA, 5SB, 5SC and 5WB

Ni Sulfammate "High Speed"						Ni Watts	
Powder concentration						Powder concentration	
20 g/L		40 g/L		40 g/L		60 g/L	
5SA		5SB		5SC		5WB	
1		1		1	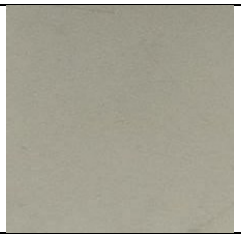	1	
2		2		2		2	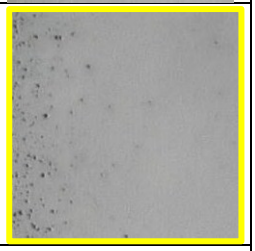
3		3		3		3	
4	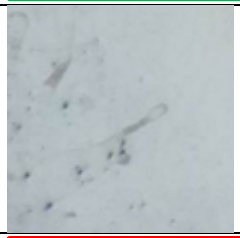					4	
5							

The Al content measured by EDXS analysis on all the produced specimens is reported in Table 4-15 and Table 4-16. The correlation between the Al content in the deposit and the particles concentration in the plating baths (both Watts and sullfammate) is reported in Figure 4-11. For this graph only the first specimen produced with each plating bath is considered.

Observing the graph, we can notice that the Al content of the coatings produced with 40 g/L and the Ni sulfammate plating bath is higher in comparison to those produced with the Ni Watts plating bath and same powder concentration.

Regarding the series 5WB, the further increase of the powder concentration to 60 g/L does not lead to a marked increase of the Al content in the deposit.
The same Al content values obtained with the repeated series produced with Ni sulfammate "High speed" confirm the reproducibility of the codeposition process.

Table 4-15: Al content of the coatings produced with Ni sulfammate "High Speed" with 20 and 40 g/L of powder 5.

		Sample obtained with Ni Sullammate "High Speed"			
Powder concentration	**[g/L]**	**20**			
		5SA.1	**5SA.2**	**5SA.3**	**5SA.4**
Al content	**[Wt.%]**	1.38 ± 0.20	1.69 ± 0.26	1.44 ± 0.29	1.72 ± 0.29
Powder concentration	**[g/L]**	**20**			
		5SB.1	**5SB.2**	**5SB.3**	
Al content	**[Wt.%]**	1.52 ± 0.19	0.92 ± 0.29	0.84 ± 0.27	
Powder concentration	**[g/L]**	**40**			
		5SC.1	**5SC.2**		
Al content	**[Wt.%]**	2.75 ± 0.06	2.32 ± 0.17		
Powder concentration	**[g/L]**	**40**			
		5SD.1	**5SD.2**		
Al content	**[Wt.%]**	2.60 ± 0.06	1.92 ± 0.17		

Table 4-16: Al content of the coatings produced with Ni Watts with 40 and 60g/L of powder 5.

		Sample obtained with Ni Watts			
Powder concentration	**[g/L]**	**40**			
		5WA.1	**5WA.2**	**5WA.3**	**5WA.4**
Al content	**[Wt.%]**	2.06 ± 0.12	2.60 ± 0.13	2.11 ± 0.19	1.72 ± 0.22
Powder concentration	**[g/L]**	**60**			
		5WB.1	**5WB.2**		
Al content	**[Wt.%]**	2.23 ± 0.07	1.56 ± 0.13		

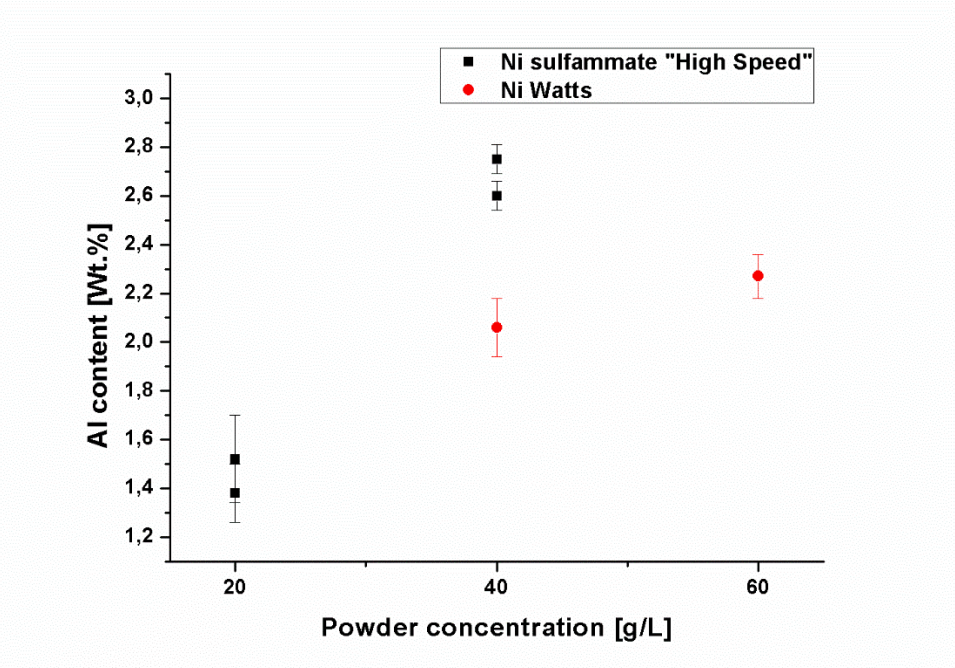

Figure 4-11: Al Content vs. powder concentration comparison between Ni Watts and Ni sulfammate "High Speed"

The produced coatings have been observed by SEM in cross section both prior and after metallographic etching. From the observations of the cross section in BSE mode it is shown that the deposit obtained with 20 g/L of Al particles does not present an uniform distribution of particles along the deposit thickness (Figure 4-12).
The particles are quite agglomerated and the agglomerates are not uniformly distributed.
An increase of the powder concentration to 40 g/L allow to produce coatings with a higher content of particles and more uniform distribution (Figure 4-13)
By observing the same deposits in cross section after metallographic etching and under higher magnifications it is clear that the deposit produced with the lower amount of Al particles maintains the pseudo-columnar structure of pure Ni deposits (Figure 4-14), this is due to the low amount of codeposited particles mainly in the form of aggregates placed on the columns boundaries.
The codeposition of a higher amount of Al nano particles with a powder concentration of 40 g/L leads to a marked microstructural refinement (Figure 4-15). The typical pseudo-columnar microstructure of the pure Ni sulfammate deposit is no longer observable and the composite coatings consist of shorter and more narrow columns.

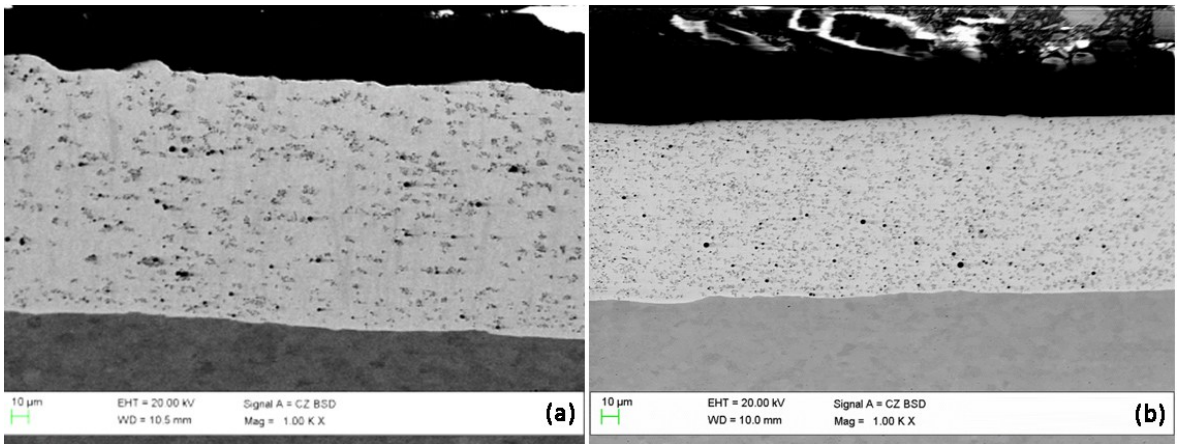

Figure 4-12: Cross section micrograph of the whole deposits: (a) Sample 5SA.1 - 20g/L and (b) Sample 5SB.1 - 40 g/L

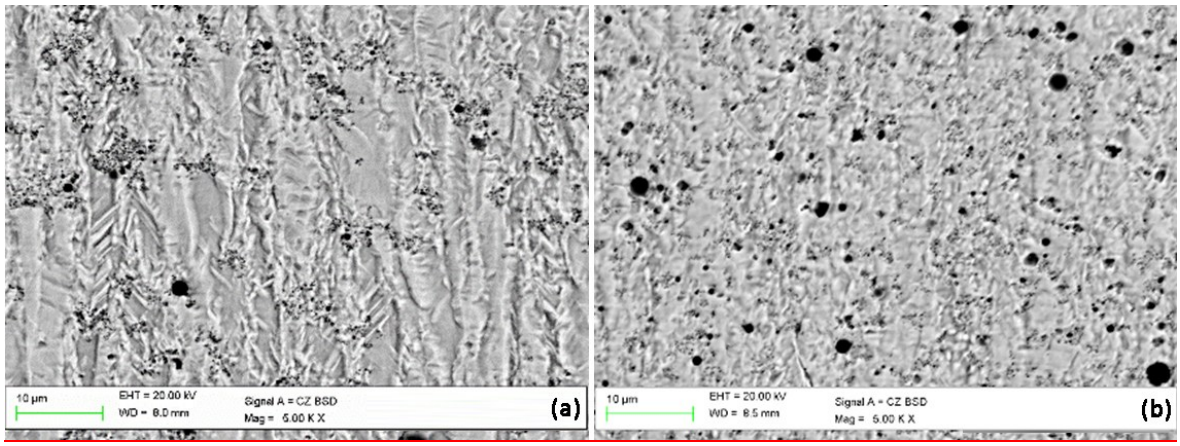

Figure 4-13: Cross section micrograph after metallographic etching of: (a) Sample 5SA.1 - 20g/L and (b) Sample 5SB.1 - 40g/L

The same trend was observed also with the coatings produced using a Ni Watts plating bath. (Figure 4-14 and Figure 4-15). The higher the Al powder concentration in the plating bath, the higher the content of Al in the deposit and the microstructure refinement that they produce.

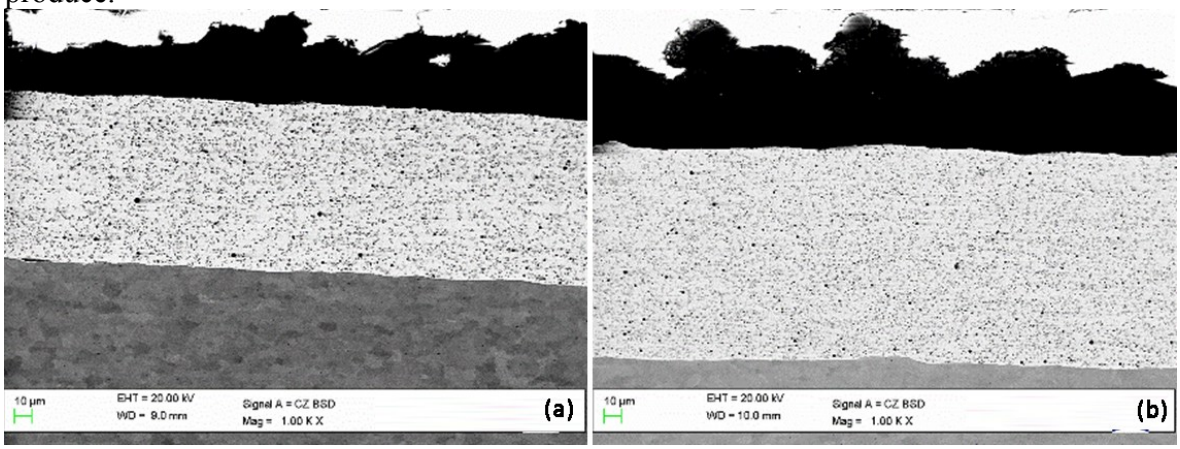

Figure 4-14: Cross section micrograph of the whole deposit: (a) Sample 5WA.1 - 40g/L and (b) Sample 5WB.1-60 g/L

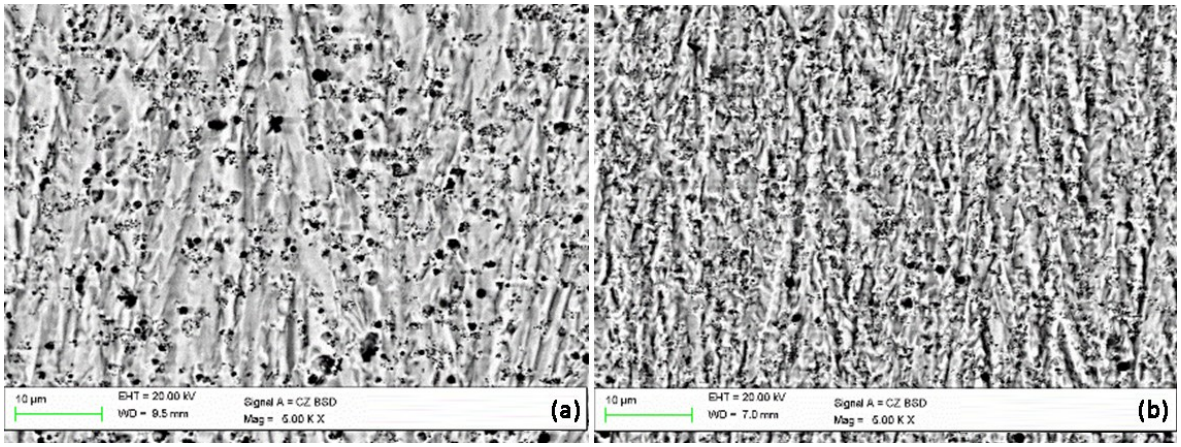

Figure 4-15: Cross section micrograph after metallographic etching of: (a) Sample 5WA.1 - 40g/L and (b) Sample 5WB.1 - 60g/L

4.1.2.5 Study of the Electrodeposition process with Al micro powders

The study of the electrodeposition process with the micro powder was performed by depositing three series of coatings using Ni sulfammate "High Speed" plating baths. Three concentrations of Al micro powders were used: 20, 30 and 40 g/L. The series with 30 g/L was carried out using also 0.2 g/L of a cationic surfactant CTAB ($C_{16}H_{33}N(CH_3)_3Br$, Cetyl-trimethyl-ammonium bromide). The surface active agent was used in order to evaluate if the formation of positive head groups on the Al particles surface could lead to an increase of the Al content in the deposit.
After the addition of Al micro powder, the plating baths were treated by ultrasounds for 15 min in order to disaggregate the Al particles agglomerates and to obtain a homogeneous dispersion. After the sonication the baths were maintained in continuous stirring using a mechanical stirrer. Sequential electrodepositions were performed changing the current density in a range around the optimal value of the deposition of the pure Ni.
The lists of the produced samples and the electrodeposition parameters are reported in Table 4-17, Table 4-18 and Table 4-19.

Table 4-17: Powder 1 Series 1SA produced with Ni Sulfammate "High Speed" plating baths

Sample	Powder concentration	Current density	Time	Stirring	Temperature
	[g/L]	[A/dm^2]	[h]	[rpm]	[°C]
1SA.1	20	4	2	600	45
1SA.2	20	5	2	600	45
1SA.3	20	4	2	600	45

Table 4-18: Powder 1 Series 1SB produced with Ni Sulfammate "High Speed" plating baths and CTAB

Sample	Powder concentration	CTAB	Current density	Time	Stirring	Temperature
	[g/L]	[g/L]	[A/dm^2]	[h]	[rpm]	[°C]
1SB.1	30	0.2	4	2	600	45
1SB.2	30	0.2	4	2	600	45
1SB.3	30	0.2	5	2	600	45

Table 4-19: Powder 1 Series 1SC produced with Ni Sulfammate "High Speed" plating baths

Sample	Powder concentration	Current density	Time	Stirring	Temperature
	[g/L]	[A/dm^2]	[h]	[rpm]	[°C]
1SC.1	40	4	2	600	45
1SC.2	40	5	2	600	45

Also using the Al micro powders the sulfammate plating bath showed instability demonstrated by a decrease of the pH going on with the sequential depositions.
The detected pH drop was lower in comparison to the pH drop observed with the nano particles test, this could be due to the lower reactivity of the micro particles surface.
The main problem observed with the Al micro powder was the marked tendency to remain attached on the plating cell glass suggesting a noticeable decrease of the Al concentration in the plating baths. Higher the powder concentration, higher the Al particles inclination to precipitate and stick on the plating cell surface.
Ultrasound treatments of the plating bath did not help to the detachment of the micro particles from the plating cell surfaces, while the use of the cationic surfactant seems to reduce the intensity of this phenomenon.
The Al content in the deposits measured in cross section is reported in Table 4-20.
From this table it is possible to notice that the Al content is not affected significantly by the powder concentration in the investigated range. After the first electrodeposition the decrease of the Al content observed with both concentrations of 20 and 40 g/L suggests a modification of the surface state of the particles and/or a rapid decrease of the powder concentration in the baths.
The addiction of the cationic surfactant even if it reduced the tendency of the particles to remain attached on the plating cell glass did not lead to an increase of the Al content in the deposits.
In comparison with the electrodeposits obtained with the Al nano powder and the same Ni sulfammate plating bath the amount of codeposited Al is almost five times higher in the case of the micro-composites. In many cases, a decrease of the particle size leads to a decrease of the amount in weight or in volume percentage of codeposited particles [2]. Transforming the weight or the volume percentage to a number of codeposited particles per unit of mass, volume or surface of composite deposit, this number is always much higher in the case of use of smaller size particles. This way of evaluating the particles content can help in explaining the remarkable microstructural differences between micro- and nano-composite coatings.

Table 4-20: Al content of the coatings produced with Ni sulfammate "High Speed" with 20, 30 and 40 g/L of powder 1.

Powder concentration	**[g/L]**	**20**		
		1SA.1	**1SA.2**	**1SA.3**
Al content	**[Wt.%]**	11.2 ± 2.5	3.4 ± 0.4	0.6 ± 0.1
Powder concentration	**[g/L]**	**30**		
CTAB concentration	**[g/L]**	**0.2**		
		1SB.1	**1SB.2**	**1SB.3**
Al content	**[Wt.%]**	10.6 ± 0.9	3.0 ± 0.5	0.8 ± 0.5
Powder concentration	**[g/L]**	**40**		
		5SC.1	**5SC.2**	
Al content	**[Wt.%]**	13.6 ± 0.7	3.6 ± 0.4	

SEM cross section micrographs of the deposited coatings are reported in Figure 4-16.
If we consider the first deposit of each series we can notice that the increase of the powder concentration allowed to produce a more uniform distribution of the micro particles along the deposit thickness.
Indeed the coating produced with 20 g/L of Al micro powders in the plating bath (a in Figure 4-16) shows some areas free of particles. On the other hand, the specimen produced with 30 or 40 g/L of Al powder show an almost uniform distribution along the coating thickness (b and c in Figure 4-16).

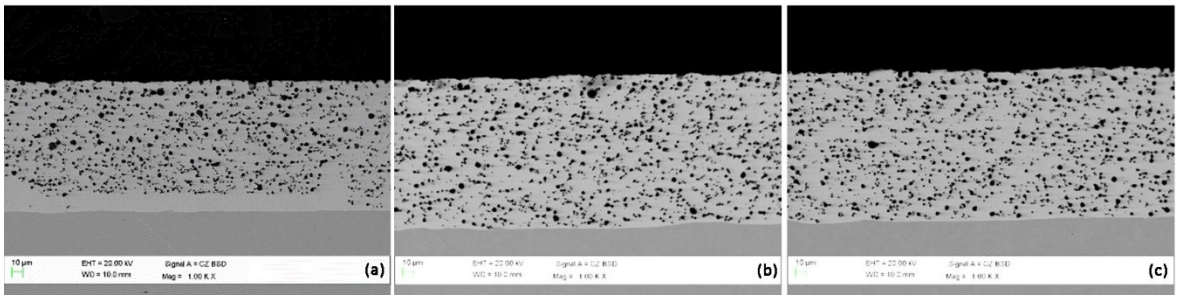

Figure 4-16: Cross section micrograph of the whole deposits: (a) Sample 1SA.1-20g/L, (b) Sample 1SB.1-30g/L+0.2 g/L CTAB, (c) Sample 1SC.1-40g/L.

Cross section micrographs after metallographic etching are reported in Figure 4-17.
The pseudo columnar structure of Ni coatings produced by a sulfammate bath is observable for specimen 1SA.1 and 1SC.1 ((a) and (c) in Figure 4-17). The Al micro particles interrupt the columns growth. On the other hand the specimen 1SB.1 ((b) in Figure 4-17) presents a mixed lamellar-columnar structure which could be attributed to the CTAB which modified the growth mechanism of the Ni matrix.

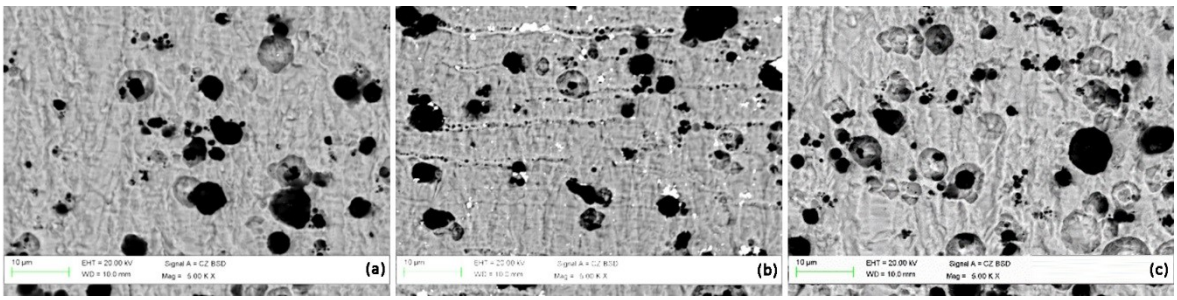

Figure 4-17: Cross section micrographs after metallographic etching of (a) Sample 1SA.1-20g/L, (b) Sample 1SB.1-30g/L+0.2 g/L CTAB, (c) Sample 1SC.1-40g/L.

4.1.3 Bath/Particles stability

To better investigate the degradation of plating bath with Al nano-powders and to better understand the physicochemical phenomena occurring after the addition of the particles some test were performed in collaboration with University of Mons in Belgium (UMONS) in the Department of Materials Science, Engineering Faculty.
In order to evaluate if the pH drop noticed during the electrodepositions was only related to the electrochemical reactions that regard the galvanic process four Ni watts plating bath containing 20 g/L of Al nano-powders 5, 6, 7 and 8 have been prepared and their pH has been monitored for 10 days at regulars intervals.
The plating baths were prepared adding the powder and treating for 15 minutes with ultrasounds and then maintaining a continuous stirring. The seventh day an electrodeposition at 2 A/dm^2 for one hour has been carried out with each electroplating bath. To study the agglomeration phenomena of the Al nano-particles, particles size distribution (PSD) and ζ potential measurements were performed immediately after the US treatments and after two, three and seven (after the deposition) days of permanence in the plating baths. To investigate whether the pH drop was the cause of the particles degradation or the effect of other reactions between the particles and the plating bath species, PSD and ζ potential measurements have been also performed immediately after the sonication at different pH, acidifying the bath with controlled addition of HCl.

4.1.3.1 pH measurements

In Figure 4-18 is reported the pH evolution with time of the Ni Watts plating baths with each Al nano-powder.

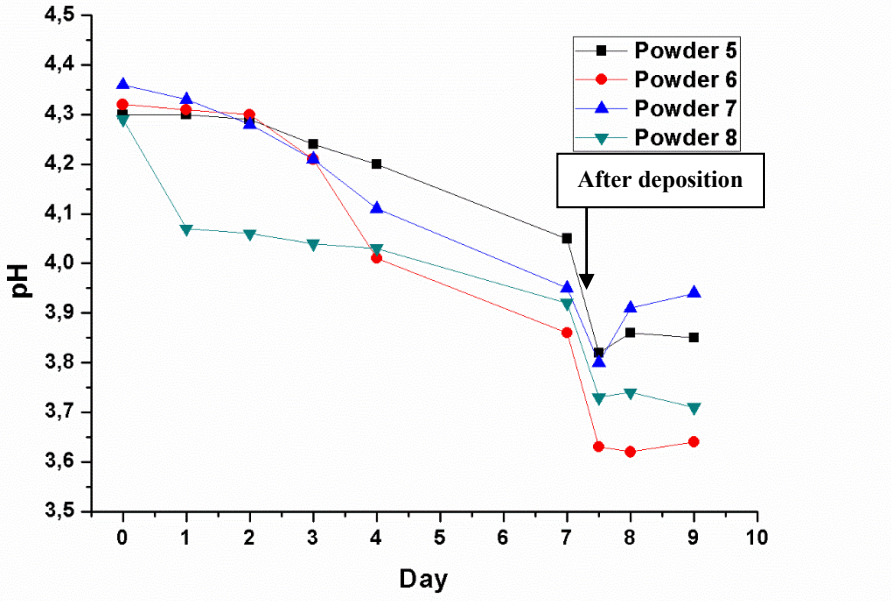

Figure 4-18: pH evolution with time of Ni Watts plating baths with Al powders

A progressive decrease of the pH was observed for each plating bath. The plating bath with nano-powder 8 showed a marked drop after the first day, followed by the powder 6 and the

powder 7 after 4 days. The plating bath with powder 5 showed the lower decrease maintaining values above 4.1 until the seventh day.
These results indicate that the reaction between the particles and the bath species take place also without using the bath and cause the pH drop. After the electrodeposition the pH decrease is more marked for all plating baths showing that the electrochemical reactions accelerate this phenomenon.
The slight recovery of the pH after the electrodeposition of the plating bath with powders 7 and 5 could be related to the buffer effect of the boric acid. The plating baths with powders 6 and 8 that reached values below 3.8 did not show any recovery.

4.1.3.2 Zeta potential/Particles size measurements

ζ potential and PSD measurements were performed in order to investigate the modification of the surface charge of the Al particles and the agglomeration phenomena.
The measurements of the PSD of each powder after the sonication and after 2, 3, and 7 days are reported in Figure 4-19. The measurements at the seventh day were performed after the electrodepositions.
The measurements were performed after appropriate dilution of the plating baths since the Ni ions concentration interferes with the light scattering, not allowing a correct measure.

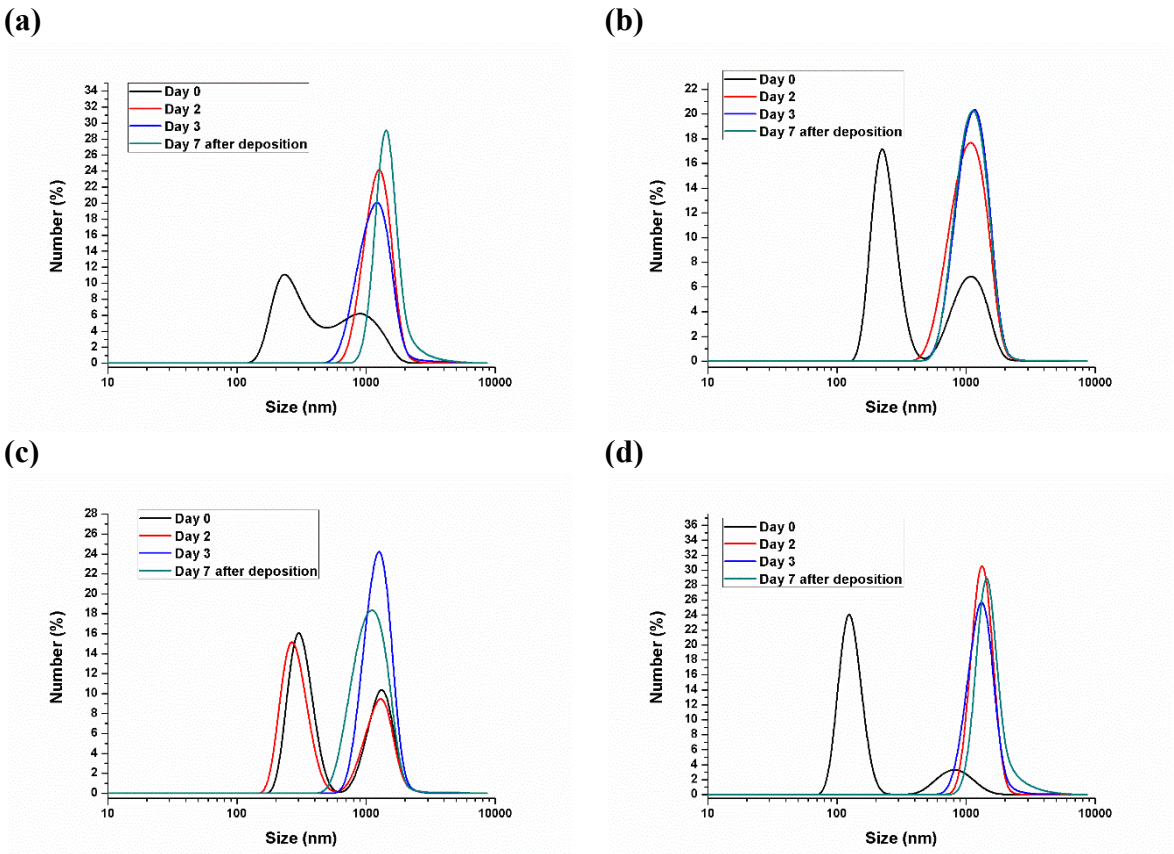

Figure 4-19: PSD measurements for: (a) powder 5, (b) powder 6, (c) powder 7 and (d) powder 8

All the particles presented already a certain grade of agglomeration after the sonication.
In fact, the PSD of each powder at the first day is bimodal with a first peak around 100-300 nm and a second peak around 1 µm. The powder 5, 6 and 8 showed a complete

agglomeration already after 2 days of permanence in the plating bath showing a monomodal distribution with a peak at about 1 µm. The powder 7 showed the complete formation of micrometric agglomerates after 4 days but observing the first peak of the PSD performed immediately after the sonication (peak at about 300nm) and considering the declared size of 40-60 nm it is possible to conclude that the powder 7 was the most agglomerated after the treatment with US.

The ζ potential values of the nano-particles measured immediately after the sonication and till the 7th day of permanence in the Ni Watts plating bath are reported in Table 4-21 and in Figure 4-20.

Table 4-21: ζ potential values of the Al nano-particles at different days of permanence in the Ni Watts plating bath

Day	Powder 5	Powder 6	Powder 7	Powder 8
	ζ potential	ζ potential	ζ potential	ζ potential
	[mV]	[mV]	[mV]	[mV]
1	0.489	-0.738	-2.5	4.68
3	3.75	4.24	5.65	7.49
4	3.7	4.5	3.57	5.06
7	4.79	4.83	4.91	5.55

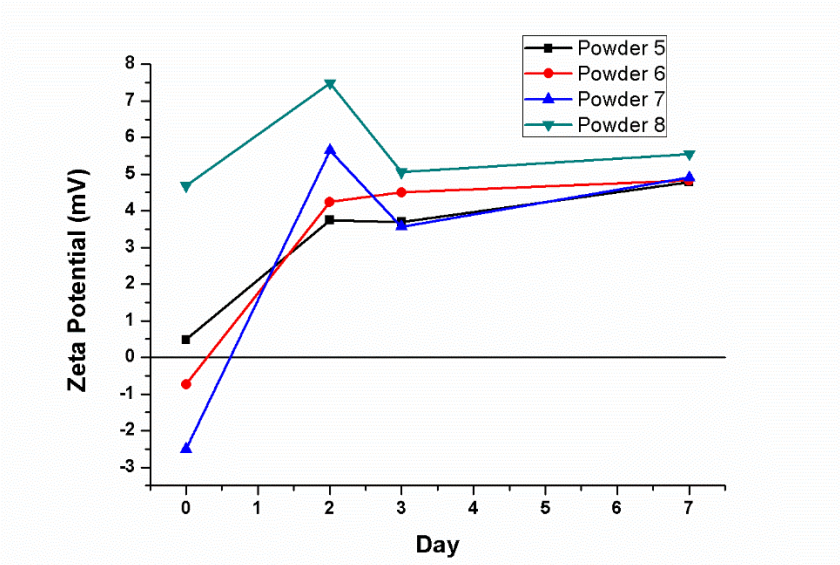

Figure 4-20: ζ potential values of the Al nano-particles at different days of permanence in the Ni Watts plating bath

All nano powders showed values of ζ potential within the range of +8 and -3 mV. Therefore, the attractive force prevails on the repulsive force and the rapid agglomeration of the Al particles is favored. At the first day, the powders 6 and 7 show a negative value and the powder 5 and 8 a positive one, at the third day all the particles show a positive value. The zeta potential values of each particle converge to about +5 mV after 7 days.
In order to investigate the effect of the variation of the pH bath on the Al particles, measurements of PSD and ζ potential were performed acidifying the electrolyte with controlled adding of HCl. The graphs related to the powder 5, that are representative of the behavior of all the powders tested, are reported in Figure 4-21 and Figure 4-22.

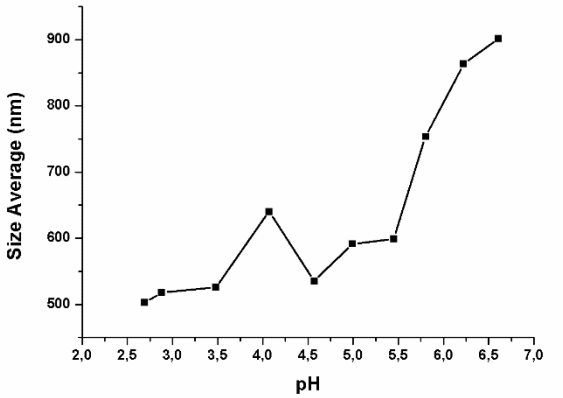

Figure 4-21: Size average vs pH

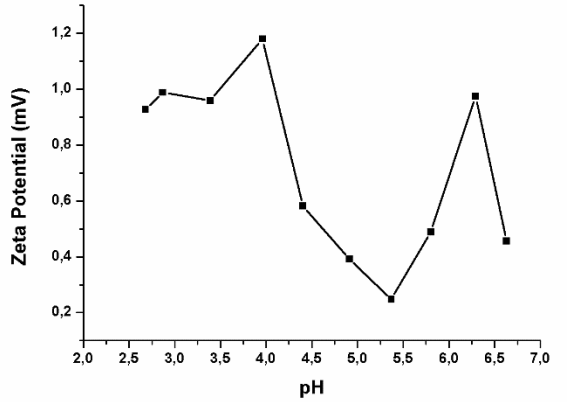

Figure 4-22: Zeta Potential vs pH

The measures show that a decrease of the electrolyte pH leads to a decrease of the agglomerates size due to a dissolution of the Aluminum. The irregular changes of the ζ potential due to the modification of the surface charge caused by the acidification of the electrolyte confirm the dissolution of the Al.

Considering that the pH drop of the plating bath and the agglomeration phenomena of the nano-particles are concomitant and established that an induced decrease of the plating bath pH leads to a dissolution of the Al particles with a decrease of the Al particles agglomerates size, it is possible to conclude that the pH drop of the Ni plating baths with Al powders is the consequence of the relative slow dissolution reaction of the Al particles and the rapid growth of the Al particles agglomerates is the consequence of the very low ζ potential also during the dissolution process.

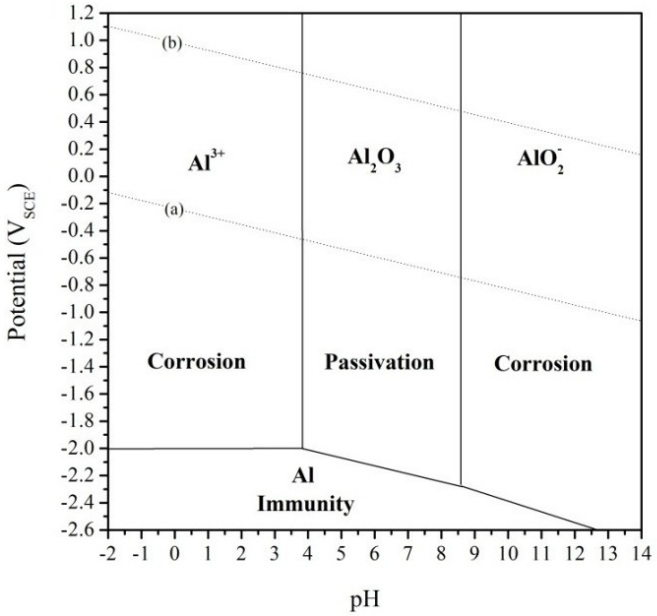

Figure 4-23: Pourbaix diagram for pure Al at 25°C in acqueous solution. The lines (a) and (b) correspond to water stability and its decomposed product

Although it might be inappropriate to refer to the Al Pourbaix diagram (Figure 4-23) as different ionic species are present in the plating bath, the Pourbaix diagram can still give some clues about the phenomena possibly occurring in the bath with particles. The particles should be stable at pH 4.5 but the small dimensions of the particles which make them more reactive and the presence of other species could lead to their dissolution:

$$Al \rightarrow Al^{3+} + 3e^{-}$$

and to a displacement deposition of Ni on their surface:

$$Ni^{2+} + 2e^{-} \rightarrow Ni$$

enhancing the formation of large aggregates.
This hypothesis was confirmed by the fact that the powder recovered from the degraded baths was magnetic. SEM micrographs of both as received and recovered from the plating bath powders are reported in Figure 4-24. The relative EDXS analyses are reported in Table 4-22 and Table 4-23. As can be noticed the particles recovered after the deposition are partially "bonded" together and covered by Al oxides. The morphology of the particles surface indicates a strong dissolution of the Al particles (Figure 4-24 d, e). As demonstrated both by the EDXS analyses and by Figure 4-24 e,f, Ni grains nucleate on the surface of the partially dissolved Al particles.
The dissolution of the Al particles is accelerated during the deposition due to the local decrease of pH near the anode caused by the parallel reaction:

$$2H_2O \rightarrow O_2 + 2H^{+} + 4e^{-}$$

Based on all the above statements it is clear that there are some issues regarding the stability of the particles in the plating baths and thus each bath can be used for the production of a limited number of deposits. More investigations are needed to modify the particles surface and make them more stable in the specific environment. However, the produced samples can exhibit enhanced mechanical properties at high temperatures which could justify a high production cost. For this reason both micro- and nano-composite deposits have been produced under the same conditions and characterized both as plated and after heat treatments.

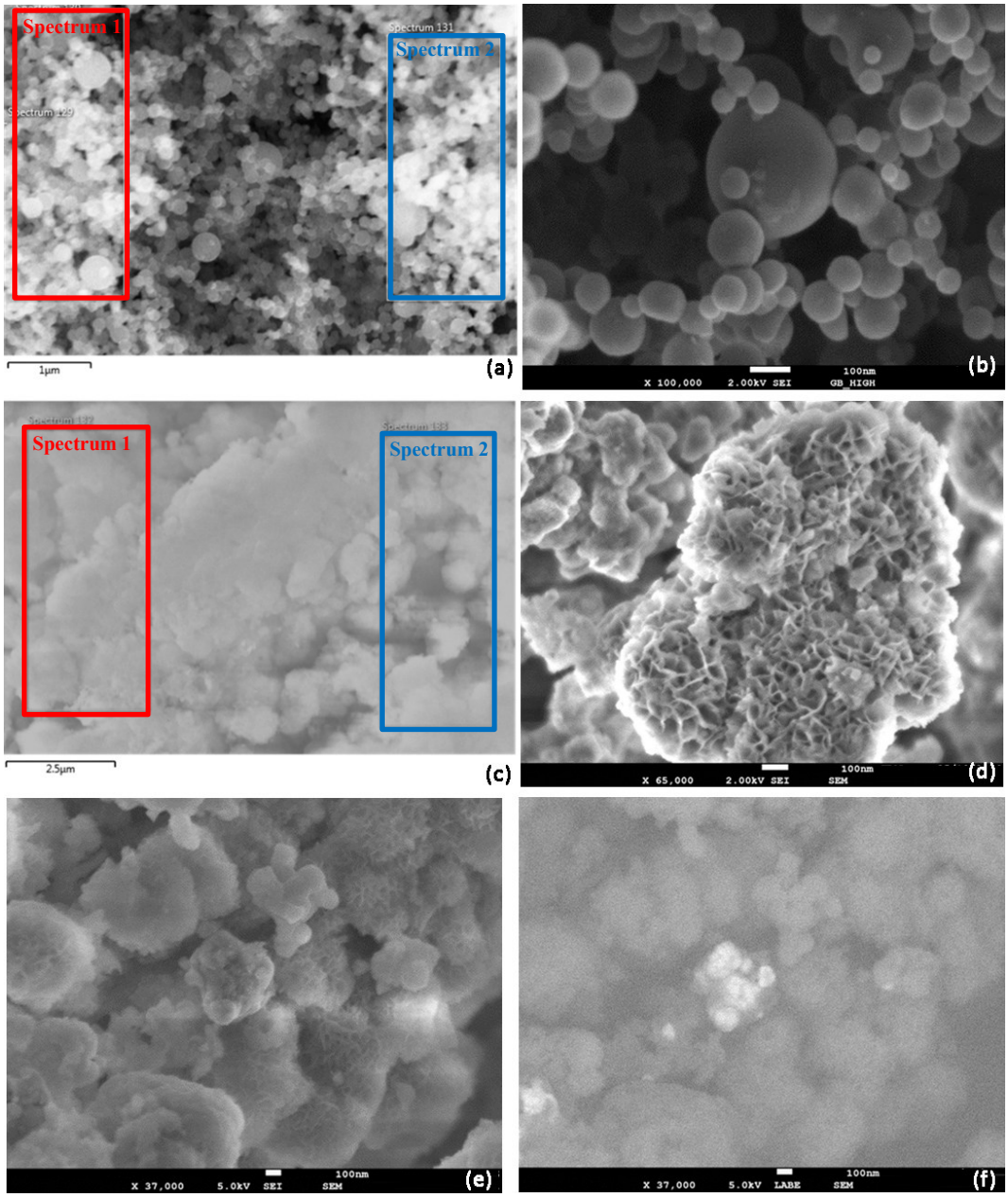

Figure 4-24:SEM micrographs of Al powder (a) and (b) as received; (c)-(e) recovered after deposition in Secondary Electron mode and (f) recovered after deposition in Backscattered mode

Table 4-22: EDXS analyses results on the marked areas of Figure 4-24-a

	C	O	Al	Ni
Spectrum	**[At.%]**	**[At.%]**	**[At.%]**	**[At.%]**
1	14.4	16.8	68.8	-
2	11.9	18.5	69.6	-

Table 4-23: EDXS analyses results on the marked areas of Figure 4-24-c

	C	O	Al	Ni
Spectrum	**[At.%]**	**[At.%]**	**[At.%]**	**[At.%]**
1	31.7	47.3	17.0	2.9
2	22.1	50.5	20.6	5.4

4.2 Microstructural characterization of Ni/Al composite coatings

Based on the preliminary results obtained during the study of the Ni/Al composite coatings production it was decided to continue the research with a comparison between the micro and the nano composite coatings produced with a Ni sulfammate "High Speed" containing 40 g/L of either micrometric powder 1 or nanometric powder 5.
The study regarded the characterization of the obtained electrodeposits and the evaluation of the mechanical and protective properties both before and after heat treatments at different temperatures.
The analyses of the as plated deposits microstructure and its modification after the different heat treatments were performed by means of SEM observations and EDXS analyses on both top surface and cross section and by means of X ray diffraction analyses.
The mechanical properties were evaluated by means of Vickers micro hardness measurements performed on the coatings cross section after metallographic preparation. Potentiodynamic polarization curves have been used to evaluate the protective properties of the coatings. In order to better understand the electrochemical behavior of the different coatings Scanning Kelvin Probe Force Microscope measurements (AFM-SKPFM) were conducted.

4.2.1 Microstructural characterization of the As Plated

SEM cross section micrographs of the selected Ni/µAl and the Ni/nAl composite coatings are reported in Figure 4-25. Both deposits are compact and porous free. In the case of the Ni/µAl composite deposit (Figure 4-25-a) the Al particles distribution is almost uniform along the coating thickness. The nano-particles in the Ni/nAl composite deposit are uniformly distributed along the coating thickness (Figure 4-25-b). The nanoparticles are quite agglomerated even if US treatment has been used to better disperse them in the plating bath.

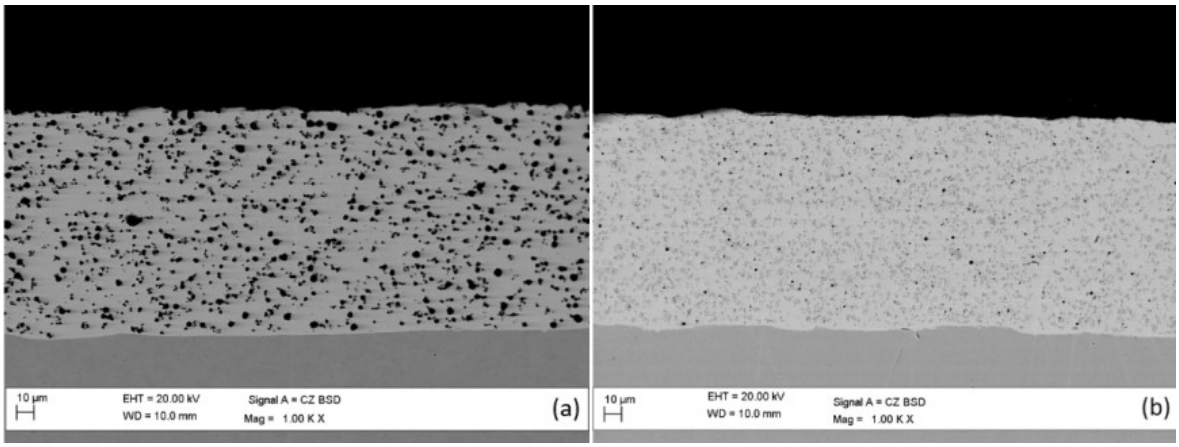

Figure 4-25:cross section micrographs of (a) Ni/µAl and (b) Ni /nAl

The EDXS analyses revealed that, using the same Al powder concentration in the bath, the Al content in the micro-composite coating is 12.4 ± 1.1 % wt. and in the nano-composite coating is 2.7 ± 0.1 % wt. In many cases, a decrease of the particle size leads to a decrease

of the amount in weight or in volume percentage of codeposited particles[5] [2]. Transforming the weight or the volume percentage to a number of codeposited particles per unit of mass, volume or surface of composite deposit, this number is always much higher in the case of use of smaller size particles. This way of evaluating the particles content can help in explaining the remarkable microstructural differences between micro- and nano-composite coatings.
Figure 4-26 shows the cross section micrographs of the three types of coatings after metallographic etching. The pure Ni coating has a pseudo-columnar microstructure typical for electrodeposited nickel coatings with the columns oriented along the direction of the electrical field (Figure 4-26-a). The incorporation of the Al micro-particles in the Ni matrix causes a structural refinement effect. Indeed, as reported by Susan et al.[6], the interruption of the Ni columns growth and nucleation of new small nickel grains onto the surface of the Al particles lead to a reduction of the columns dimension and to slight changes in the growth direction (Figure 4-26-b). The same effect but much more intense is observable in the Ni/nAl composite coatings. In this case, even if the Al content is lower and the nano-particles are quite agglomerated, the smaller dimension and the more uniform distribution lead to a marked refinement of the microstructure (Figure 4-26-c). The codeposition of nano-particles, even if quite agglomerated, increased the nucleation rate leading to the formation of thinner and shorter not oriented Ni columns.

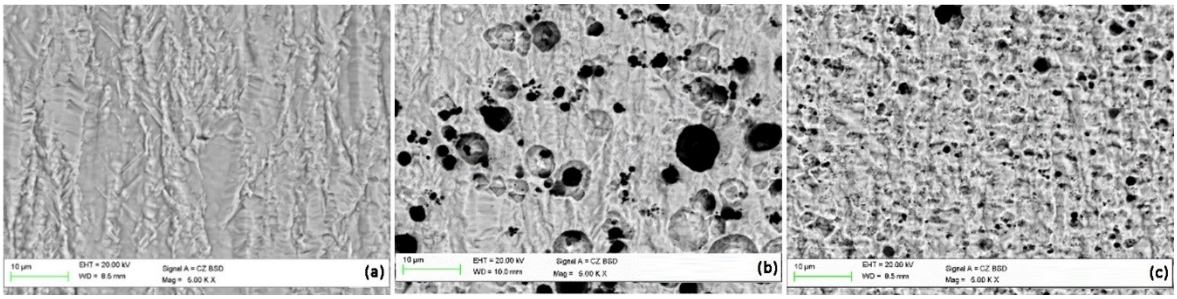

Figure 4-26: Cross section micrographs after metallographic etching of: a) pure Ni, b)Ni/µAl and c)Ni/nAl

4.2.2 Microstructural characterization after heat treatments

Pure Ni coating
The microstructural modifications caused by the incorporation of the particles in the metal matrix and the intermetallic phases which are formed after thermal treatments modify the mechanical properties of the composite coating when compared to the pure nickel deposits. Pure Ni, Ni/µAl and Ni/nAl specimens have been heat treated in oven in air atmosphere for three hours at 400°C, 600°C and 800°C and cooled to room temperature in the oven.
The cross section micrographs after metallographic etching show a partial recrystallization of the Ni grains after heat treatment at 400°C (Figure 4-27-b). The formation of some small equiassic grains is noticed starting from the boundaries of the large columnar grains. After heat treatment at 600°C the pure Ni microstructure presents complete recrystallization with

[5] M. Lekka, Electrochemical Deposition of Composite Coatings, Elsevier Reference Module in Chemistry, Molecular Sciences and Chemical Engineering, 2016, Reedijk, J. (Ed.)Waltham, MA: Elsevier
[6] D. F. Susan, K. Barmak, A. R. Marder, Thin Solid Films 307 (1997), 133-140

the formation of large equiassic grains (Figure 4-27-c). After heat treatment at 800°C a further increase of the grains dimension is observable (Figure 4-27-d).

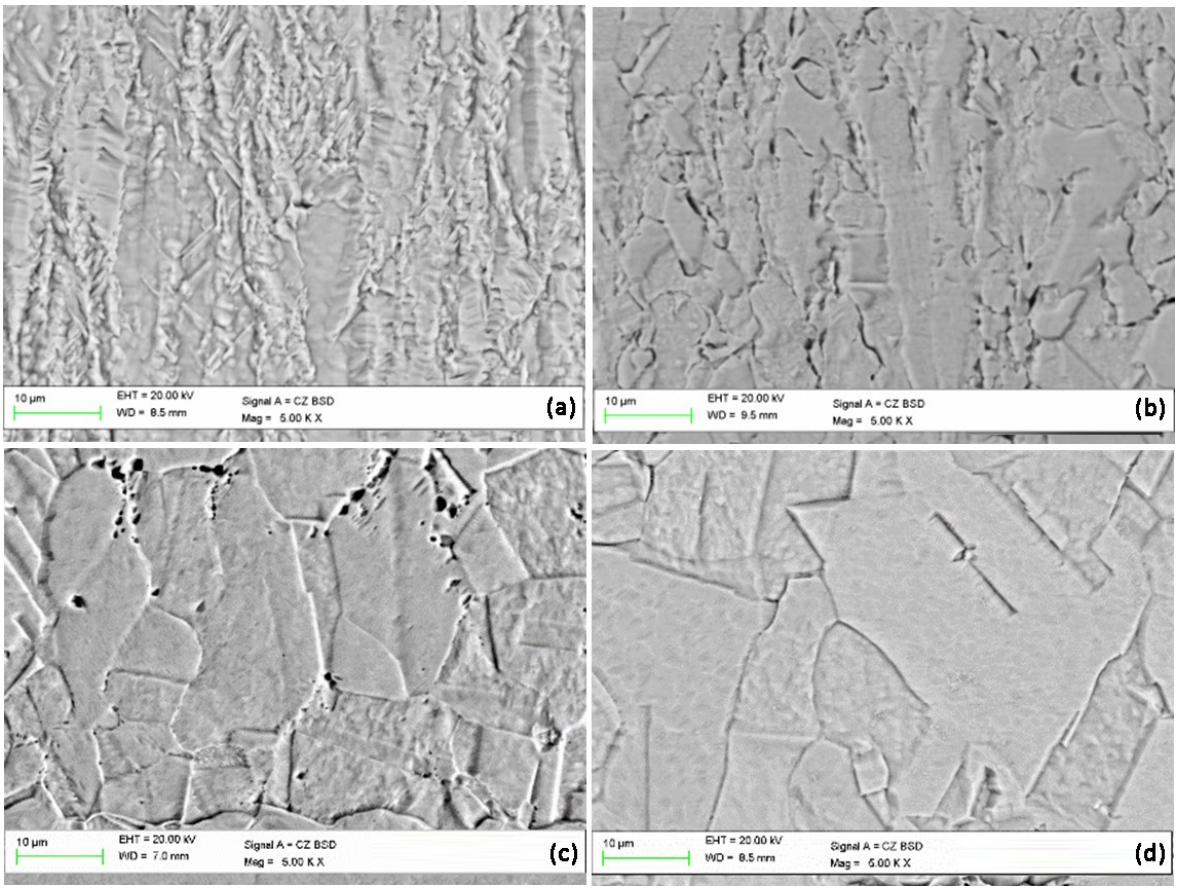

Figure 4-27: Cross section micrographs after metallographic etching of pure Ni sulfammate "High Speed" as plated (a) and after heat treatments at: 400°C (b), 600°C (c) and 800°C (d)

Ni/Al micro composite coatings

The not etched Ni/µAl composite coating after heat treatment at 400°C (Figure 4-28-b) shows a similar structure of the as-plated coating (Figure 4-28-a), indicating a very limited diffusion of Al in the Ni matrix at this temperature.

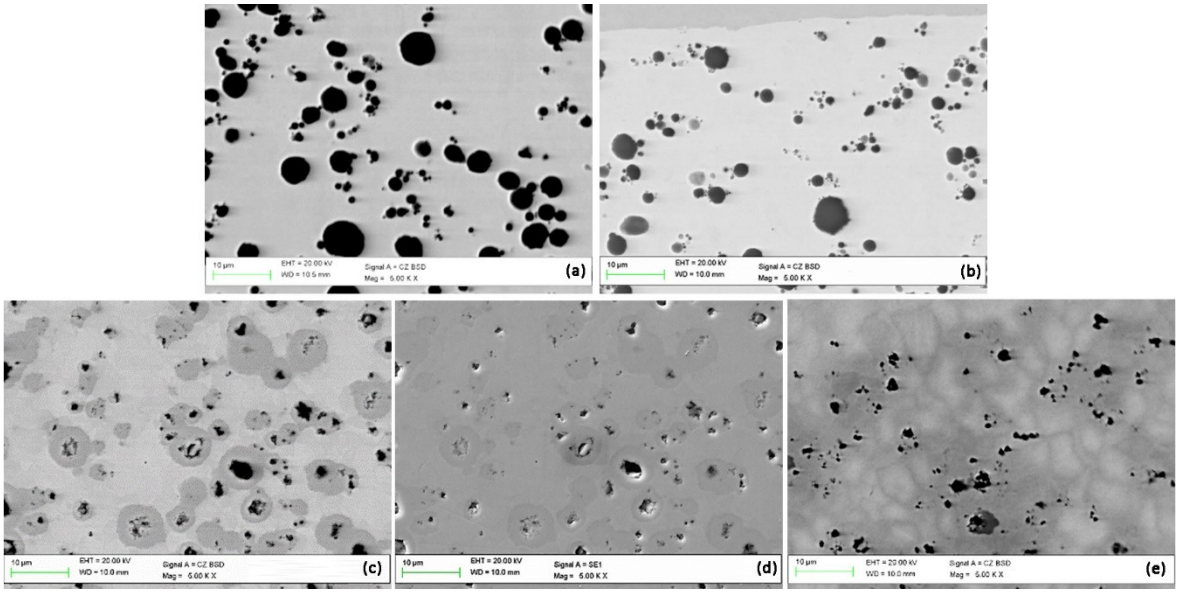

Figure 4-28: Cross section micrographs of Ni/µAl as plated (a) and after heat treatments at: 400°C (b), 600°C (c and d in Secondary Electron mode) and 800°C (e)

The Ni/µAl coating heat treated at 600°C (Figure 4-28-c) presents a dark grey ring that surrounds the Al particles suggesting a remarkable interdiffusion between the Al of the particles and the Ni matrix.
EDXS analyses performed on the different grey areas (Figure 4-29 and Table 4-24) and in agreement with the Al-Ni phase diagram (Figure 4-30) revealed that the dark grey zones (Figure 4-29 spectrum 3) possibly correspond to the intermetallic γ'(Ni_3Al phase).

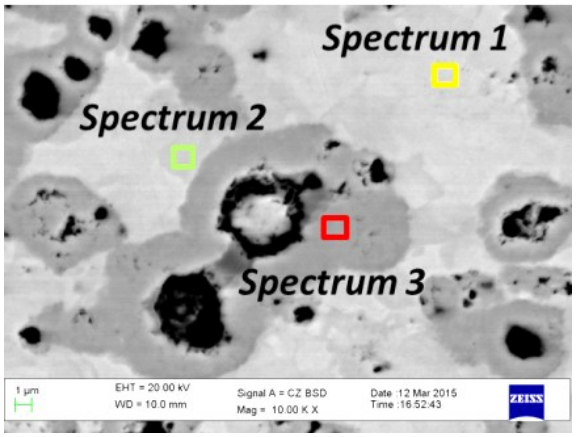

Figure 4-29: EDXS analyses performed on the different grey zones of the Ni/µAl H.T. at 600°C

Table 4-24: EDXS analyses performed on the different grey zones of the Ni/µAl H.T. at 600°C

	Al	Ni	Total
Spectrum	**[Wt.%]**	**[Wt.%]**	**[Wt.%]**
1	0.42	99.58	100
2	5.66	94.34	100
3	12.74	87.26	100

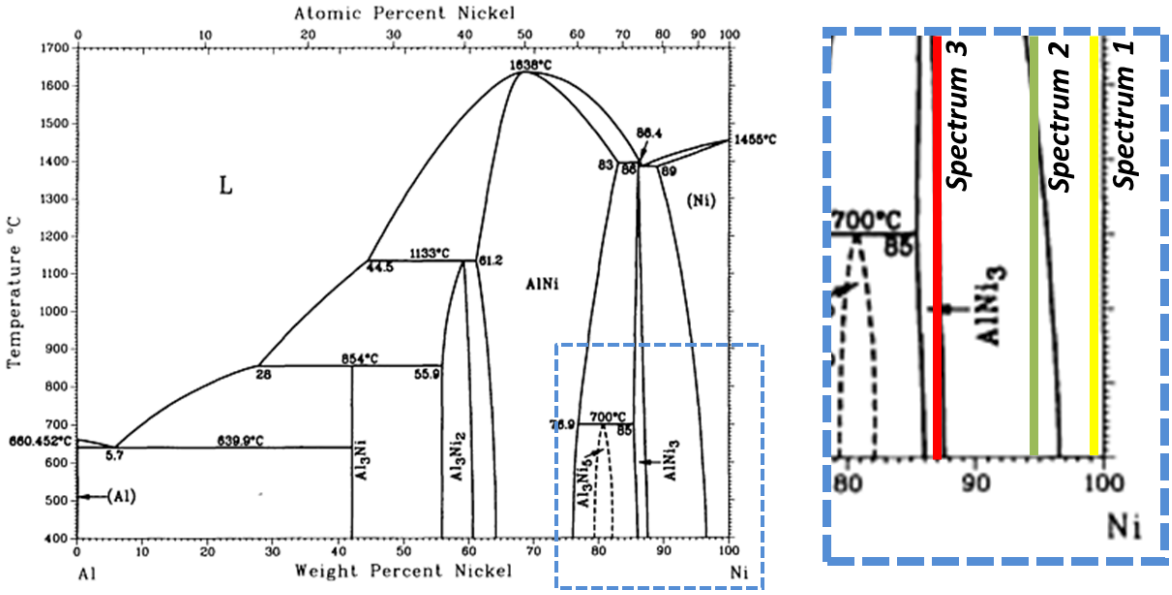

Figure 4-30: Al-Ni Phase diagram and zoom of the area of interest

By increasing the distance from the Al particles (light grey zones in Figure 4-29 spectrum 1 and 2) the Al content decreases, indicating the formation of a γNi phase containing lower amounts of Al in a substitutional solid solution. Observing the same areas in Secondary Electron mode (Figure 4-28-d) it is possible to notice the formation of voids in the places previously occupied by the Al particles. These pores were formed due to the fast diffusion of Al and the formation of the γ´ phase which has a lower specific volume, as reported also by Liu et al.[7] and Susan et al.[8].

After heat treatment at 800°C a more homogenous microstructure is observable, indicating a further in deep diffusion of the Al into the Ni matrix (Figure 4-28-e).

XRD diffraction diagrams of the nano-composite deposits are reported in Figure 4-31. The analyses performed both prior and after each H.T. showed the presence of small peaks related to pure Al for the as plated and H.T. at 400°C deposits and high intensity peaks related to the Ni matrix (Figure 4-31-a and Figure 4-31-b). The H.T. 600°C deposit's diffractogram confirmed the presence of the γ' intermetallic phase and the presence of γNi (Figure 4-31-c). In the X Ray diffractogram obtained on the Ni/μAl coating after heat treatment at 800°C no peaks related to the presence of intermetallic phases are present, indicating that the coating consists of a substitutional solid solution of Al in the Ni elementary cell γ(Ni) (Figure 4-31-d). These results indicate also that the codeposited Al amount is not enough to form an intermetallic phase overall the coating volume.

[7] H.Liu, W.Chen, Intermetallics 13 (2005) 805-817

[8] D.F.Susan, W.Z.Misiolek, A.R.Marder Metallurgical and Materials Transactions A 32A (2001), 379-390

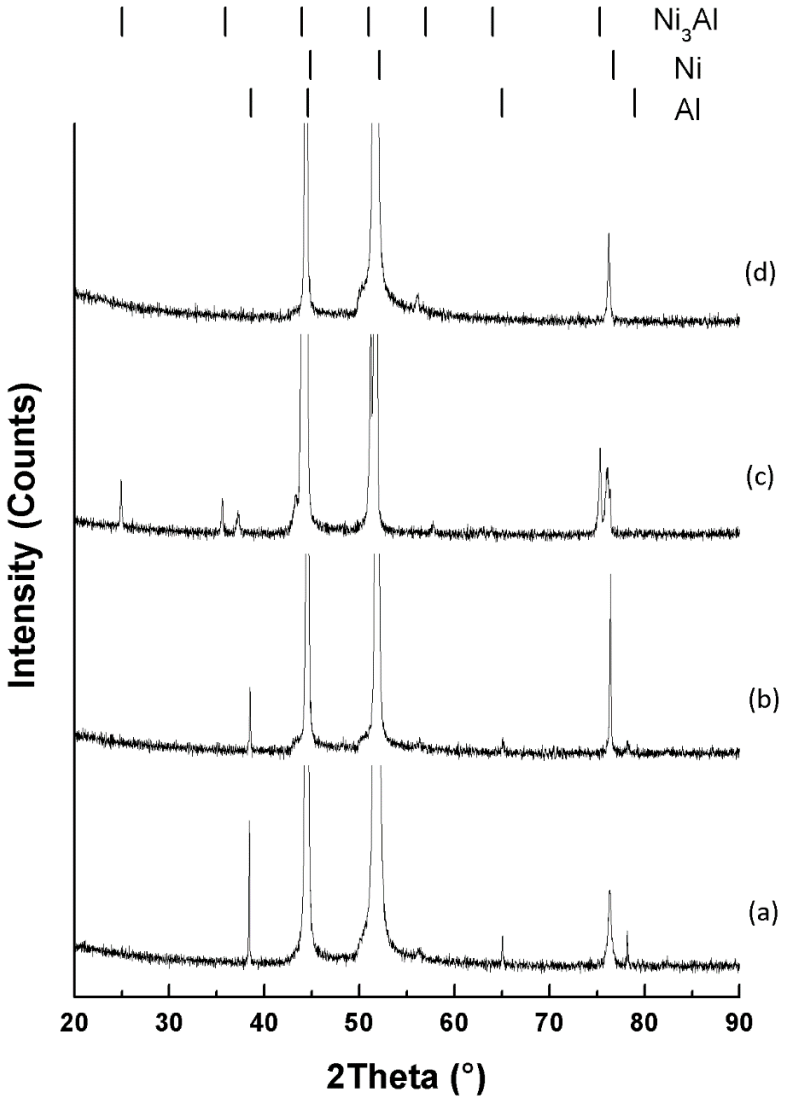

Figure 4-31: X-ray diffraction diagrams of Ni/μAl deposits (a) as plated, (b) after H.T. at 400°C, (c) after H.T. at 600°C, (d) after H.T. at 800°C

Cross section micrographs after metallographic etching of the micro-composite deposits after each H.T. are reported in Figure 4-32.

By observing these micrographs, it was possible to appreciate that by heating at 400°C the limited diffusion of Al in the Ni matrix doesn't sufficiently hinder the recrystallization of the Ni matrix (Figure 4-32-b). The formation of small equiassic Ni grains is observed as in the pure Ni coatings treated at the same temperature (Figure 4-32-b). After heat treatment at 600°C it is possible to distinguish a mixed microstructure with small equiassic grains of γ(Ni) and small grains γ'(Ni_3Al) that surround the voids created by the fast diffusion of Al from the micro-particles into the Ni matrix (Figure 4-32-c). After heat treatment at 800°C the microstructure is more homogenous, consisting in prevalence of small equiassic grains of γ(Ni). Also in this case, pores are observable (Figure 4-32-d). The diffusion of Al after heat treatments at 600 and 800°C hindered the recrystallization of the Ni matrix leading to the formation of much smaller grains compared to the pure Ni coatings.

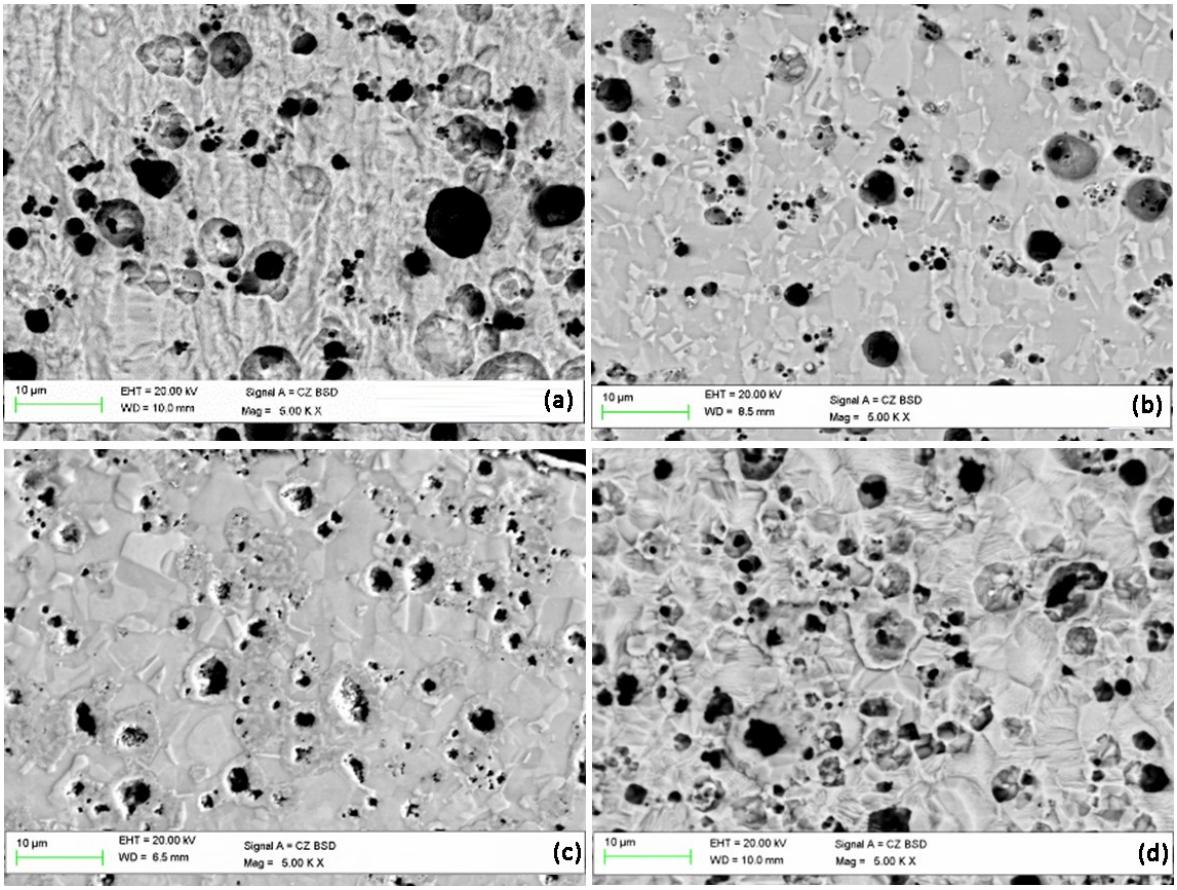

Figure 4-32: Cross section micrographs after metallographic etching of Ni/µAl as plated (a) and after heat treatments at: 400°C (b), 600°C (c) and 800°C (d)

Ni/Al nano composite coatings

Cross section micrographs and Al EDXS maps of the nano-composite deposits both as plated and after each H.T. are reported in Figure 4-33. In the case of the Ni/nAl composite coatings after all heat treatment temperatures, due to the small particles size and the lower Al content, it was not possible to clearly distinguish the formation of different phases by BSE observation at SEM as it was in the case of the micro-composite coatings. Even at higher magnification, the only feature suggesting that diffusion occurs is the interface line between the Al nano-particles and the Ni matrix which becomes more blurry (Figure 4-33-a,c,e,g). Al EDXS maps obtained at the same areas (Figure 4-33-b,d,f,h) revealed a progressive diffusion of Al in the Ni matrix by increasing the heat treatment temperature. The coatings treated at 800°C present a uniform distribution of Al in the overall volume (Figure 4-33-h).

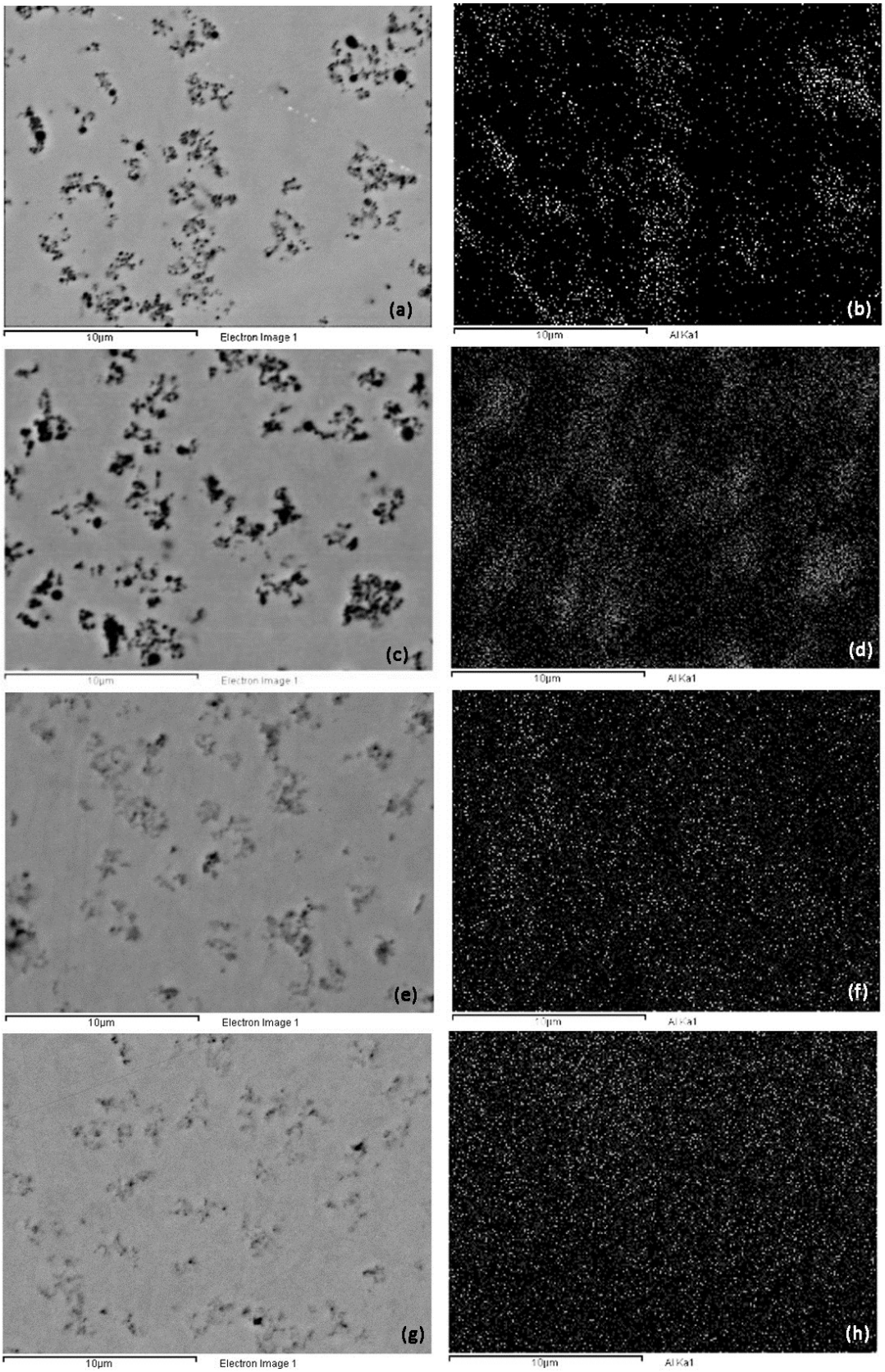

Figure 4-33: Cross section micrographs and Al EDXS Maps of Ni/nAl as plated (a,b) and after heat treatments at: 400°C (c,d), 600°C (e,f) and 800°C (g,h)

XRD diffraction diagrams of the nano-composite deposits are reported in Figure 4-34. The diffractograms obtained on the as plated and H.T. at 400°C deposits present small peaks related to the Al and high intensity peaks related to the Ni matrix. After H.T. at 600oC and 800oC no peaks related to Al or Ni/Al intermetallic phases are present (Figure 4-34-a,b,c,d). It could be thus deduced that the amount of codeposited Al is too low to form intermetallic phases or if these were locally formed, the amount is below the detection limit of the XRD. The coatings consist just of a substitutional solid solution of Al in the Ni elementary cell.

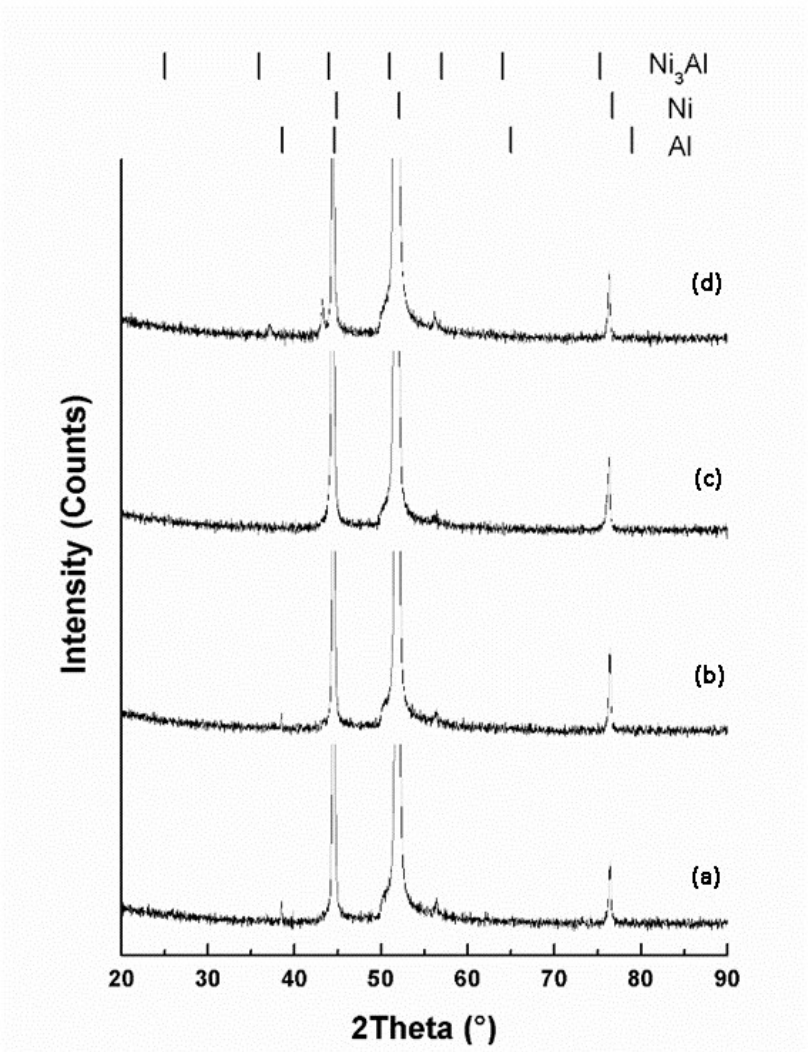

Figure 4-34: X-ray diffraction diagrams of Ni/nAl deposits (a) as plated, (b) after H.T. at 400°C, (c) after H.T. at 600°C, (d) after H.T. at 800°C

The cross section micrographs of the coatings after metallographic etching show that all deposits preserve a predominant columnar structure after each heat treatment temperature (Figure 4-35-a,b,c,d). The small dimensions of the particles and their more uniform distribution in the matrix in comparison to the micro-composites, lead to an advance of the inter-diffusion at lower heat treatment temperature[9]. The diffusion of Al at 400°C blocks the recrystallization of the Ni grains and "freezes" the already quite refined columnar

[9] L. Zheng, X. Peng, F. Wang, J. Mater Sci 47 (2012) 7759-7763

structure (Figure 4-35-b). After heat treatment at 600°C (Figure 4-35-c) some smaller grains, probably consisting of γ´Ni_3Al are observable around the nano-particles agglomerates. The small γ Ni grains are still present in the matrix (Figure 4-35-c). After heat treatment at 800°C the microstructure is more homogeneous with a single phase consisting of a substitutional solid solution of Al in the Ni elementary cell (γ Ni), forming small grains (Figure 4-35-d).

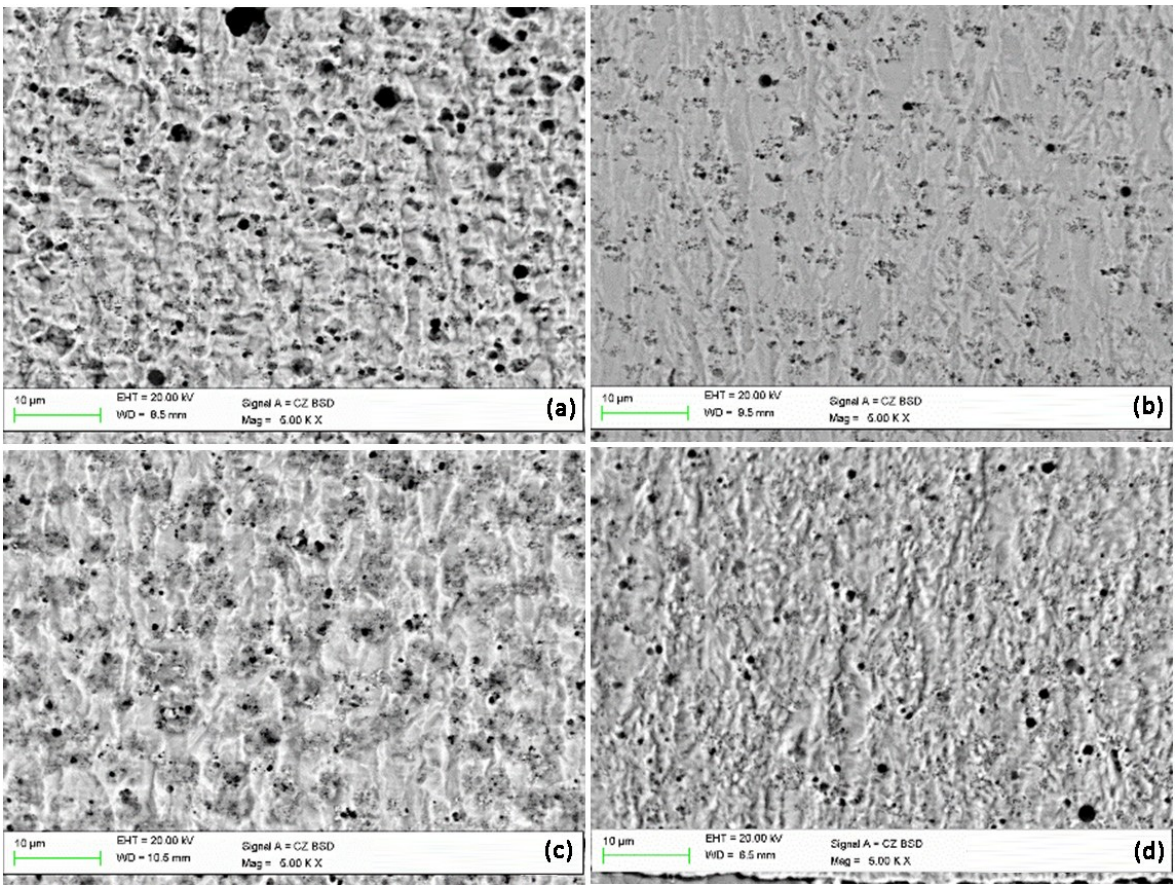

Figure 4-35: Cross section micrographs after metallographic etching of Ni/nAl as plated (a) and after heat treatments at: 400°C (b), 600°C (c) and 800°C (d)

The XRD measurements have been also used to examine the preferred orientation of the three types of coatings prior and after the H.T.

The preferred orientation was evaluated by calculating the RTC $_{(h,k,l)}$ (relative texture coefficient) of a given orientation of the studied samples according to the method described by Ye et al[10], using the following equation:

$$RTC_{(h,k,l)} = \frac{R_{(h,k,l)}}{\sum R_{(h,k,l)}} \times 100\%$$

For each reflection line the ratio $R_{(h,k,l)} = I_{(h,k,l)} / I_{p(h,k,l)}$ was first calculated, where $I_{p(h,k,l)}$ is relative of the corresponding reflection peak for a nickel powder reference sample measured with the same method used for the nickel matrix coatings.

The RTC values of the crystallographic orientations of both the as plated and heat treated pure Ni coatings are reported in Figure 4-36-a. As can be observed, the as plated coating presents a preferential [100] orientation. At 400°C the partial recrystallization of the Ni

[10] X. Ye, J.P. Celis, M. De Bonte, J.R. Roos, J. Electrochem. Soc. 141 (1994) 2698-2708

grains leads to a loss of the preferential [100] orientation and an increase of the RTC along [111] and [110] orientation. After heat treatment at 600°C and 800°C the complete recrystallization leads to a further loss of the [100] orientation and to a remarkable increase of the orientation [111].

The RTC values of the crystallographic orientations of both the as plated and heat treated Ni/µAl coatings are reported in Figure 4-36-b. The as plated Ni/µAl coating shows a lower value of the preferential [100] orientation as compared to the pure Ni coating due to the interruption of the Ni columns growth on the Al micro particles and to slight changes in the growth direction. After heat treatment at 400°C and 600°C a progressive loss of the [100] orientation and an increase of both [111] and [110] can be observed. At 400°C this change can be mainly attributed to the recrystallization of the Ni matrix, while at 600°C to the formation of the intermetallic γ'(Ni_3Al). After heat treatment at 800°C the preferential [100] orientation was maintained as the coating consists of a solid solution of Al in the γNi.

The RTC values of the crystallographic orientations of both the as plated and heat treated Ni/nAl coatings are reported in Figure 4-36-c. The Ni/nAl coating as plated and heat treated at each temperature present the same preferential [100] orientation. As observed in the cross section micrographs after metallographic etching (Figure 4-35), the uniform distribution of the nano-particles in the Ni matrix in the as plated coating and the diffusion of the Al after the different heat treatments block the refined columnar structure preserving the initial preferential growth direction of the deposit.

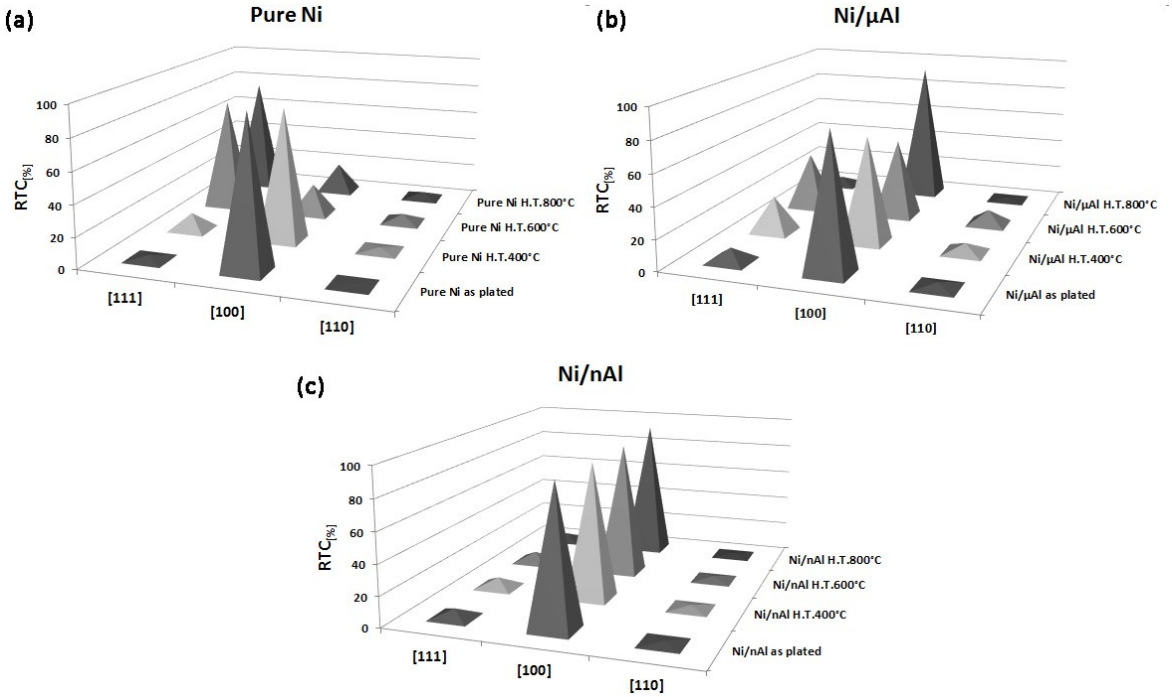

Figure 4-36: Relative texture coefficient (RTC) for the different reflection lines of (a) pure Ni deposits, (b) Ni/µAl deposits and (c) Ni/nAl deposits both prior and after H.T. at different temperatures

4.3 Microhardness

The deposits hardness has been evaluated as mean value of 15 $HV_{0,05}$ microhardness measures performed on polished coatings cross sections using a Struers Duramin Vickers micro-indenter.
In Table 4-25 are reported the microhardness values of the three types of coatings both as plated and after heat treatments and in Figure 4-37 the relative graph.

Table 4-25: Vickers microhardnes $HV_{0.05}$ values of pure Ni, Ni/µAl and Ni/nAl deposits both as plated and H.T. at 400, 600, 800°C

	Pure Ni	**Ni/µAl**	**Ni/nAl**
	[$HV_{00.5}$]	**[$HV_{00.5}$]**	**[$HV_{00.5}$]**
As plated	163 ± 5	199 ± 8	248 ± 8
H.T. 400°C	116 ± 19	146 ± 4	271 ± 5
H.T. 600°C	96 ± 10	225 ± 12	246 ± 8
H.T. 800°C	85 ± 3	208 ± 12	248 ± 8

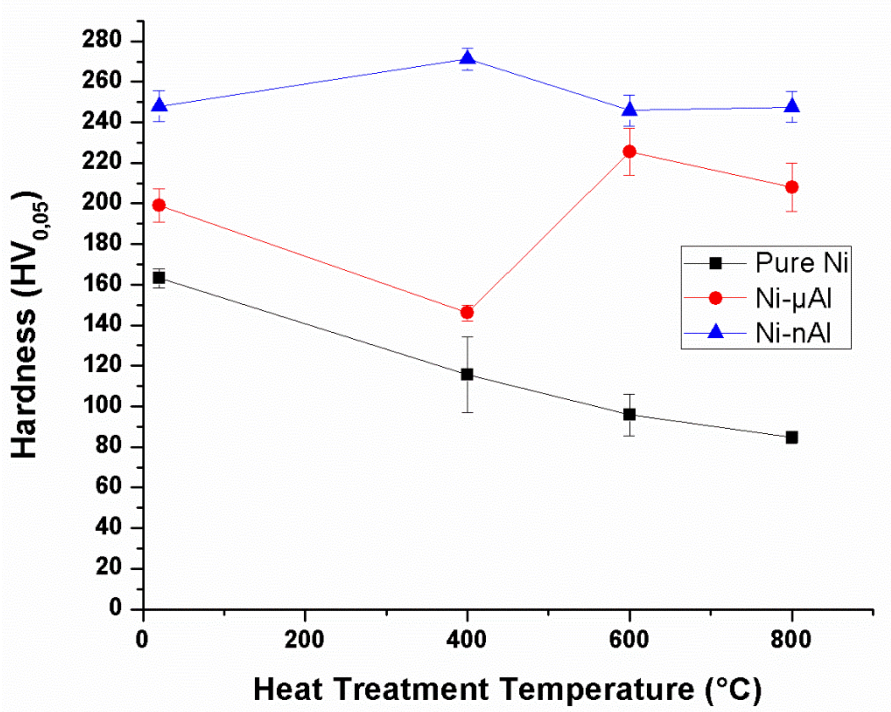

Figure 4-37: Vickers microhardnes $HV_{0.05}$ of pure Ni, Ni/µAl and Ni/nAl deposits as a function of H.T. temperature

The pure Ni coating presents a relative low microhardness of about 163±5 $HV_{0.05}$. The codeposition of both micro- and nano- Al particles leads to an increase of the composite coatings hardness. In comparison to the pure Ni the as plated Ni/µAl presents an increase of about 22% and in the case of Ni/nAl an increase of about 52%. Considering that the hardness of the Al particle is lower with respect to the Ni matrix, the marked increase of the composite coating hardness is due to the microstructural refinement caused by the codeposition of the particles.

Regarding the hardness modifications after the heat treatments, the pure Ni coating shows a progressive decrease of the hardness by increasing the heat treatment temperature. As described before, this decrease is strictly correlated to the recrystallization and the Ni grains growth and is proportional to the grain size.
Regarding the Ni/μAl, the recrystallization of the Ni matrix that occurs at 400°C leads to a similar decrease of the hardness as observed for the pure Ni. The formation of the harder intermetallic phase γ'(Ni_3Al) that occurs at 600°C leads then to an increase of about 13% respect to the as plated coating. The deeper diffusion of the Al in the Ni matrix that occurs at 800°C and the formation of a microstructure consisting of grains of a substitutional solid solution of Al in the Ni elementary cell finally leads to a slight increase of the hardness of about 5% with respect to the as plated coating, but to a slight decrease with respect to the coating treated at 600°C.
The Ni/nAl composite coating presented an almost stable hardness after every heat treatment due to the preservation of the columnar microstructure.

4.4 Corrosion resistance

The electrochemical behavior of the different phases formed during the H.T. was studied by means of Atomic Force Microscopy (AFM) and Scanning Kelvin Probe Force Microscopy (SKPFM). Topographic and Volta potential maps of 100x100 µm on the top surface of the polished deposits were performed in order to better understand the electrochemical behavior and the eventual formation of galvanic couples between the different phases. SEM micrographs of the same areas analyzed with the localized electrochemical technique were obtained in order to identify the different analyzed areas.
The corrosion resistance of the three types of coatings both prior and after heat treatments was evaluated by potentiodynamic polarization measurements in a 3.5% wt. NaCl solution.

4.4.1 Micro-electrochemical behavior: Topographic and Volta potential maps

4.4.1.1 Pure Ni deposits

The topographic AFM and Volta potential maps obtained by SKPFM as well as the SEM micrograph of the same area of a pure as plated Ni deposit is reported in Figure 4-38.

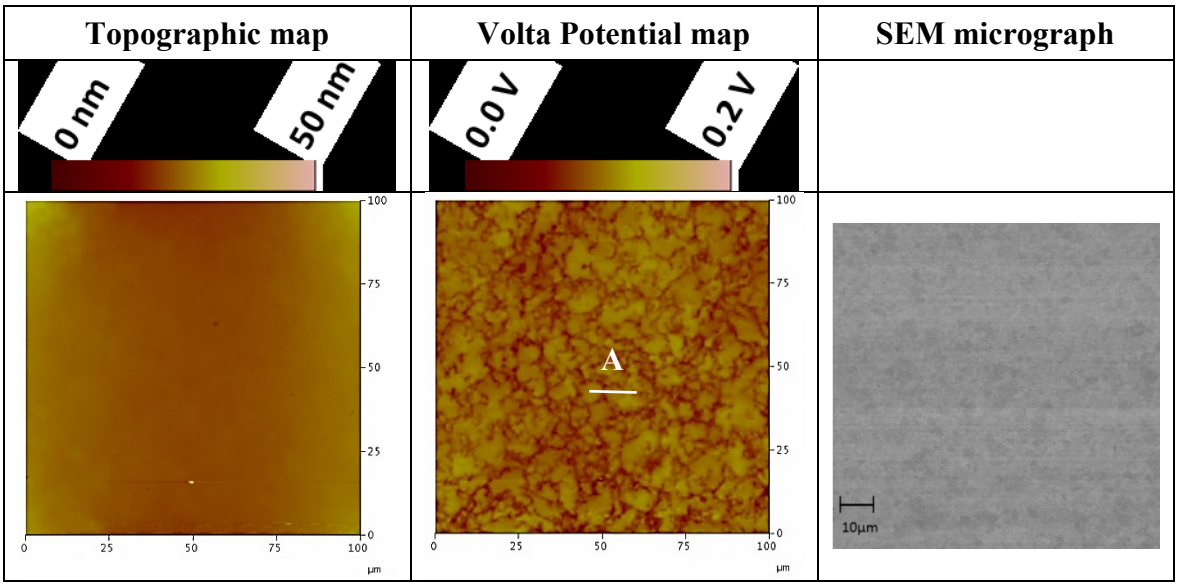

Figure 4-38: Topographic AFM and Volta potential maps and SEM micrographs of pure Ni as plated

By observing the topographic map and the SEM micrograph is possible to notice that the surface of the deposit is perfectly flat. The Volta potential map shows that the maximum Volta potential difference is between the columnar grain boundaries and the center of the grains. This difference could be attributed to the segregation at the grain boundaries, during the electrodeposition process, of the impurities that are present in the Ni plating bath.
The potential scan line A in Figure 4-38, shows that the Volta potential difference is only of about 30 mV.

The Volta potential map of the pure Ni H.T. at 600°C reported in Figure 4-39 shows that the recrystallization of the Ni grains leads to a uniform distribution of the impurities in the whole microstructure. The Volta potential line scan B in Figure 4-39 indicates that the potential difference is about 25 mV but in this case the difference is between the differents Ni grains.

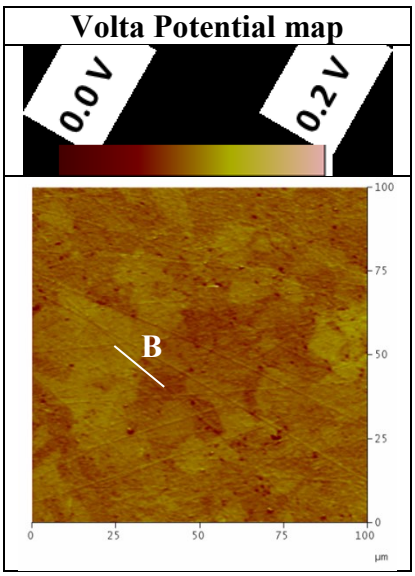

Figure 4-39: Volta potential maps of pure Ni H.T. at 600°C

4.4.1.2 Ni/µAl composite deposits

The topographic AFM and Volta potential maps obtained by SKPFM as well as the SEM micrograph of the same areas of both as plated and after H.T. micro-composite deposits are reported in Figure 4-40. The different phases present in the maps have been identified by EDXS analyses on the same areas (Figure 4-41, Figure 4-42, Table 4-26 and Table 4-27).

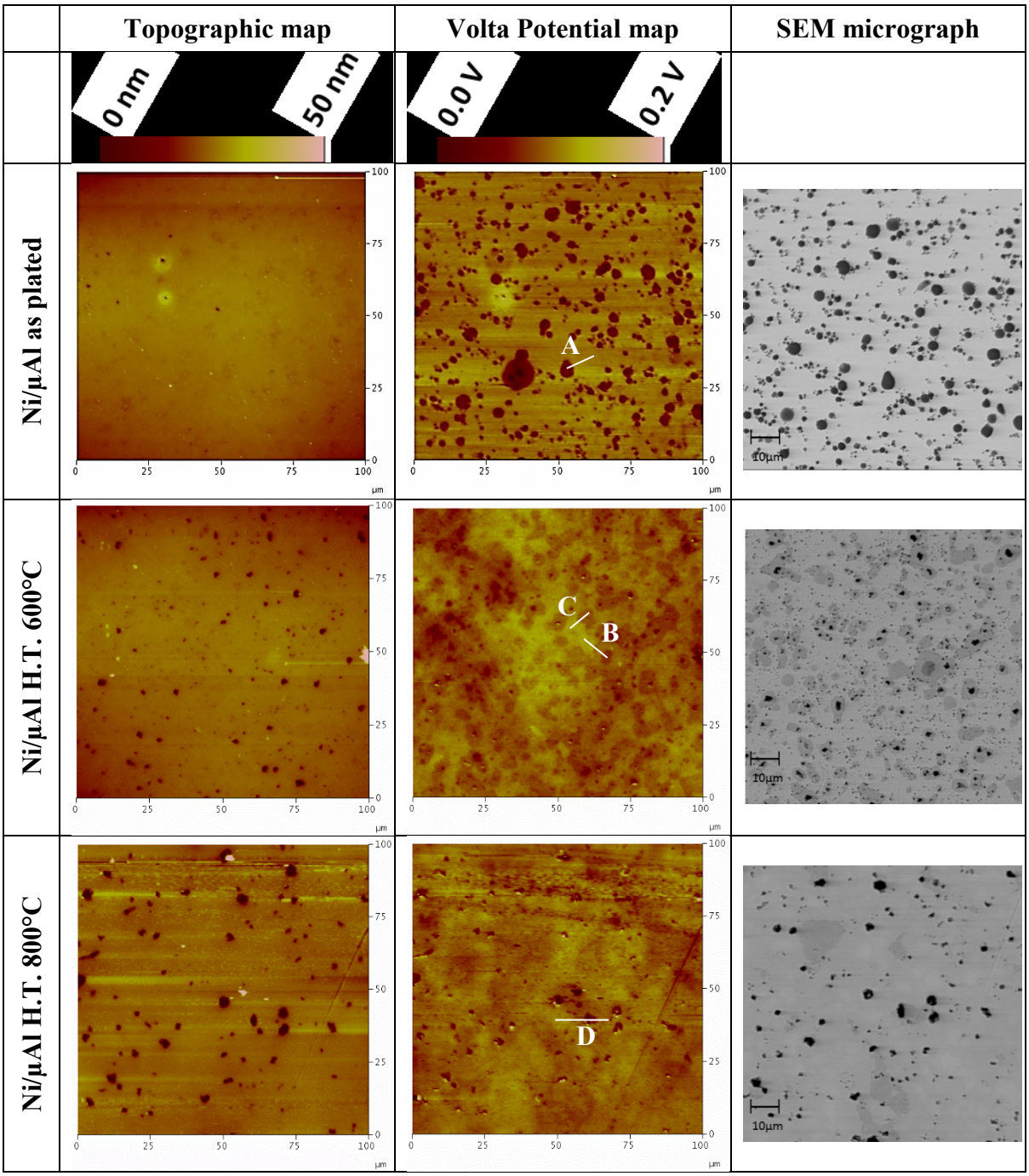

Figure 4-40: Topographic AFM and Volta potential maps and SEM micrographs of Ni/µAL as plated and H.T. at 600°C and 800°C

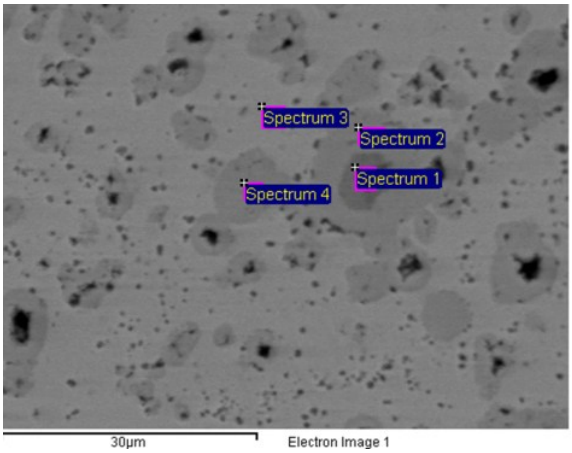

Figure 4-41: EDXS analyses performed on the different grey zones of the Ni/µAl H.T. at 600°C

Table 4-26: EDXS analyses performed on the different grey zones of the Ni/µAl H.T. at 600°C

	Al	Ni	Total
Spectrum	**[Wt.%]**	**[Wt.%]**	**[Wt.%]**
1	31.31	68.69	100.00
2	14.68	85.32	100.00
3	1.2	98.80	100.00
4	13.74	86.26	100.00

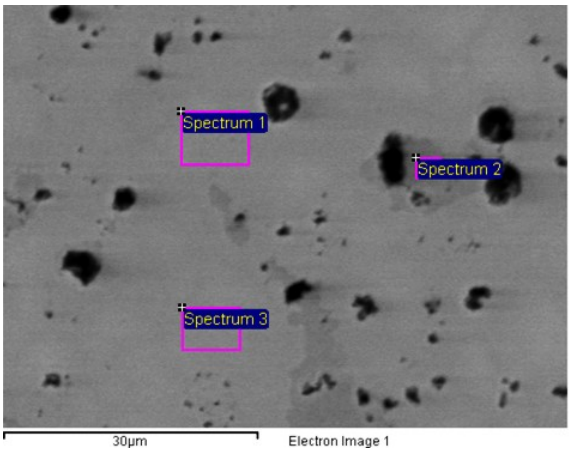

Figure 4-42: EDXS analyses performed on the different grey zones of the Ni/µAl H.T. at 800°C

Table 4-27: EDXS analyses performed on the different grey zones of the Ni/µAl H.T. at 800°C

	Al	Ni	Total
Spectrum	**[Wt.%]**	**[Wt.%]**	**[Wt.%]**
1	4.49	95.51	100.00
2	13.39	86.61	100.00
3	4.15	95.85	100.00

The topographic map of the as plated deposit shows that the surface is almost flat, only few pores are observable. These voids are due to the metallographic polishing which has removed some Al particles.

As described in the chapter 3.2.2, the diffusion of the Al in the Ni matrix during the heat treatments leads to the formation of voids in the places previously occupied by the Al particles. The AFM maps performed on the deposits H.T. at 600°C and 800°C confirms the presence of voids in the same places observed with the SEM. Higher the heat treatment temperature, faster and deeper the Al diffusion and also higher the voids size.

By observing the SKPFM map of the as plated coating it is possible to notice the high Volta potential difference between the Ni matrix and the Al particles. From the potential scan performed along the line A in Fig. 3-40 a Volta potential difference of about 110mV was measured.. This high potential difference indicates a strong tendency to form galvanic couples. The Volta potential map performed on the sample H.T. at 600°C shows that the diffusion of the Al leads to a formation of phases with lower potential differences. In fact, from the potential scans performed along the lines B and C in Fig. 3-40 a Volta potential difference of about 60mV was measured between the Al and the γ(Ni) phase and a Volta potential difference of about 42mV was measured between the Ni_3Al phase and the γ(Ni) phase. Both Volta potential differences are lower than that between the Al particles and the

Ni matrix in the as plated deposits. The Volta potential map performed on the sample H.T. at 800°C shows that the formation of a more homogenous microstructure consisting in prevalence of small grains of γ(Ni) phase leads to a more uniform and homogeneous distribution of the Volta potential in the deposit. The potential scan performed along the D line in Figure 4-40 showed that the potential difference between a residual Ni_3Al grain and the γ(Ni) phase is about 30mV similar to the Pure Ni coatings. The SKPFM measurements indicate that Ni/Al micro composite coatings heat treated at 600°C and 800°C have a significantly lower tendency to form galvanic couples in comparison to the as plated coating.

4.4.1.3 Ni/nAl composite deposits

The topographic AFM and Volta potential maps obtained by SKPFM as well as the SEM micrograph of the same area of both as plated and after H.T. nano-composite deposits are reported in Figure 4-43.

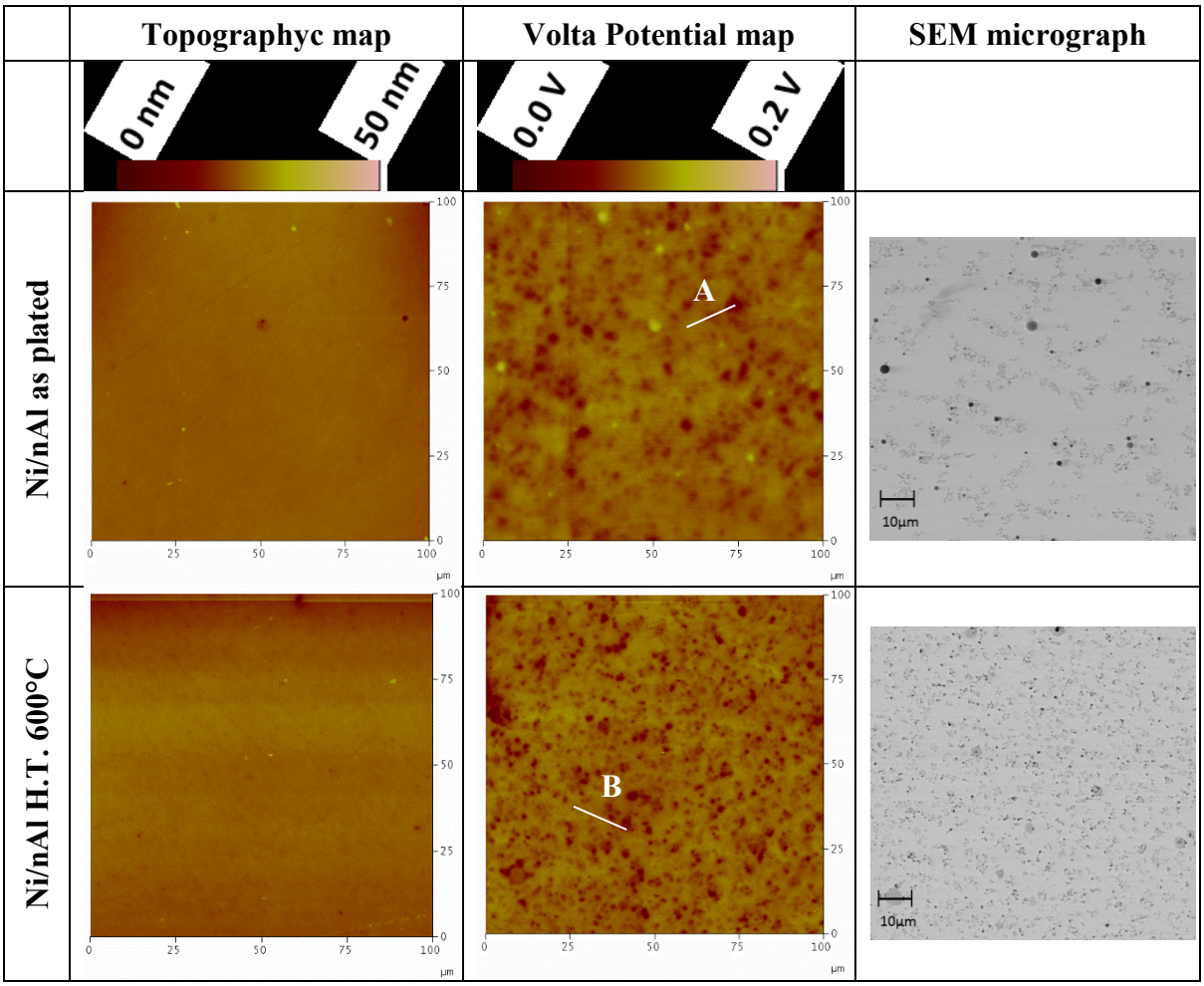

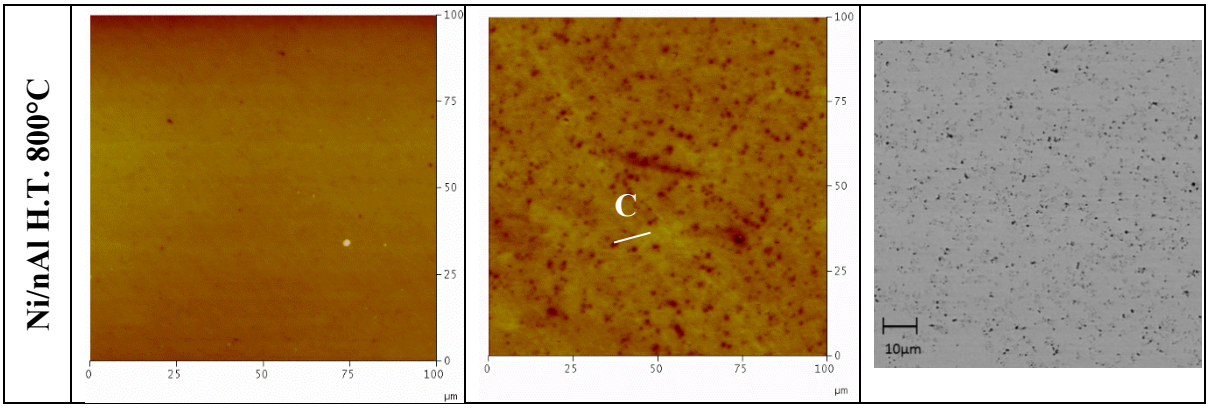

Figure 4-43: Topographic AFM and Volta potential maps and SEM micrographs of Ni/nAL as plated and H.T. at 600°C and 800°C

By observing the topographic maps in Figure 4-43 of the Ni/Al nano composite coatings prior and after the heat treatments is it possible to notice that despite the Al nano particles agglomeration, the uniform distribution and the smaller dimension lead to the formation, after the heat treatments, of nano-voids and the surface results to be practically flat.
By observing the Volta potential maps in Figure 4-43 of the Ni/Al nano composite coatings prior and after the heat treatments is it possible to notice that the nano particles allow to obtain a more uniform distribution of anodic and cathodic sites in comparison to the micro composite deposit.
However, the potential scan performed along line A in Figure 4-43 shows that the potential difference of about 90mV between the Al agglomerates and the Ni matrix is enough high to indicate also in this case the tendency to form galvanic couples.
The potential scan performed along the line B in Figure 4-43 performed on the deposit H.T. at 600°C shows that, as in the case of the micro composite deposit, the diffusion of the Al in the Ni matrix and the formation of a more uniform microstructure consisting in prevalence of γ(Ni) phase leads to a decrease of the maximum potential difference at about 45mV.
The potential scan performed along line C in Figure 4-43 on the deposit H.T. at 800°C shows that a further deeper diffusion of Al in the Ni matrix and the formation of an even more uniform microstructure with maximum potential differences of about 20mV further decreases the tendency to form galvanic couples.

4.4.2 Potentiodynamic polarization measurements

The polarization measurements were performed using an Avesta cell to avoid crevice corrosion and a three-electrodes system. A Pt wire and an $Ag/AgCl/kCl_{3M}$ electrode were used as counter and reference electrode, respectively. The exposed surface area of the working electrode was 0.7 cm^2. The scan rate was 0.2mV/s and all measurements have been performed in aqueous solution with 3.5% wt. of NaCl. The scan range was from -250mV vs. OCP till reaching $10^{-3}A/cm^2$.

4.4.2.1 As plated deposits

Representative potentiodynamic curves obtained on the as plated deposits are reported in Figure 4-44.

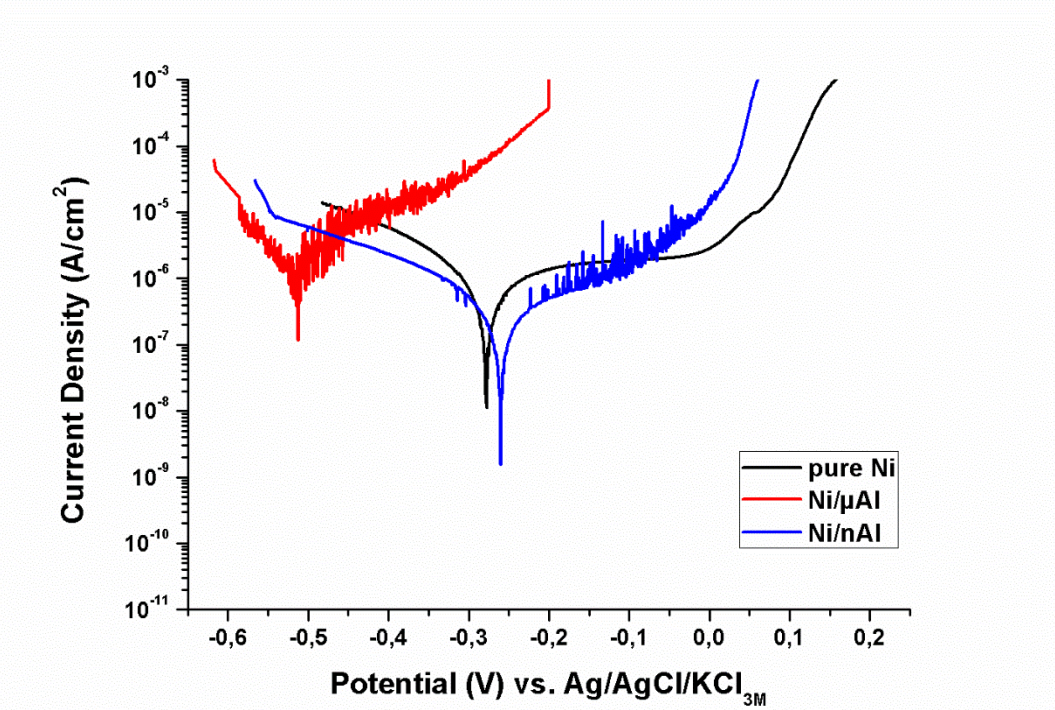

Figure 4-44: Potentiondynamic polarization curves of pure Ni, Ni/µAl and Ni/nAl as plated coatings

The corrosion resistance of the three as plated coatings is rather different due to the presence of the nano- and the micro- Al particles in the composite coatings.
The as plated pure Ni coating presents a passive behavior with a passive current of 10^{-6} A/dm^2 and a breakdown potential at about +0.15 V.
The Ni/Al micro-composite coating shows an active behavior with a marked decrease of the corrosion resistance. The potentiodynamic polarization curve of the Ni/µAl shows a noticeable decrease of the corrosion potential, related to the formation of a mixed potential between the Ni matrix and the Al particles, and an increase of the corrosion current. This behavior is due to the formation of a strong galvanic coupling between the Al particles and the Ni matrix as pointed out by the SKPFM measurements.
Furthermore, the marked current density oscillations both at the anodic and the cathodic branches indicate a dissolution of the Al micro-particles present on the surface. In particular, the variations of the current along the cathodic branch indicate that the Al of the particles is in anodic state also at these potentials. The preferential dissolution of the Al micro-particles causes the formation of micro pores that became preferential points to chlorides attack of the Ni matrix.
Regarding the Ni/nAl coating, due to the lower amount of Al, the small size of the particles and the uniform distribution in the Ni matrix, the corrosion behavior is in-between that of the pure Ni and the Ni/µAl coatings. Observing the polarization curve of the Ni/nAl coating it is possible to notice that the corrosion potential is similar to the pure Ni one and the corrosion current is slightly lower probably due to the finer microstructure. As well as in the case of Ni/µAl coating and demonstrated by the SKPFM map, the galvanic coupling between the Al particles and the Ni matrix leads to a preferential dissolution of the nano-particles agglomerates on the surface. This selective dissolution, proved by the sudden

variations of the current in the anodic branch during the potential scan, leads to a formation of nano-defects that became preferential points for the chlorides attack.
Even if the Ni/Al nano composite coating present a passive behavior, the preferential dissolution causes a progressive increase of the current during the anodic polarization and an advance of the breakdown potential respect to the pure Ni coating.

4.4.2.2 Pure Ni and composite deposits after heat treatments

The potentiodynamic polarization curves of pure Ni, Ni/µAl and Ni/nAl both prior and after the H.T. are reported in Figure 4-45, Figure 4-46 and Figure 4-47 respectively.

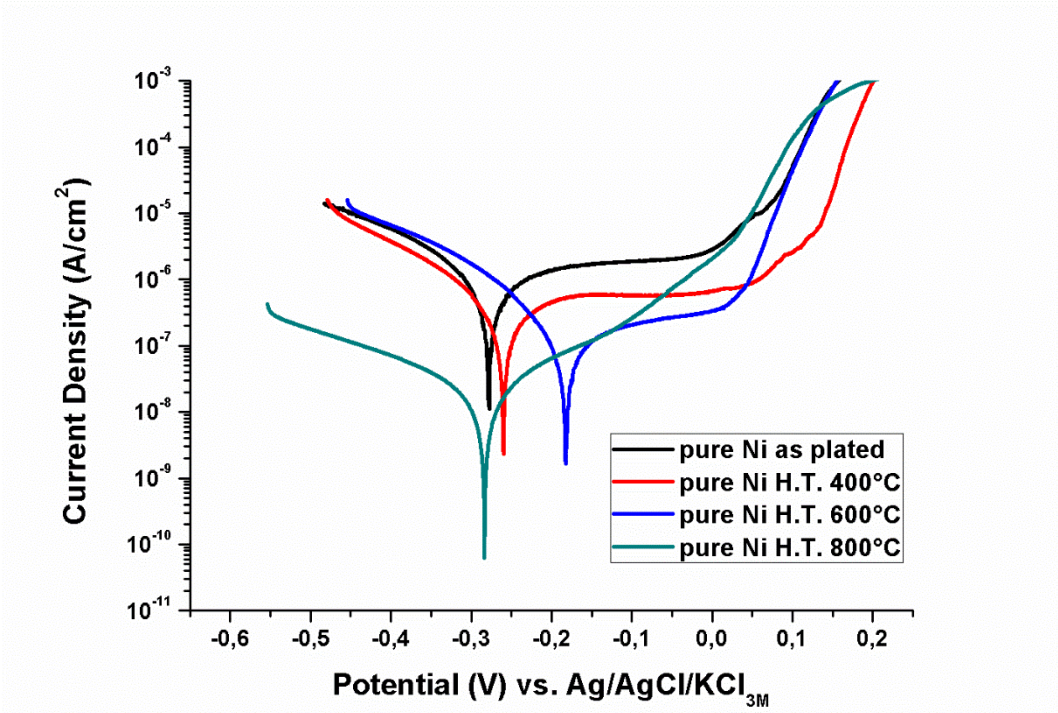

Figure 4-45: Potentiondynamic polarization curves of as plated pure Ni and pure Ni after H.T. at 400°C, 600°C and 800°C

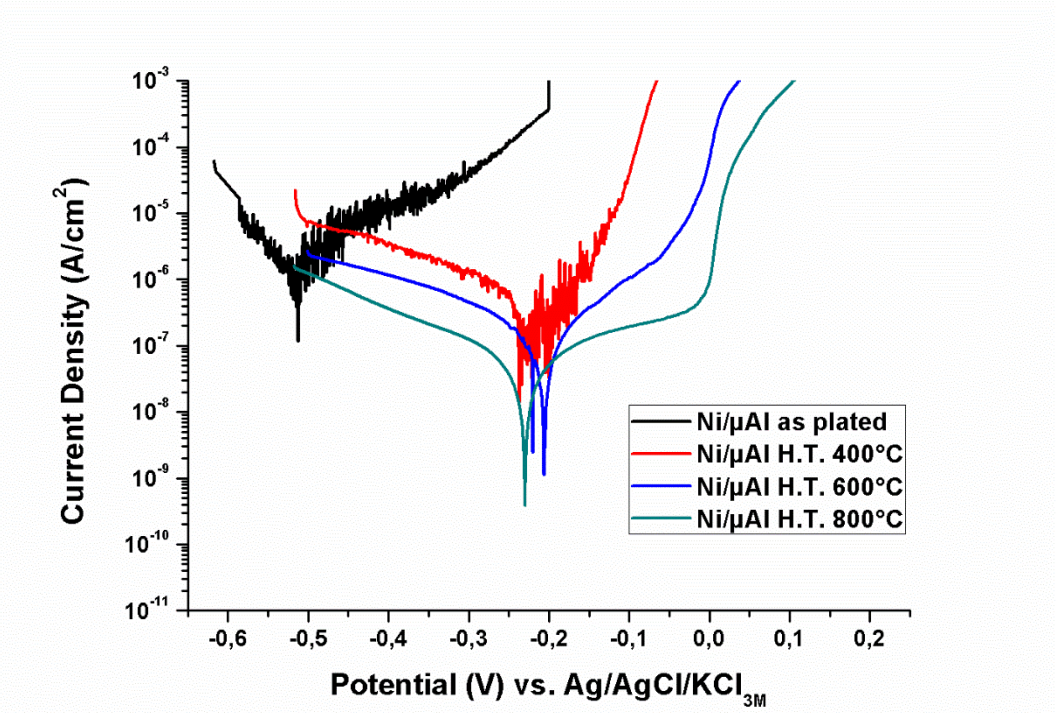

Figure 4-46: Potentiondynamic polarization curves of as plated Ni/μAl and Ni/μAl after H.T. at 400°C, 600°C and 800°C

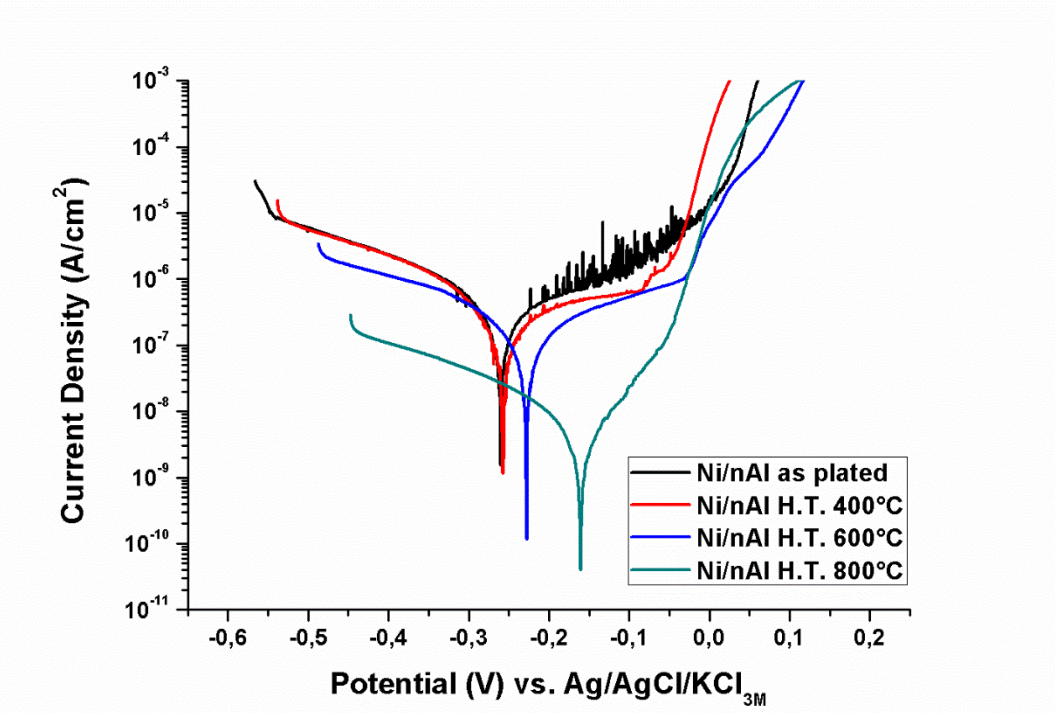

Figure 4-47: Potentiondynamic polarization curves of as plated Ni/nAl and Ni/nAl after H.T. at 400°C, 600°C and 800°C

By observing the curves related to the pure Ni deposits it is possible to notice that the increase of the heat treatment temperature leads to a decrease of the passive current while

the breakdown potentials are all in a range from 0V to 0.15V. The decrease of the passive current density could be attributed to the formation of a more stable oxide on the deposits surface after heat treatments.

The potentiodynamic curves related to the micro-composite deposits present marked differences. After H.T. at 400°C a considerable increase of the corrosion potential is shown compared to the as plated coating. As the deposits microstructure are almost the same due to the irrelevant diffusion of Al in the Ni matrix, this increase could only be attributed to the formation of a thin oxide layer on the deposit surface. Indeed, the anodic behavior of the deposit H.T. at 400°C is quite similar to the as plated one. Also in this case, the galvanic coupling between the nickel matrix and the Al particles leads to the dissolution of the Al and the coating presents an active behavior. The oscillations both at the anodic and the cathodic branches are related to the selective dissolution of the micro-particles. This dissolution and the successive formation of voids can accelerate the corrosion of the Ni matrix as they act as preferential points for the chlorides attack. The specimen H.T. at 600°C presents a quite different behavior. The corrosion potential is similar to that of pure Ni and there is a limited passive zone. This is due to both the formation of an oxide on the deposit surface and the decrease of the potential difference between the Ni/Al phases as demonstrated by the SKPFM map. The diffusion of Al in the Ni matrix and the formation of a more resistant Ni_3Al phase decreases the driving force for the formation of galvanic couples. The corrosion behavior of the specimen heat treated at 800°C is even better. The complete diffusion of Al and the formation of an uniform substitutional solid solution of Al in the Ni matrix leads to a passive behavior with a passive current density similar to that of the pure Ni coating. The breakdown potential is still lower in comparison to the pure Ni and this could be attributed to the formation of voids due to the fast diffusion of Al. These pores are always preferential attack points for the Cl^-.

The potentiodynamic curves related to the nano-composite deposits after the heat treatments present lower differences respect to the micro composite deposits but the trend is the same.

The Ni/nAl deposit heat treated at 400°C shows a decrease of the oscillations of the anodic current in comparison to the as plated coating. This could be related to the formation of a thin oxide layer on the surface but also to the faster diffusion of the Al in the Ni matrix at lower temperature in comparison to the micro composite deposit. By increasing the heat treatment temperature is it possible to notice a progressive decrease of both the corrosion and passive currents and a shift to more noble corrosion potentials. Instead, no marked changes are noticed in the breakdown potentials that remain all in a range from -0.5V to 0.10V, slightly lower in comparison to the pure Ni coatings probably due to the presence even in this sample of small pores,.

4.5 Partial conclusions

For the production of Ni matrix composite electrodeposits containing Al particles, some preliminary experiments have been performed in order to identify the optimum process parameters. To this aim 9 different Al powders and 2 Ni plating baths have been combined and different series of specimens have been produced and characterized varying also the plating process parameters. The produced deposits have been observed in cross section and analysed by EDXS in order to evaluate the Al content and the distribution of particles along the deposits. After these preliminary tests, two different Al powders have been selected, a micro-metric one with a particles mean size of 4-5μm and a nano-metric one with a particles mean size of 130nm. It was also decided to use a Ni sulfammate "high speed" plating bath as electrolyte containing 40g/L of either mico- or nano-particles.
Pure and composite nickel deposits containing either micro- or nano-particles of Al have been produced. The obtained deposits have been characterized regarding the Al content and its distribution, their microstructure, microhardness and protective properties both prior and after heat treatments up to 800^{o}C.
The as plated pure Ni deposits have a columnar structure with the columns oriented along the direction of the electrical field and with a strong [100] preferential orientation. After H.T. at 400°C a partial recrystallization occurs with the formation of small equiassic grains which also leads to a loss of the preferential [100] orientation and an increase of the RTC along [111] and [110] orientation. After H. T. at 600^{o}C and 800^{o}C the recrystallization is complete and the deposits consist of large equassic grains with a preferential [111] orientation. The microhardness decreases by increasing the heat treatment temperature following the grain dimensions. All pure Ni deposits, both prior and after heat treatments present a good corrosion resistance. The as plated pure Ni coatings present a passive behavior with a passive current of 10^{-4} A/dm^2 and a breakdown potential at about 0,5-0,15 V. The increase of the heat treatment temperature leads to a decrease of the passive corrosion current while the breakdown potentials are all in a range from 0V to 0.15V. The decrease of the passive current density is attributed to the formation of a more stable oxide on the deposits surface after heat treatments.
The addition of 40g/L of Al micro-particles into the plating bath leads to the deposition of a composite coating with a 12.4±1.1 % wt. of Al particles distributed in an almost uniform way along the coating's thickness. The codeposition of Al micro-particles causes a reduction of the Ni columns dimensions and a slight change in the growth direction. The structural refinement is due to the interruption of the columns growth. The structural modifications caused also an increase to the microhardness of about 22% in comparison to the pure Ni. After H.T. at 600^{o}C there is a fast diffusion of Al into the metal matrix which leads to the formation of a mixed γNi and γ´Ni_3Al structure. After H.T. at 800^{o}C the diffusion of Al is almost complete and the coating consists of a substitutional solid solution of Al in the Ni matrix. The diffusion of Al hinders the recrystallization of the Ni matrix and thus the micro-composite coatings present smaller equiassic grains and maintained the preferential [100] orientation and a high microhardness.
The SKPFM analyses revealed the presence of strong galvanic couples between the Al particles and the Ni matrix for the as plated deposits. The diffusion of Al occurred after H.T. at 600°C and 800°C lead to the formation of Ni/Al phases presenting lower Volta potential differences. The potentiodynamic curves showed that the as plated deposits presents a low corrosion resistance sue to the galvanic coupling between the Al particles and the matrix. This coupling leads to the preferential dissolution of the particles and the

formation of voids which may act as preferential points for the chlorides attack of the nickel matrix, further lowering the overall resistance. After H.T. at 600°C and 800°C the corrosion resistance increases as demonstrated by the increase of the corrosion potential, the decrease of the corrosion current and the presence of a limited passive zone. The passive zone extent is lower if compared to the pure Ni deposits.
The codeposition of Al nano-particles leads to a strong grain refinement with the formation of shorter and more narrow columns. The amount of codeposited Al is about 2.7±0.1 % wt. and the particles are uniformly distributed along the coatings thickness. The structural modifications due to the incorporation of the fine particles lead to an increase of about 52% in the microhardness with respect to the pure Ni deposits. The small dimensions of the nano-particles and the more uniform distribution in comparison to the micro-composite coatings lead to an activation of the inter-diffusion at lower heat treatment temperature (400^{o}C). The fast diffusion of Al blocks the recrystallization of the Ni matrix up to 800^{o}C and all heat treated deposits maintain the fine columnar structure consisting of a solid substitutional solution of Al in the γ Ni and having a [100] preferential orientation. The preservation of the microstructure is reflected also on the deposits microhardness which remains almost stable after each heat treatment. The Volta potential differences, observed by SKPFM between the particles and the metal matrix are slightly lower in comparison to the micro-composite deposits for the as plated deposits. The H.T. lead to a further decrease of the potential differences due to the formation of a uniform solid solution of Al in the Ni matrix. This behavior was reflected to the overall corrosion resistance as demonstrated by the potentiodynamic curves. The as plated deposits present a passive behavior, but a lower extent of the passive zone if compared to the pure nickel deposits. Also in this case there is a preferential dissolution of the Al particles, which leads to a decrease of the breakdown potential. The more uniform distribution, the lower amount and the smaller dimensions of the particles allowed the formation of a passive film even if the galvanic coupling between particles and matrix is still present. The H.T. increased the corrosion resistance and lead to decrease of the passive current density.
The obtained results have been very promising by means of mechanical and protective properties of the composite coatings. On the other hand, during the preliminary research activity, a strong instability of the plating baths containing the Al particles has been observed. The dissolution of the Al particles and a consequent drop of the pH of the plating bath that occur both for the only permanence of the particles in the Ni plating bath and, mainly, for the electrochemical reaction of the deposition process does not allow to produce a high number of specimens in sequence. The production of Ni/Al deposits thus requires a high amount of Al powders and the use of “new” plating baths. For this reason, it is difficult to industrialize the process without previously “stabilizing” the particles.
For this reason the research for the production of a high temperature resistant coating, proceed with the study of a different family of Ni based coatings: Ni-B alloys with a low amount of B.

5 Ni-B galvanic coatings

5.1 Study of the Ni-B alloy plating process

The second part of the research was focused on the study of the electrodeposition of Ni-B alloy coatings.
The addition of small amounts of boron should assist the preservation of both mechanical and protective properties of Ni in a temperature range between 400°C and 500°C.
The introduction of B in the alloy enhance the mechanical properties of the coatings but the B content must be kept low in order to avoid the formation of cracks which worsen the protective properties.
To this aim the study of the plating process started with a preliminary study on laboratory scale using electroplating cells with volumes of 600 mL and 1500 mL.
Dymethylamine borane (DMAB) was used as B source in the plating bath.
Different series of coatings have been produced and characterized using two different Ni plating baths and different DMAB concentrations.
The Ni plating bath used was initially a Ni Watts plating bath, the more widely used due to its higher stability, and then the tests continued with a Ni sulfammate "High Speed" plating bath, which allows to produce thick deposits with low internal stresses.
The preliminary study has been developed producing several series of specimens in order to:

1. Identify the relation between the DMAB concentration in the plating baths and the content of B in the deposits
2. Evaluate the distribution of the B along the deposit thickness and the "topographic distribution" of B in the coatings
3. Evaluate the consumption of the DMAB during the electrodepositions
4. Investigate the influence of the pulsed current
5. Investigate the influence of the saccharin as stress reduction agent
6. Feasibility study of multilayer coatings production

The results of the characterization of the different series of coatings have been used as feedback for the optimization of the plating process. As the final goal was the industrialization of the process, the study of the plating process was finally scaled up in a galvanic pilot plant with 10L deposition tanks.
At the same time, the activity was focused on the definition of a method for the determination of the DMAB concentration in order to monitor the stability of the plating baths, its consumption during the electrodepositions and facilitate the replenishment.

5.1.1 Study of the Ni-B alloy plating process at laboratory scale and microstructural characterization

5.1.1.1 Substrate preparation and characterization of the Ni-B alloy coatings

Q panels of carbon steel have been used as substrate for the preliminary study of the Ni-B alloy plating process. The substrates, before each electrodeposition, have been pretreated following the same steps described in the paragraph *4.1.2.1.*
The B content in the Ni-B coatings was determined by Glow Discharge Optical Emission Spectroscopy (GDOES). The GDOES method allows the detection of B that can not be revealed using EDXS and gives information about the distribution along the deposit thickness. A demonstrative GDOES measurement both at full scale and zoomed at 0.1% wt. in order to see the B profile is reported in Figure 5-1.

(a) (b)

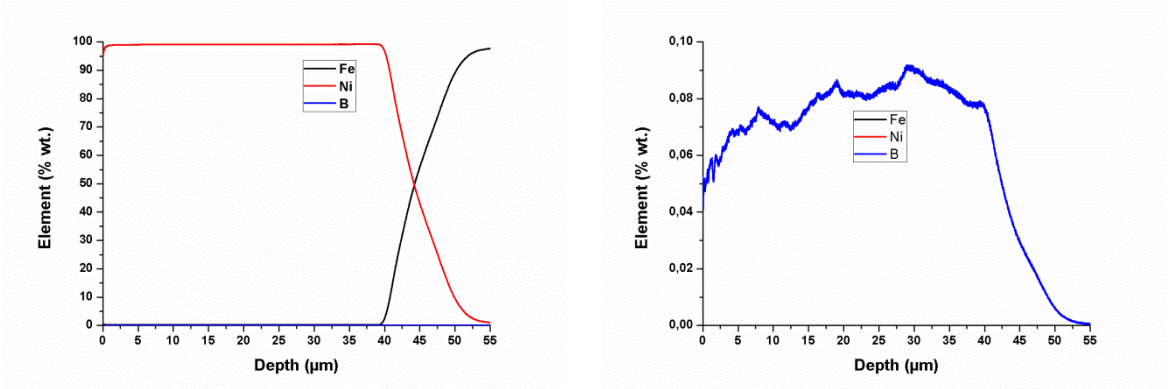

Figure 5-1: Demonstrative GDOES measurement: (a) at full scale and (b) zoom at 0.1% wt.

Selected Ni-B coatings were also observed both on top surface and in cross section, prior and after metallographic etching, by means of SEM in order to evaluate the presence of defects and the deposits microstructure.
The coating hardness has been evaluated as mean value of 15 $HV_{0.05}$ microhardness measures performed in cross section using a Struers Duramin Vickers micro-indenter.

5.1.1.2 Preliminary study with Ni Watts plating bath

Relationship between the DMAB concentration in the plating bath and the B content in the deposits

The study of the Ni-B electrodeposition process has started with the individuation of a range of DMAB concentration that allow to produce samples without macro defects.
A series of sample have been produced using Ni Watts baths in which 0.02 - 1.5 g/L of DMAB have been added. The depositions were carried out at 2 A/dm^2, optimal current density for pure Ni coatings from Watts baths. The list of the produced samples and the electrodeposition parameters are reported in Table 5-1. The images of the deposits surface are reported in Table 5-2.

Table 5-1: DMAB range - Ni Watts plating baths - Electrodeposition parameters

Sample	Bath volume	DMAB concentration	Current density	Time	Stirring	Temperature
	[mL]	[g/L]	[A/dm^2]	[min]	[rpm]	[°C]
A1	600	1.5	2	120	30	45
B1	600	0.75	2	120	30	45
C1	600	0.5	2	120	30	45
D1	600	0.3	2	120	30	45
E1	600	0.1	2	120	30	45
F1	600	0.05	2	120	30	45
G1	600	0.02	2	120	30	45
H1	600	0.01	2	120	30	45

Table 5-2: Images of the coatings surface

DMAB concentration [g/L]			
1.5 (A1)	**0.75 (B1)**	**0.5 (C1)**	**0.3 (D1)**
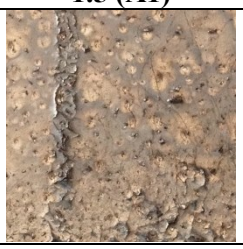			
DMAB concentration [g/L]			
0.1 (E1)	**0.05 (F1)**	**0.02 (G1)**	**0.01 (H1)**
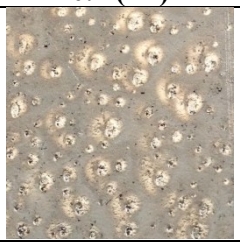		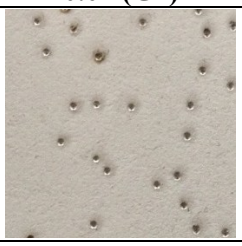	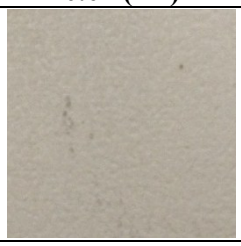

The coatings produced with concentrations in the range from 0.3 to 1.5 g/L present large cracks and blistering on the surface which lead to delamination. The coatings are very brittle indicating the presence of high residual stresses due to a high B content.
The coatings produced with DMAB concentrations in the range from 0.02 to 0.1 g/L are characterized by a marked presence of pits due to the formation of H_2 during the electrodeposition on the cathode surface. It seems that the concentration of surfactant added to the bath to help the detachment of the H_2 bubbles was not sufficient.
It can be noticed that only the samples produced with 0.01 g/L of DMAB do not present defects on the surface and the aspect is similar to that of the pure Ni coatings.
GDOES profiles of the B content along the deposits thickness are reported in Figure 5-2.

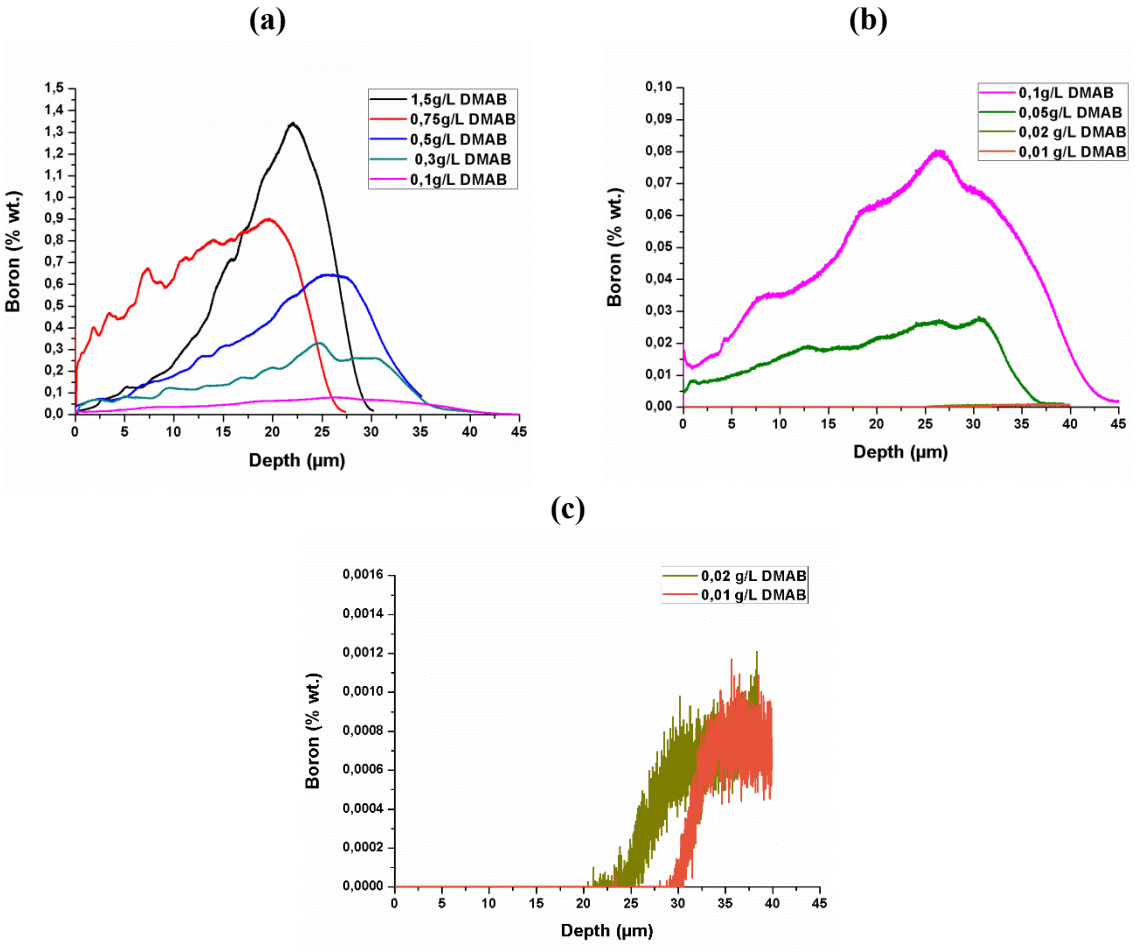

Figure 5-2: Boron content along the deposit thickness obtained with GDOES of the deposits produced with different concentration of DMAB in the plating bath: (a) range 0-1.5% wt., (b) range 0-0.1% wt., (c) range 0-0.0016% wt.

By observing the distribution of B along the deposits thickness it is possible to notice that there is a decrease from the interface, between the substrate and the coating, to the external surface of the coatings. This evidence indicates a fast decrease of the DMAB concentration during the electrodeposition using a plating bath with a volume of 600 mL and a deposition time of 120min. The B content of the deposits produced with 0.02 and 0.01g/L of DMAB is close to zero.

By organizing the data in a graph putting in relation the DMAB concentration in the plating bath and the B content at interface with the substrate (Figure 5-3) it is possible to notice that by increasing the DMAB concentration there is an almost linear increase of the B content in the deposit.

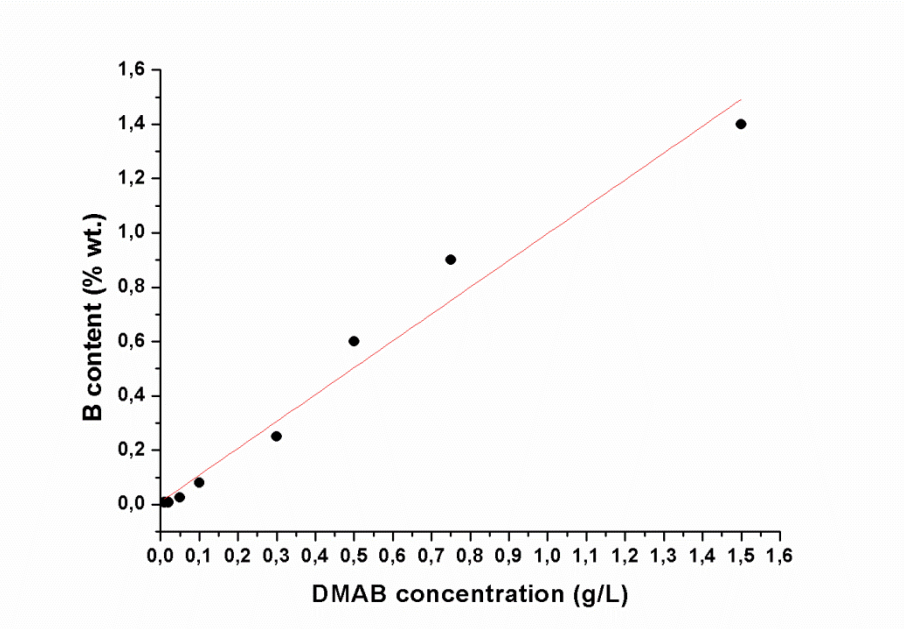

Figure 5-3: DMAB concentration in the bath vs. B content in the deposit at interface

Based on these results it was decided to proceed with the successive electrodepositions by:

- increasing the concentration of the surfactant in order to facilitate the detachment of the H_2 bubbles
- using a DMAB concentration of 0.5 and 0.3 g/L
- reducing the deposition time and carrying out sequential depositions with the same plating bath in order to investigate if the decrease of the B along the deposits thickness is due to a DMAB consumption in the bath.

Investigation of the DMAB consumption and the "spatial distribution" of B in the coatings

Three samples have been electrodeposited in sequence using the same plating baths containing 0.5 and 0.3 g/L of DMAB. The surfactant concentration has been increased to 0.4 g/L and the deposition time was reduced to 30 min. The electrodepositions performed with the plating bath containing 0.3 g/L have been carried out varying the mechanical stirrer speed.
The lists of the produced sample and the electrodeposition parameters are reported in Table 5-3 and Table 5-4. The images of the coatings series C2 and D2 surface are reported in Table 5-5.

Table 5-3: Series C2 of deposits produced with Ni Watts plating baths with 0.5 g/L of DMAB

Sample	Bath volume	DMAB concentration	Current density	Time	Stirring	Temperature	Surfactant
	[mL]	[g/L]	[A/dm^2]	[min]	[rpm]	[°C]	[mL/L]
C2-1	600	0.5	2	30	30	45	0.4
C2-2	600	0.5	2	30	30	45	0.4
C2-3	600	0.5	2	30	30	45	0.4

Table 5-4: Series D2 of deposits produced with Ni Watts plating baths with 0.3 g/L of DMAB at different mechanical stirrer speed

Sample	Bath volume	DMAB concentration	Current density	Time	Stirring	Temperature	Surfactant
	[mL]	[g/L]	[A/dm^2]	[min]	[rpm]	[°C]	[mL/L]
D2-1	600	0.3	2	30	180	45	0.4
D2-2	600	0.3	2	30	120	45	0.4
D2-3	600	0.3	2	30	60	45	0.4

Table 5-5: Images of the coatings surface of series C2 and D2

C2-1 (0.5 g/L DMAB)	C2-2	C2-3
		
D2-1 (0.3 g/L DMAB)	**D2-2**	**D2-3**
	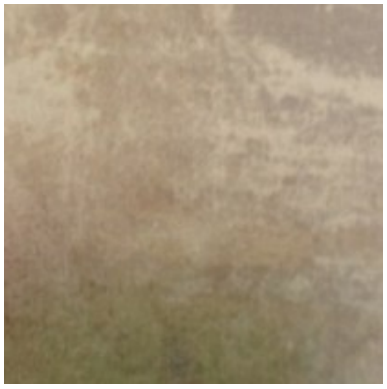	

The images show that the increase of the surfactant concentration allow to avoid the formation of pits due to the marked H_2 evolution during the electrodeposition of Ni-B deposits. The coatings are uniform and do not present macroscopic defects. The deposits have also a shiny aspect, more evident for the deposits produced with the higher concentration of DMAB.

GDOES analyses have been performed on different areas on the specimens surface as reported in Figure 5-4. These analyses were made in order to investigate the "spatial distribution" of B content on the plates surface. GDOES profiles of the B content along the deposits thickness are reported in Figure 5-5 and Figure 5-6.

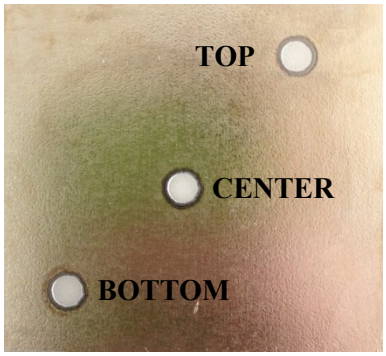

Figure 5-4: Position of the GDOES analyses

C2-1

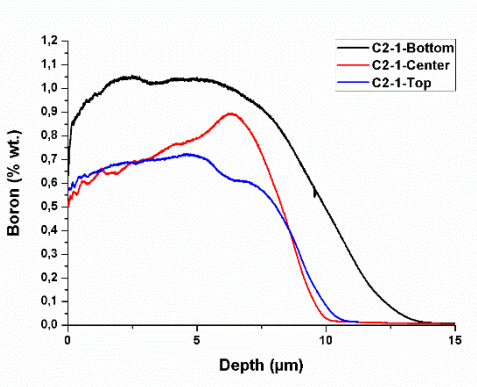

C2-2

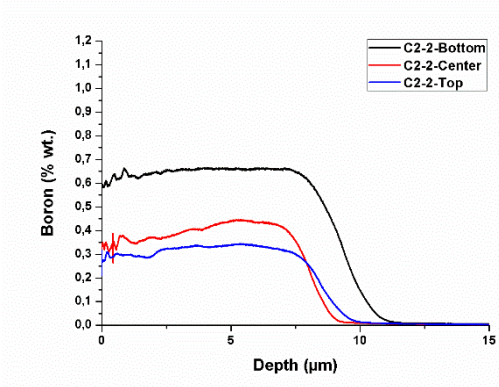

C2-3

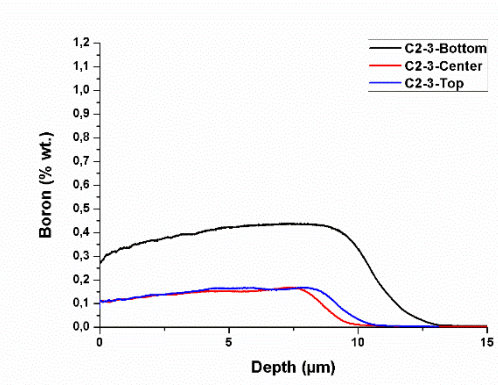

Figure 5-5: GDOES profiles of the B of the C2 series samples

D2-1 (stirring 180 rpm)

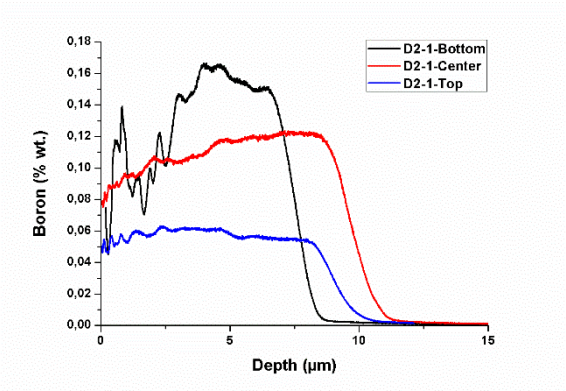

D2-2 (stirring 120 rpm)

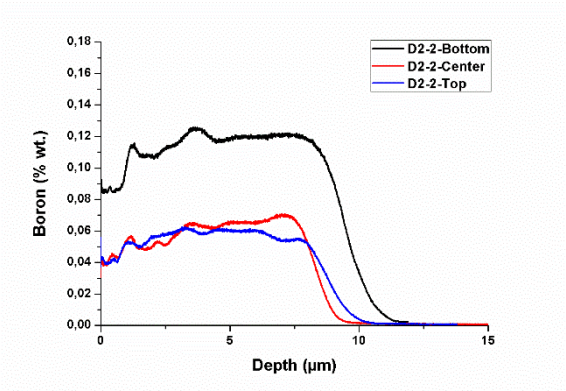

D2-3 (stirring 60 rpm)

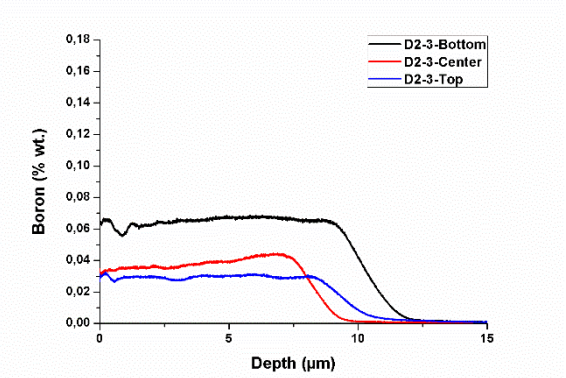

Figure 5-6: GDOES profiles of the B of the D2 series samples

The GDOES measurements of both series D2 and C2 show that the coatings produced in sequence with the same plating bath have a decreasing content of B. This indicates that there is a fast consumption of DMAB in the plating bath.
Moreover, it is noticed that the content of B at the bottom part of the samples is always higher in comparison to the content at the top part. This evidence indicates a stratification of the DMAB in the plating baths. The D2 series produced with higher stirrer speed show that an increase of the stirring of the plating bath does not allow to homogenize the "spatial distribution" of B and leads to a formation of coatings with not uniform distribution of B even along the deposits thickness.
Micrographs in top view and in cross section prior and after the metallographic etching of the samples C2-1 and D2-1 are reported in Figure 5-7 and Figure 5-8.

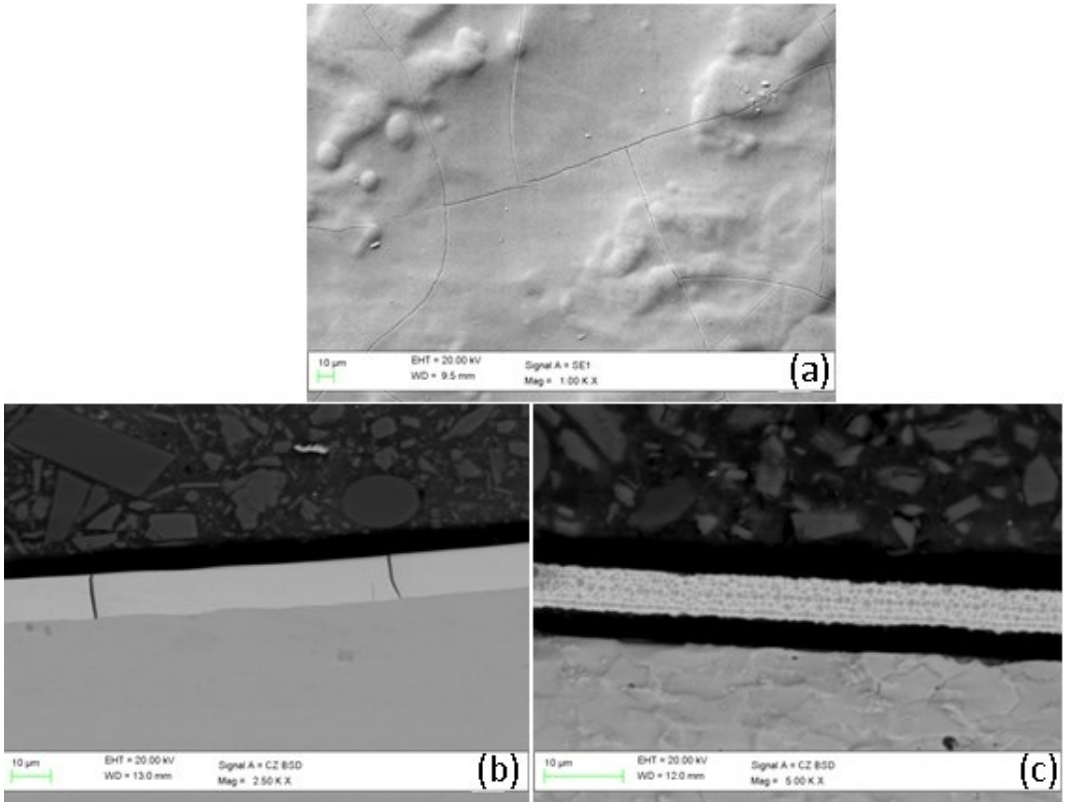

Figure 5-7: SEM micrographs of C2-1 coating: (a) top view morphology, (b)cross section and (c)cross section after metallographic etching

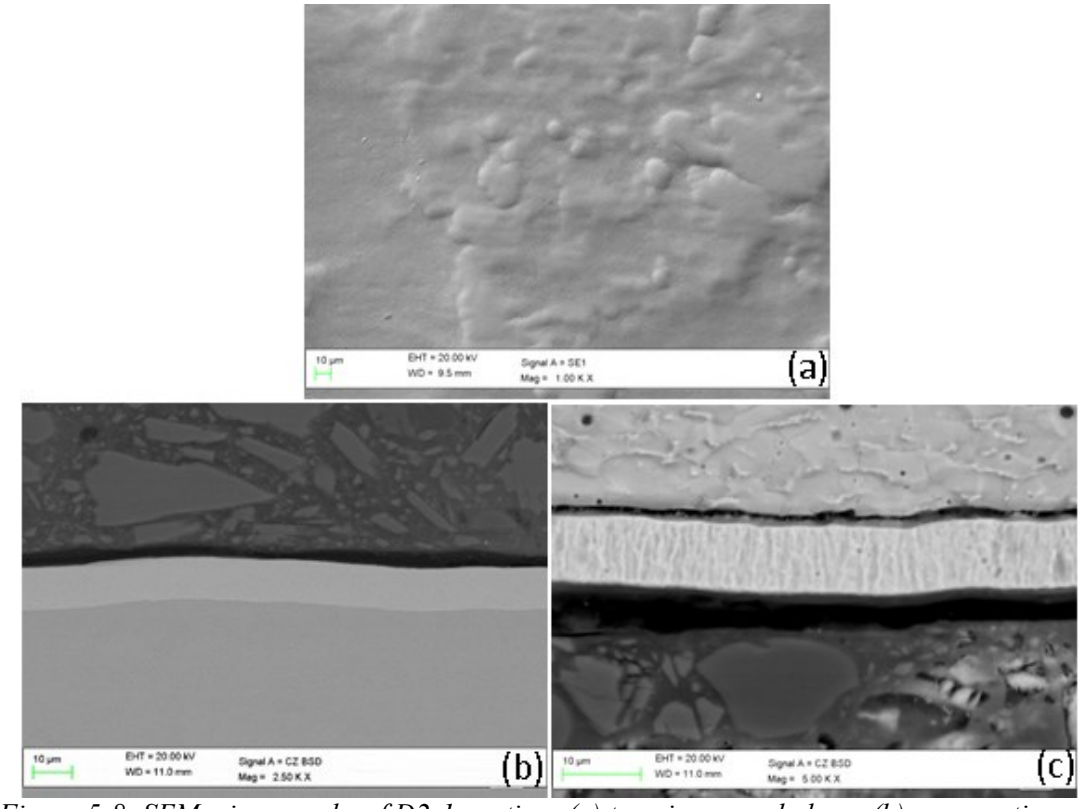

Figure 5-8: SEM micrographs of D2-1 coating: (a) top view morphology, (b)cross section and (c)cross section after metallographic etching

From the SEM micrographs above, it is possible to notice that the C2-1 coating, having a B content ten times higher in comparison to the D2-1 coating, presents a net of cracks that concern the whole deposit thickness. The metallographic etching pointed out also a very fine, nano-crystalline microstructure. The coating D2-1 instead, is compact and crack-free. The microstructure is columnar with thin columns oriented along the electrical field direction.
Based on these results it was decided to proceed with the successive series of samples:

- using the DMAB concentration of 0.3 g/L
- increasing the volume of the bath to 1500mL
- increasing the deposition time in order to produce thicker deposits

Influence of the increasing of the bath volume and deposition time

Four samples have been electrodeposited in sequence using a plating bath containing 0.3 g/L of DMAB with a volume of 1500 mL. The list of the produced samples and the electrodeposition parameters are reported in Table 5-6.

Table 5-6: Bath Series D3 of deposit produced with Ni Watts plating baths with 0.3 g/L of DMAB

Sample	Bath volume	DMAB concentration	Current density	Time	Stirring	Temperature	Surfactant
	[mL]	[g/L]	[A/dm^2]	[min]	[rpm]	[°C]	[mL/L]
D3-1	1500	0.3	2	120	30	45	0.4
D3-2	1500	0.3	2	120	30	45	0.4
D3-3	1500	0.3	2	120	30	45	0.4
D3-4	1500	0.3	2	120	30	45	0.4

GDOES profiles of the B content of the D3 series coatings are reported in Figure 5-9.

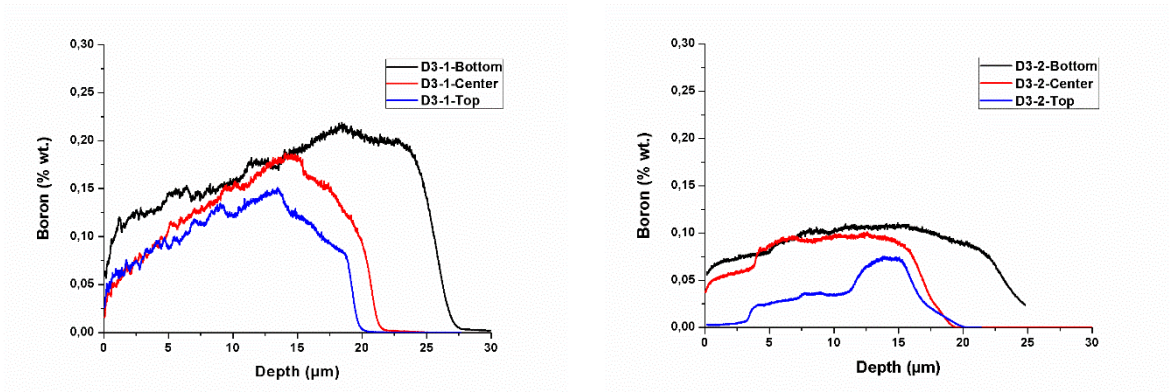

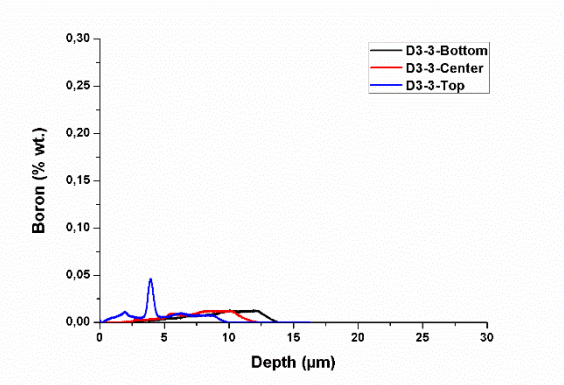

Figure 5-9: GDOES profiles of B of the D3 series coatings

The GDOES analyses show a marked decrease of the B content in the deposits after few depositions. These results indicate a fast consumption of the DMAB also using a plating bath with a volume of 1500 mL. Considering that the surface of the sample is the same used in the previous tests, the use of a bigger cell helps to reduce the differences in the distribution of the B between the bottom and the top parts of the specimens due to the stratification of the DMAB in the plating bath. The B content along the deposits thickness is decreasing but the drop is lower in comparison to the coatings produced with a 600 mL volume bath thanks to a higher total amount of DMAB.
This evidence suggests that an increase of the ratio *bath volume/coated surface* should allow to produce thick deposits with a more constant B content along the coating thickness. SEM micrographs obtained on top surface of D3-1 and D3-2 coatings (Figure 5-10) show the presence of cracks on the coating with the higher content of B. This indicates that by increasing the deposition time, and thus the deposit thickness, there is an increase of the internal stresses that leads to cracks formation even using the DMAB concentration of 0.3 g/L.

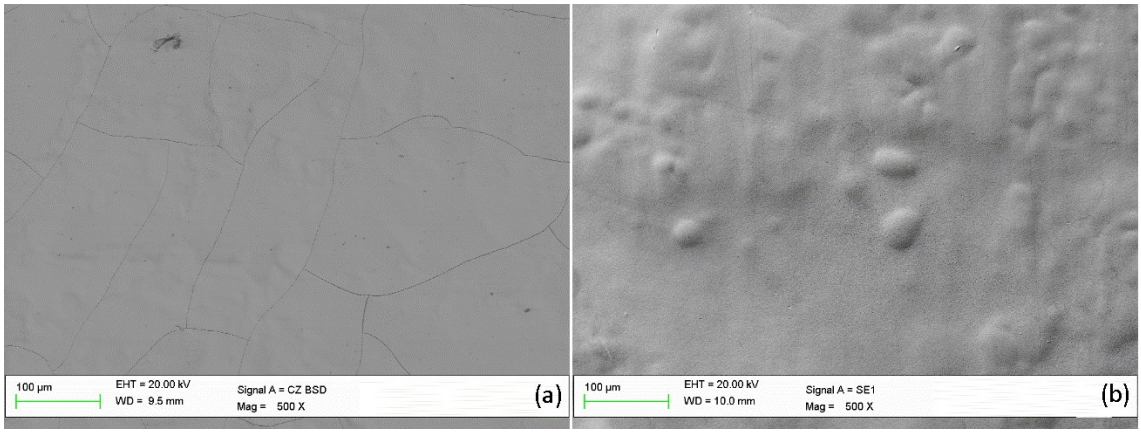

Figure 5-10: SEM micrographs of the coatings surface: (a)sample D3-1 and (b)sample D3-2

Microhardness $HV_{0.05}$ of the coatings D3-1 and D3-2 are reported in Table 5-7.

Table 5-7: Vickers microhardness $HV_{0.05}$ values of Sample D3-1 and D3-2

Sample	Mean content of B	Microhardness
	[%wt.]	[$HV_{0.05}$]
D3-1	0.14	450±16
D3-2	0.07	365±20

The microhardness values (Table 5-7) show that even a very low B content in the deposit causes a strong hardness increase.
Considering that pure Ni deposits produced by a Watts bath usually present a Vickers microhardness of about 200-230 HV, the hardness increase of the Ni-B coatings is proportional to the B content.

Pulsed current

In the following series was investigated the influence of the pulsed current. The use of the pulsed current could help to produce Ni-B coatings with low internal stresses thanks to the interruption of the deposit growth. The produced samples and the deposition parameters are reported in Table 5-8. GDOES profiles of the B content are reported in Figure 5-11.

Table 5-8: Series D4 of deposit produced with pulsed current ting baths with 0.3 g/L of DMAB

Sample	Bath volume	DMAB concentration	Current density	Time	Duty Cycle	Frequency	Surfactant
	[mL]	[g/L]	[A/dm^2]	[min]	[%]	[Hz]	[mL/L]
D4-1	1500	0.3	2	240	50	0.5	0.4
D4-2	1500	0.3	2	240	50	0.5	0.4
D4-3	1500	0.3	2	240	50	0.5	0.4

(a) (b)

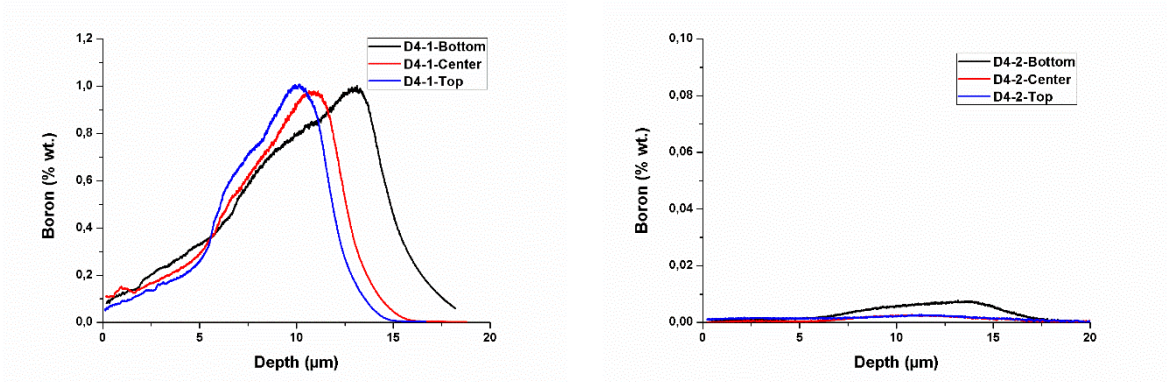

Figure 5-11: GDOES Boron profiles of the samples: (a) D4-1, (b) D4-2

The GDOES analyses show that the first coating D4-1 has a decreasing B content along the thickness with a high content of B at interface with the substrate. The B content is much higher in comparison to the coating D3-1 produced with the same parameters but under direct current. This could be attributed to a decrease of the diffusion layer thickness that allows to a higher amount of DMAB to reach the cathode in shorter time, leading to an increase of the deposited B at the first microns off the coating and hence to a faster

decrease of the DMAB in the plating bath. In fact, the very low B content of the second specimen indicates that the reagent is practically finished.
It was also noticed a decrease of the overall deposit thickness, even if the overall charge is the same as in the D3-1 deposit.
The higher amount of DMAB reaching the cathode surface interferes with the electrocrystallization and growth rate of the Ni deposit.

Effect of the Saccharin

As the pulsed current leads to strongly dishomogeneous deposits a second attempt to reduce the internal stresses was made by adding saccharin to the plating bath as a stress reduction agent.
Three series of sample have been produced in order to investigate the effect of a stress reduction agent on the microstructure of the Ni-B coatings. Two Ni Watts plating baths with concentration of 0.1 g/L (bath L) and 0.2 g/L (bath E) of DMAB have been prepared with and without adding saccharin ($C_7H_5NO_3$) in a concentration of 0.2 g/L. Two Ni-B coatings have been produced in sequence with each plating bath. In order to understand the only effect of the saccharin, two samples of pure Ni have been produced as references using Ni Watts plating baths with and without saccharin.
The lists of the produced coatings and the deposition parameters are reported in Table 5-9, Table 5-10 and Table 5-11 and the images of the samples surface are reported in Figure 5-12.

Table 5-9: Pure Ni deposit produced with Ni Watts plating baths without and with 0.2 g/L Saccharin

Sample	Bath volume	DMAB concentration	Saccharin concentration	Current density	Time
	[mL]	[g/L]	[g/L]	[A/dm^2]	[min]
Pure Ni	1500	-	-	2	120
Pure Ni-Sac	1500	-	0.2	2	120

Table 5-10: Saccharin effect - Electrodeposition parameters E2 and E3sac series coatings

Sample	Bath volume	DMAB concentration	Saccharin concentration	Current density	Time
	[mL]	[g/L]	[g/L]	[A/dm^2]	[min]
E2-1	1500	0.1	-	2	120
E2-2	1500	0.1	-	2	120
E3sac-1	1500	0.1	0.2	2	120
E3sac-2	1500	0.1	0.2	2	120

Table 5-11: L2 and L3sac series coatings without and with 0.1 g/L of Saccharin

Sample	Bath volume	DMAB concentration	Saccharin concentration	Current density	Time
	[mL]	[g/L]	[g/L]	[A/dm^2]	[min]
L2-1	1500	0.2	-	2	120
L2-2	1500	0.2	-	2	120
L3sac-1	1500	0.2	0.2	2	120
L3sac-2	1500	0.2	0.2	2	120

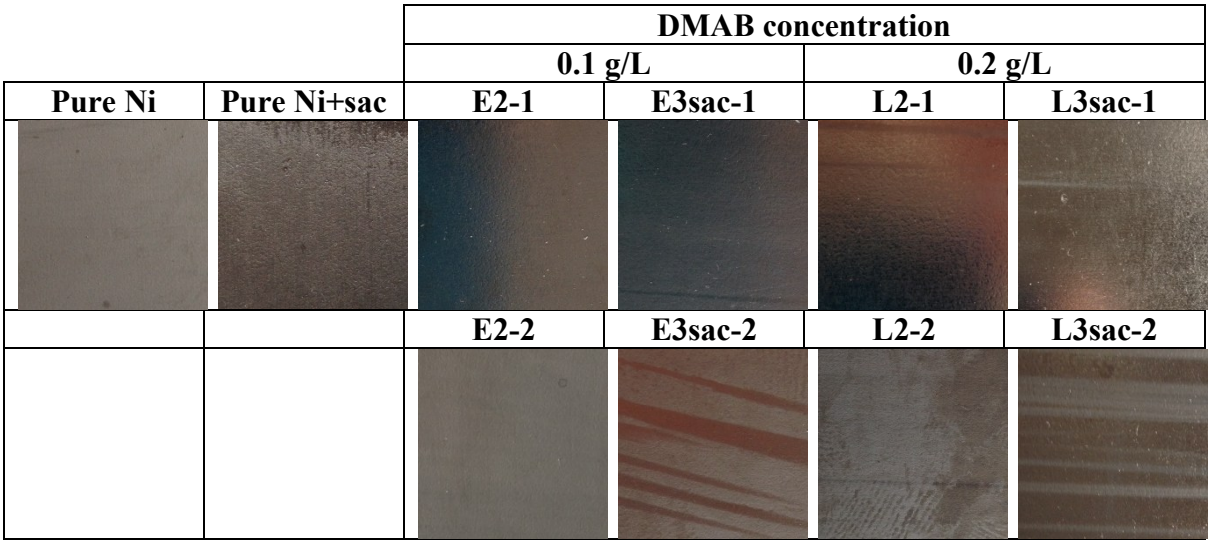

Figure 5-12:Images of the coatings surface of the series produced with and without saccharin.

All the specimens are uniform, without macroscopic defects. The first sample produced with each plating bath (E2-1, E3sac-1,L2-1, L3sac-1) is more glossy than the second sample produced with the same bath. The addition of saccharin seems also to increase the gloss of the deposits. The glossy aspect is correlated either to the higher amount of B or to the presence of saccharin indicating usually a finer microstructure.
The Boron GDOES profiles along the deposit thickness are reported in Figure 5-13 and Figure 5-14. A graph showing the relation between the mean B content and the DMAB concentration for the Ni-B coatings produced either with or without saccharin is reported in Figure 5-15.

(a)

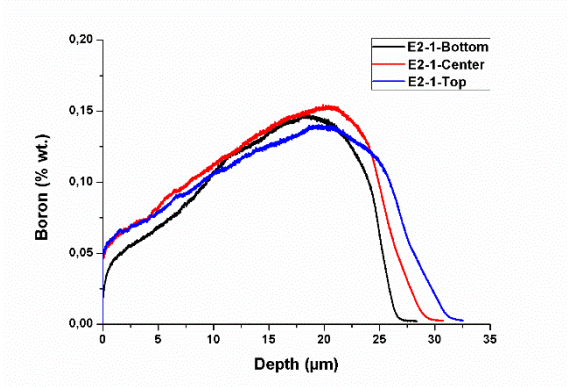

(b)

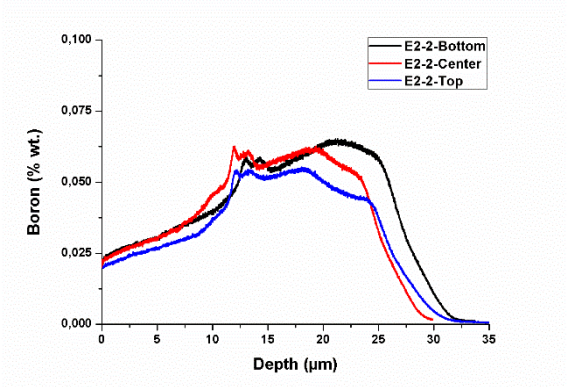

(c) (d)

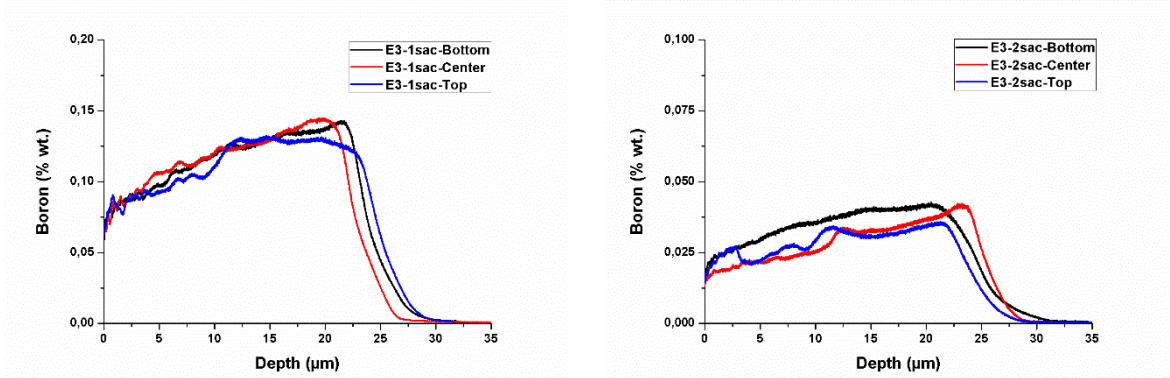

Figure 5-13: GDOES Boron profiles of samples without saccharin E2-1 (a) and E2-2 (b) and with saccharin E3sac-1 (c) and E3sac-2 (d)

(a) (b)

(c) (d)

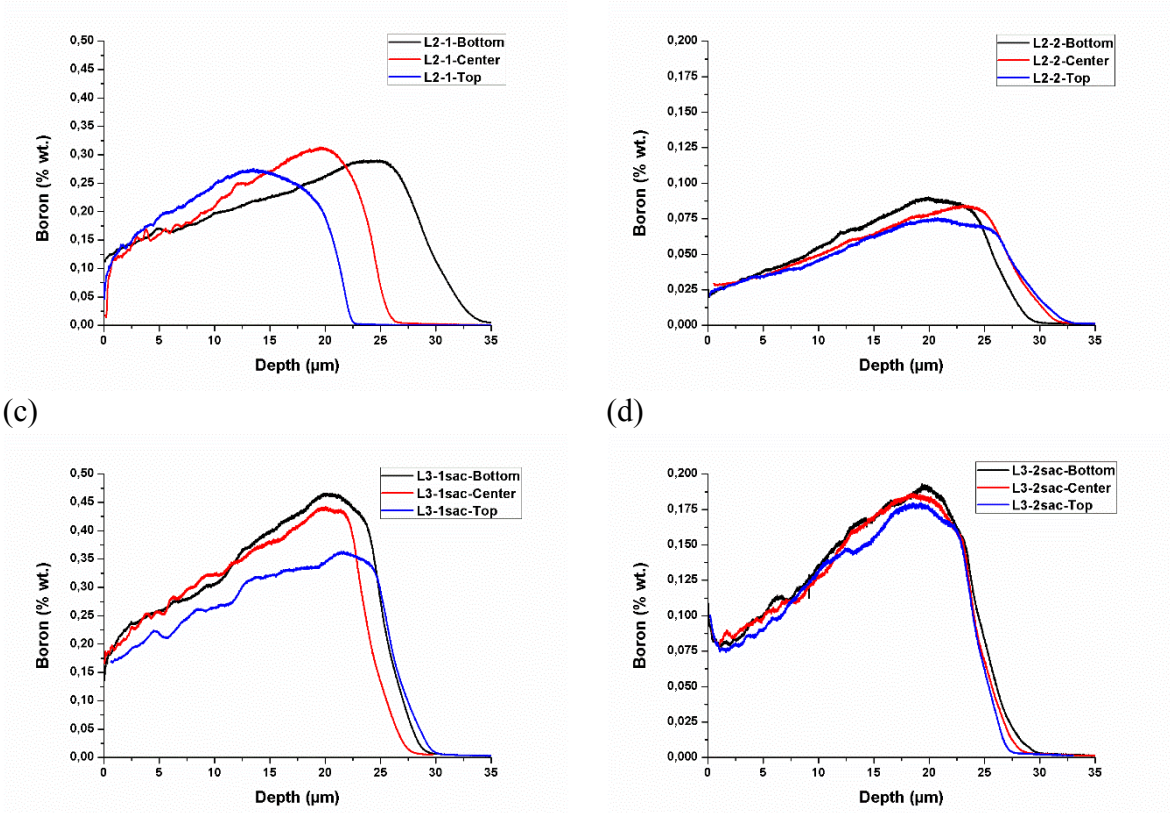

Figure 5-14: GDOES Boron profiles of samples without saccharin L2-1 (a) and L2-2 (b) and with saccharin L3sac-1 (c) and L3sac-2 (d)

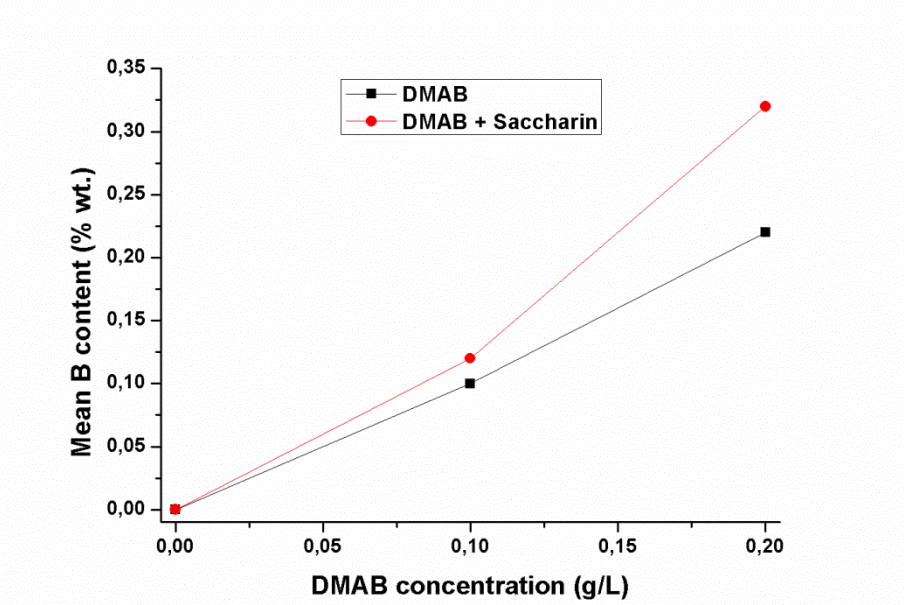

Figure 5-15: Mean B content vs. DMAB concentration for the first samples produced with Ni plating bath without and with Saccharin

The GDOES analyses show that all deposits present a B content which decreases by increasing the thickness.
The second deposits produced with each plating bath show a B content at the interface with the substrate equal to the B content at the external surface of the first samples indicating a linear decrease of the DMAB concentration in the baths by increasing the deposition time.
The addition of saccharin does not seem to influence particularly the B content at least for the lower concentration of DMAB.
As can be seen by Figure 5-15 there is a slight increase of the mean B content for the specimen produced with baths coating 0.2g/L of DMAB by using saccharin.
The micrographs in top view and in cross section after metallographic etching of the samples are reported in Figure 5-16, Figure 5-17 and Figure 5-18.

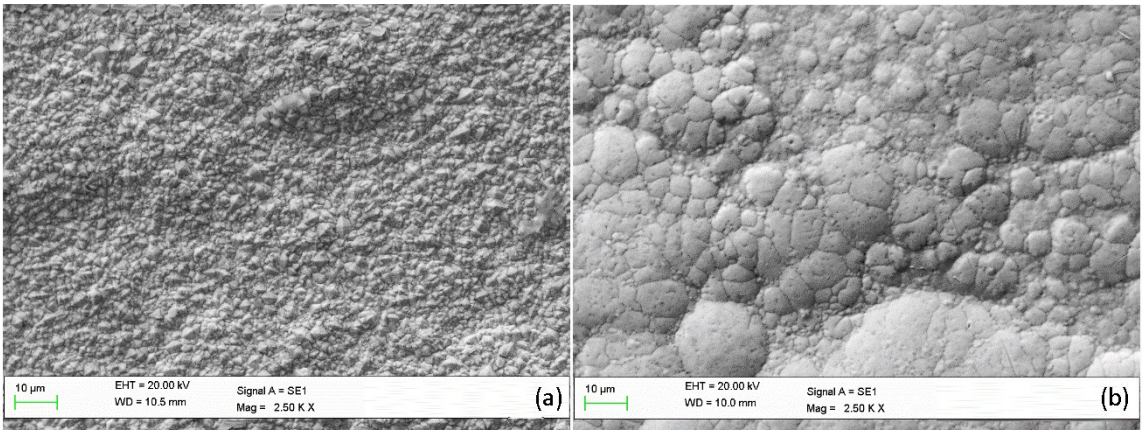

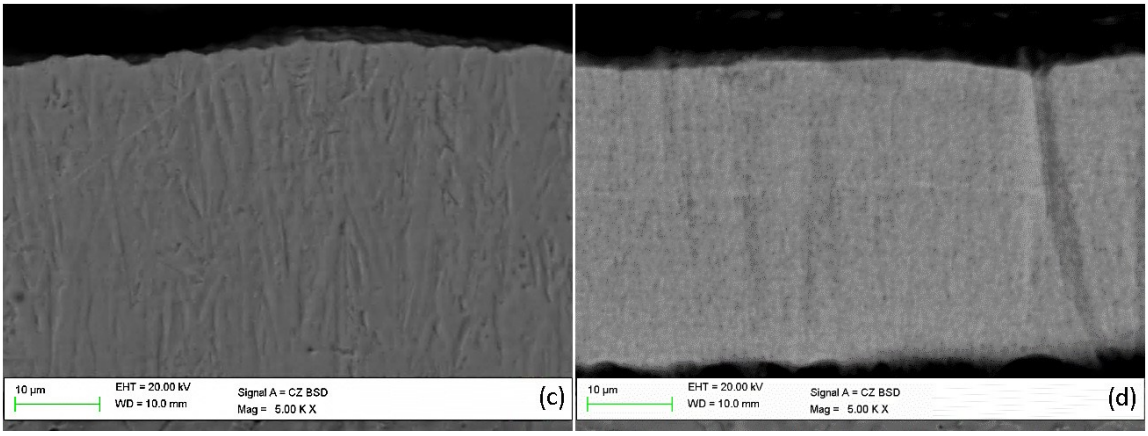

Figure 5-16: SEM micrographs in top view and in cross section after metallographic etching of pure Ni deposit produced without (a and c) and with saccharin (b and d)

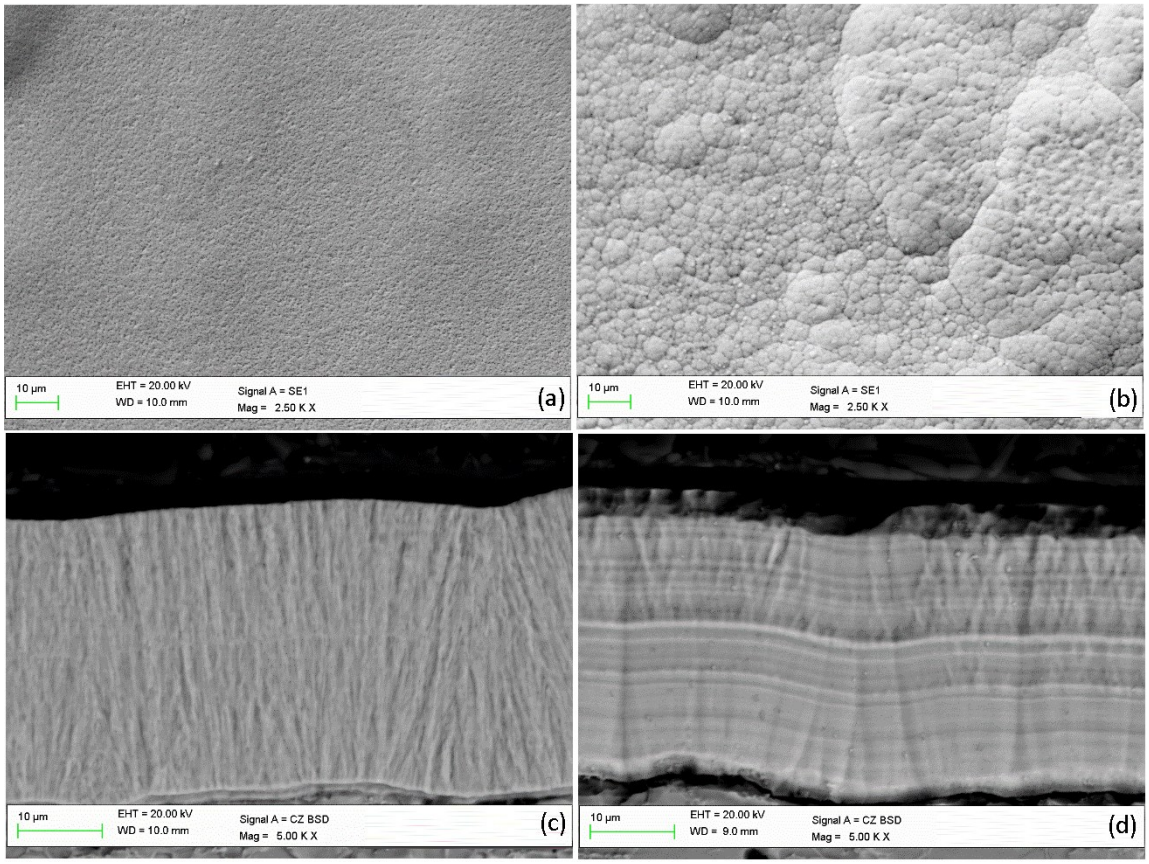

Figure 5-17: SEM micrographs in top view and in cross section after metallographic etching of deposits E2-1 (a and c) and E3sac-1 (b and d)

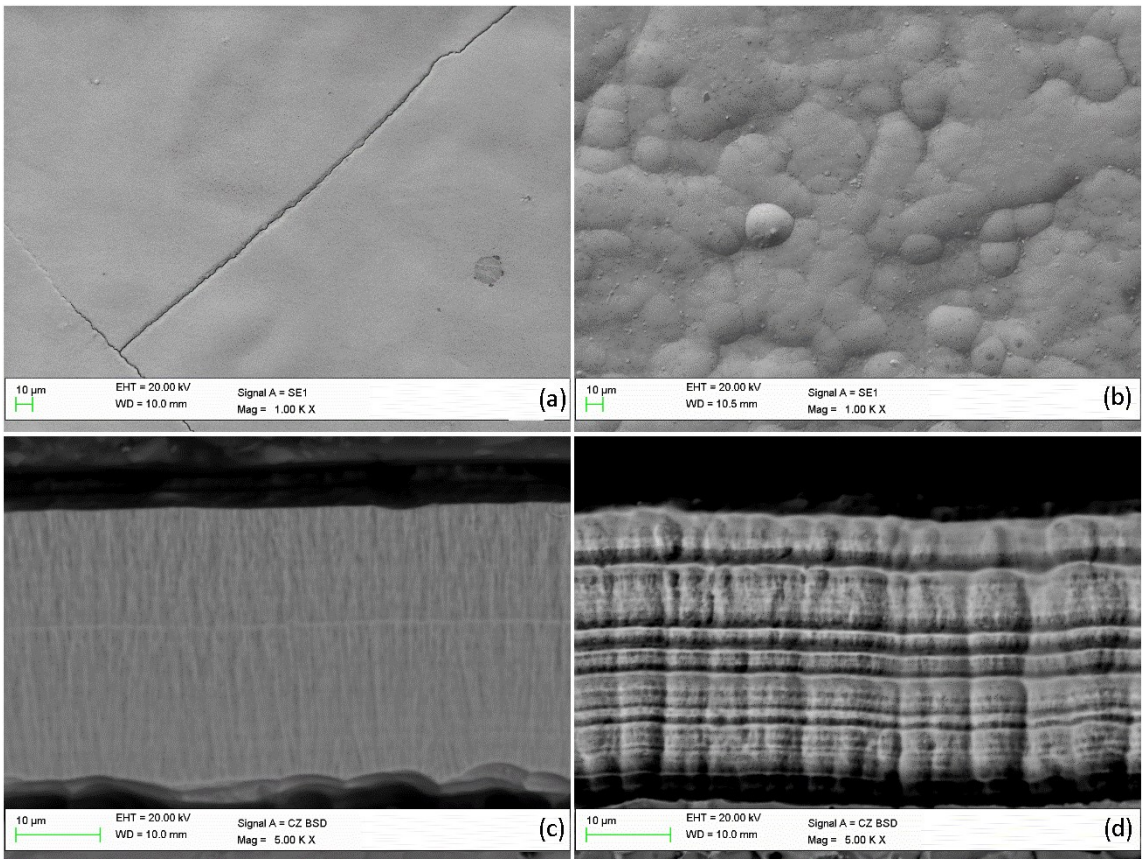

Figure 5-18: SEM micrographs in top view and in cross section after metallographic etching of deposits L2-1 (a and c) and L3sac-1 (b and d)

The addition of saccharin in the Ni Watts plating bath leads to a production of pure Ni deposit with a marked fine microstructure. The top view morphology changes from "pyramidal" to "cauliflower" and the cross section microstructure from columnar to a mixed columnar-lamellar structure (Figure 5-16). The Ni-B deposits E2-1 and L2-1, produced without saccharin ((a) and (c) in Figure 5-17 and Figure 5-18) are nano-crystalline with a very fine columnar structure. The higher the B content, the narrower the columns width. The top view observation showed also that the coating produced with 0.2 g/l of DMAB presents a net of cracks, while the coatings produced with 0.1 g/L of DMAB is free of cracks. Both Ni-B coatings produced with saccharin ((b) and (d) in Figure 5-17 and Figure 5-18) present a lamellar microstructure and no cracks have been observed on the surfaces of the samples. The microhardness values of the coatings are reported in Table 5-7 and a graph correlating the mean B content in the deposits and the hardness of the coatings produced with and without saccharin is reported in Figure 5-19:.

Table 5-12: Vickers microhardness $HV_{0.05}$ values of Sample D3-1 and D3-2

Sample	Mean content of B	Microhardness	Sample	Mean content of B	Microhardness
	[%wt.]	[$HV_{0.05}$]		[%wt.]	[$HV_{0.05}$]
Pure Ni	**-**	**204 ± 12**	**Pure Ni + sac**	**-**	**481 ± 7**
E2-1	**0.1**	**446 ± 10**	**E3sac-1**	**0.12**	**652 ± 17**
E2-2	**0.05**	**342 ± 9**	**E3sac-2**	**0.035**	**572 ± 17**
L2-1	**0.22**	**625 ± 16**	**L3sac-1**	**0.32**	**852 ± 33**
L2-2	**0.07**	**402 ± 11**	**L3sac-2**	**0.13**	**661 ± 30**

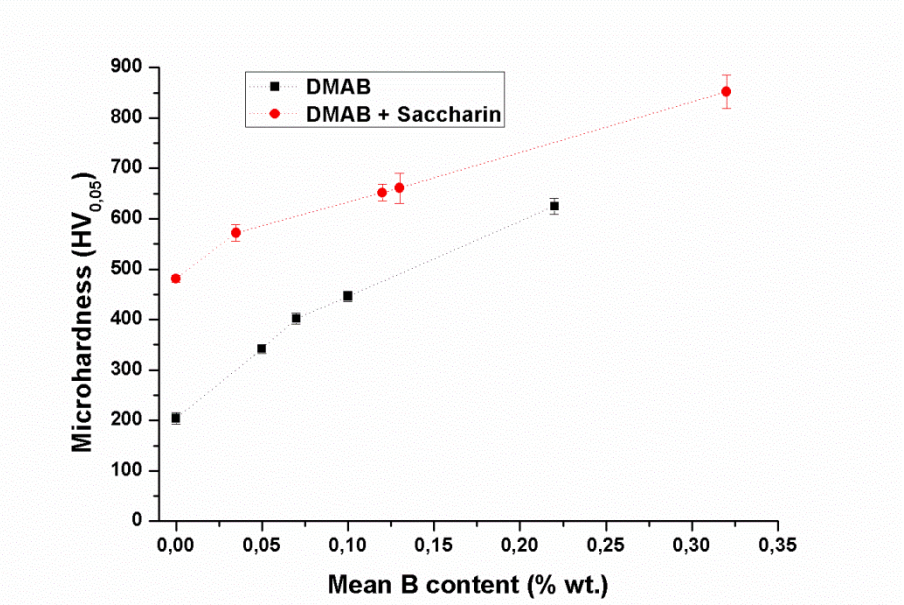

Figure 5-19: Relation between the mean B content in the deposits and the microhardness of the Ni-B coatings produced with and without saccharin.

By observing the graph it is possible to notice that both pure Ni and Ni-B coatings, produced with baths containing saccharin, present a higher hardness in comparison to the coatings produced without the stress reduction agent. This increase of hardness follow the microstructure refinement caused by the saccharin. Also the Ni-B coatings produced with saccharin show an increase of the hardness by increasing the B content, but the increase is more moderated.

The saccharin is one of the possible stress reduction agent that in combination with DMAB could be used in order to produce deposits with higher content without cracks.
To do so, the concentration of saccharin should remain constant during the deposition.
The stress reducers generally are consumed by drag out, hence it is difficult to control the concentration, especially in industry where the dimensions of parts to be coated are big.
Furthermore, as reported by J. Matovic and D. Mockute et al., the organic stress-reducers usually incorporate sulphur into the Ni deposits during the plating process[1,2].
This is an issue for the coatings that have to work at high temperature.
Indeed the incorporation of even small amounts of sulphur leads to a deposit embrittlement when the working temperature is above 200°C.
For this reason, even if the saccharin could be a candidate for the production of crack free Ni-B deposits with higher B content, it was decided to continue the study without using stress reduction agents.

[1] J. Matovic, Proc. IMechE Part C: J. Mechanical Engineering Science 220 (2006), 1645-1654
[2] D. Mockute, G. Bernotiene, R. Vilkaite, Surface and Coatings Technology 160 (2002) 152–157

Multilayer deposits

Another method that could be used in order to increase the overall deposit thickness without risking the formation of cracks is to deposit different layers forming a multilayer coating. This method could also help to obtain a more uniform distribution of the B in the deposit if new or replenished plating baths are used. A series of specimens have been produced using two DMAB concentrations, 0.1 and 0.08 g/L, and carrying out three sequential depositions on the same sample using new plating baths for each layer. The introduction of an intermediate step of acid etching (50% HCl) between the sequential depositions was also tested in order to increase the adhesion between the different Ni-B layers. The influence of the current density was also investigated.
The lists of the produced specimens are reported in Table 5-13 and Table 5-14 and the images of the coatings surface are reported in Figure 5-20 and Figure 5-21.

Table 5-13: Multilayer deposits produced with and without intermediate acid pickling

Sample	Bath volume	DMAB concentration	Current density	Time	Acid pickling
	[mL]	[g/L]	[A/dm^2]	[min]	[min]
E4-1	1500	0.1	2	3x60	-
E5-1	1500	0.1	2	3x60	10
I1-1	1500	0.08	2	3x60	-
I2-1	1500	0.08	2	3x60	10

Table 5-14: Multilayer deposits produced with different current density

Sample	Bath volume	DMAB concentration	Current density	Time	Acid pickling
	[mL]	[g/L]	[A/dm^2]	[min]	[min]
I3-1	1500	0.08	1.5	3x60	10
I4-1	1500	0.08	2	3x60	10
I5-1	1500	0.08	2.5	3x60	10

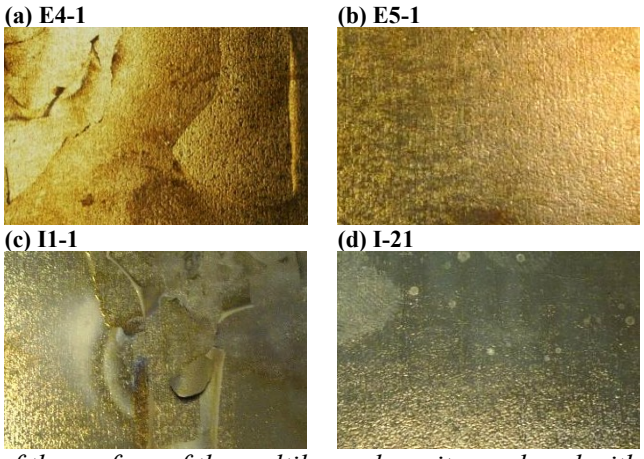

Figure 5-20: Images of the surface of the multilayer deposits produced without (a and c) and with (b and c) intermediate acid etching

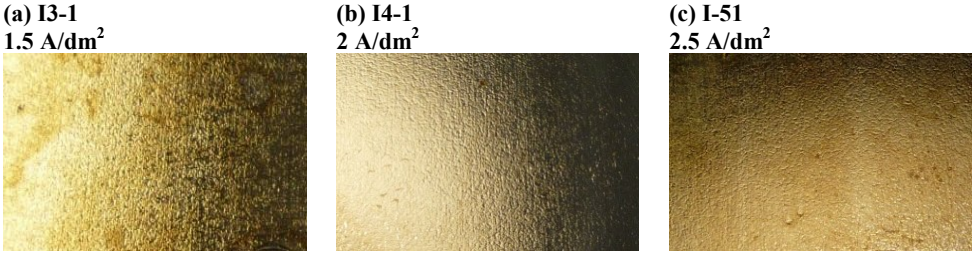

Figure 5-21: Images of the surface of the multilayer deposits produced with different current density: (a)1.5 A/dm^2, (b) 2 A/dm^2 and (c) 2.5 A/dm^2

By observing the images in Figure 5-20 it is possible to notice a strong delamination at the interface between the Ni-B layers (a and c in Figure 5-20).
This could be attributed to the formation of the Ni oxides passive film on the coatings surface immediately after the extraction from the plating bath. This thin oxide layer does not allow the adhesion of the successive deposit. The coatings produced with the intermediate step of acid etching do not present any adhesion problem. The multilayer deposition, therefore, is possible but requires an intermediate acid etching between the Ni-B layers.
GDOES analyses have been performed on the undamaged areas in the center of the deposits. GDOES boron profiles are reported in Figure 5-22 and Figure 5-23.

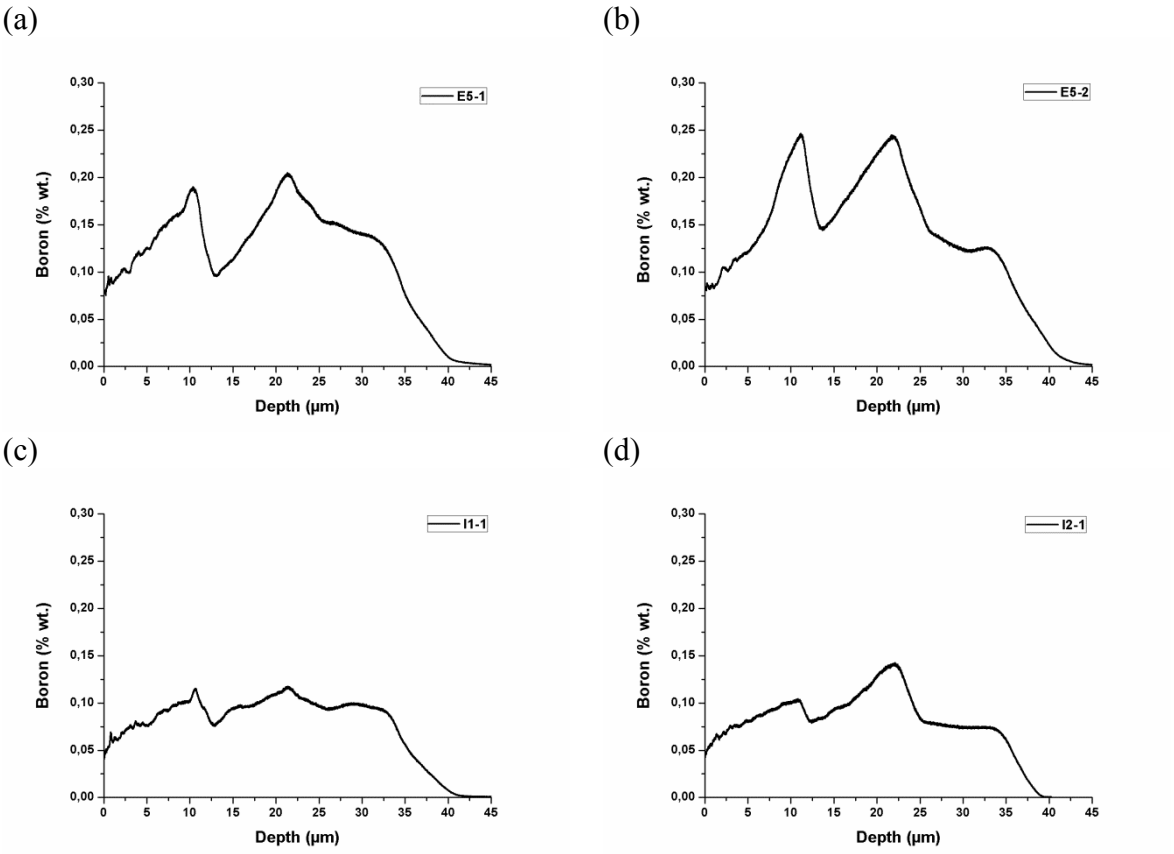

Figure 5-22: GDOES boron profiles of the multilayer deposits produced with (a and c) and without (b and d) intermediate acid pickling

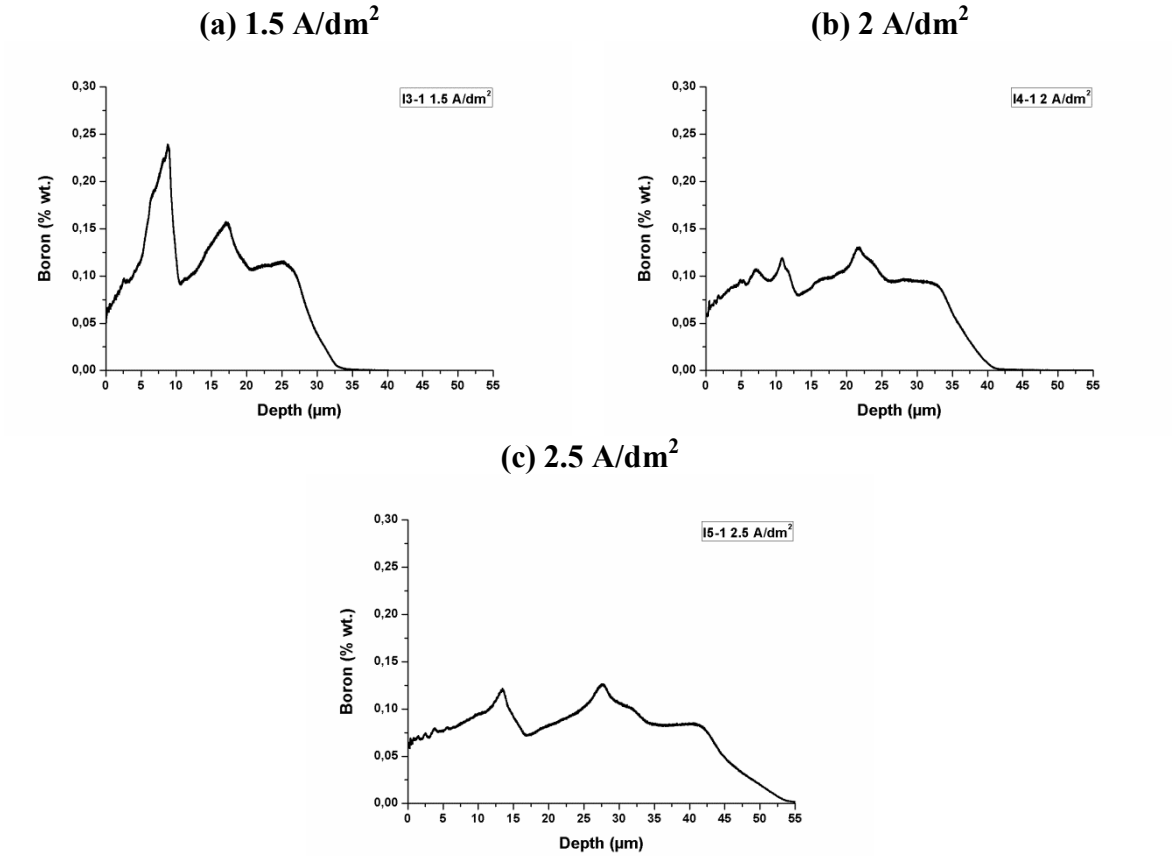

Figure 5-23: GDOES Boron profiles the multilayer deposits produced with different current density: (a)1.5 A/dm^2, (b) 2 A/dm^2 and (c) 2.5 A/dm^2

The GDOES analyses in Figure 5-22 show that the multilayer deposits produced with and without acid etching present similar distributions of B along the deposit thickness.
The GDOES analyses in Figure 5-23 show that by decreasing the current density there is a decrease of the deposit thickness but the B content in the deposits increases.
The same trend was also observed by other researcher[3].
The SEM micrographs of the produced deposits in cross section after metallographic etching are reported in Figure 5-24 and Figure 5-25.

[3] K. Krishnaveni, T.S.N. Sankara Narayanan, S.K.Seshadri, Materials Chemistry and Physics 99 (2006) 300-308

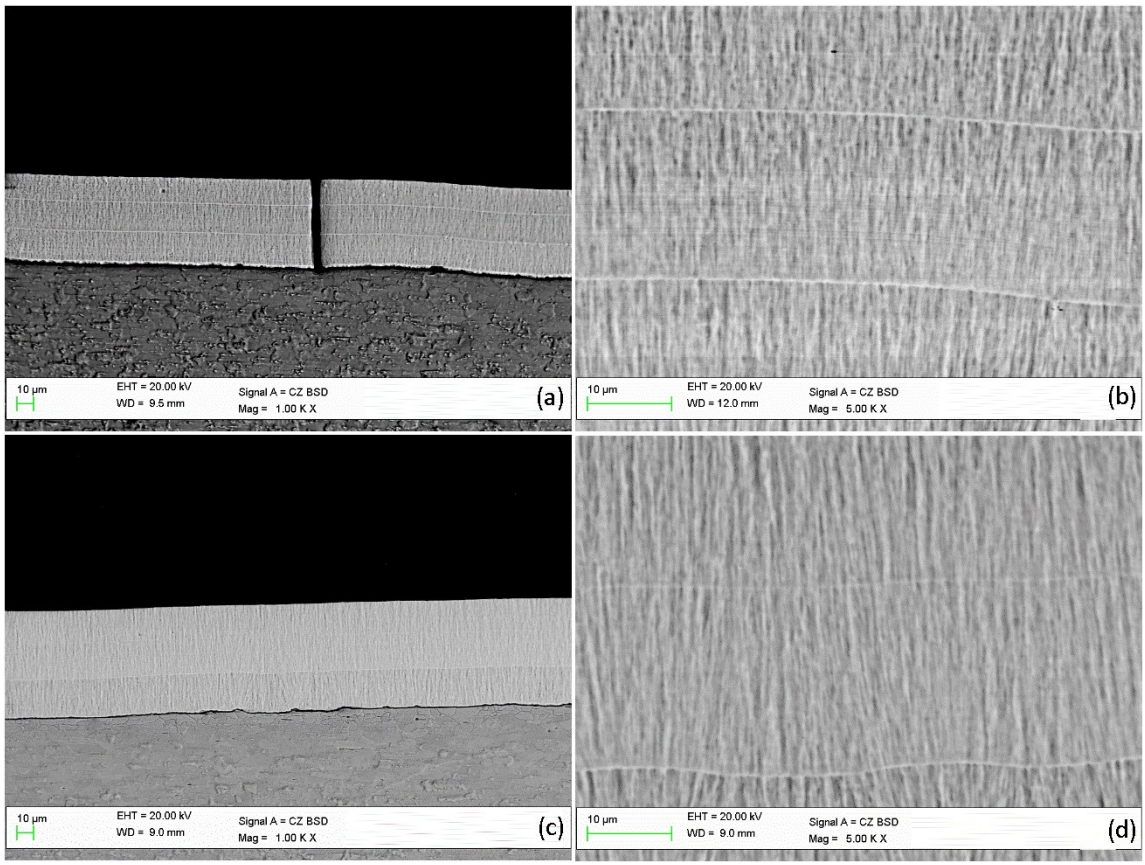

Figure 5-24: SEM micrographs in cross section after metallographic etching of the multilayer coatings: E5-2 produced with 0.1 g/L of DMAB (a and b) and E5-2 produced with 0.08 g/L of DMAB (c and d)

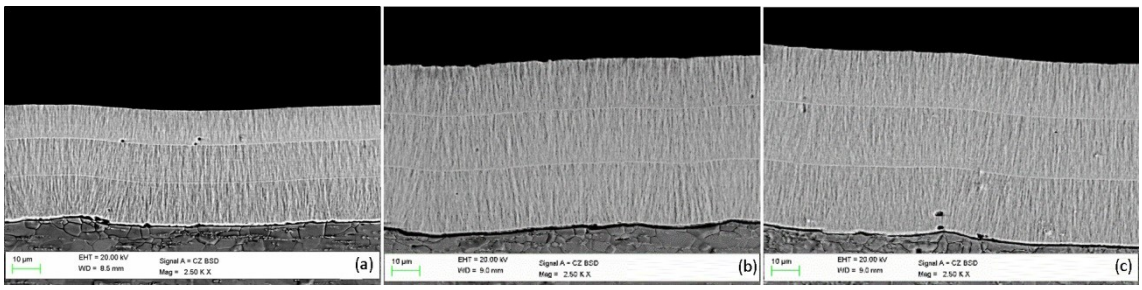

Figure 5-25: SEM micrographs in cross section after metallographic etching of the coatings produced with different current density: (a)1.5 A/dm^2, (b) 2 A/dm^2 and (c) 2.5 A/dm^2

The SEM micrographs show that the microstructure of all deposits is columnar with thin columns oriented along the electrical field direction. The multilayer coating produced with 0.1 g/L of DMAB (Figure 5-24-a-b), which has the higher content of B, presents cracks that concern the whole deposit thickness. All deposits produced with 0.08 g/L of DMAB do not present cracks (Figure 5-24-c-d and Figure 5-25-c-d) even if the B content is high for the coating produced at low current density. Observing the micrographs in Figure 5-25 it is possible to notice the increase of the deposits thickness by increasing the current density.

The microhardness values of the produced coatings are reported in Table 5-15.

Table 5-15 Vickers microhardness $HV_{0.05}$ values of multilayer coatings

Sample	Microhardness
	[$HV_{0.05}$]
E4-1	460 ± 16
E5-1	487 ± 18
I1-1	424 ± 11
I2-1	430 ± 13
I3-1	435 ± 22
I4-1	427 ± 12
I5-1	421 ± 13

The microhardness of the multilayers coatings is strictly correlated to the B content. The higher the B content, the higher the grain refinement and the microhardness of the deposits.

5.1.1.3 Preliminary study with Ni Sulfammate "High speed" bath

First series with plating bath volume of 600mL

Extensive bibliographic research revealed the lack of publications on the production of Ni-B coatings using Ni sulfammate plating baths.
The lower internal stresses of the pure Ni deposits produced with Ni sulfammate "High Speed" plating baths in comparison to the deposits produced with Ni Watts plating baths lead us to investigate the feasibility of the production of Ni-B using Ni sulfammate plating bath. Based on the results obtained with the Ni Watts plating bath, the study started with the production of a series of coatings using a 600mL bath volume and using three DMAB concentration of 0.05 g/L, 0.1 g/L and 0.15g/L. The produced coatings and the electrodeposition parameters are reported in Table 5-16.

Table 5-16: Lists of sample produced with Ni sulfammate "High speed" baths of 600mL

Sample	Bath volume	DMAB concentration	Current density	Time	Stirring	Temperature	Surfactant
	[mL]	[g/L]	[A/dm^2]	[min]	[rpm]	[°C]	[mL/L]
Ms	600	0.05	4	60	30 rpm	45	0.4
Es	600	0.1	4	60	30 rpm	45	0.4
Ls	600	0.15	4	60	30 rpm	45	0.4

All the deposits are uniform, without macroscopic defects. By increasing the DMAB concentration the coatings became more glossy.

The GDOES boron profiles are reported in Figure 5-26.

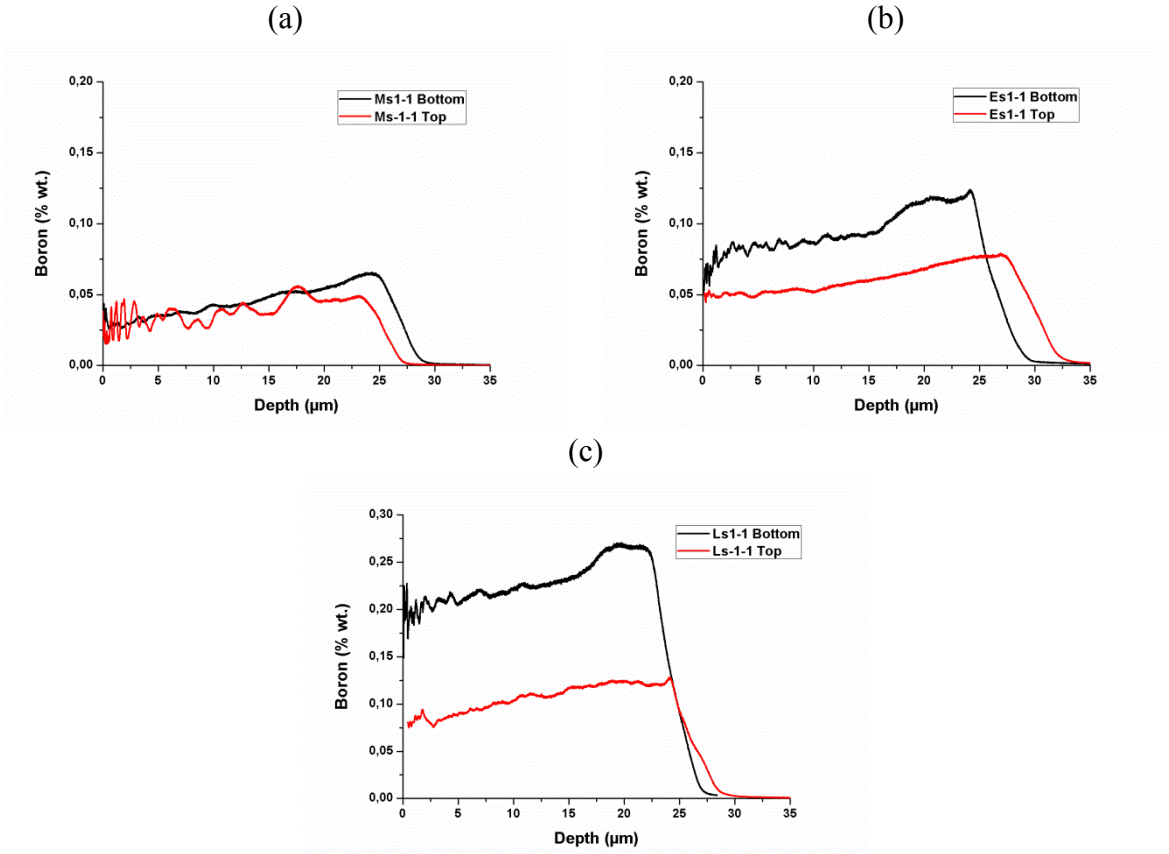

Figure 5-26: GDOE Boron profiles of the Ni-B deposits produced with Ni sulfammate "High speed" bath of 600 mL volume

The GDOES analyses show that the B content in the deposits increased by increasing the DMAB concentration in the baths. By increasing the deposit thickness it is possible to notice a decrease of the B content due to the consumption of the DMAB in the plating bath. Comparing the results obtained with Ni watts plating bath it is clear that, using the same DMAB concentration, the coatings produced with Ni sulfammate bath have a lower content of B. This fact could be related to the different mechanism of electrodeposition of the two Ni plating baths. The process, in the case of Ni Watts plating bath, is under charge transfer control, instead in the case of Ni sulfammte bath, the slower step that controls the electrodepostion process is the diffusion. A thicker diffusion layer could slow down the deposition of B.
The Ni-B deposits, especially those produced with higher concentration of DMAB, present noticeable differences in the content of B between the bottom and the top part indicating that, also with Ni sulfammate baths, there is a stratification of the reagent.
The SEM micrographs of the deposit in cross section after metallographic etching and in top view are reported in Figure 5-27.

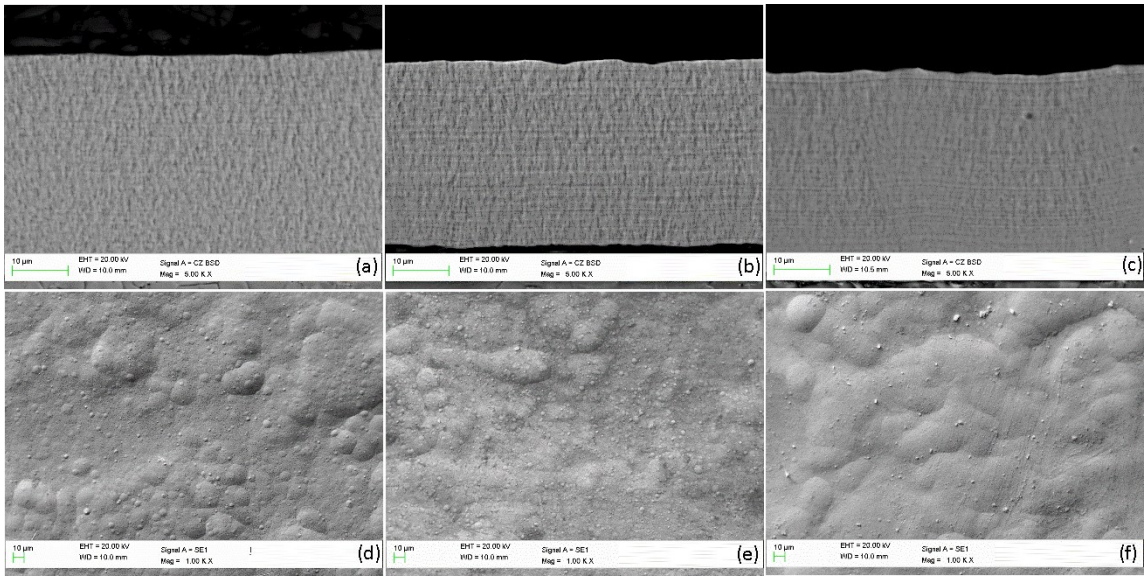

Figure 5-27: SEM micrographs in cross section after metallographic etching and in top view of the coatings produced with: (a and d) 0.05 g/L, (b and e) 0.1 g/L and (c and f) 0.15 g/L of DMAB

All the deposits are compact and cracks free and the top view analyses show a "cauliflower" morphology. The coatings have a nanocrystalline structure and the microstructure changes from a very fine columnar structure to a mixed columnar-lamellar one. Based on these results it was decided to increase the electrolyte volume to 1500mL, extend the DMAB concentrations range and increase the deposition time.

Second series with plating bath volume of 1500mL

A pure Ni deposit and five Ni-B deposits have been produced with a volume bath of 1500mL and concentrations of DMAB up to 0.25 g/L.
The list of the produced samples and the deposition parameters are reported in Table 5-17 and the images of the coatings surface are reported in Figure 5-28.

Table 5-17: Lists of sample produced with Ni sulfammate "High speed" baths of 1500mL

Sample	Bath volume	DMAB concentration	Current density	Time	Stirring	Temperature	Surfactant
	[mL]	[g/L]	[A/dm^2]	[min]	[rpm]	[°C]	[mL/L]
Pure Ni	1500						
Ms	1500	0.05	4	120	none	45	0.4
Es	1500	0.1	4	120	none	45	0.4
Ns	1500	0.15	4	120	none	45	0.4
Ls	1500	0.2	4	120	none	45	0.4
Ps	1500	0.25	4	120	none	45	0.4

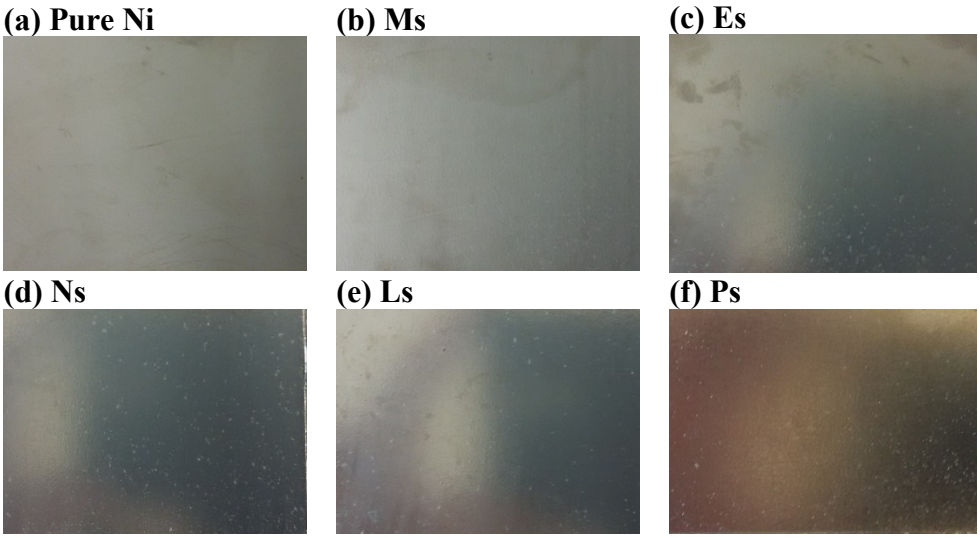

Figure 5-28: Photographs deposits produced with a volume bath of 1500mL: (a)Pure Ni, (b) 0.05g/L, (c) 0.1g/L,(d) 0.15 g/L,(e)0.2g/L and (f)0.25g/L of DMAB

All deposits are uniform without macro defects. By increasing the DMAB concentration in the plating baths the coatings become more glossy.
The GDOES boron profiles are reported in Figure 5-29 and a graph of the mean B content in the deposit vs. DMAB concentration in the plating bath in Figure 5-30.

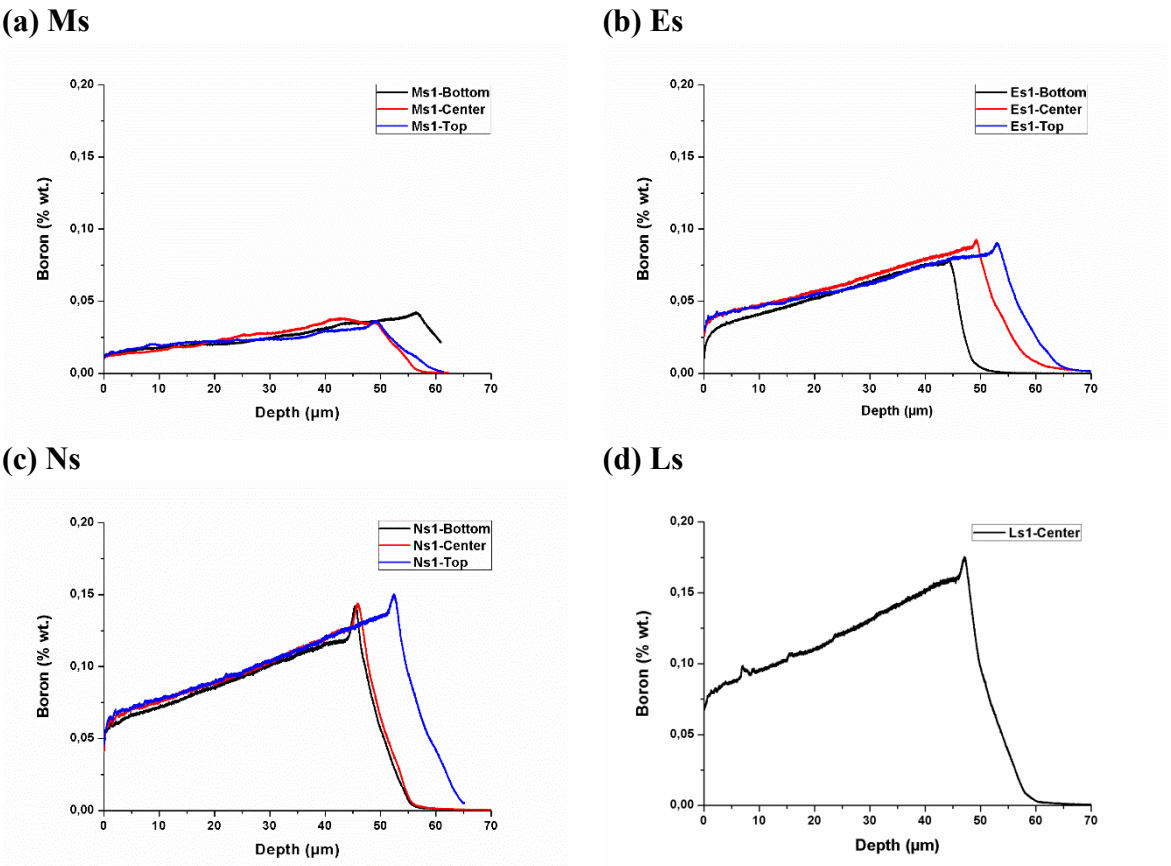

Figure 5-29: GDOES boron profiles of the Ni-B deposits produced with Ni sulfammate "High speed" baths in the plating cell of 1500mL: (a) 0.05g/L, (b) 0.1g/L,(c) 0.15 g/L,(d) 0.2 g/L of DMAB

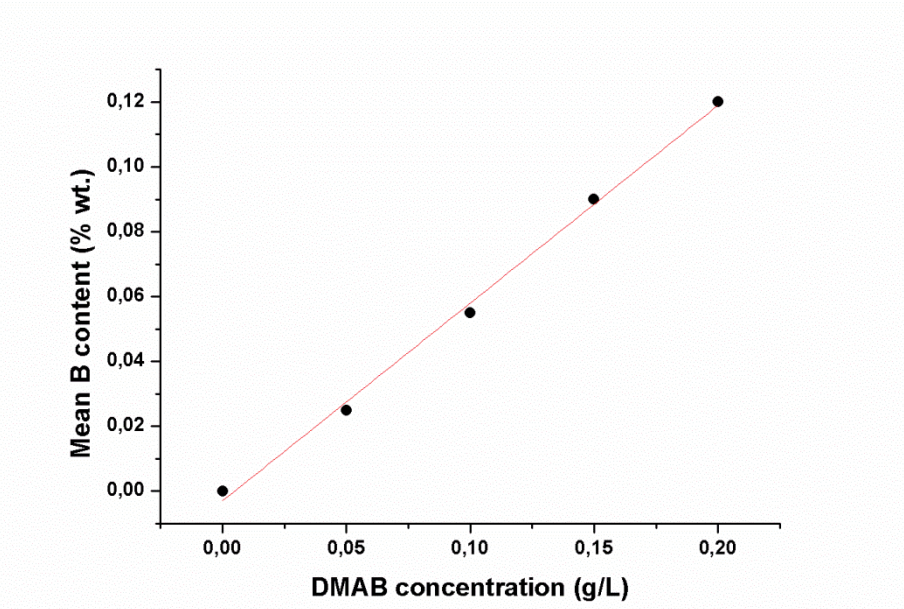

Figure 5-30: Mean B content in the deposit vs. DMAB concentration in the plating bath for Ni-B coatings produced with Ni sulfammate "High Speed" plating bath in the plating cell of 1500mL

It was not possible to perform all the GDOES analyses on the coatings produced with the higher concentration of DMAB probably due to the formation of a net of cracks which did not allow to produce the necessary vacuum for the measurements.
However, the GDOES performed show that an increase of the bath volume has led to a more uniform "spatial distribution" of the B in the coating. All the coatings present a linear decrease of the B content along the deposit thickness caused by the consumption of the DMAB. By observing the graph in Figure 5-30 it is possible to notice that, by increasing the DMAB concentration in the plating baht, the B content in the deposit increases linearly. Comparing the results with those obtained with a Watts plating bath, it was noticed that the same concentration of DMAB in the plating baths leads generally to a lower B content in the Ni/B deposits when a sulfammate bath is used.
LOM (light optical microscope) micrographs of the coating surfaces are reported in Figure 5-31.

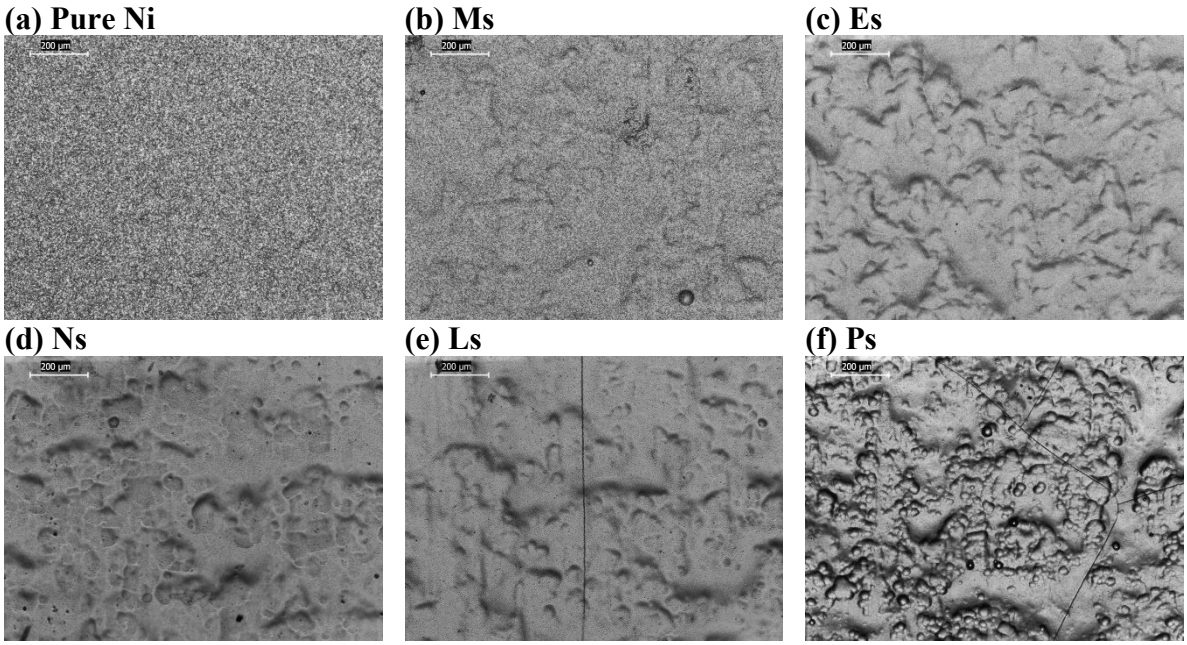

Figure 5-31: LOM micrographs in top view of the coatings produced with Ni sulfammate "High Speed" plating bath in the plating cell of 1500mL: (a) Pure Ni, (b) 0.05 g/L, (c) 0.1 g/L,(d) 0.15 g/L,(e) 0.2 g/L and (f) 0.25 g/L of DMAB

By observing the micrographs it is possible to notice that the coatings produced with DMAB concentration above 0.2 g/L present cracks.
SEM micrographs in cross section after metallographic etching are reported in Figure 5-32.

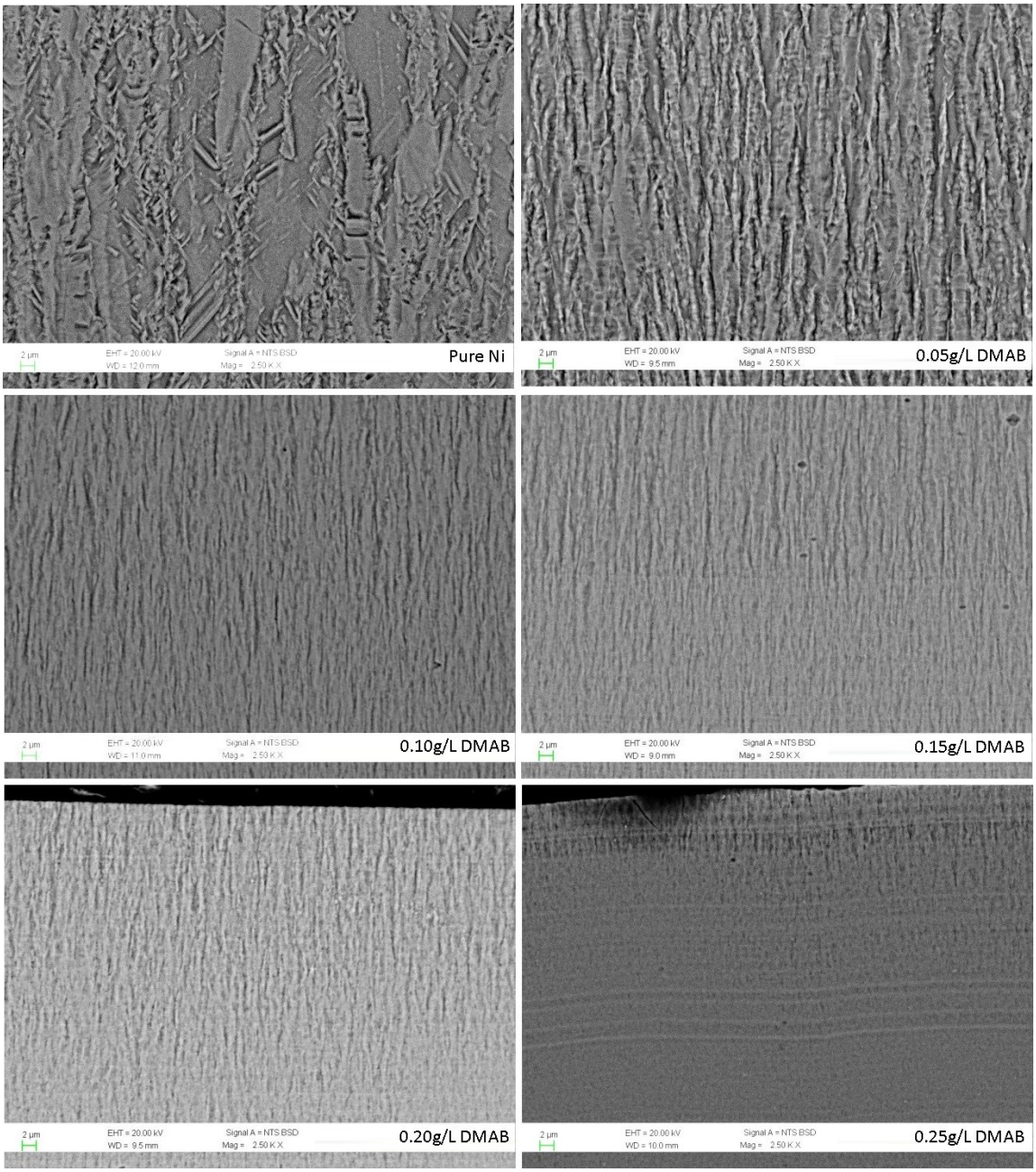

Figure 5-32: SEM micrographs in cross section after metallographic etching of the coatings produced with Ni sulfammate "High Speed" plating bath in the plating cell of 1500mL

The deposition of B leads to a marked grain refinement. By increasing the B content the microstructure change from a columnar structure to a very fine fiber structure and finally to a lamellar structure for the coating produced with 0.25 g/L.

The microhardness values of the coatings are reported in Table 5-18 and graphs of the microhardness as function of both DMAB concentration in the plating bath and mean B content in the deposit are reported respectively in Figure 5-33 and Figure 5-34.

Table 5-18: Vickers microhardness $HV_{0.05}$ of the deposits produced with Ni sulfammate "High Speed" plating bath with a volume of 1500mL

Sample	Microhardness
	[$HV_{0.05}$]
Pure Ni	173 ± 11
Ms-1	273 ± 11
Es-1	409 ± 21
Ns-1	468 ± 18
Ls-1	594 ± 35
Ps-1	643 ± 38

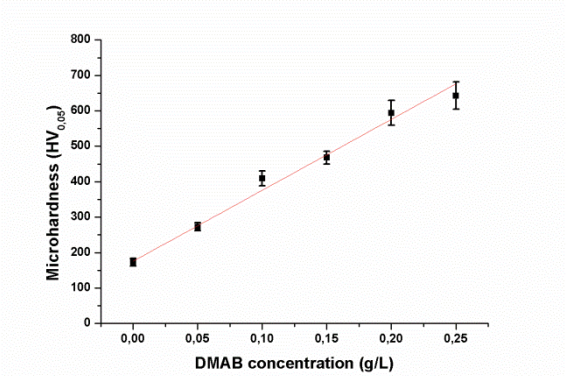

Figure 5-33: Microhardness $HV_{0.05}$ vs. DMAB concentration in the plating bath

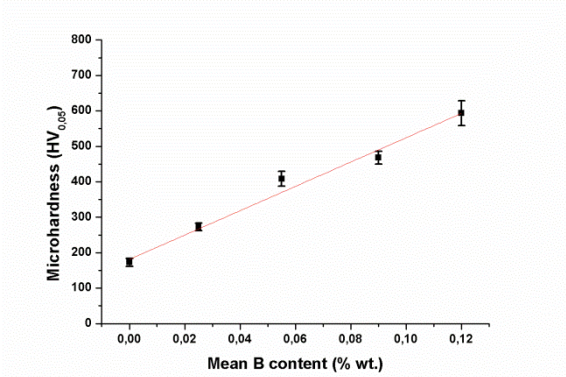

Figure 5-34: Microhardness $HV_{0.05}$ vs. mean B content in the deposit

The graphs show that the microhardness of the Ni-B deposits produced with Ni sulfammate plating bath presents a marked increase by increasing the DMAB concentration in the plating bath and hence by increasing the B content in the deposits as observed with the Ni-B coatings produced with Ni Watts plating baths.
In literature many works describe the marked increase of the hardness of Ni-B coating produced with Ni Watts plating baths with small increase of the B content or small increase of reduction agents in the plating bath[4,5].
In this work, Ni-B coatings produced with Ni sulfammate "High Speed" plating bath show a lower microhardness in comparison to coatings produced with the same concentration of DMAB but using Ni Watts plating bath. The different mechanism of co-depositon of B using Ni sulfammate "High Speed" plating bath leads to a production of Ni-B coatings with lower internal stresses and thus a slight lower microhardness.
Based on these results and considering that Ni sulfammate "High Speed" plating bath allows to produce thicker deposits with lower deposition time, it was chosen to proceed with the scaling up of the process in the galvanic pilot plant using the Ni sulfammate "High Speed" plating bath.

[4] K. H. Lee, D. Chang, S.C. Kwon, Electrochimica Acta 50 (2005), 4538-4543
[5] H. Ogihara, K. Udagawa, T. Saji, Surface & Coatings Technology 206 (2012), 2933-2940

5.1.2 DMAB titration and plating baths stability

In parallel with the optimization of the electroplating process, different methods for the determination of the DMAB concentration in the plating baths have been studied.
The determination of DMAB concentration in the plating bath is extremely important for the scaling-up of the process. In order to provide not only coatings with the desired properties but also a well-defined process for their production in industrial scale. The determination of the DMAB amount is not easy due to three main factors:

- it is not possible to use method for the elementary determination of B, as the B is present also in the H_3BO_3 (buffer for the plating baths) and in much higher concentrations
- The DMAB concentration range is very low
- The concentration of other species in the plating baths is too high.

For this reason the research was focused on the use of potentiometric methods which could allow the selective reduction of the DMAB. Two different methods have been tested.
The first one is based on a potentiometric method developed for the electroless Ni-B baths[6].
The solution to be tested is titrated in a solution containing a known amount of $PdCl_2$, a Pd electrode and a Ag/AgCl electrode as reference. During the titration, the potential of the Pd electrode vs. the reference electrode is monitored. The DMAB reduces the $PdCl_2$ according the reaction:

$$(CH_3)_2HN \cdot BH_3 + 3Pd^{2+} + 3H_2O \rightarrow 3Pd^0 + H_3BO_3 + (CH_3)_2HN + 6H^+$$

When all Pd^{2+} ions in the solution have reacted the DMAB reduced the H^+ present in the solution according the reaction:

$$(CH_3)_2HN \cdot BH_3 + 3H_2O \rightarrow 3H_2 \uparrow + H_3BO_3 + (CH_3)_2HN$$

The potential at the Pd electrode changes abruptly as hydrogen is formed, thus indicating the end point of the titration. Known the concentration of Pd^{2+} in the solution and the volume of the Ni plating bath added until the change of the potential, it is possible to calculate the concentration of the DMAB in the Ni plating bath.
Since the method is developed for Ni electroless baths, the measures are more accurate for baths that contain high amounts of DMAB and lower amounts of Ni^{2+}. As the Ni^{2+} can influence the reduction reactions taking place during the titration, a high number of tests have been performed with known concentrations of DMAB in the Ni Watts plating baths in order to "calibrate" the method.
In order to evaluate the efficiency of this method and the feasibility of the plating baths replenishment, a series of electrodepositions has been performed using the same plating bath containing 0.2g/L of DMAB and replenishing the DMAB concentration according to the titration results after each deposition.
The list of the deposit produced and the electrodeposition parameters are reported in Table 5-19 and the GDOES Boron profiles are reported in Figure 5-36.

[6] A.F. Schmeckenbecher, J.A. Lindholm, Analytical Chemistry 39-8 (1967) 1014-1016

Table 5-19: Series of deposit produced with Ni Watts plating baths with 0.2 g/L of DMAB

Sample	Bath volume	DMAB concentration	Current density	Time	Stirring	Temperature	Surfactant
	[mL]	[g/L]	[A/dm^2]	[min]	[rpm]	[°C]	[mL/L]
L1-1	**1500**	**0.2**	**2**	**60**	**30**	**45**	**0.4**
L1-2	**1500**	**0.2 replenished**	**2**	**60**	**30**	**45**	**0.4**
L1-3	**1500**	**0.2 replenished**	**2**	**60**	**30**	**45**	**0.4**

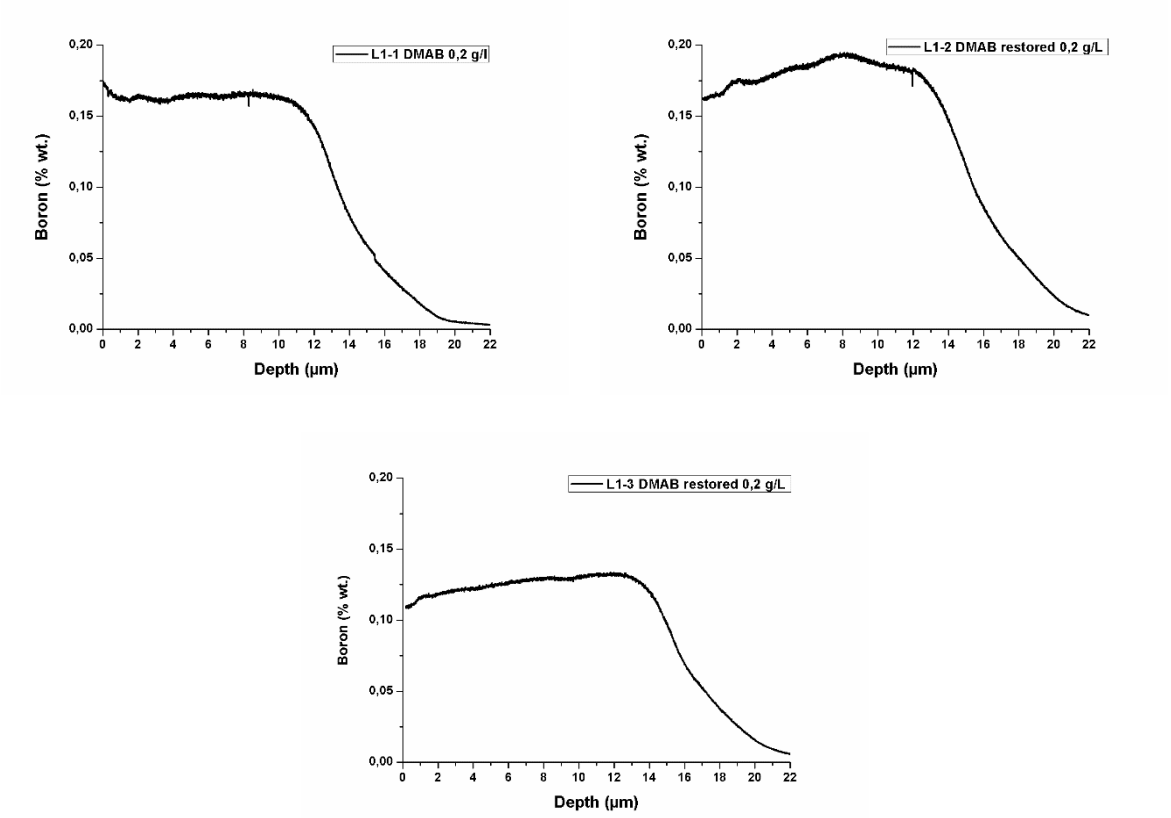

Figure 5-35: GDOES boron profiles of the coatings produced with the same Ni watts plating bath with replenishments of the DMAB concentration

The GDOES boron profiles showed that the three samples present similar B content along the deposit thickness (within the experimental error), indicating that the DMAB concentration can be restored after the deposition based on the titration method results. The method was also used to verify the "baths aging". The DMAB concentration in Ni Watts plating bath was monitored during several days of storage in order to evaluate if the concentration of DMAB remains stable without using the plating baths.
The potentiometric titrations performed during 4 days of storage of a in Ni Watts plating bath containing 0.25g/L of DMAB are reported in Figure 5-36 and the graph of the DMAB concentration measured is reported in Figure 5-37.

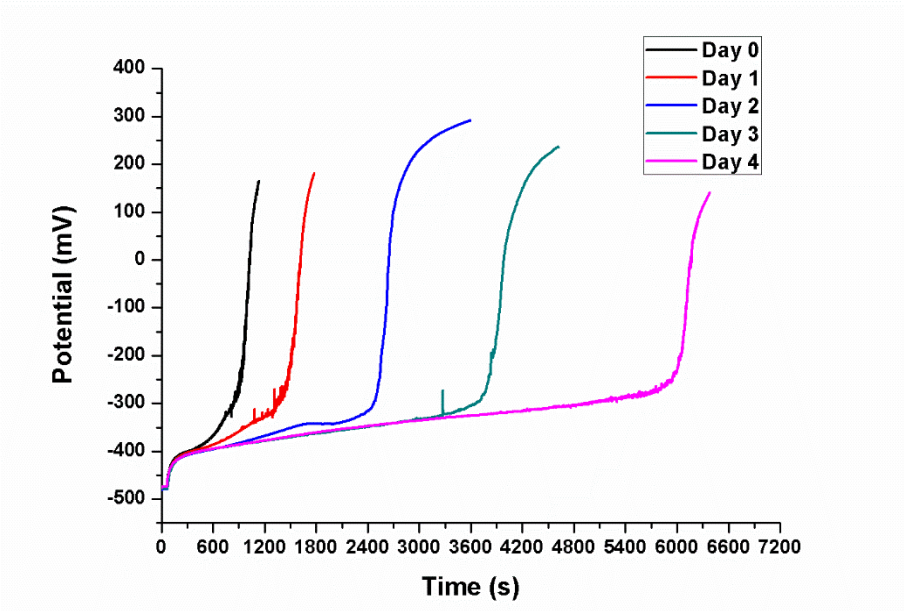

Figure 5-36: Potentiometric titrations with $PdCl_2$ method of DMAB in Ni Watts plating bath during 4 days of storage.

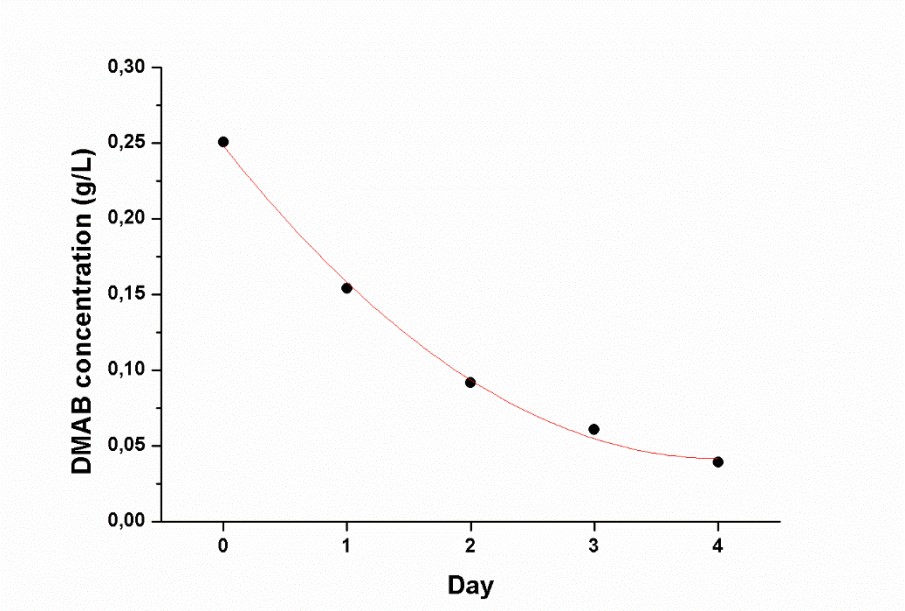

Figure 5-37: DMAB concentrations in Ni Watts plating bath during 4 days of storage

The potentiometric curves in Figure 5-36 have a typical sigmoid shape. The end point of the titration is easily identifiable allowing to measure accurately the DMAB concentration. The graph in Figure 5-37 shows that there is a noticeable decrease of the DMAB concentration during few days of storage. The consumption of DMAB during the storage indicates that there is a redox reaction between the DMAB and the Ni^{2+} ions of the plating bath, even if both the DMAB concentration and the bath temperature are much below the

limits which should allow an electroless deposition. In fact, filtrations of the plating bath showed the presence of metallic Ni particles in the electrolyte. The phenomenum have been also deducted during the study of the production of Ni-B coatings. Deposits produced with Ni plating baths stored for some days always present lower B content in comparison to coatings produce with fresh plating baths.
Even if the works in literature[3,7] reports contradictory opinions about the activation of the electroless deposition of Ni Watts plating baths containing small amount of DMAB, the tests in this study it was demonstrated that the electroless deposition process it is not completely suppressed in the case of Watts plating baths containing low amount of DMAB at 4.5 pH and at room temperature but rather that the rate of the redox reaction is very low.
The potentiometric titration with $PdCl_2$ has been also used with Ni sulfammate "high Speed" plating baths. The potentiometric titrations performed during 8 days of storage of a Ni sulfammate "high Speed" plating bath containing 0.3 g/L of DMAB are reported in Figure 5-38.

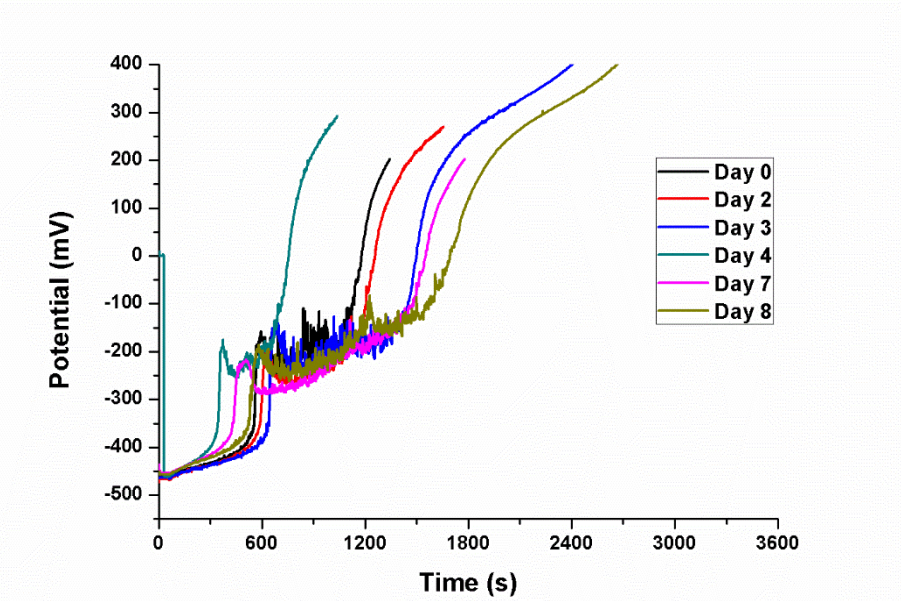

Figure 5-38: Potentiometric titrations with $PdCl_2$ of DMAB in a Ni sulfammate plating bath during 8 days of storage

From the potentiometric curves obtained with the Ni sulfammate "High Speed" plating bath it is not easy to determine the end point of the titration and thus calculate the DMAB concentration. In fact, the shape of the curves suggests that other reactions take place contemporaneously, involving other species present in the plating baths. A possible cause of this behavior could be attributed to the higher content of Ni^{2+} ions present in the Ni sulfammate plating bath. However, the shift of the curves at higher times indicate a consumption of the DMAB also in the case of Ni sulfammate "High Speed" plating bath.
An alternative method has been investigated in order to determine the DMAB concentration in the Ni sulfammate "High Speed" plating baths. The second method tested is an iodometric method.

[7] H. Ogihara, K. Udagawa, T. Saji, Surface & Coatings Technology 206 (2012) 2933–2940

The bath to be analyzed ia added in an acqueous solution containing an excess of triiodide, suitably calculated. The DMAB is reduced according the reaction:

$$(CH_3)_2HN \cdot BH_3 + 3I_3^- + 3H_2O \rightarrow 9I^- + H_3BO_3 + (CH_3)_2HN + 6H^+$$

Afterwards the excess of triiodide is titrated with thiosulfate monitoring the potential of a Pt electrode in the solution. The thiosulfate reacts with the triiodide according to the reaction:

$$I_3^- + 2S_2O_3^{2-} \rightarrow 3I^- + S_4O_6^{2-}$$

When all the triiodide in the solution has reacted with the added thiosulfate the potential of the Pt electrode instantly changes indicating the end of the titration. Known the total amount of triiodide that reacted with the thiosulfate and it is possible to calculate the DMAB concentration in the plating bath.
Some titration curves obtained for the same concentration of DMAB, in water, Ni Watts plating bath and Ni sulfamate plating bath are reported Figure 5-39. The solution type and the DMAB concentration are reported in Table 5-20

Table 5-20: DMAB concentrations of the solution titrated with thiosulfate

Solution	DMAB concentration
	[g/L]
Excess of I_3^-	0
H_2O	0.25
Ni Watts	0.25
Ni sulfammate "High Speed"_1	0.25
Ni sulfammate "High Speed"_2	0.125

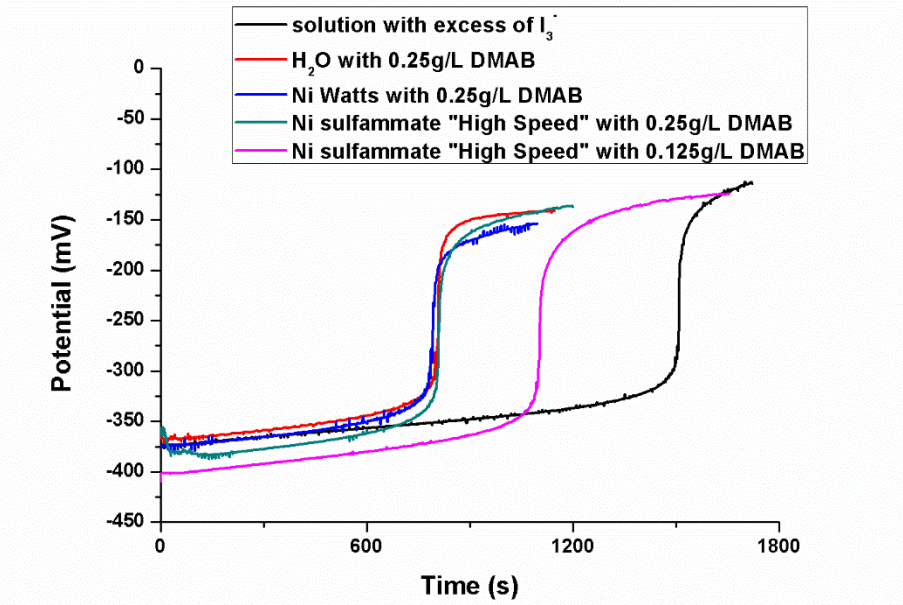

Figure 5-39:Potentiometric titration with Tiosulphate of I_3^- for the determination of DMAB concetrationin different solution: Water, Ni Watts plating bath and Ni sulfammate "high Speed" plating bath

By observing the shape of the curves it is possible to notice that the iodometric method, opportunely calibrated, allow to determine the DMAB concentrations of both Ni Watt and Ni sulfammate "High Speed" plating baths. The accuracy of the method is high and it does not seem to be influenced by the presence of Ni^{2+} as the curves obtained for solution with the same DMAB concentration are almost perfectly overlapped.
From all the above analyses it was clear that the iodometric method could be used in order to determine the DMAB concentration in the plating baths and thus replenish them to the desired concentration. On the other hand, it is not possible to store Ni plating baths containing DMAB as it is consumed during the storage. The DMAB addition should be done just before the electrodeposition.

5.1.3 Production of Ni-B deposits in the galvanic pilot plant and microstructural characterization

Considering the good results obtained in the preliminary study, the Ni sulfammate "High Speed" plating bath was chosen for the scaling up of the process in the galvanic pilot plant. Two different types of coatings have been produced: a series of monolayer coatings with different contents of B and a multilayer coating composed of 4 layers with different B contents.
The series of Ni-B monolayer coatings produced with DMAB concentration in a range from 0.1g/L to 0.25g/L have been used for the evaluation of the wear, the tribocorrosion and corrosion resistance while the multilayer coatings have been used for the evaluation of the effect of heat treatments on the microstructural modification.

5.1.3.1 Substrate

The Ni-B coatings produced in the galvanic pilot plant have been electrodeposited on low carbon steel substrates with dimensions of 6 x 11 cm with a thickness of 6 mm. Before each electrodeposition the substrates have been pretreated following the same steps described in the paragraph *4.1.2.1* .

5.1.3.2 Monolayer Ni-B coatings

The series of monolayer Ni-B coatings has been deposited with concentration of DMAB in the range from 0.1 to 0.25 g/L.
Particular attention in the characterization has been done in order to identify the maximum content of B that allows to produce crack-free Ni-B deposits.
The list of the produced samples and the deposition parameters are reported in Figure 5-22.

Table 5-21: List GPP of the Ni-B coatings produced in the galvanic pilot plant

Sample	Bath volume	DMAB concentration	Current density	Time	Stirring	Temperature	Surfactant
	[L]	[g/L]	[A/dm^2]	[min]	[intensity]	[°C]	[mL/L]
Pure Ni	10	0	4	120	Low	45	0.4
GPP 1	10	0.1	4	120	Low	45	0.4
GPP 2	10	0.15	4	120	Low	45	0.4
GPP 3	10	0.2	4	120	Low	45	0.4
GPP 4	10	0.25	4	120	Low	45	0.4

All deposits were uniform without macro defects. By increasing the DMAB concentration in the plating baths the coatings became more shiny. The boron profiles obtained with

GDOES are reported in Figure 5-40 and a graph of the mean B content in the deposits vs. the DMAB concentration in the plating bath is reported in Figure 5-46.

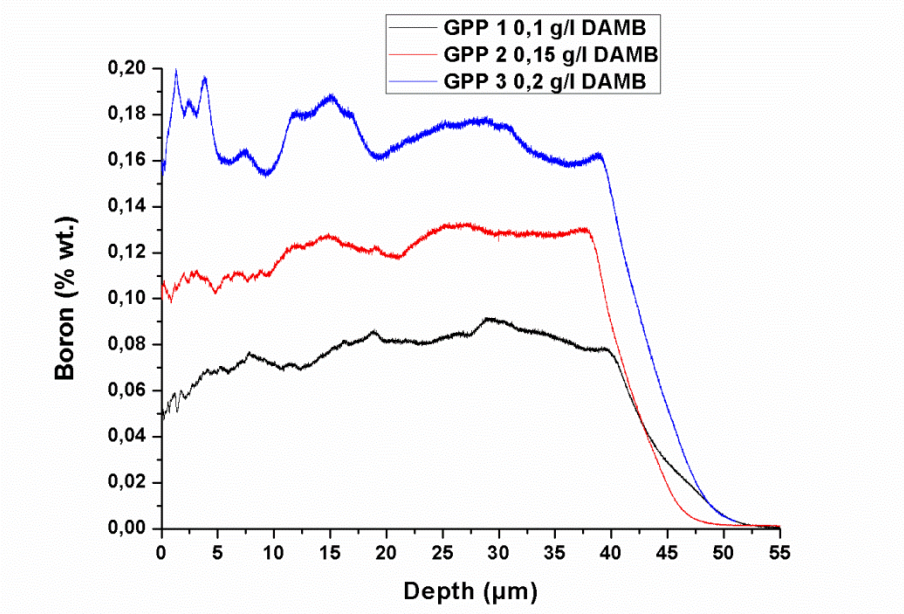

Figure 5-40: GDOES B profiles of the Ni-B coatings produced in the galvanic pilot plant with Ni sulfammate "High Speed" plating baths.

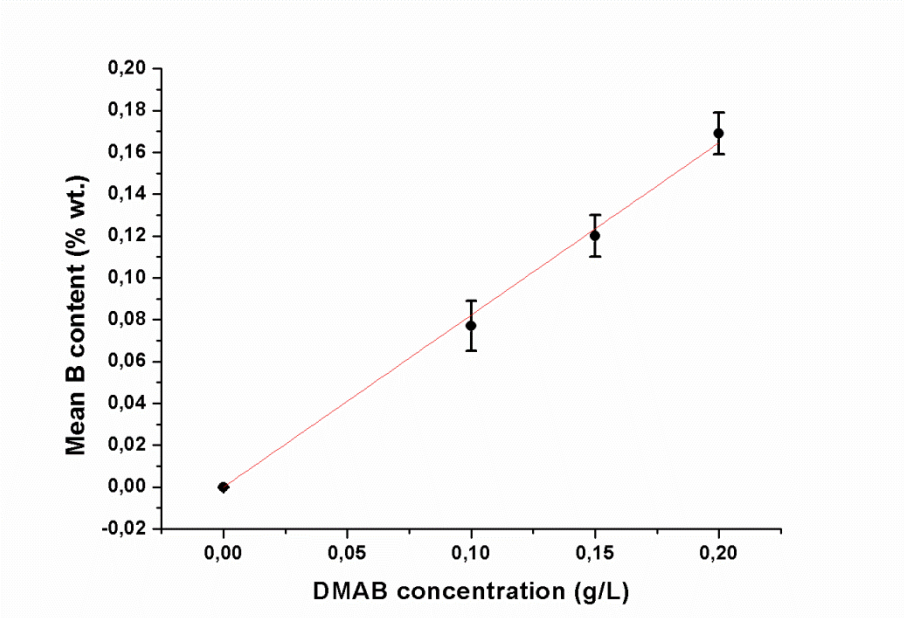

Figure 5-41: Mean B content in the deposit vs. DMAB concentration in the plating bath for Ni-B coatings produced in the galvanic pilot plant with Ni sulfammate "High Speed" plating baths.

The GDOES analyses showed that by increasing the ratio *Volume bath/coated surface* the Ni-B electrodeposition process allows the production of thick deposits with a more constant distribution of B along the deposit thickness. It was noticed also that the use of a bigger deposition tank helps to reduce the differences in the "spatial distribution" of the B in the deposits. Nevertheless, the increase of the deposit thickness, especially for deposits

with a constant content of B along the thickness, is accompanied by an increase of the internal stresses that leads to the formation of cracks. In fact, due to the presence of a net of cracks on the sample produced with 0.25 g/L of DMAB it was not possible to perform the GDOES analysis. However, considering the previous results, it is licit to hypothesize that the amount of B of the coating GPP4 follows the linear increase observable in the graph in Figure 5-41.
The SEM micrographs in top view of the surface of the samples are reported in Figure 5-42 and the micrographs in cross section after metallographic etching in Figure 5-43.

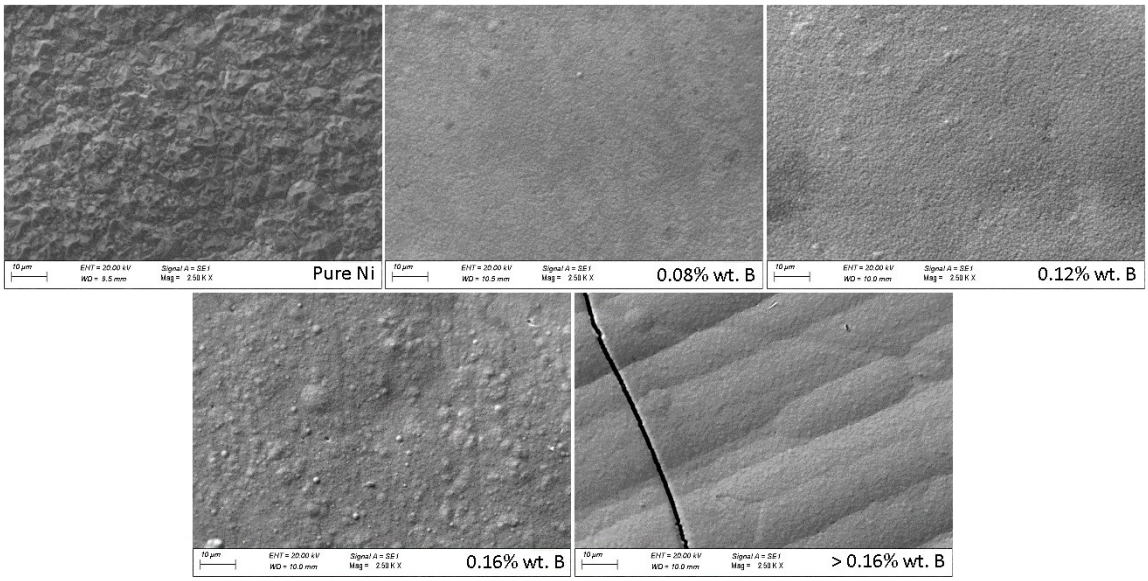

Figure 5-42: SEM micrographs in top view of the coatings produced in the galvanic pilot plant using Ni sulfammate "High Speed" plating baths

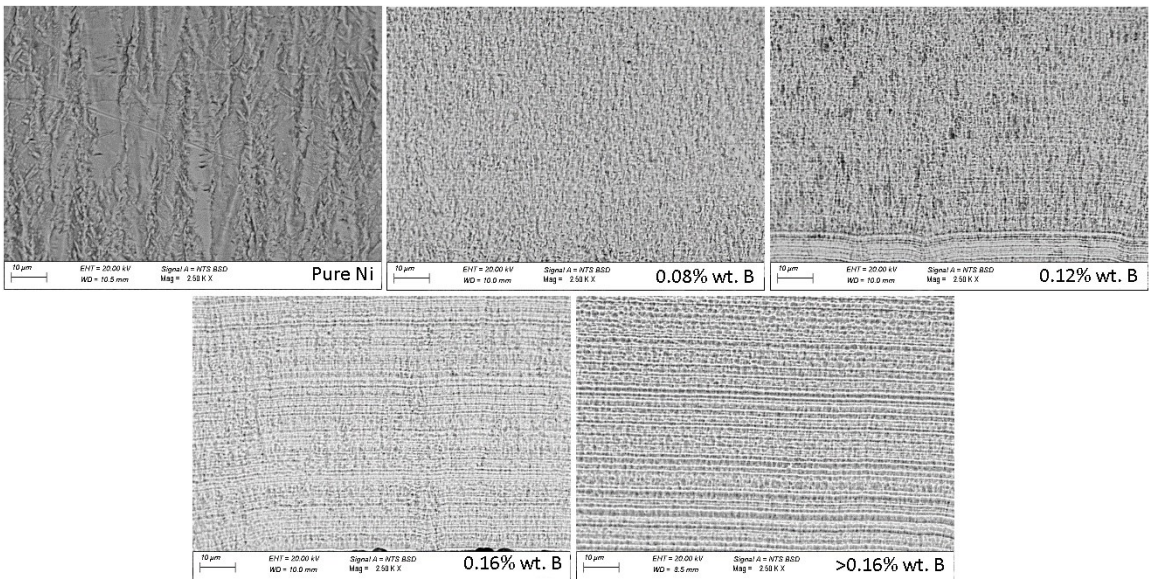

Figure 5-43: SEM micrographs in cross section after metallographic etching of the coatings produced with Ni sulfammate "High Speed" plating bath in the plating cell of 1500mL

The deposition of B leads to a remarkable refinement of the microstructure, which can be noticed both on top surface (Figure 5-42) and in cross section (Figure 5-43).
The deposits with the higher amount of B (Figure 5-43-a-b) are characterized by the presence of cracks due to marked residual stresses.
Some cracks have been observed also on the deposits produced with 0.16% wt. of B even if they are not observable in the reported micrograph.
The pure Ni coating has a pseudo-columnar structure, with large columnar grains oriented along the electrical field direction (Figure 5-43-a). The deposition of even very low amount of B leads to the formation of fine fibrous grains (Figure 5-43-b). By increasing the amount of B the microstructure changes progressively from fine-columnar to lamellar (Figure 5-43-c-d-e).
The microstructure of the coatings was further characterized by means of X ray diffraction analyses. XRD diffraction diagrams of pure Ni deposits and Ni-B deposits with mean contents of B of 0.08% wt., 0.12% wt. and 0.16% wt. are reported in Figure 5-44 and the RTC values of the crystallographic orientations of the same deposits are reported in Figure 5-45.

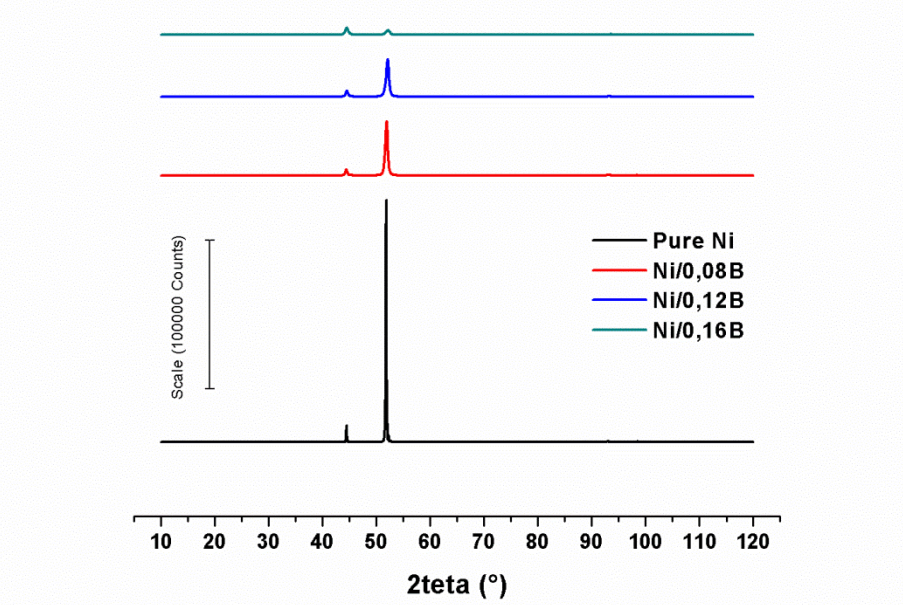

Figure 5-44: X-ray diffraction diagrams of pure Ni deposit and Ni-B deposits with 0.08% wt., 0.12% wt. and 0.16% wt. of B content

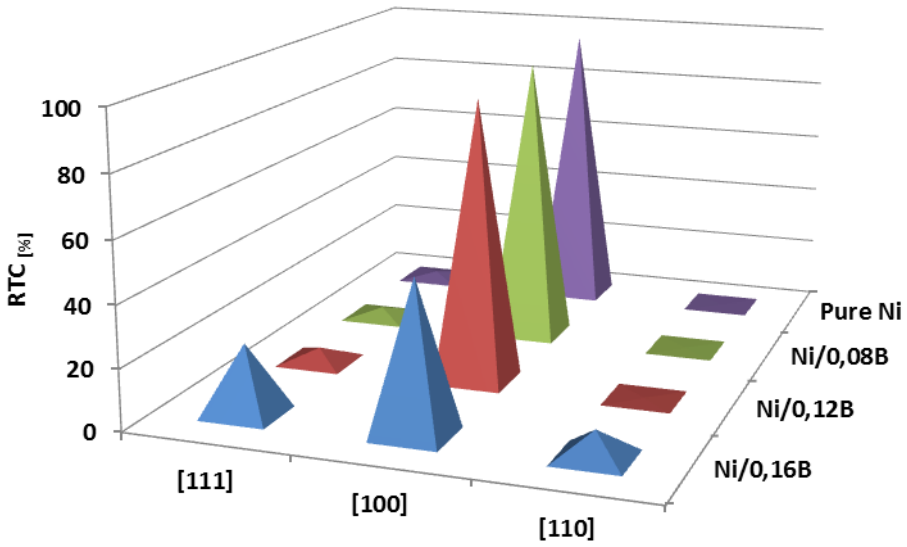

Figure 5-45: Relative texture coefficient (RTC) for the different reflection lines of pure Ni deposit and Ni-B deposits with 0.08% wt., 0.12% wt. and 0.16% wt. of B content

By increasing the B content there is a broadening of the peaks and a marked decrease of their intensity indicating a decrease of the crystal size.
The pure Ni deposit presents an intense (200) peak indicating a strong [100] preferential orientation. The RTC graph shows a progressive loss of the preferential orientation [100] by increasing the B content. This trend follows the microstructural modifications observed by SEM.
The microhardness $HV_{0.05}$ of the coatings as function of B content is reported in the graph of Figure 5-46.

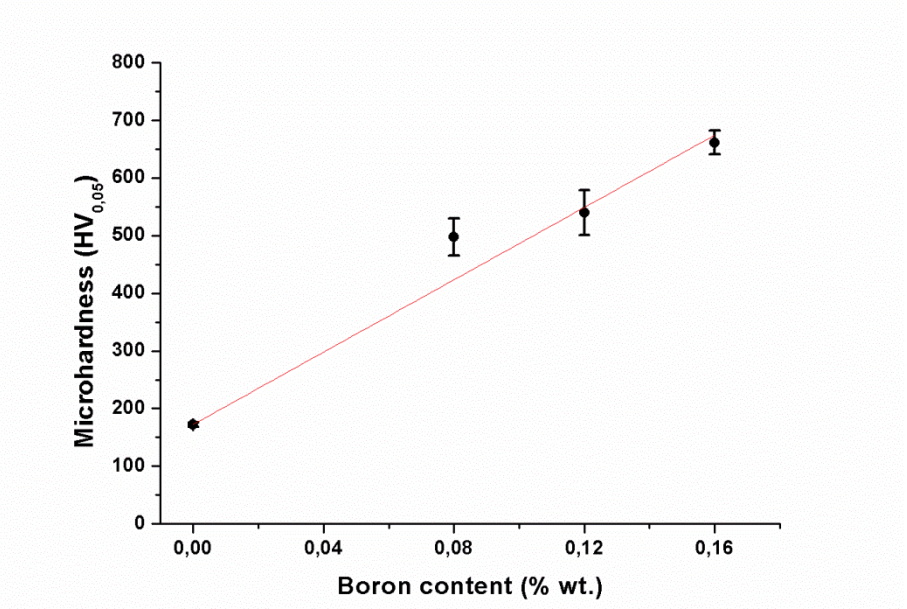

Figure 5-46: Vickers Microhardness $HV_{0.05}$ of Ni-B coatings produced in the galvanic pilot plant with Ni sulfammate "High Speed" plating baths.

The microhardness of the coatings increases linearly by increasing the B content. The marked increase of the microhardness follows the microstructural modifications and can be attributed to:

- the solid solution hardening due to the presence of B as interstitial atom in the Ni elementary cell
- the reduction of grain size
- the loss of preferential orientation
- the presence of high internal stresses.

These results demonstrate that it is possible to produce thick Ni-B coatings with a constant B content of 0.12% wt. along the thickness without the formation of cracks using a Ni sulfammate "High Speed" plating bath with a DMAB concentration of 0.15 g/L.

5.1.3.3 Multilayer Ni-B coating

A multilayer coating with an increased B content along the deposit thickness has been produced with 4 sequential electrodepositions using 4 new plating baths with an increasing DMAB concentration. The multilayer coating is composed by one layer of pure Ni and three Ni-B layers produced with baths containing 0.08 g/L, 0.1 g/L and 0.12 g/L of DMAB.
Between the depositions the sample was etched in a 50% HCl solution for 10 min in order to provide a good adhesion between the deposits. The electrodeposition parameters used for the production of each layer are reported in Table 5-22 and the image of the surface of the coating is reported in Figure 5-47.

Table 5-22: Electrodeposition parameters used the multilayer Ni-B coating produced in the galvanic pilot plant.

Layer	Bath volume	DMAB concentration	Current density	Time	Stirring	Temperature	Surfactant
	[mL]	[g/L]	[A/dm^2]	[min]	[intensity]	[°C]	[mL/L]
1	10	0	4	30	Low	45	0.4
2	10	0.08	4	30	Low	45	0.4
3	10	0.1	4	30	Low	45	0.4
4	10	0.12	4	30	Low	45	0.4

Figure 5-47: Image of the multilayer coating produced in the galvanic pilot plant.

The surface of the sample was uniform without macro defects and had a glossy aspect. The GDOES B profile along the coating thickness is reported in Figure 5-48.

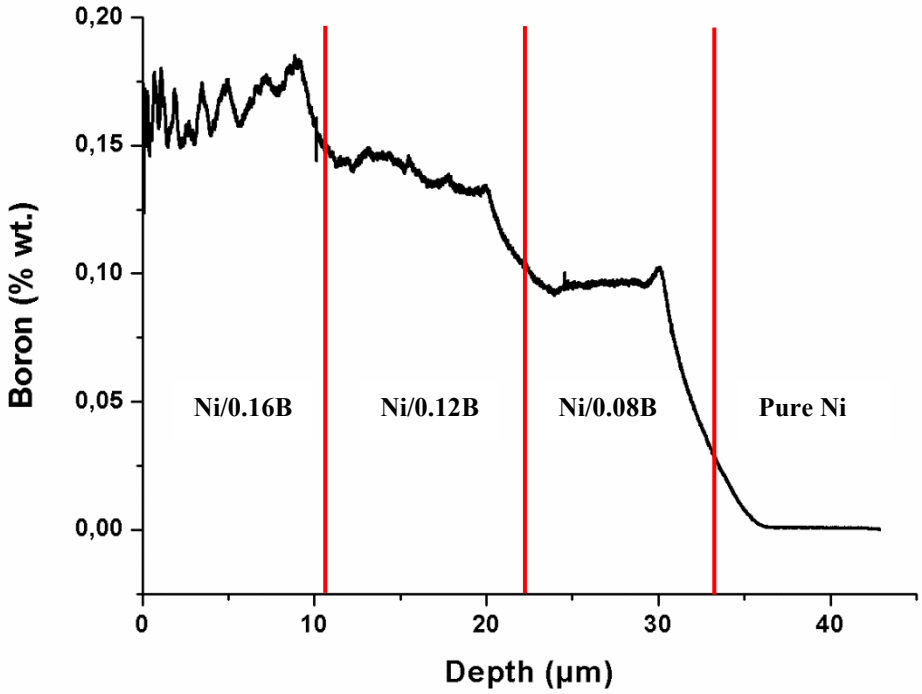

Figure 5-48: GDOES boron profile of the multilayer Ni-B coating produced in the galvanic pilot plant with Ni sulfammate "High Speed" plating baths.

The increasing DMAB concentration in the four plating baths is reflected in an increasing B content along the overall coating thickness. Instead, the distribution of B within every single deposit is quite constant. The last layer presents some oscillations of the B content caused probably by the non-uniform fluid dynamic conditions due to the positioning of the

sample too close to the nozzle for the bath recirculation. No important differences have been noticed in the "spatial distribution" of B in the deposits.
The SEM micrograph in cross section after metallographic etching of the multilayer Ni-B coating is reported in Figure 5-49.

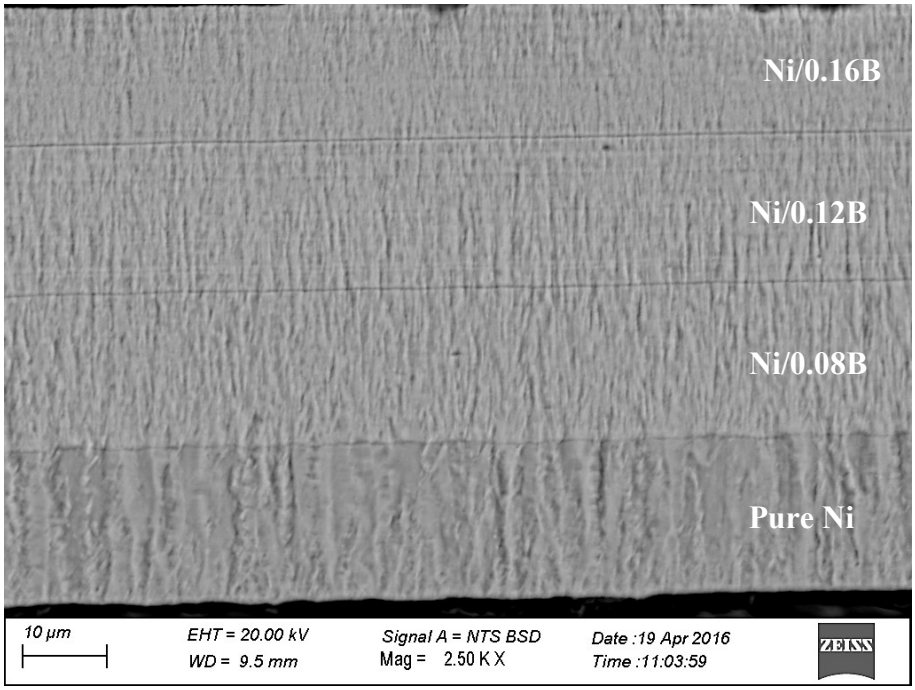

Figure 5-49: SEM micrograph in cross section after metallographic etching of the multilayer Ni-B coating produced in the galvanic pilot plant with Ni sulfammate "High Speed" plating baths.

By observing the deposit cross section it is possible to notice that the metallographic etching pointed out the interface between the different layers which was not observable without etching. No adhesion problems were detected. The first layer of pure Ni presents a pseudo-columnar microstructure. The microstructure of the Ni-B layers is columnar with thinner columns. The increase of the B content in the different layers lead to a gradual refinement of the microstructure. The higher the B content the thinner the columns width. No cracks have been observed both in top view and in cross section. Vickers microhardness $HV_{0.025}$ have been performed in cross section on each layer. The microhardness of the different layers as a function of the mean B content are reported in the graph in Figure 5-50.

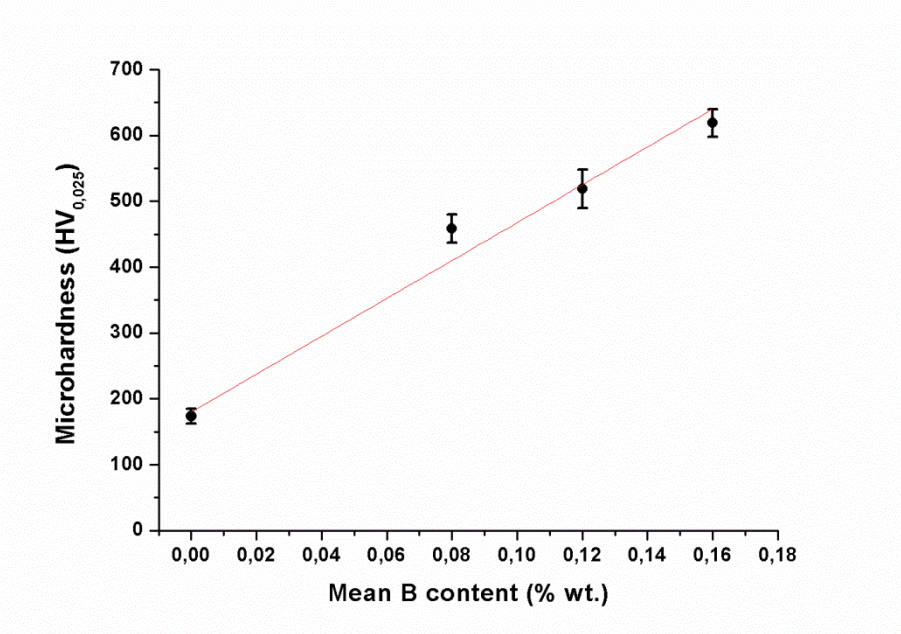

Figure 5-50: Vickers Microhardness $HV_{0.025}$ of the layers of the multilayer Ni-B coating produced in the galvanic pilot plant with Ni sulfammate "High Speed" plating baths.

The microhardness of the different layers follows the B content in the layers. The higher the B content, the higher the hardness of the layer.
This result shows that it is possible to produce thick Ni-B coatings performing sequential depositions with controlled B content and with different properties along the thickness.
For example, in this case a deposit with an increased microhardness from the substrate to the external surface has been produced.

5.2 Evaluation of the performances of Ni-B alloy coatings

5.2.1 Microstructural and microhardness modification after heat treatments

Heat treatments have been performed on specimens extracted from the multilayer Ni-B coating in order to study the microstructural modifications and the variation of the microhardness of the different layers. The specimens have been heat treated in air for 1 hour at temperatures of 200°C, 300°C, 400°C, 500°C and 600°C and cooled to room temperature in the oven.

5.2.1.1 Microstructure after heat treatments

The SEM micrographs in cross section after metallographic etching of the multilayer coating heat treated at different temperatures are reported in Figure 5-51.

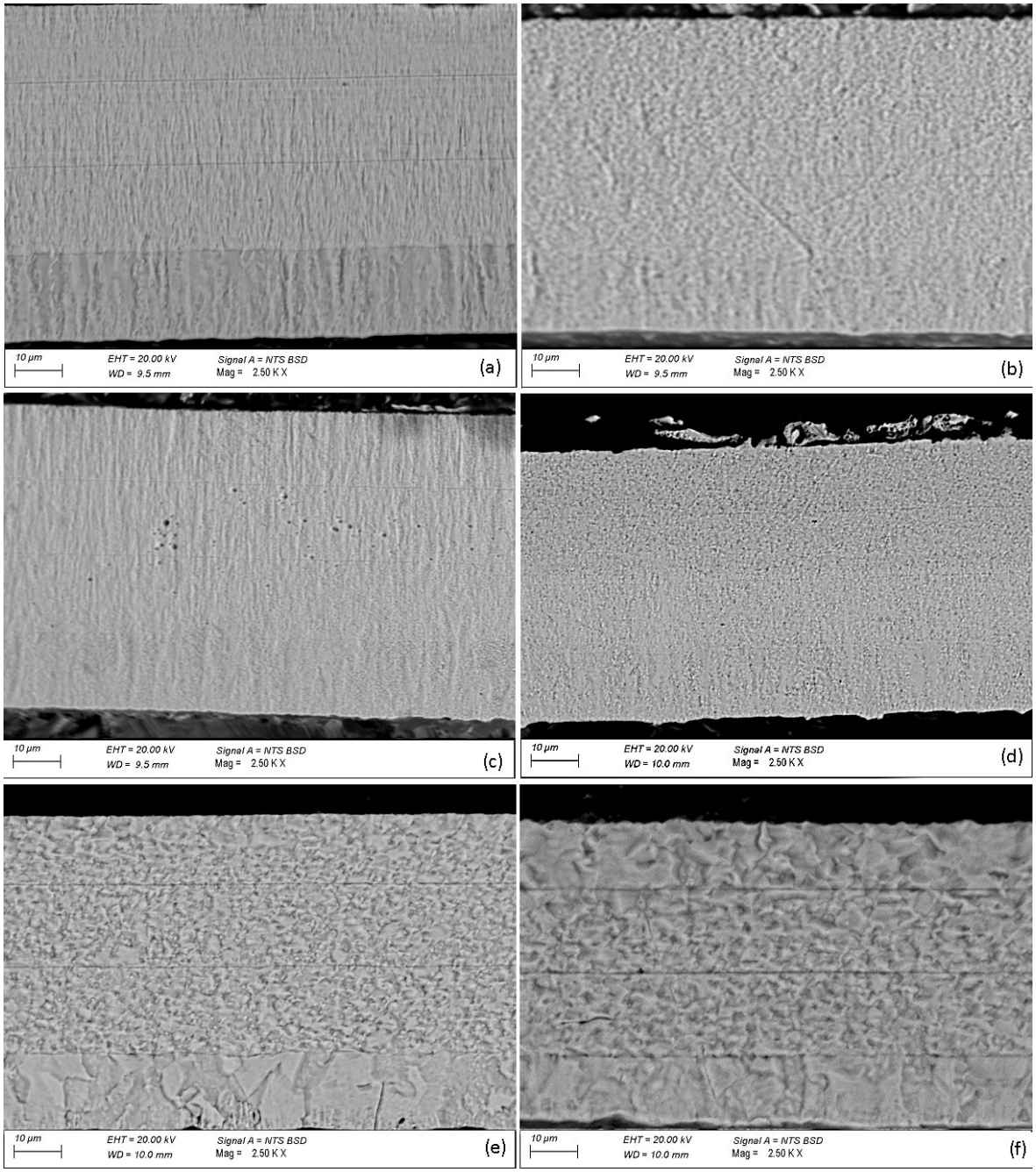

Figure 5-51:SEM micrographs in cross section after metallografic etching of multilayer coatings at different heat treatment temperatures: (a) R..T. , (b) H.T. 200°C, (c) H.T. 300°C, (d) H.T.400°C , (e) H.T. 500°C, (f) H.T. 600°C

As can be observed from the SEM micrographs no significant modifications occur in the microstructure after H.T. up to 300°C of both pure Ni layer and Ni-B layers. A partial recrystallization of the Ni grains in the pure Ni layer is noticed after heat treatment at 400°C. Also in the Ni-B layers heat treated at 400°C it is possible to observe a slight modification of the microstructure indicating the initiation of the recrystallization of the layers. The microstructure of all Ni-B layers is however finer in comparison to the pure Ni layer. The pure Ni layer shows a complete recrystallization after heat treatment at 500°C with the formation of large equiassic grains of dimensions of the layer thickness. The

recrystallization of Ni-B layers is more evident after H.T. at 500°C with the formation of small equiassic grains. No particular differences are observable among the different Ni-B layers due to the different contents of B. After H.T. at 600°C it is noticed a further increase of the dimensions of the equiassic grains but they are still smaller in comparison to the pure Ni grains.

5.2.1.2 Microhardness after heat treatments

The microhardness $HV_{0.025}$ values, measured in cross section on the four layers, as a function of the heat treatment temperatures are reported in the graph in Figure 5-50.

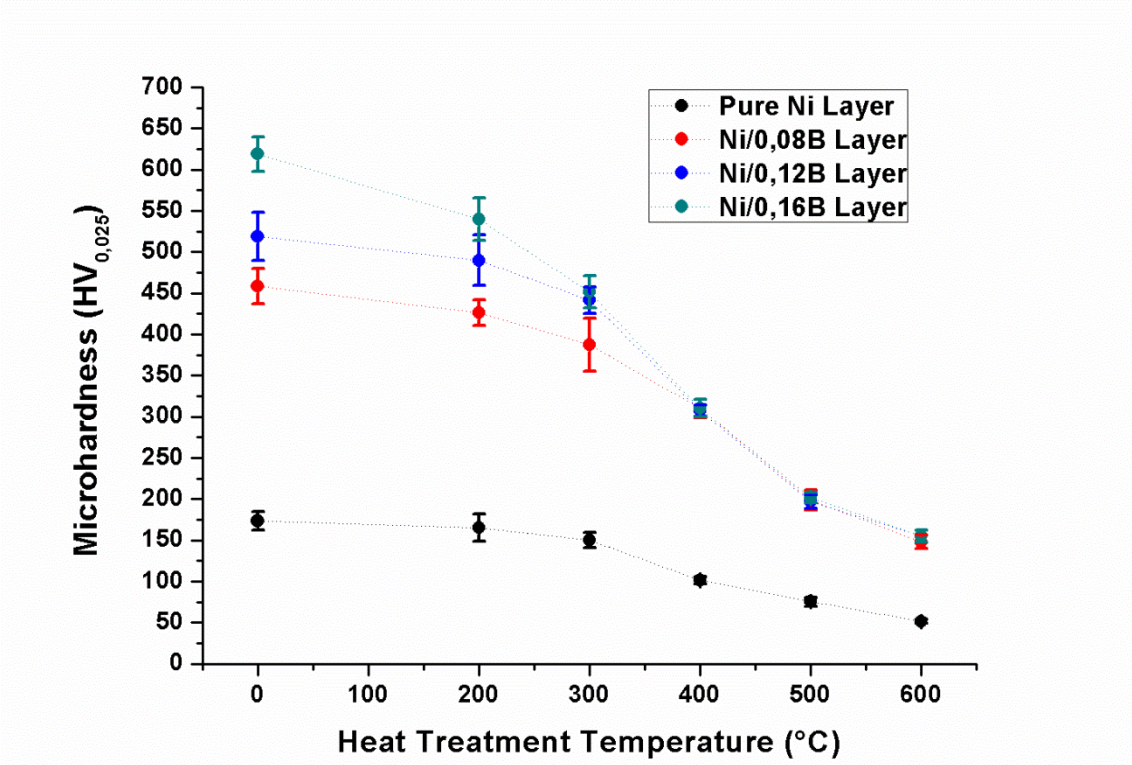

Figure 5-52: Vickers microhardnes $HV_{0.025}$ of pure Ni and the different Ni-B coatings as a function of H.T. temperature

The microstructure modifications observed in cross section by SEM are reflected into the microhardness values of the heat treated layers.
Both pure Ni and Ni-B layers present a decrease of the hardness by increasing the heat treatment temperature but the Ni-B layers present always higher values in comparison to the pure Ni layer. The different content of B and the different microstructure of the three Ni-B layers influence the microhardness values till 300°C. After heat treatment at 400°C or higher the microhardness curves are overlapped indicating that the different content of B of the three Ni-B layers does not influence neither the microstructure nor the hardness. The presence of small amount of B however is enough to hinder the recrystallization of all Ni-B layers that present for all the heat treatment temperatures more fine microstructure and higher hardness in comparison to the pure Ni layers.

5.2.2 Wear and Tribocorrosion resistance

The monolayer Ni-B coatings with 0.08 %wt., 0.12 %wt. and 0.16 %wt. of boron have been used for the evaluation of the wear and tribocorrosion resistance of the Ni-B coatings. Wear tests have been performed for 1 hour in a ball-on-disc configuration using as counter an alumina ball with a diameter of 3 mm and an applied load of 20N. The frequency of the wear test was 0.5 Hz, the test radius 5mm corresponding thus to a sliding speed of 0.0157m/s. A scheme of the ball on disc configuration is reported in Figure 5-53.
The tribocorrosion tests have been performed in the same condition using as electrolyte a 3.5% wt. NaCl solution. The open circuit potential OCP was monitored before, during and after the tribocorrosion tests.

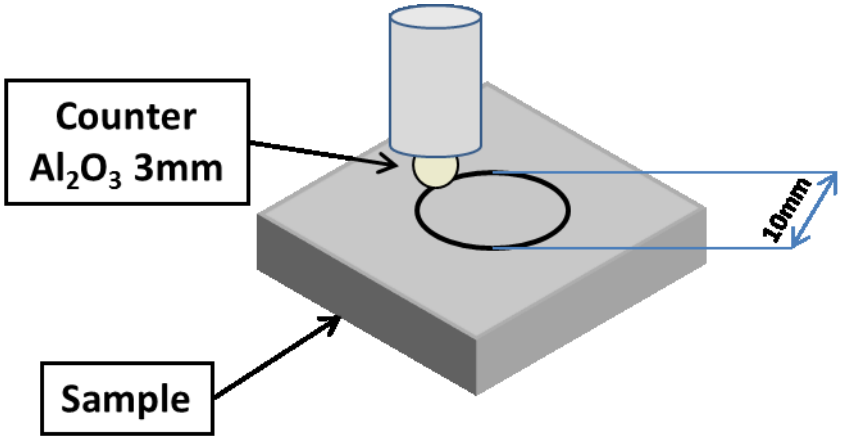

Figure 5-53: Scheme of the tribological test

The wear tracks have been characterized by means of stylus profilometer in order to acquire 8 wear track profiles along 8 radius equally distributed along the circumference. The wear track profiles have been used for the calculation of 8 wear areas and the average value of the areas has been used for the calculation of the volume loss. The volume loss has been used for the calculation of the wear coefficient according to the formula:

$$K = \frac{V_{loss}}{S \cdot F_z} \qquad (5.1)$$

Where: V_{loss} is the volume of the material removed [mm^3], S is the total wear distance [m] and F_z is the applied load [N].
The wear tracks have been also observed by SEM on both top surface and cross section in order to better understand the wear mechanism. Two tests have been performed for each type of coating.
The SEM micrographs of the top surface of all specimens wear tracks performed in dry condition are reported in Figure 5-54 and EDXS analyses performed on the different grey zones of the wear tracks of pure Ni and Ni/0.16B coatings are reported in Figure 5-55 and Figure 5-56.

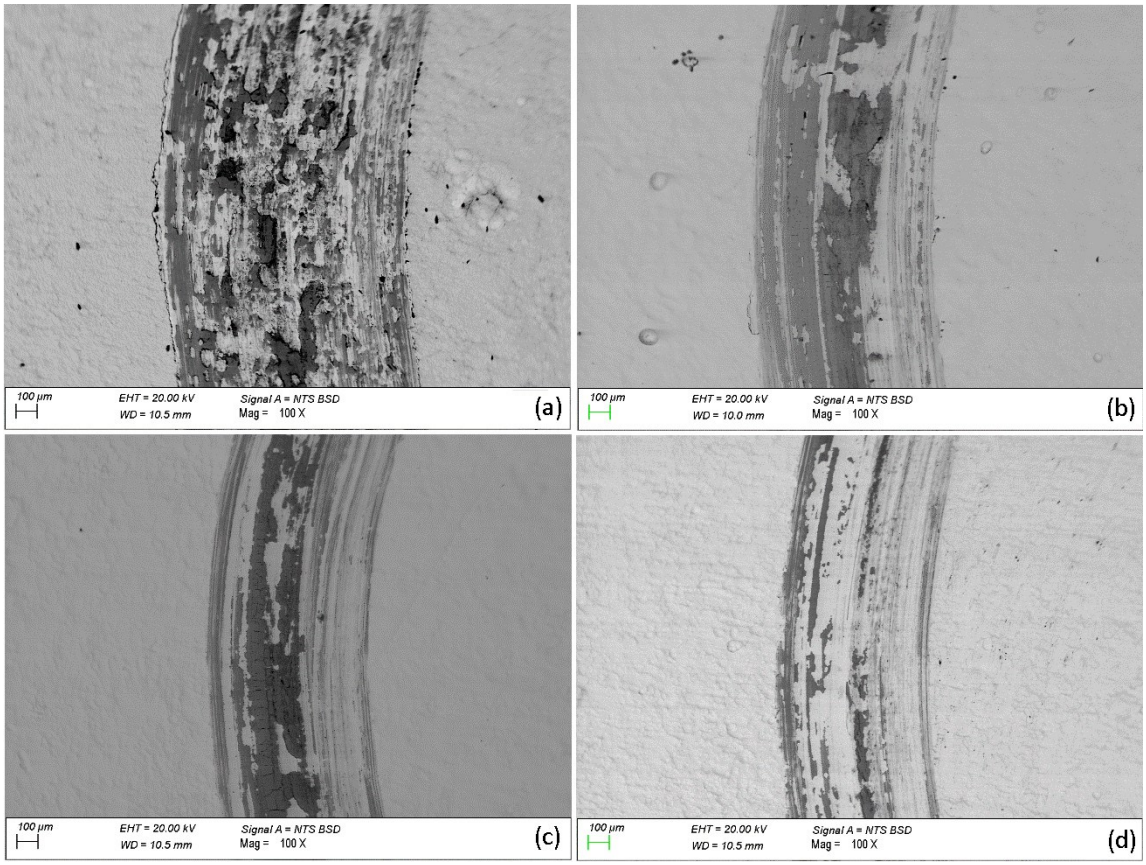

Figure 5-54: SEM micrographs in top view of the wear tracks after tribological tests of (a) Pure Ni, (b) Ni/0.08B, (c) Ni/0.12B and (d) Ni/0.16B

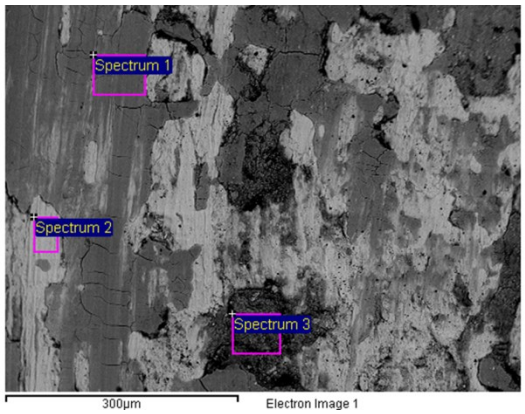

Figure 5-55: EDXS analyses performed on the different grey zones of of the pure Ni wear track

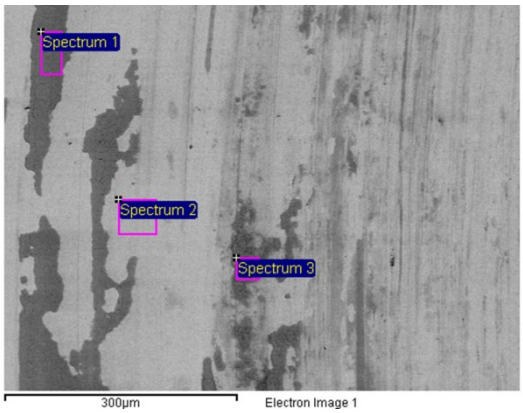

Figure 5-56: EDXS analyses performed on the different grey zones of the Ni/0.16B wear track

Table 5-23: EDXS analyses performed on the different grey zones of the pure Ni wear track

	O	Al	Ni
Spectrum	**[wt.%]**	**[wt.%]**	**[wt.%]**
1	28.52	3.49	67.99
2	3.63	0.36	96.00
3	27.05	3.78	69.18

Table 5-24: EDXS analyses performed on the different grey zones of the Ni/0.16B wear track

	O	Al	Ni
Spectrum	**[wt.%]**	**[wt.%]**	**[wt.%]**
1	28.35	2.52	69.14
2	3.21		96.79
3	23.42	1.37	75.21

By observing the top surface of the wear tracks it is possible to notice that the pure Ni wear track is the wider one and the more damaged.
EDXS analyses performed on the different grey areas of the wear tracks show that both pure Ni and Ni/0.16B coatings are partially covered by a Ni oxide layer (Figure 5-55 and Table 5-23 ; Figure 5-56 and Table 5-24). This indicate that all types of deposits underwent to triboxidative wear.
The observations of the top surface by SEM revealed also a progressive decrease of the amount of the Ni oxide in the wear tracks in the Ni-B coatings (dark grey areas) by increasing the B content in the deposits.
The SEM micrographs of the top surface of the wear tracks performed in wet condition are reported in Figure 5-57.

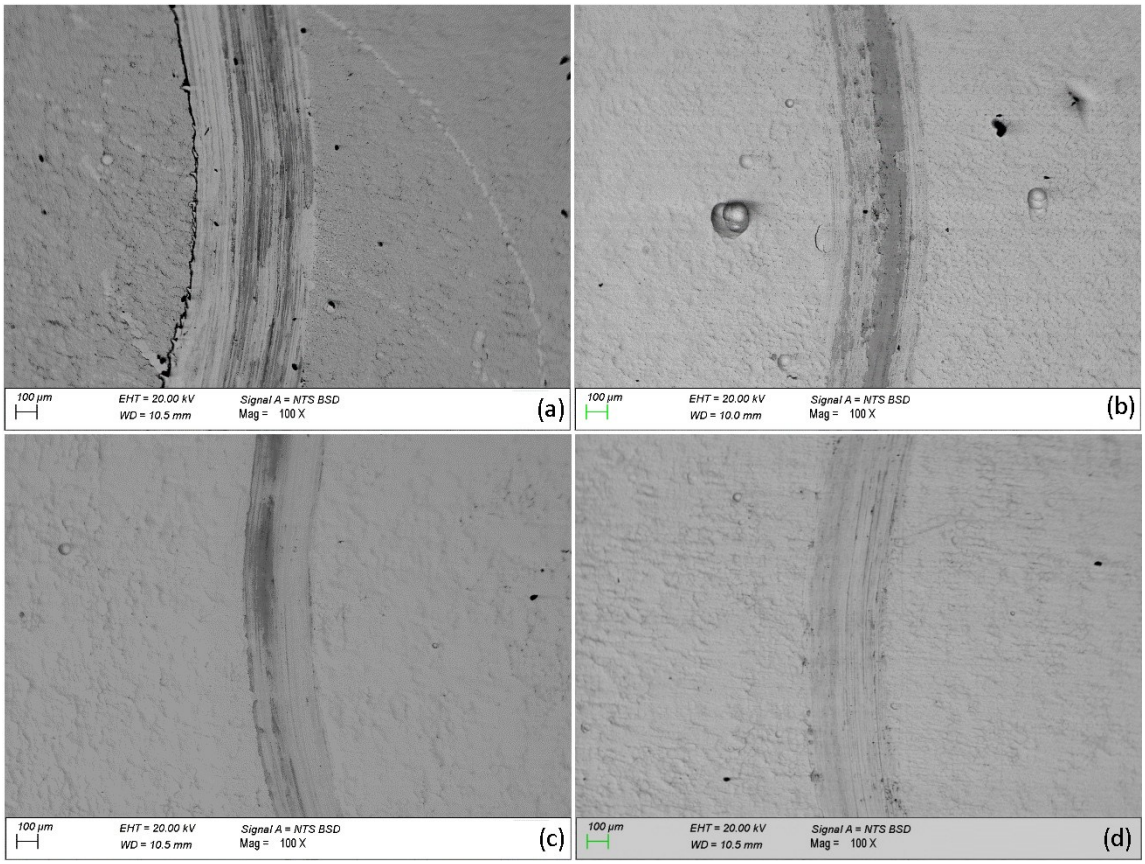

Figure 5-57: SEM micrographs in top view of the wear tracks after tribocorrosion tests(a) Pure Ni, (b) Ni/0.08B, (c) Ni/0.12B and (d) Ni/0.16B

By observing the top surface of the wear tracks after the tribocorrosion tests it is possible to notice that also in wet condition the pure Ni wear track is the wider one indicating an higher damage of the coating in comparison to the Ni-B coatings. EDXS analyses performed on the different grey areas of the wear tracks revealed the presence of chlorides and Ni oxide but in lower amounts in comparison to the wear tracks obtained in dry conditions. This is due to the lubricant effect of the electrolyte and the solution flow induced by the movement which helps the oxides removal. All types of deposit underwent to triboxidative wear also under wet condition. The SEM micrographs of the wear tracks in

cross section after metallographic etching reported in Figure 5-54 are representative of both wear and tribocorrosion tests.

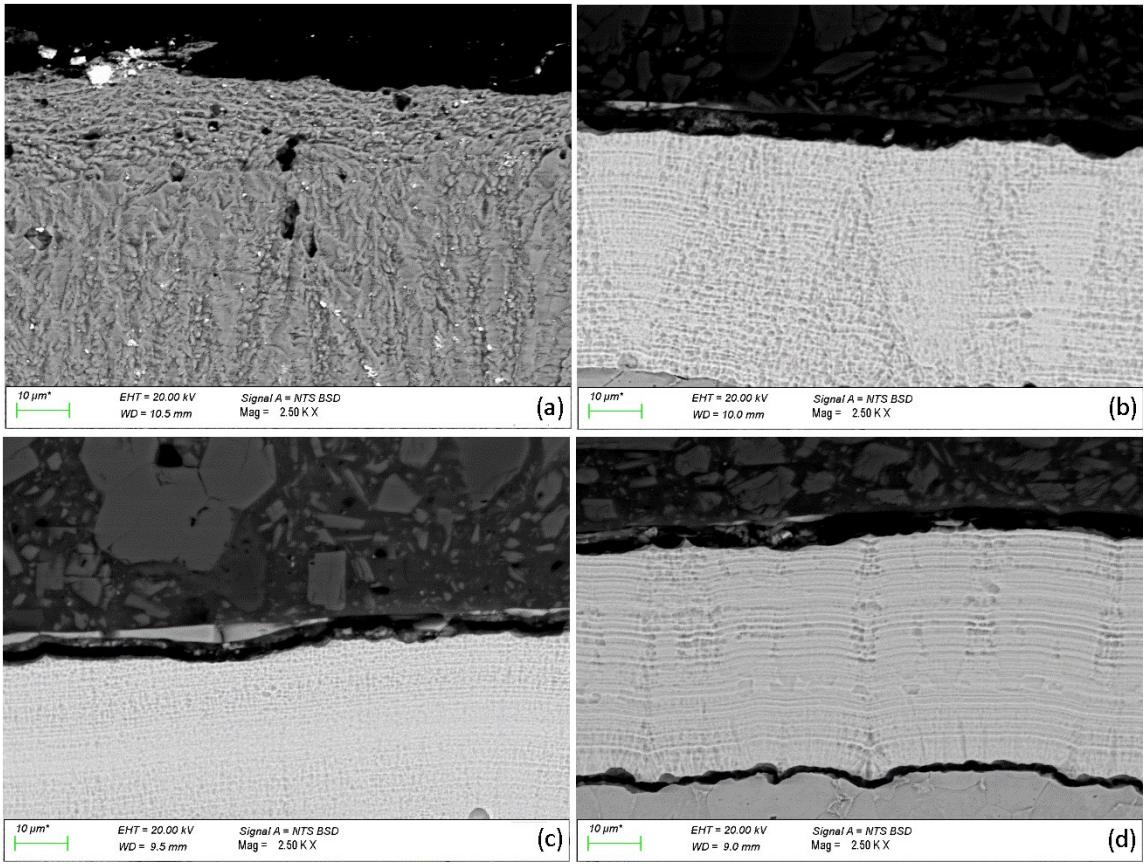

Figure 5-58: SEM micrographs of the wear tracks after wear tests in cross section and after metallographic etching of (a) Pure Ni, (b) Ni/0.08B, (c) Ni/0.12B and (d) Ni/0.16B

The analyses by SEM of the wear tracks cross section at high magnification showed that both under dry and wet conditions the pure Ni underwent a severe plastic deformation of the Ni columns during the sliding.

No one of the Ni/B coatings presents plastic deformation due probably to the higher hardness and the fine, not oriented microstructure. The lower ductility of the Ni/B coatings in comparison to the pure Ni facilitates the detachment of the Ni oxide scales which are formed on the coatings surface under wear.

The wear coefficient values calculated using the *(5.1)* equation are reported in Figure 5-59.

(a) **(b)**

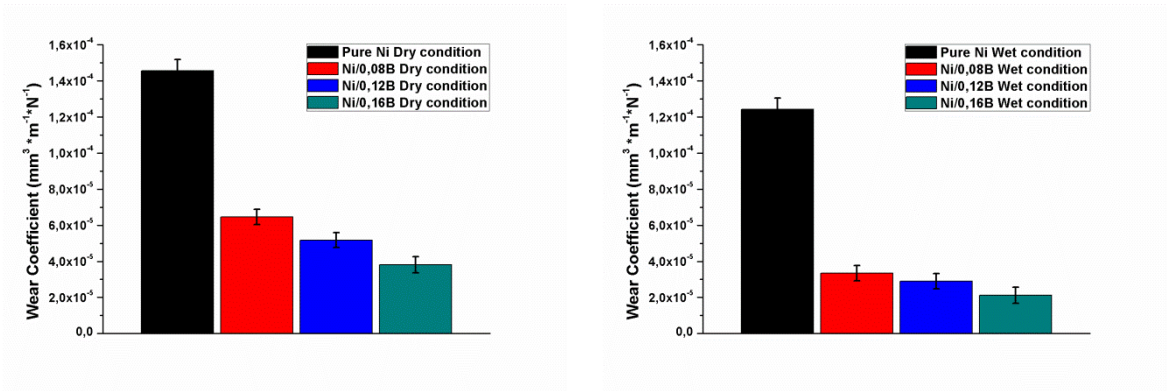

Figure 5-59: Wear coefficient of the pure Ni and Ni-B coatings tested in dry (a) and in wet (b) conditions

By observing the wear coefficient values it is possible to notice that in both dry and wet conditions all Ni/B coatings present remarkable high wear resistance in comparison to the pure Ni coatings. The decrease of the wear coefficient of the Ni-B coatings by increasing the B content indicates that Ni-B coatings with higher hardness present a higher wear resistance. In general, comparing the results obtained in dry and wet condition, the lubricant effect of the electrolyte leads to a decrease of the wear coefficient values. Furthermore, the flow of the solution produced by the sliding between the sample and the counterpart hinders the formation of a solid and adherent Ni oxide and facilitates the removal of the wear debris and oxides, reducing the third-body damage. With this test configuration, no synergic effect between wear damage and corrosion attack was detected.
OCP measurements of pure Ni and Ni-B coatings before, during and after tribocorrosion tests are reported in the graph in Figure 5-60.

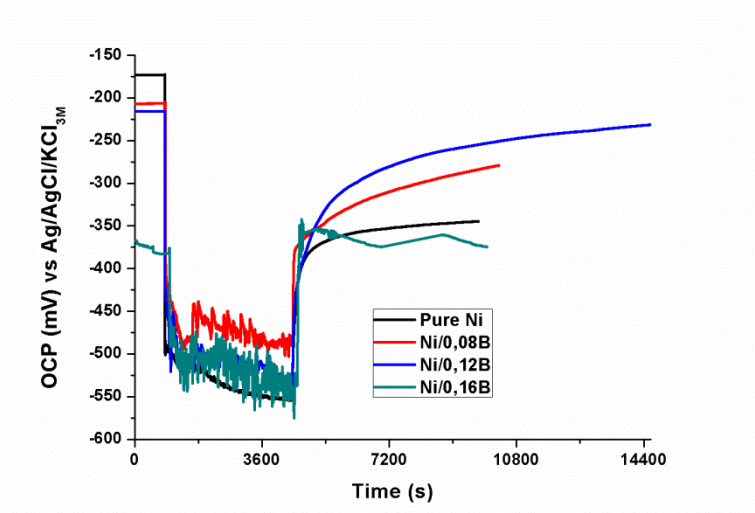

Figure 5-60: OCP measurements of pure Ni and Ni-B coatings before, during and after tribocorrosion tests

The graph shows that the damage of the passive layer during the sliding and the exposure of the bare metal to the electrolyte leads to a drop of the OCP (in a range of about -450 – -550 mV vs. Ag/AgCl) for all tested specimens.

At the end of the tribocorrosion tests, when the wear load is removed, it is possible to notice that the crack-free Ni/B coatings (Ni/0.08B and Ni/0.12B) exhibit a faster recovery of the OCP in comparison to the pure Ni.
The Ni/0.12B specimen shows a complete recovery of the OCP 2 hours after the load removal, reaching the same value monitored prior to the load application. The Ni/0.08B specimen shows a similar behavior. On the contrary the pure Ni coated specimen, 1 hour after the load removal, presents OCP values of about 200 mV lower than those monitored prior to the load application. This behavior could be related to the severe plastic deformation of the pure Ni coating during the test (determining the presence of a more stressed surface layer even after the load removal) which does not allow the formation of an uniform passive layer. The Ni/0.16B coating with cracks shows the same OCP of the others coatings during the sliding but lower values before and after the test due to the presence of cracks both inside and outside of the wear tracks (allowing a substrate interference in the OCP value). Based on these results it is possible to affirm that the crack free Ni-B deposits exhibit both a higher wear and tribocorrosion resistance in comparison to the pure Ni coatings.

5.2.3 Corrosion resistance

The protective properties of the Ni-B coatings have been evaluated by potentiodynamic polarization measurements in a 3.5% wt. NaCl solution both in large scale and in small scale. The measurements in large scale have been performed using an Avesta cell to avoid the crevice corrosion and in order to evaluate the overall performance of the coatings. In small scale, an electrochemical microcell with a capillary with a mean diameter of 800µm has been used to better understand the influence of the chemical composition and the microstructure to the electrochemical behavior of the coatings.
The potentiodynamic polarization curves performed in large scale and in small scale are reported respectively in Figure 5-61 and Figure 5-62.

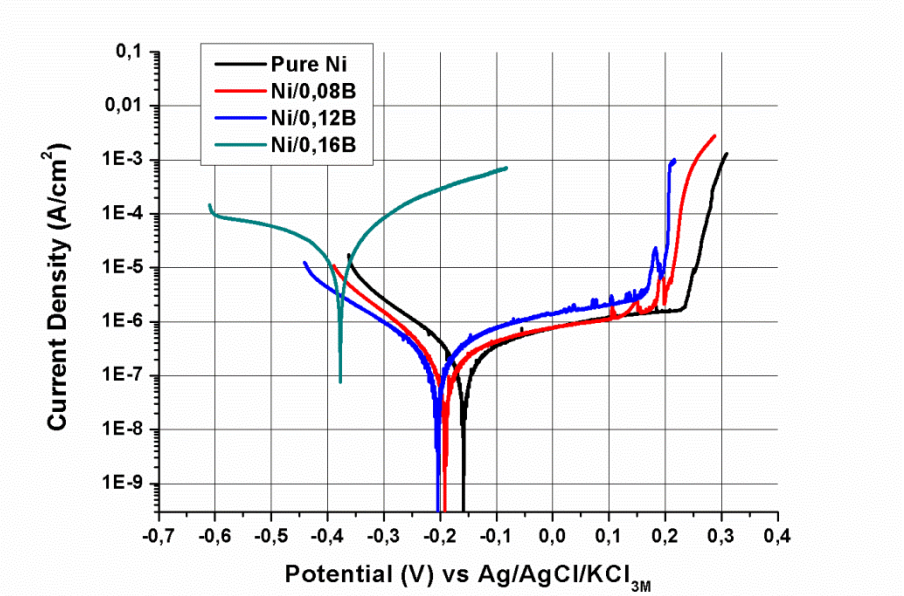

Figure 5-61: Potentiondynamic polarization curves performed with Avesta cell of pure Ni coating and Ni-B coatings with 0.08% wt. , 0.12% wt. and 0.16% wt. of B content

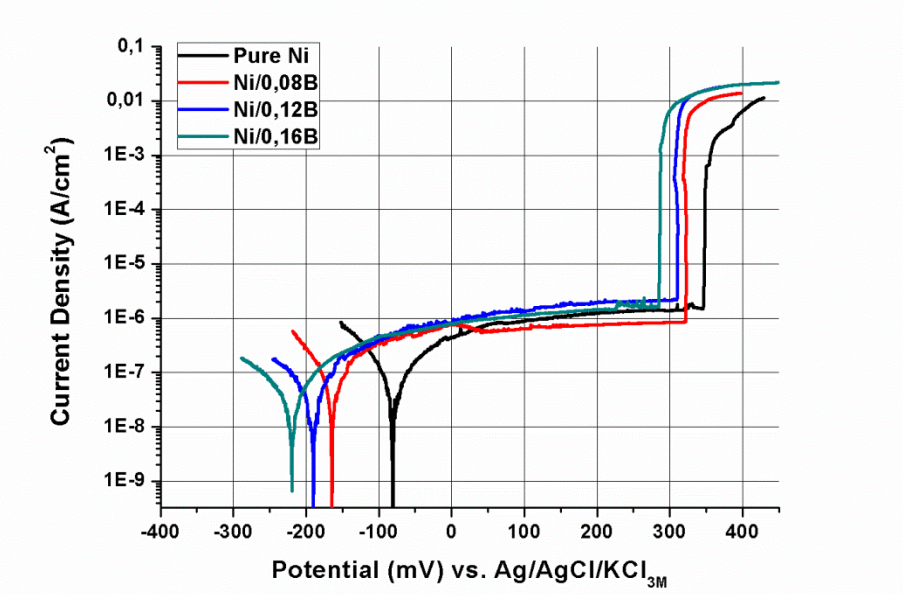

Figure 5-62: Potentiondynamic polarization curves performed with micro-cell of pure Ni coating and Ni-B coatings with 0.08% wt., 0.12% wt. and 0.16% wt. of B content

By observing the potentiodynamic polarization curves obtained in large scale it is possible to notice that the Ni-B coating with the higher content of B presents the higher corrosion current, the lower corrosion potential and an active behavior due the presence of cracks that allow to the electrolyte to reach the substrate. Instead, the crack free Ni/B coatings and the pure Ni show a passive behavior. A slight decrease of the pitting potential is observed by increasing the B content.
The measurements performed in small scale in areas without cracks confirm that, the active behavior observed in large scale, is caused by cracks. In fact, all coatings present a passive behavior. It is possible to notice also a progressive decrease of the corrosion potential by increasing the B content correlated to the different chemical composition.
The measurements at small scale confirm the progressive decrease of the pitting potential by increasing the B content. This phenomena is quite strange considering that usually grain refined coatings present a higher pitting resistance[8,9].
A possible explanation of this decrease of the pitting potential could be correlated to the increase of the deposit internal stresses that accompany the marked grain refinement.
By increasing the Boron content, the internal stresses increase causing the formation of micro defects into the passive layer thus favoring the chlorides attack.

5.3 Partial conclusions

The second part of the research was focused on the study of the electrodeposition of crack free Ni-B alloy coatings using Dymethylamine borane (DMAB) as boron source. The work started with the production, on laboratory scale, of different series of deposits using a Ni Watts plating bath and varying the plating process parameters. The preliminary study has

[8] M. Lekka, A. Lanzutti, C. Zanella, G. Zendron, L. Fedrizzi, P.L. Bonora, Pure and Applied Chemistry, 83(2) (2011), 295-308
[9] C. Zanella, M. Lekka, P.L. Bonora, Journal of Applied Electrochemistry 39 (2009), 31-38

been developed in order to identify the range of DMAB concentration that allow to produce crack free deposits, evaluate the distribution of the B along the deposit thickness, evaluate the consumption of the DMAB in the plating bath, investigate the influence of the pulsed current and the saccharin as stress reduction agent and feasibility of multilayer coatings production. The produced samples have been characterized regarding their microstructure, the chemical composition and the hardness. The results of the characterizations have been used as feedback for the optimization of the plating process.

The results of the preliminary study show that DMAB concentrations above 0.5 g/L lead to delamination of the coatings due to high internal stresses. The formation of H_2 during the electrodeposition of the Ni-B coatings is higher in comparison to the electrodeposition of pure Ni. Hence a higher concentration of surfactant is required. By increasing the DMAB concentration in the plating bath the B content in the deposits increases linearly. Due to the low DMAB concentrations the distribution of B along the deposit thickness is strictly correlated to the ratio *volume bath/coated surface* and the deposition time. The higher the ratio *volume bath/coated surface*, the more uniform the distribution of B along the thickness. The DMAB stratification in the plating bath causes a dis-homogeneous "spatial distribution" of B in the deposit, a more vigorous stirring does not allow to solve the issue while an higher ratio *volume bath/coated surface* can help to obtain a more uniform distribution.

The formation of cracks due to the internal stresses is strictly dependent to the B content and the deposit thickness. Crack-free Ni-B deposit with a B content of about 0.1% wt. can be obtain with a DMAB concentration in the order of 0.1-0.2 g/L approximately. However in general, at equal B content, deposits with a higher thickness have higher internal stresses and hence are more prone to the cracks formation. The attempt to reduce the internal stresses with the use of the pulsed current did not give the expected results instead a marked increase of the amount of the co-deposited B was noticed. An explanation of the increase of the co-deposition of B could be due to a thinning of the diffusion layer that allows a higher amount of DMAB to reach the cathode surface. The use of the saccharin as stress reduction agent leads to the production of crack-free Ni-B deposits with a higher content of B, but the incorporation of sulphur could worsen the performances at high temperatures due to embrittlement effect. The production of multilayer coatings is feasible and lead to a more uniform distribution of B along the whole coating thickness. However it requires intermediate steps of acid etching to ensure a good adhesion between the different Ni-B layers.

The microhardness of the Ni-B coatings increases linearly by increasing the B content due to the solid solution hardening caused by the presence of B as interstitial atom in the Ni elementary cell, the reduction of grain size and the loss of preferential orientation.

Based on the results obtained with Ni Watts plating bath, the feasibility of the production of Ni-B deposits using Ni sulfammate "High speed" plating bath has been also investigated.

The Ni-B coatings produced with Ni sulfammate "High Speed" plating bath show a lower microhardness in comparison to coatings produced with the same DMAB concentration using Ni Watts plating bath due to the different deposition mechanism. This is mainly due to the lower internal stresses in the coatings with the Ni sulfammate plating bath. The range of DMAB concentration that is possible to use in order to produce crack-free Ni-B deposit is slightly higher.

Since the determination of DMAB concentration in the plating bath is extremely important for the scaling-up of the process, in parallel with the optimization of the electroplating

process, different methods for its determination have been investigated and a method based on iodometric titration resulted the most accurate.
The developed method was used for the plating baths replenishment and to investigate the plating baths stability. The titration pointed out a consumption of the DMAB during the storage due to the activation of the electroless deposition mechanism. Even if the deposition rate is very low, the consumption is significant for the low DMAB concentration for this reason the reagent has to be added in the plating bath just before the deposition.
After the optimization of the plating parameters and the determination of an optimum DMAB concentration range in order to produce crack free deposits the plating process was scaled up in a galvanic pilot plant with 10L deposition tank. Considering the good results on laboratory scale and the higher deposition rate, the Ni sulfammate "High Speed" plating bath was chosen to proceed with the deposition in large scale. Two different types of coatings have been produced: a series of monolayer coatings with DMAB concentration in a range from 0.1g/L to 0.25g/L and a multilayer coating composed of 1 pure Ni layer and 3 Ni-B layers produced with new plating baths with DMAB concentration of 0.08g/L, 0.1g/L and 0.12 g/L.
The characterization of the monolayer coatings allowed to demonstrate that it is possible to produce crack-free Ni-B deposits with a B content of 0.12% wt. with a thickness of about 40-50 μm and a constant B content along the thickness. Above this B content the increase of the internal stresses causes the formation of cracks. The electrodeposition of the Ni-B multilayer coating demonstrates the possibility to produce deposits with an increasing gradient of microhardness.
The coatings produced in the galvanic pilot plant have been used for the evaluation of the wear, the tribocorrosion and the corrosion resistance and the effect of the heat treatments on both the microstructure and the hardness.
All crack-free Ni-B deposits (up to 0.12% wt. of B) present a passive behavior in a 3.5%wt. NaCl solution similar to the pure Ni deposits. A slight decrease of the E_{pit} is noticed by increasing the B content which could be attributed to the internal stresses. On the other hand the presence of cracks (B content above 0.16% in wt.) leads to an active behavior.
All Ni/B coatings exhibit a higher wear resistance in comparison to the pure Ni coating. The higher the B content, the higher the wear resistance.
Crack free Ni-B deposit present a higher tribocorrosion resistance in comparison to the pure Ni. The absence of plastic deformation of the Ni grains allows a faster recovery of the OCP for the crack-free Ni-B deposits, at same values exhibited before the sliding, in comparison to the pure Ni, which does not recover the initial values of OCP due to a severe plastic deformation of Ni columns.
The results of characterization of the multilayer deposits heat treated at different temperatures up to 600°C show that both pure Ni and Ni-B layers present a decrease of the hardness by increasing the heat treatment temperature due to the recrystallization.
The different B content but in particularly the different microstructure of the three Ni-B layers influence the microhardness till 300°C. Above this temperature the crystallographic rearrangement of the microstructure is not affected by the small differences in the B content between the different Ni-B layers and the hardness is the same for all Ni-B layers. However the small amount of B is enough to hinder the recrystallization of all Ni-B layers, that present, for all the heat treatment temperatures, a more fine microstructure and a higher hardness in comparison to the pure Ni layers.

6 Conclusions

In this work two different types of Ni based coatings, which should guarantee higher performances at high temperature applications in comparison to the Pure Ni coatings, have been developed by electrodeposition. The work was divided in two parts, the first one regards the production and characterization of Ni matrix composite coatings containing either micro- or nano- particles of Al and the second one regards the production and characterization of Ni-B alloy coatings with low B content produced using DMAB as boron source.

Pure and composite Ni deposits containing either micro- or nano-particles of Al have been produced using a Ni sulfammate "High Speed" plating bath. The concentration of Al powders was fixed at 40g/L considering both the high cost of powders and the plating bath management difficulties in a potential use in industry.

The obtained deposits have been characterized regarding the Al content and its distribution, their microstructure, microhardness and protective properties both prior and after heat treatments up to 800^{o}C.

Pure Ni coatings present recrystallization starting from heat treatment temperature of 400°C and a progressive decrease of the microhardness, following the grain growth, by increasing the heat treatment temperature.

In comparison to pure Ni coatings, the co-deposition of both micro- and nano particles causes a refinement of the deposit columnar microstructure, and an increase of the hardness, more intense in the case of use of nano-particles. The nano-composite coatings present a more uniform distribution of Al particles but an Al content in weight 4-5 time lower in comparison to the micro-composite coatings.

Regarding the Ni/Al micro-composite coatings, the limited diffusion of Al that occurs after heat treatment at 400°C does not hinder the recrystallization of the Ni matrix leading to a decrease of the coating hardness. The fast diffusion of Al into the Ni matrix that occur at heat treatment temperature of 600°C leads to the formation of a mixed γNi and $\gamma'Ni_3Al$ structure. After heat treatment at 800°C the diffusion of Al is almost complete and the coating consists of a substitutional solid solution of Al in the Ni elementary cell. In both cases, the diffusion of Al hinders the recrystallization of the Ni matrix leading to the formation of coatings consisting of smaller equiassic grains maintaining microhardness values similar to those of the as plated deposit.

The small dimensions of the nano-particles and the more uniform distribution lead to an activation of the diffusion at lower heat treatment temperatures, even at 400°C. The fast diffusion of Al, that occurs after each heat treatment temperature up to 800°C, blocks the recrystallization of the Ni matrix maintaining a fine columnar structure and stable microhardness values.

All pure Ni deposits, both prior and after heat treatments, present a good corrosion resistance presenting a passive behavior.

The as plated and the heat treated at 400°C Ni/Al micro composite deposits present a low corrosion resistance, showing an active behavior, due to a strong galvanic coupling,

revealed also by SKPFM analyses, which causes the preferential dissolution of Al micro particles. Heat treatments at 600°C and 800°C lead to the formation of Ni/Al phases with lower Volta potential differences which enhanced the overall corrosion resistance.
The as plated and the heat treated at 400°C Ni/Al nano-composite deposits, instead, thanks to a lower Al content, a more uniform distribution and a smaller dimensions of the Al nano particles exhibit a higher corrosion resistance with the formation of a protective passive film. After heat treatment at 600°C or 800°C, the formation of more stable oxide on the deposit surface and the formation of Ni/Al phases increases the corrosion resistance of both composite coatings.
Even if this kind of composite coatings have been developed for high temperatures application the corrosion study revealed the potential risk to suffer galvanic corrosion before the putting in service or during the periods of plant shutdown.
During the preliminary research activity, a strong instability of the plating baths containing the Al particles has been observed. The dissolution of the Al particles and the consequent drop of the plating bath pH below the operative range does not allow to scale up the process. A possible solution, that nevertheless requires further experimental tests, may be the "stabilization" of the particles by depositing on the external surface a thin layer of Ni. Among the different techniques that could be used to functionalize the Al particles, electroless deposition or PVD and CVD could be used. However, considering the already high cost of the Al particles, the addition of a further process step in the production of the coatings could be justified only for applications with a high added value.
The study of the electroplating processes of Ni-B alloy coatings started with the production of different series of sample in order to identify the range of DMAB concentration that allows to produce crack free deposits, to evaluate the feasibility of the production of Ni-B coatings using Ni sulfammate "High Speed" plating bath, and the feasibility of the production of multilayer coatings.
In comparison to the previous studies on Ni-B deposits the use of GDOES has allowed to determine precisely the amount and the distribution of co-deposited B and hence determine with a higher accuracy the relationship between DMAB concentration and the electrodeposition parameters with the B content in the deposit.
After the initial laboratory scale tests, the plating process was successfully scaled up in a galvanic pilot plant with 10L deposition tank. Big samples have been produced for the evaluation of the wear, the tribocorrosion and the corrosion resistance and the effect of the heat treatments on both the microstructure and the hardness.
Based on the results of the characterization it is possible to assert that B content of 0.12% wt. allows to produce crack-free Ni-B deposits with a thickness of about 40-50 μm and a constant B content along the thickness. Above this B content the Ni-B coatings present cracks. The microhardness of the Ni-B coatings increases linearly by increasing the B content due to the solid solution hardening caused by the presence of B as interstitial atom in the Ni elementary cell, the reduction of grain size and the loss of preferential orientation. Nevertheless the increase of the B content leads to an increase of the internal stresses that could cause the formation of cracks that concern the whole deposit thickness. The electrodeposition of Ni-B multilayer coatings demonstrated the possibility to produce thick deposits with an increasing gradient of microhardness. Heat treatments at different temperatures up to 600°C showed that Ni-B coatings present a decrease of the hardness by increasing the heat treatment temperature due to the recrystallization. The different B content but in particular the different microstructure of the Ni-B coatings influence the microhardness till 300°C. Above this temperature the crystallographic rearrangement of

the microstructure is not affected by the small differences in the B content between the different Ni-B coatings and the hardness is the same for all Ni-B deposits. However the small amount of B is enough to hinder the recrystallization of all Ni-B coatings, that present, for all the heat treatment temperatures, a more fine microstructure and a higher hardness in comparison to the pure Ni. Regarding the corrosion resistance, all crack-free Ni-B deposits present similar protective properties to the pure Ni deposits. On the other hand, Ni-B deposits with cracks present an active behavior with a marked decrease of the protective properties. All crack free Ni/B coatings exhibit a higher wear and tribocorrosion resistance in comparison to the pure Ni coating. The higher the B content, the higher the wear resistance.

Since the determination of DMAB concentration in the plating bath is extremely important for the scaling-up of the process, in parallel with the optimization of the electroplating process, different methods for its determination have been investigated and a method based on iodometric titration resulted the most accurate. The titration pointed out a consumption of the DMAB during the storage due to the activation of the electroless deposition mechanism. Even if the electroless deposition rate is very low, the consumption is significant for the low DMAB concentration, for this reason the reagent has to be added in the plating bath just before the deposition.

Comparing the two types of galvanic coatings it is possible to assert that the Ni-B coatings are more suitable for application that require high hardness and high wear resistance in an operating range temperature up to 400°C - 450°C. Ni/Al composite coatings, thanks to the preservation of the hardness at higher temperatures, are more indicated for operating temperatures in a range from 500°C to 800°C.

The study of the comparison between the use of nano and micro particles showed that the use of nano-particles even if does not allow to reach the highest content of Al allows to produce coatings with higher performances thanks to the small dimensions and a more homogenous distribution of the particles.

The developed Ni-B production process could be easily industrialized with existing deposition plants. Particular attention has to be done on the electroplating parameters and the plating baths replenishment.

The developed Ni/Al production process can not be industrialized as it is, due to the Al dissolution issues. Further studies, both scientific and economic, are needed to exploit the feasibility of the industrialization.